Modeling of Coal Fired Boiler

A thesis submitted to

University of Pune

for the degree of

DOCTOR OF PHILOSOPHY

In

Chemical Engineering

By

Devkumar F. Gupta

Under guidance of

Dr. Vivek V. Ranade

Catalysis, Reactor and Separation Unit, CEPD,
National Chemical Laboratory (NCL)
Pune-411 008, INDIA

December 2009

CERTIFICATE

This is to certify that the work incorporated in the thesis, "**Modeling of Coal Fired Boiler**" submitted by Mr. Devkumar F. Gupta, for the degree of Doctor of Philosophy, was carried out by the candidate under my supervision at Chemical Engineering and Process Development Division, National Chemical Laboratory, Pune 411008, India. Such material as has been obtained from other sources has been duly acknowledged in the thesis.

Dr. V. V. Ranade

(Research Supervisor)

DECLARATION

I hereby declare that the thesis entitled "**Modeling of Coal Fired Boiler**", submitted for the Degree of Doctor of Philosophy to the University of Pune, has been carried out by me at the National Chemical Laboratory (NCL), Pune under the supervision of Dr. V. V. Ranade. The work is original and has not been submitted in part or full by me for any other degree or diploma to this or any other University.

Date: (Devkumar F. Gupta)

Place:

ACKNOWLEDGEMENT

I am highly indebted to Dr. V.V. Ranade, my supervisor at National Chemical Laboratory (NCL), Pune. Working with him was one of the most fortunate things that have happened in my life. I could not have imagined having a better advisor and mentor for my PhD, and without his knowledge, perceptiveness and approach to crack problems, I would never have finished in time. With very high standards of quality work set by him in our group at NCL, Pune, I would like to repeat my colleague Dr. Vivek Buwa's words "I hope this work at least partly satisfies his expectations."

There are several friends whom I would like to acknowledge whom I met during my stay at our group Industrial Flow Modeling Group (IFMG) at NCL, Pune. I would like to acknowledge my seniors Vivek, Gunjal, Ranjeet, Khopkar and Kaustubh whose interactions at different intervals have been encouraging. Special thanks to one of my colleague Naren for helping me several times during my work. Interacting with Naren has always helped me in getting some new ideas to tackle a problem. I would also like to thank my other colleagues Mohan, Ajay, Madhavi, Latif, Chaitanya, Amit, Shashi, Ganesh, Chandrashekar, Ram Ratan Ratnakar (IIT-D) and Mohanshyam (IIT-D) for making my stay at iFMg very pleasant.

I sincerely acknowledge Dr. B. D. Kulkarni, head CEPD and Dr. Amol Kulkarni for their valuable help and co-operation during my research stay in NCL. I would like to thank all other members of homogeneous catalysis division, for a healthy working atmosphere. I am grateful to Council of Scientific and Industrial Research (CSIR), India for the research fellowship and to NCL research foundation, ISCRE20 and Society of Japan for providing travel grant to present my work in ISCRE20, Japan. I am thankful to director Dr. S. Sivaram, Director, NCL for allowing me to carry out research work and extending me all the possible infrastructural facilities.

I would also like to say thanks to my entire family particularly to in-laws and most importantly to my wife Maya for standing by me at all times, may be good or bad. I would also like to thank God for blessing me and my wife with our baby kid "Suhani" who has added some of very sweet memories during my Ph.D and has now grown tall with the progress of my research work.

DEV GUPTA

Dedicated to my wife "Maya"

Abstract

Pulverized coal fired boilers (PCFB) generate nearly 40% of world's electricity output. With stringent environmental regulations and escalating electricity demands, there is a greater drive towards performance enhancement of such units. The performance of PCFB is influenced by hardware configuration (furnace volume, burner type, burner settings etc.) and operating protocols/procedures (coal characteristics and composition, particle size distribution, air flow rate, burner tilt and so on). Understanding influence of these parameters on boiler performance is crucial for improving efficiency of PCFBs. Variety of complex processes with different time and length scales (like turbulent, multiphase recirculating flows, chemical reactions and radiative heat transfer) exist in the boiler. Proper understanding of all these processes will help in devising better operating strategies for coal fired boiler. The thesis is aimed at improving the understanding of underlying various aspects of the coal fired boiler.

A multilayer methodology was developed to study various aspects of the coal fired boiler. TGA experiments were performed to estimate the devolatilization and intrinsic char oxidation kinetic parameters of the Indian coal. Computational model for the drop tube furnace was developed to estimate the kinetics of char oxidation from the available literature data on char burnout. This study emphasized the importance and use of 2D axisymmetric CFD model over conventional plug flow model in estimation of kinetic parameters.

A detailed CFD model was developed for 200 MW_e boilers and the effects of various operating parameters were studied. The Eulerian-Lagrangian approach was used to simulate the flow, mass and heat transfer in the boiler. The model was used to understand flow, temperature and species concentration field within a typical boiler. The crossover pass characteristic (uneven distribution of flow and temperature) of tangentially fired boiler was predicted. The model was also used to quantify sensitivity of these fields with key design and operating parameters. The predictions of the developed CFD model were

validated with the plant data. The base case was used to understand the sensitivity of excess air, burner tilt and thermal heat load on boiler performance. Simulations were performed to understand the performance of boiler when the Indian coal was blended with imported lignite coal in various ratios.

Based on the outcomes of the CFD models, appropriate methodology was adopted to develop a state of art phenomenological model (Boiler Optimization and Simulation Tool, BOST). This model framework translates the information gained from detailed CFD model to readily usable engineering scale model for actual plant implementation. The phenomenological model was based on the mixing cell approach, each zone representing key section of boiler. The positioning and sizes of different zones depends upon the underlying fluid dynamics. The effect of key operating protocols like burner tilt was accounted through appropriate correlations developed from the CFD simulations. The developed framework provides a powerful platform to simulate coal fired boilers with reasonable computing resources and in real time.

The research work of this thesis presents systematic approach in developing state of art models for boilers. Studies were performed to understand various aspects like chemistry (kinetics of devolatilization and char oxidation), physics (two phase reactive turbulent flow, radiative heat transfer) and engineering (effect of operational parameters) to predict the performance of the boiler.

Table of Contents

List of Figures

List of Tables

Nomenclature

a	Absorption coefficient of gas	m^{-1}
A	Empirical constant = 4.0	--
A_c	Pre exponential factor for char oxidation	kg m^{-2} s^{-1} Pa^{-1}
A_p	Particle surface area	m^2
a_p	Equivalent absorption coefficient due to the presence of particulates	m^{-1}
A_v	Pre exponential factor for devolatilization	s^{-1}
B	empirical constant = 0.5	--
c	Constant	--
C_0	Viscous resistance coefficients	m^{-2}
C_2	Inertial resistance coefficients	m^{-1}
C_D	Drag coefficient	--
$C_{l,r}$	Molar concentration of each reactant l^{th} species in reaction r	kmol m^{-3}
Cpp	Heat capacity	J kg^{-1} K^{-1}
D	Characteristic dimension of heat exchanger tube	m
D_{km}	Diffusion coefficient for species k in the mixture	m^2 s^{-1}
d_p	Particle diameter	m
E_c	Activation energy for char oxidation	J $kmol^{-1}$
E_p	Equivalent emission	W m^{-3}
E_v	Activation energy for devolatilization	J $kmol^{-1}$
F	Momentum source term	kg m^{-2} s^{-2}
f_{heat}	Fraction of char oxidation heat absorbed by the particle	--
f_{pn}	Particle scattering factor associated with the n^{th} particle	--
g	Gravitational constant	m^2 s^{-1}
G	Turbulence generation term	
h	Gas enthalpy	J kg^{-1}
h	Heat transfer coefficient	$Wm^{-2}K^{-1}$
h_k^0	Enthalpy of formation of species k at the reference temperature, T_{ref}	J kg^{-1}
H	Total enthalpy	J kg^{-1}

H_c	Heat released during char oxidation	J kg^{-1}
HR	Ramp heating rate	K s^{-1}
I	Radiant intensity	W m^{-2}
k	Thermal conductivity of gas	W m^{-1} K^{-1}
k	Turbulent kinetic energy	
K_c	Char oxidation kinetic rate constant	kg m^{-2} s^{-1} Pa^{-1}
K_d	Gas phase diffusion coefficient for oxygen	kg m^{-2} s^{-1} Pa^{-1}
K_r	the kinetic rate constant for reaction r	
k_t	Turbulent thermal conductivity of gas	W m^{-1} K^{-1}
K_v	Devolatilization kinetic rate constant	s^{-1}
L	Characteristic dimension of the furnace	m
m	Exponent of Pr number (constant)	--
M_f	Final mass of sample after the devolatilization is over	kg
m_k	Mass fraction of species k	--
M_p	Mass of particle	kg
M_v	Mass of volatile at any time	kg
m_v , m_c	Mass fraction of volatile and char respectively	--
MW	Molecular weight	kg $kmol^{-1}$
$\dot{m}$	Mass flow rate of particle	kg s^{-1}
n	Order of the char oxidation reaction (n=1)	--
N_p	Number of particles	s^{-1}
N_r	Number of reactions	--
p	Static pressure	Pa
Pr	Prandtl number	--
$P_{O_2}^n$	O_2 partial pressure	Pa
Q_{conv}	Heat flow towards the particle by convection	W
Q_{rad}	Heat flow towards the particle by radiation	W
r	Radial direction	--
Re	Reynolds number	--
R_k	Net rate of production of species k by chemical reaction	kg $s^{-1}m^{-3}$
$S_{h,rxn}$	Source term for heat of gas phase chemical reactions	Wm^{-3}
S_k	Source of species k from dispersed phase	kg $s^{-1}m^{-3}$
S_m	Source term for the total mass added from the discrete phase	kg $s^{-1}m^{-3}$
S_Q	Source term for heat added from discrete phase	W m^{-3}

T_p	Particle temperature	K
$T_{ref,k}$	Reference temperature = 298.16 K	K
T_R	Radiation temperature $=\left(\frac{I}{4\sigma}\right)^{1/4}$	K
U	Fluid velocity in radial direction r	m s^{-1}
U	unburnt fraction of coal	--
$u_{p,i,j}$	Velocity components of the particle of size j in i^{th} direction (r or z)	m s^{-1}
v_i	Gas velocity in i^{th} direction (U or W)	m s^{-1}
V	cell volume	m^3
W	Fluid velocity in axial direction z	m s^{-1}
Y_p	mass fraction of any product species, p	--
Y_R	mass fraction of a particular reactant, R	--
z	Axial direction	--

Subscript

db	Dry basis
g	gas
i	Direction
j	Particle size
p	Particle
O_2	Oxygen

Greek letter

μ_T	Turbulent or eddy viscosity	kg m^{-1} s^{-1}
δij	Kronecker delta function	--
σ_p	Equivalent particle scattering factor	--
σ	Stefan Boltzmann constant $=5.67\times10^{-8}$	$Wm^{-2}K^{-4}$
ε_{pn}	Emissivity of particle	--
Δ	change in the property across that cell	--
ρ	Density	kg m^{-3}
μ_{eff}	Effective viscosity	kg m^{-1} s^{-1}
μ	Viscosity of gas phase	kg m^{-1} s^{-1}
ε	Turbulent energy dissipation rate	m^2 s^{-3}
$v'_{k,r}$ and $v_{k,r}$	Stoichiometric coefficient for k^{th} species as product and reactant respectively	--

$\phi(\vec{s},\vec{s}')$	Scattering phase function	--
$\eta'_{l,r}$	Exponent for each l^{th} reactant in reaction r	--

Chapter 1

Introduction

1.1 Coal fired boiler

Majority of the large scale electricity generation power plants derive their energy from burning of pulverized coal in boilers to generate high pressure steam that drives turbines to generate electricity. Worldwide coal-fired generating capacity is expected to reach approximately 2,500 GW by the end of 2020, an increase of nearly 60% from 2008 and more than 55% of the projected new generating capacity is expected to be in Asia (Mcllvaine, 2008). The capacity enhancement is based on the addition of advanced low-emission boiler systems and as well as continuous efforts are being made on existing power plants to achieve higher efficiency, reliability and availability with low maintenance, while complying with stringent emissions regulations for CO_2, SO_x, NO_x and particulates. The research work on performance enhancement of power plants is majorly based on the areas like new emission control technologies, state-of-the-art boiler designs and low-temperature heat recovery systems for improved plant efficiencies, systems for improved ash disposability and reduced waste generation, optimum system integration and plant controls. There have been several improvements in electricity generation technology in many such different areas, including boilers, turbines, generators, fluegas cleaning and these areas are still re-inventing themselves.

Boilers have been there over past century of time and have undergone major innovations in order to satisfy economics and increasing stringent environmental regulations. In principle, the solid-fuel combustion technologies are divided into three categories as (i) Fixed bed or grate combustion, (ii) Suspension or pulverized combustion and (iii) Fluidized bed combustion. The traveling grate stoker was the early coal combustion system for power generation. Traveling grate stokers are capable of burning coals of a wide range of coal rank (from anthracite to lignite). The typical particle sizes are 1-5 cm with residence time of 3000-5000 s. The flame temperature is around 1750 K (Essenhigh, 1981). Stoker firing was not able to scale beyond 25 MW_e unit capacities. The boiler efficiency gets suppressed by the high excess air (about 40%), which was required for acceptable coal burnout. Hence traveling grate stokers were retrofitted with topping pulverized coal (TPC) combustion. The arrangement of TPC allowed for flash drying of

the coal with controlled separation of fines from the larger coal particles. The lumps of coal were fed to the grate and the fines (< 0.3 mm) were carried pneumatically to a small grinding mill, ground to pulverized coal fineness, and injected through burners into the combustion chamber above the grate. TPC was successful in improving the boiler efficiency and raising the steaming capacity, but it required to retrofit some additional screen tubes in the combustion chamber and improved flue gas cleaning equipments to capture fly ash particles (Baranski, 2002).

In 1946, Babcock & Wilcox introduced the cyclone furnace for use with slagging coal (i.e. coals that contains inorganic constituents that will form a liquid ash at temperature of ~1700 K or lower) which was most significant advance in coal firing since introduction of the pulverized coal firing (Miller, 2005). Cyclone furnace provide benefits obtained with pc firing but have the advantages of utilizing slagging coals, reducing costs due to less fuel preparation (i.e. fuel can be coarser and does not need to be pulverized). In slagging combustion, the boiler tubes in the lower part of the furnace are covered by refractory to reduce heat extraction and to al1ow the combustion temperature to rise beyond the melting point of the ash. The temperature has to be sufficiently high for the viscosity of the slag to be reduced to about 150 Poise that is necessary for removal in liquid form. The most notable application of slagging combustion technology in the USA was the Cyclone Furnace in which about 85% of the coal ash could be removed in molten form in a single pass without ash recirculation. Because of the high temperature and the oxidizing atmosphere, slagging furnaces produced very high NO_x emissions and they fell in disfavor in the 1970s.

Fluidized-bed boilers for utilizing coal were originally developed in the 1960s and 1970s and offer several inherent advantages over conventional combustion systems including the ability to burn coal cleanly by reducing sulfur dioxide emissions during combustion (i.e. in situ sulfur capture) and generating lower emissions of nitrogen oxide. In addition fluidized bed boilers provide fuel flexibility as a range of low-grade fuels can be burned efficiently. In fluidized bed combustion (FBC), crushed coal of 5–10 mm is burned in a hot fluidized bed of 0.5 – 3.0 mm size inert solids. The typical particle residence time is

around 100-500 s (Essenhigh, 1981). Less than 2% of the bed material is coal; the rest are coal ash and limestone, or dolomite, which are added to capture sulfur in the course of combustion. The bed is cooled by steam generating tubes immersed in the bed to a temperature in the range of 1050 – 1170 K. This prevents the softening of the coal ash and the decomposition of $CaSO_4$, the product of sulfur capture. The heated precipitate after coming in direct contact with the tubes (heating by conduction) helps to improve the efficiency of heat transfer. Since this allows coal plants to burn at cooler temperatures, less NO_x is also emitted. But this technology was limited to small industrial sized fluidized boilers and was not useful for very large steam capacities that of pulverized coal-fired units.

Pulverized coal (pc) combustion became widely accepted combustion system for power generation in the period of 1900-1920. This was the major development in order to take advantage of the higher volumetric heat release rates of pulverized coal; increasing system efficiencies by using super heaters (heat-exchange surface to increase the steam temperature), Economizer (heat exchanger surface to preheat the boiler feed water) and combustion air pre heaters (heat exchange surface to preheat combustion air); and improving material of construction, allowing for steam generator to achieve steam pressures in excess of 83 barg. The typical particle sizes are 10-100 μm with residence time of ~ 1 s (Essenhigh, 1981). The flame temperature is around 1750 K. The development of superheater, reheater, economizer and air pre-heater played significant role in improving overall system efficiency because by absorbing most of the heat generated from burning the coal. The separation of steam from water and the use of super heaters and reheaters allowed for higher boiler pressure and larger capacities. Hence, pulverized coal combustion system became widespread due to increased boiler capacity, improved combustion and boiler efficiencies over stoker-fired boilers. Pulverized-coal boiler was found to be most the suitable for the utility power plants and contributes to more than 50% of world's electricity demand. Advances in material of construction, system designs and fuel firing have led to increasing capacity and higher steam operating temperatures and pressures. There are two basic pulverized coal-fired water tube steam generators: sub critical drum type boilers with nominal operating pressures of either 131

or 179 barg or once through super critical units operating at 262 barg. These units typically range in 300 to 800 MW (i.e. producing steam in the range 900 to 3000 ton $hour^{-1}$); however ultra-supercritical units entered into service in 1988 and operate at steam pressure of 310 barg and steam temperatures of 838 K with capacities as high as 1300 MW. This thesis work was focused on understanding various processes occurring in the most widely adopted pc boiler and the details of the same are discussed in the next paragraph.

In pc combustion, the coal is dried and ground to specified fineness and the powdered coal is pneumatically transported to the burners where it is injected in the form of particle-laden jets into the combustion chamber. The system of coal preparation: feeding, drying, and grinding of the coal and the pneumatic transport of the pulverized coal to the burners is fully integrated with the boiler. The transport air that carries the coal from the mill to the burners is a fraction of the total combustion air required mainly because its temperature is limited to about 373 K for reasons of safety against ignition and explosion in the mill and the transport pipeline between the mill and the burners. Upon injection into the combustion chamber, the coal particle-laden jet entrains hot combustion products, which raises its temperature and assists the ignition of the cloud of coal particles. The rest of the combustion air, which can be more strongly preheated, is injected separately and admixed with the burning fuel jet in the combustion chamber. The particles burn in a mode in which both external diffusion of oxygen to the particle surface and chemisorption of the oxygen at the particle surface/ pores of the solid char play roles in determining the progress of combustion, with diffusion controlling the burning rate of larger particles at the higher temperatures, and chemical kinetics controlling the burning rate of the small particles as the char bums out in the tail end of the flame.

Typical tangentially fired pulverized coal boiler is shown in Figure 1.1-a. There are three major parts of the boiler: Furnace, Cross over pass and Second pass. In a tangentially-fired furnace, the burners engender a rotational flow in the furnace by directing the jets tangent to an imaginary circle whose centre is located at the centre of the furnace. The resultant swirling and combusting flow generates a fireball at the centre of the furnace

where the majority of combustion occurs (Figure 1.1-c). The design of the combustion chamber has to provide for sufficient residence time of the burning particle to complete combustion, and for the cooling of the fly ash to below its "softening temperature" to prevent the build up of ash deposits on heat exchanger surfaces. While there is a great variety of a burner type, the most widespread are circular burners and vertical nozzle arrays. Circular burners are usually positioned perpendicularly to the combustion chamber walls, while the vertical nozzle arrays are

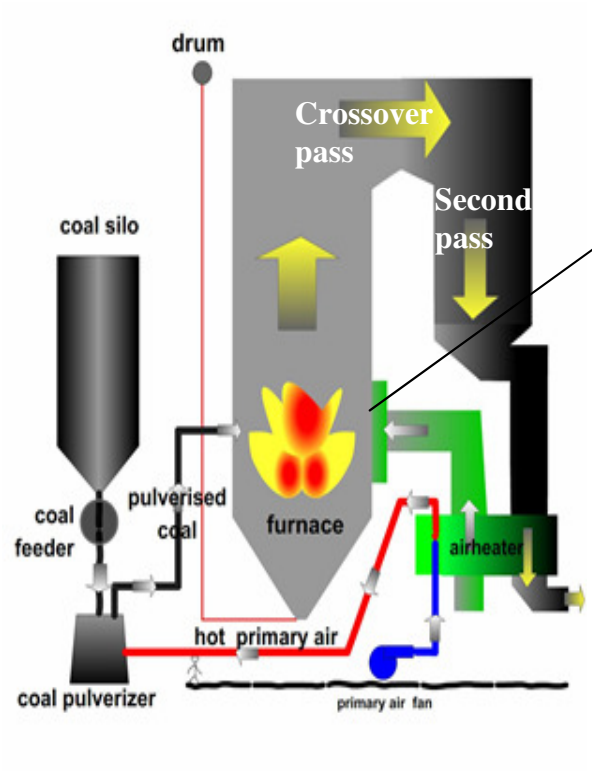

(a) Boiler

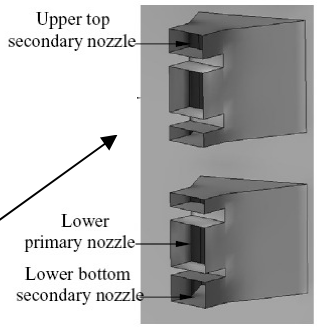

(b) Primary and secondary air burner

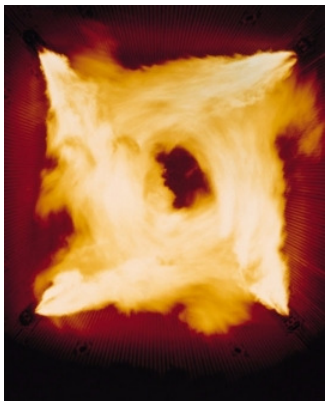

(c) Fire ball (Alstom)

Figure 1.1: Tangentially fired pulverized coal fired boiler

in the corners, firing tangentially to the circumference of an imaginary cylinder in the middle of the combustion chamber. The design of circular burners is more concerned with the tailoring of the individual burner-flame while those of vertical nozzle arrays in tangential1y fired furnaces rely more on the bulk of the furnace volume for the mixing of

the fuel and air streams injected through the nozzle arrays. The majority of the boilers is tangentially fired which use rectangular slotted burners. Pulverized coal, air mixture (primary air) and secondary air is injected from 16–24 burners located in the four corners of the furnace (Figure 1.1-b). These boilers limit the NO_x production by using staged combustion and lowering the excess air requirement. The heat generated due to combustion reaction is radiated and transported to the water walls of boiler to generate steam. This steam is further superheated in super heaters at crossover pass by radiative and convective heat transfer. The last few percentages of the residual carbon in the char burns in an environment of depleted O_2 concentration and reduced temperature before the fly ash leave the combustion chamber and enter the pass of convective heat exchangers. In the majority of cases, most of the fly ash formed in pulverized coal combustion is removed from the flue gas in the form of dry particulate matter, with a small proportion (about 10%) of the coal ash falling off the tube walls as semi molten agglomerated ash which is collected from the bottom hopper of the combustion chamber ("bottom ash"). Pulverized coal fired boiler offers high combustion intensities (0.5-1 MWm^{-3}) and high heat transfer rates (0.1-1 MWm^{-2}) (Williams et al., 2001).

During pulverized coal combustion, the coal particles get heated, moisture and volatile materials are released and char particles are yielded. The general processes that take place during coal combustion are summarized in Figure 1.2. Pyrolysis yields vast array of products like CO, CO_2, tar, H_2, H_2O, HCN, hydrocarbon liquids and gases, etc. These products react with oxygen in the vicinity of char particles depleting oxygen and increasing the temperature. These complex reaction processes are very important to the control of nitrogen oxides, formation of soot, stability of coal flames and ignition of char. The char combustion then occurs simultaneously with the combustion of the volatile species in gas phase. After the completion of char combustion, the inorganic constituents decompose to form ash that has typical composition as SiO_2, Al_2O_3, Fe_2O_3, TiO_2, CaO, MgO, Na_2O, K_2O, SO_3 and P_2O_5, primarily containing first three compounds (composition varies with the rank of coal). The ash material can further decompose to form slag. The nitrogen is released from the coal and forms nitrogen oxide as shown in

Figure 1.2. The sulfur released during coal combustion forms sulfur oxide with some toxic metals.

During devolatilization, gas formation can be related to the thermal decomposition of specific functional groups in the coal and can be predicted with the reasonable accuracy by models employing first order reaction with ultimate yields (Solomon, et al., 1992). The complexity of proposed devolatilization models varies substantially. There are number of approaches that have been used to model the complex devolatilization process and are summarized in Table 1.1.

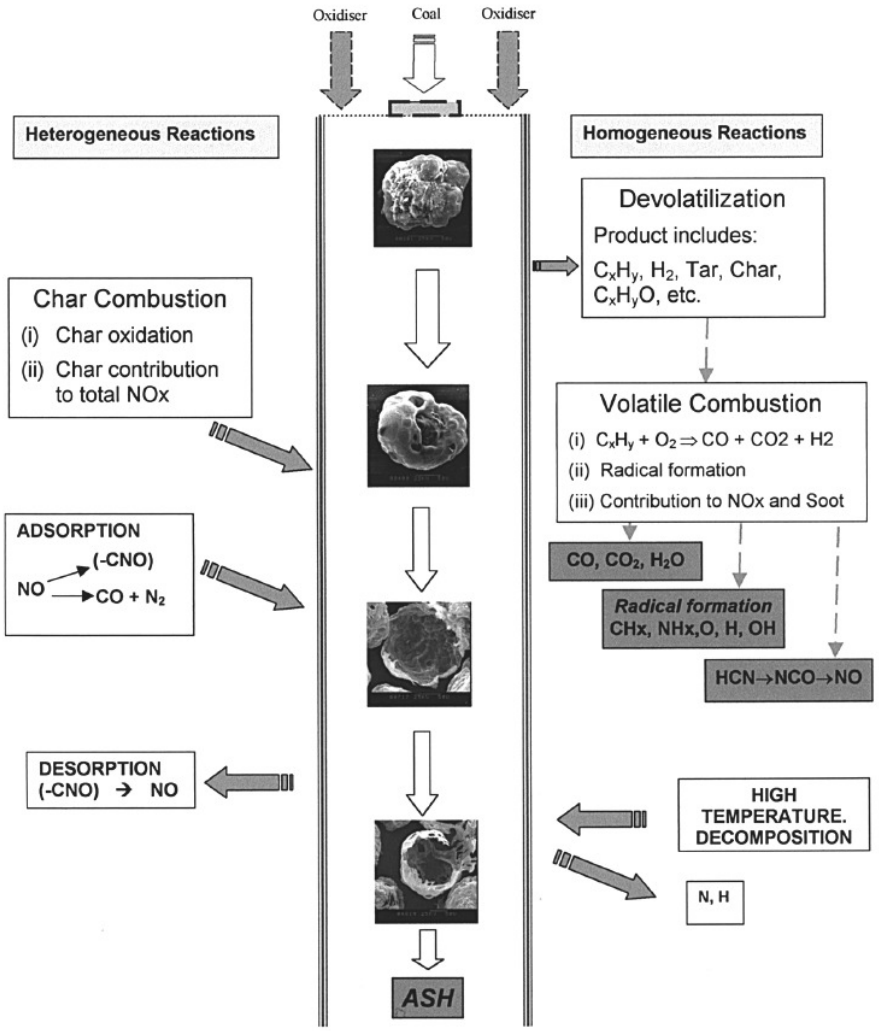

Figure 1.2: Schematic of coal combustion processes (Williams et al., 2000)

On the other hand, tar and char formation processes are more complicated and success in mechanistic modeling of tar formation has been rather limited. In combustion or gasification, tar is often the volatile product of highest initial yield and thus controls ignition and flame stability. It is precursor to soot, which is important to radiative heat transfer. The process of tar formation is linked to the char viscosity and the subsequent physical and chemical structure of the char and so is important to char swelling and reactivity.

Table 1.1: Kinetic expression used for devolatilization (Williams et al., 2000)

Mechanism	Kinetic Expression	Sources of Information
Single step	$\text{Coal} \xrightarrow{k_1} \text{X(volatile)} + (1 - \text{X})\ \text{(Char)}$ $k_1 = A_1 \exp(-E_1/RT)$ $dV/dt = k(v^* - v)$	Howard et al. (1987) devolatilization rate parameters may depend upon the specific coal and the reaction conditio 23]
Two step Coal → 1, 2	$\xrightarrow{k_1}$ Volatile 1 + Residue 1 $\xrightarrow{k_2}$ Volatile 2 + Residue 2 $\frac{dx_{coal}}{dt} = -k_1 x_{coal} - k_2 x_{coal}$ $k_1 = A_1 \exp(-E_1'/RT)$ $k_2 = A_2 \exp(-E_2'/RT)$	$A_1 = 3.7 \times 10^5\ s^{-1}\ E_1/R = 8857$ K $A_2 = 1.46 \times 10^{13}\ s^{-1}\ E_2/R = 30200$ K Generality limitation: as one step Kobayashi et al. (1976)
Distributed kinetics (DAEP) Number of independent parallel, first-order reactions	$\frac{dv_i}{dt} = k_{o,i} \exp\left(\frac{-E_i \pm \sigma_{E,i}}{RT_p}\right)(v_o - v_i)$	Miura (1995); Serio et al. (1987)
Functional Group	Based on Elementary Reaction	Gavalas (1982)
FG-DVC	Network pyrolysis computer code	Solomon and Fletcher (1994)
FLASHCHAIN	Network pyrolysis computer code	Niksa (1996)
CPD	Network pyrolysis computer code	Juntgen and Van Heek (1979); Smith et al. (1993)

The process of char combustion is of central importance in industrial pc fired applications. However, despite extensive investigations over the last half-century, the mechanism of the char/oxygen reaction is not completely understood because of a number of factors such as the reaction due to the pore growth and mass transfer effects (William et al., 2001). It is further complicated by the influence of particle size distribution, char mineral content and fragmentation of the char particle. The rate limiting

step in the combustion of a char particle can be chemical reactions or gaseous diffusion to the particle or a combination of these factors. Generally three zones are defined, namely:

Zone I: Chemical reaction is the controlling step, occurs at low temperatures or with small particles

Zone II: Both chemical and pore diffusion control

Zone III: Occurs at high temperature where bulk mass transfer limitations are controlling or the particles are large

In actual practice the difficulty arises in exactly defining the zone where the combustion occurs: generally, this takes place in inter-zone territory. In zone I, because chemical reaction is rate controlling, the experimentally observed activation energy is the true chemical activation energy and the reaction order is the true chemical reaction order. Since the reaction rate in the pores is slow, any oxygen that reacts is soon replaced from outside the boundary layer. In zone II, as the particle surface temperature increases the reaction between carbon and oxygen becomes so fast that the oxygen concentration in the pores is lower than the bulk gas concentration and zero at the center of the particle. The observed reaction rate is controlled by both chemical reaction rate and the rate of pore diffusion. The experimentally observed activation energy is approximately half the true value, whilst the experimentally observed order 'n' will be related to the true order 'm' thus $n = 0.5(m+1)$. In zone III, at very high temperatures, the reaction at the particle surface becomes so fast that the oxygen concentration diminishes to zero at the particle external surface. The apparent activation energy is consequently small. The transfer rate of oxygen molecules from the surrounding gas to the external surface controls the reaction rate. It has been a common practice to relate experimental char burning rates to the external char surface area, even when pore reaction may occur. The resulting rate of reaction is termed as global since it incorporates the influence of the pore surface area. There are two models or their variants, effectively in use, the Baum and Street model (1971), which is based on apparent activation energy and the more fundamental intrinsic reactivity model as set out by Smith (1971).

Table 1.2: Char burnout models (Williams et al., 2000)

	Data
Baum and Street $\frac{dm_c}{dt} = -\pi D^2 \rho RT \frac{X_{O_2}}{M_{O_2}} (R_{diff}^{-1} + R_c^{-1})^{-1}$ Where m_c is the mass of the coal particle, D is the diameter, ρ is density, R is the universal gas constant, T is the temperature, X is the mol fraction of species, M is the molecular weight of species, R_c is the chemical rate coefficient/unit external surface area, R_{diff} is the diffusional reaction coefficient. In these expressions, the rate of mass loss by combustion depends on particle density, diameter, and the ratio of reacting surface to external surface area of the particle.	E and A vary from coal to coal Baum and Street (1971)
Intrinsic Reaction Rates: Smith $\rho_i = \rho_o / \eta\gamma\sigma_a Ag[C_g(1-X)]^m$ where ρ_i is the intrinsic reactivity, ρ_o is the observed reactivity, η is the effectiveness factor, γ is the characteristic size, σ_a is the apparent density, Ag is the total surface area, C_g is the oxidizer concentration, and m is the true reaction order, X is the fractional burnout.	E = 179.4 kJ/mol 161 ± 6 kJ/m Smith (1982)
Hampartsoumian $R_c = \exp^{(-89)} \sigma^{(-7.5)} Ag^{(-0.5)} C^{(3.5)} T_p^{(9.5)}$ $[1.4 (vit_m + 0.83\ vit_{ps})] - [0.6 (In_R + 1.6\ In_{LR})]$ where vit_m and vit_{ps} are the fraction of matrix and pseudo vitrinite, respectively, In_R and In_{LR} are the fraction of low-reflectance and high-reflectance inertinite, respectively, and C is the carbon content (%).	E = 167.3 kJ/mol Hampartsoumian et al. (1989)
Hurt et al. $R = \eta A_o S\ e^{-E/RT_p} P_o^n C_p$ where A_o is the pre-exponential factor for the surface rate constant, S is the total surface area/mass, P_o is the oxygen partial pressure, n is the apparent reaction order and C is the carbon mass in the particle.	n = 0.5 E = 146.3 kJ/mol Hurt (1998)
Extended Resistance Equation $\frac{1}{R_s} = \frac{1}{k_{DYOX}} + \frac{1}{\in k_{aYOX}} + \frac{1}{\in k_d}$ where R_s is the specific reaction rate at the particle surface, k_D is the oxygen diffusion velocity constant, k_a and k_d are the adsorption and desorption velocity constants, $\in$ is the reaction penetration factor.	Essenhigh and Mescher (1996)

A number of enhancements to the basic model have been proposed, which can predict reduced oxidation rates in the high conversion range. Coal is a heterogeneous material and particle to-particle variations could cause an asymptotic decay in the conversion rate of a sample. Both size dependent (Coda and Tognotti, 2000) and random (Sahu et al., 1988) variations in A_c have been proposed; Hurt and co-workers (Hurt et al., 2003, 1998) developed a statistical model, which addresses heterogeneity in both reactivity and density. Experimental evidence of thermal annealing of the fuel matrix has been found

(Hurt and Gibbins,1995), although this effect is thought to affect mainly the initial stages, where the maximum temperatures are reached, rather than the final steps of the particle's combustion history (Sun and Hurt, 2000). The presence of inorganic material can also reduce oxidation rates through different mechanisms (Zolin et al., 2001), having increasing influence as the ash content of the particles increases with residence time. Extinction and near extinction phenomena can cause an abrupt decrease in the oxidation rate of individual particles (Zolin et al., 2001; Hurt et al., 1998 and Essenhigh et al., 1999), contributing to a reduction in the global conversion rate. However, the lack of data hinders reliable estimation of model parameters and therefore it is often desirable to use lumped models to capture relevant devolatilization and char combustion kinetics. The brief summary of the models to predict the rates of char burnout are summarized in Table 1.2.

The measurement of temperature is essential for the development of combustion theory and technology. A number of methods for measuring flame temperature in a furnace have been developed in the past. In practice, the most widely applied methods use physical probes such as thermocouples or two-color pyrometers. These techniques have some disadvantages, such as single-point measurement and degradation in harsh environments. The various measurement techniques available in literature are summarized in Table 1.3.

Table 1.3: Experimental techniques for temperature measurement inside the furnace

Experimental method	Key aspects	References
Optical method	Can measure temperatures and their distributions. But due to the large dimensions of a furnace and the limited power of lasers, these techniques are unsuitable for boiler furnaces	Ohtake and Okazaki (1988)
Acoustic method	Limited by the propagating velocity of acoustic waves and the inadequacy of the measurements provided by the transducers, so it is hard to achieve high temporal and high spatial resolutions.	Muzio and Eskinazi (1989)
Charge Coupled	A charge-coupled device (CCD) sensor can provide	Huang et al.

Device (CCD)	information on 3×10^6 pixels of a target, so the radiation image captured by a CCD camera is suitable for monitoring the temperature distribution and for analyzing combustion.	(2000); Allen et al. (1993);

Furnace is key part of the boiler where turbulent mixing, reactive two phase flow, exothermic heat generation and radiative heat transfer are dominating. Primary calculations show that the average size of 70 μm coal particle takes nearly less than 1 s to get combusted completely. But industrial data confirms the presence of unburnt carbon in fly ash (~5%) as well as in bottom ash which affects the thermal efficiency of boiler and salability (value) of ash. Turbulent and re-circulating flow affects the mixing of the fuel and oxidants and hence the rate of combustion reaction. The understanding of the behavior of coal fired boilers and translating this understanding into computational models for simulating such boilers is complicated by existence of turbulent, multi-phase re-circulating flows coupled with chemical reactions and radiative heat transfer. The existence of wide range of key spatio-temporal scales (chemical reactions occurring on molecular scales to micron size particles to tens of meters of boiler) often complicate the matter further. The thermo-fluid interaction processes between neighboring burners and between the burners and the furnace as a whole are complex and not well understood (Perry, 1982). So it is of great importance to understand the aerodynamics of near field region not only to ensure that the jets reach the centre of the furnace at the correct location but also to stabilize the flame in the centre. The performance of such a boiler can be influenced by different boiler related parameters like furnace volume, burner type, excess air, distribution of coal/air, burner settings and various coal related parameters such as quality of coal, char maceral content, particle size distribution (Hurt et al., 2003; Walsh, 1997 and Chen et al., 1992). Recent advances in understanding of multiphase flows, turbulence and combustion coupled with advances in computing power and numerical methods provide an opportunity to develop better understanding and better computational models for simulating coal fired boilers.

Table 1.4: Sub models of comprehensive CFD model for boiler

Processes	Model	References
Turbulence	Standard k–ε	Asotani et al. (2008); Belosevic et al. (2006); Pallares et al. (2005); Yin et al. (2002)
	RNG k–ε model	Fan et al. (2001); Launder and Spalding (1972); Chaudhary (1993)
Gas-solid two phase flow	Eulerian–Lagrangian approach particle source in Cell method	Shirolkar et al. (1996)
	Eulerian–Eulerian approach	Li et al. (2003); Zhou et al. (2002); Guo and Chan (2000)
Turbulent dispersion of particle	Discrete random walk (DRW) model	Shirolkar et al. (1996)
Radiative heat transfer	P1 radiation model	Asotani et al. (2008); Vuthaluru et al. (2006); Backreedy et al. (2006)
	Discrete Ordinate (DO)	He et al. (2007); Yin et al. (2002); Zhou et al. (2002)
	Six-flux model	Viskanta (1966); Gosman et al. (1969 & 1973)
	Monte Carlo model	Wall et al. (1982); Howell et al. (1968)
	Discrete transfer model	Xu et al. (2001); Lockwood and Shah (1981)
Absorption Coefficient	Weighted sum of gray gas model (WSGGM)	Raithby and Chui (1990, 1993); Murthy and Mathur (1998)
Devolatilization	Single step kinetic rate	Howard et al. (1987)
	Two step kinetic rate	Kobayashi (1976)
Char oxidation	Kinetic/ diffusion controlled	Baum and Street (1970); Field (1970)
	Intrinsic rate model	Smith (1982)
	Advanced combustion models (Char burnout kinetic model, CBK)	Hurt et al. (1998)
Gas phase combustion	Kinetic or mixing controlled reaction rate	Magnussen and Hjertager (1976)
	Single or two mixture fraction approach	Jones and Whitelaw (1982); Sivanthanu and Faeth (1990)

The development of advanced industrial burners, furnaces and boilers with the improved performance of higher efficiency and lower pollutant emissions is the major goal of combustion researchers, furnace designers and manufacturers. To realize the goal, on one hand, the new technical concepts and novelties for different combustion routes and processes have to be continuously developed. On the other hand, more efficient and economic tools, such as computer simulation by using computational fluid dynamics (CFD) technology, are also extremely important for the design and development of new advanced furnaces. In recent decade, compared with the traditionally experimental methods and physical modeling methods, the computer simulation with numerical methods is considered as a more effective design tool. Over the years, the Computational fluid dynamics (CFD) has evolved as a powerful design and predictive tool to simulate large utility boilers as it can handle multiple complex and simultaneous processes like fluid flow, heat transfer, particle trajectories and chemical reactions (Belosevic et al., 2006; Pallares et al., 2005; Yin et al., 2002; Fan et al., 2001; Smoot et al., 1999 and Boyd & Kent., 1986).

Development and application of comprehensive, multidimensional, computational combustion models are increasing at a significant pace in all over the world. While one confined to specialized research computer codes, these combustion models are becoming more readily accessible as features in commercially available CFD computer codes. A number of commercial CFD codes have been developed and those widely used for modeling coal combustion are Fluent, CFX, CINAR, PCGC, PHOENICS and STAR CD. The sub models involved in development of comprehensive CFD model for simulating boiler are shown in Table 1.4. Simulations made with such computer codes offer great potential for use in analyzing, designing, retrofitting and optimizing the performance of fossil-fuel combustion and conversion systems. However, CFD is expensive in terms of computational time & resource. Few researchers have tried in past to develop phenomenological model to simulated boiler where the key information about sizing of zones, fluid flow are extracted from CFD simulations (Falcitelli et al., 2002 and Diez et al., 2005). This is a very useful approach as information about fluid flow, particle trajectory, zoning methodologies can be formulated. Such models can be developed with

additional features for predicting effect of operating conditions and/or for better accuracy of model prediction.

Pulverized coal boiler contributes more than 53% electricity generation in India producing more than 75,000 MW of electricity (CEA, 2008). It is expected that the total electricity generation will increase from 144,000 MW (2008) to 200,000 MW by 2012 and to be 400,000 MW by 2020 and future contribution of the coal fired boiler is expected to remain same. Indian coal is typically medium volatile with high ash content (sub bituminous type). The sulfur and nitrogen content of the coal is very low (<1%) and heating value is around 12000 to 15000 $MJkg^{-1}$.High ash content causes the problem of ash handling, slagging, ash deposition on heat exchanger surfaces and char unburnt in ash, etc. which are major drawbacks for power generation. Hence to extract the same amount of energy more amount of coal is required to be burnt that will produce more gas pollutant emissions. At the same time the environmental legislation is becoming more stringent for fossil fuel boilers. Hence one of the major objectives of the boiler operators is to reduce the pollutant emissions and enhance the performance of the boiler. The availability, performance and reliability of such boiler depend upon many factors such as burner design, operational protocols, coal quality, age of boiler, furnace hardware configuration, etc. that influences the stability of the combustion process, heat transfer efficiency and wall fouling. This forms the background and motivation behind this research work where it was aimed to use computational fluid dynamics and reaction engineering models to enhance the understanding of coal fired boilers.

1.2 Objectives

The objective of the work was to develop modeling tools, computational fluid dynamics (CFD) and phenomenological model, to simulate various processes occurring in the utility 200 MW_e tangentially fired pulverized coal boiler. The present research work had following specific objectives;

a. Understand devolatilization and char combustion of Indian coal

b. Develop CFD models to simulate pulverized coal combustion in drop tube furnace

c. Develop CFD models to simulate temperature profile, velocity and concentration profile, char burnout and crossover pass characteristics of 200 MW_e boiler

d. Understand effect of operating conditions on performance of 200 MW_e boiler

e. Develop phenomenological/Reactor Engineering Network (REN) model for 200 MW_e boiler, based on the information extracted from offline CFD simulation of the boiler

1.3 Methodology and organization of thesis

The proposed work was to develop comprehensive computational models to simulate the coal fired boiler. Complex gas–solid flow in coal-fired boilers was modeled using different turbulent models approach. Coal devolatilization, reactions and combustion were included in these models. Radiation model was coupled with these flow and reaction models. Since CFD simulations of the whole boiler was extremely computation extensive and time consuming, it was also proposed to develop a phenomenological/REN model of 200 MW_e coal-fired boiler. CFD simulations provided the necessary inputs for the phenomenological model. The overall modeling approach is shown schematically in Figure 1.3. Critical analysis of strength and lacunae of different models was carried out. Geometry modeling based on detailed engineering drawings was carried out. Possible simplification and their implications on final objectives were studied. Various strategies to decompose furnace geometry to make it amenable to grid generation was developed and evaluated.

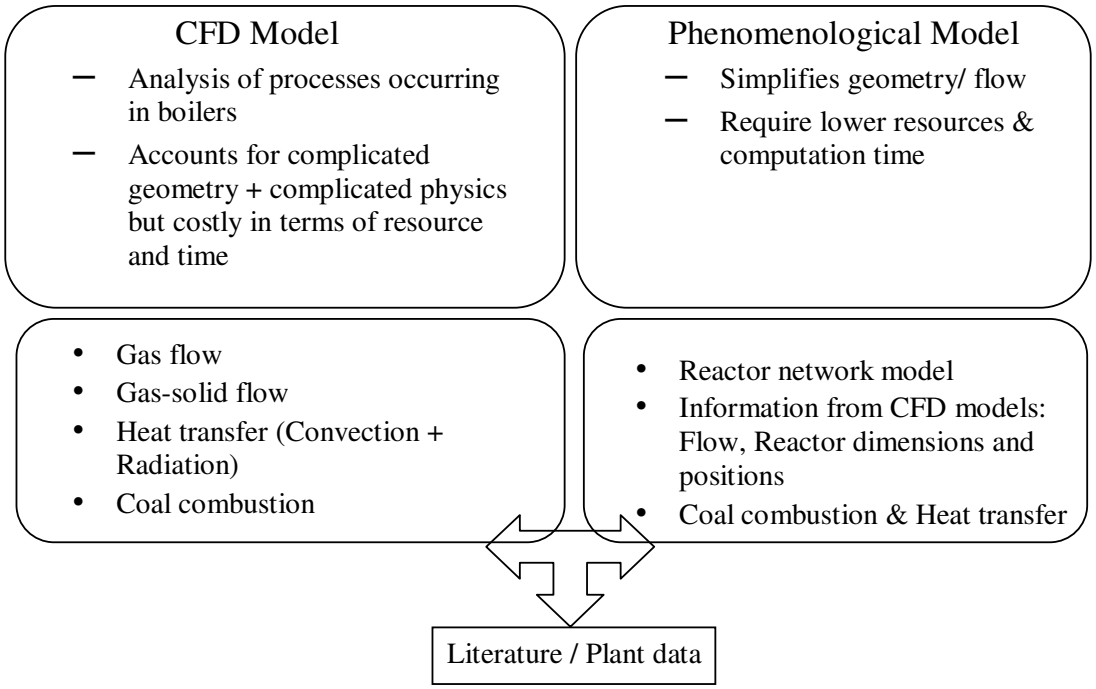

Figure1.3: Multilayered modeling for coal fired boiler

The chapter wise outline of the thesis is provided below:

Chapter 1 introduces the topic and provides background, motivation, objective and scope of the thesis.

Chapter 2 presents kinetic study of pulverized coal combustion. TGA experiments were performed and model was developed to estimate the devolatilization and intrinsic char oxidation kinetic parameters of the Indian coal (medium volatile and high ash content). Computational model for the drop tube furnace (DTF) was developed to estimate the kinetic parameters of char oxidation from the available literature data on char burnout (Ballester et al., 2005). This study emphasized the importance and use of 2D axisymmetric CFD model over conventional 1D model in estimation of kinetic parameters.

Chapter 3 provides systematic approach for the development of detailed CFD model for 200 MW_e tangentially fired pulverized coal boiler. The simulated results were useful to

understand gas flow, particle trajectories, extent of char burnout, gas temperature and species concentration field within a typical boiler. The crossover pass characteristics (uneven distribution of flow and temperature) of tangentially fired boiler were predicted. The predictions of the developed CFD model were compared with the design / literature data.

Chapter 4 demonstrates the utility of the developed model to quantify the sensitivity of operating parameters on the boiler performance. Parameters those can vary during the boiler operation such as excess air, boiler heat load and burner tilt were identified and their impact on the boiler performance was studied. Simulations were performed to understand the performance of boiler when the high ash content Indian coal was blended with low ash and high volatile lignite coal in various ratios. The key conclusions derived from the above studies are listed in the Chapter 4.

Chapter 5 describes development of a phenomenological model based on with the analysis of results obtained with the CFD model. This framework of phenomenological model translates the information gained from detailed CFD model to readily usable engineering scale model for actual plant implementation. The phenomenological model was based on the mixing cell approach, each zone representing key section of boiler. The positioning and size of different zones depend upon the underlying fluid dynamics. The effect of key operating protocols like burner tilt was accounted through appropriate correlations developed from CFD simulations. Model results were compared with the overall CFD results.

Chapter 6 summarizes the work presented in Chapters 2-5 of the thesis. Key conclusions are highlighted in this Chapter. Some suggestions for possible extensions and future work are listed here.

1.4 Key contribution of the thesis

- Developed a methodology and a CFD model to simulate 200 MW_e pulverized coal fired boiler. Implemented this in a commercial CFD solver, FLUENT

- Predicted overall performance of the 200 MW_e tangentially fired pulverized coal boiler fired with high ash content coal. Quantified crossover pass characteristics of the 200 MW_e boiler and effect of burner tilt on the same

- Effect of various operating conditions like excess air, burner tilt and thermal heat load on the performance of the boiler was predicted

- Methodology was proposed to account the effect of burner tilt on shifting of reaction zone in the furnace by developing empirical correlation based on analysis of CFD simulations

- Predicted performance of the blends of Indian coal (high ash, medium volatile and Inertinite rich) + Imported lignite (low ash, high volatile and Vitrinite rich) type coal in 200 MW_e boiler

- Developed phenomenological model and computer code, BOST to simulate performance of 200 MW_e boiler

- Developed methodology to extract information from CFD simulations of the boiler which can be readily useful in development of the phenomenological model

- Novel features and ability to predict effect of burner tilt and crossover pass characteristics of the boiler

The models developed in this work and the presented results will be useful for understanding and improving performance of pulverized coal fired boilers.

Chapter 2

Kinetics of Coal Combustion

2.1 Introduction

Coal is heterogeneous mixture of organic material, moisture and mineral matter in various compositions. Coal is generally characterized by its proximate & ultimate analysis, petrographic composition and heating value. The ultimate analysis of coal shows that it is primarily composed of carbon along with variable quantities of other elements, like sulfur, hydrogen, oxygen and nitrogen. The proximate analysis provides information about the overall composition of volatiles, fixed char, moisture and ash present in coal. The composition of coal varies widely depending upon time history under which the coal has undergone to heat and pressure (the process is termed as coalification). The rank of coal is based on the coalification stage of the coal which can be represented by proximate analysis and heating value of coal. Primarily, coals are grouped in four major types in ascending order of their rank: Lignite, Sub Bituminous, Bituminous and Anthracite. The typical grading based on the composition and heating value of coal is shown in Table 2.1.

Table 2.1: Coal composition with increasing coalification (Diessel, 1992)

Rank stages	% carbon (d.a.f.)	% volatile matter (d. a. f.)	Gross CV ($MJkg^{-1}$)	% in situ moisture	% vitrinite reflectance R_{max}
Wood	50	>65	11.7		
Peat	60	>60	14.7	75	0.20
Brown coal	71	52	23.0	30	0.42
Sub bituminous	80	40	33.5	5	0.63
High volatile bituminous	86	31	35.6	3	1.03
Medium volatile bituminous	90	22	36.0	<1	1.58
Low volatile bituminous	91	14	36.4	1	1.97
Semi-anthracite	92	8	36.0	1	2.83
Anthracite	95	2	35.2	2	7.00
d.a.f. = Dry ash free basis CV= Calorific value					

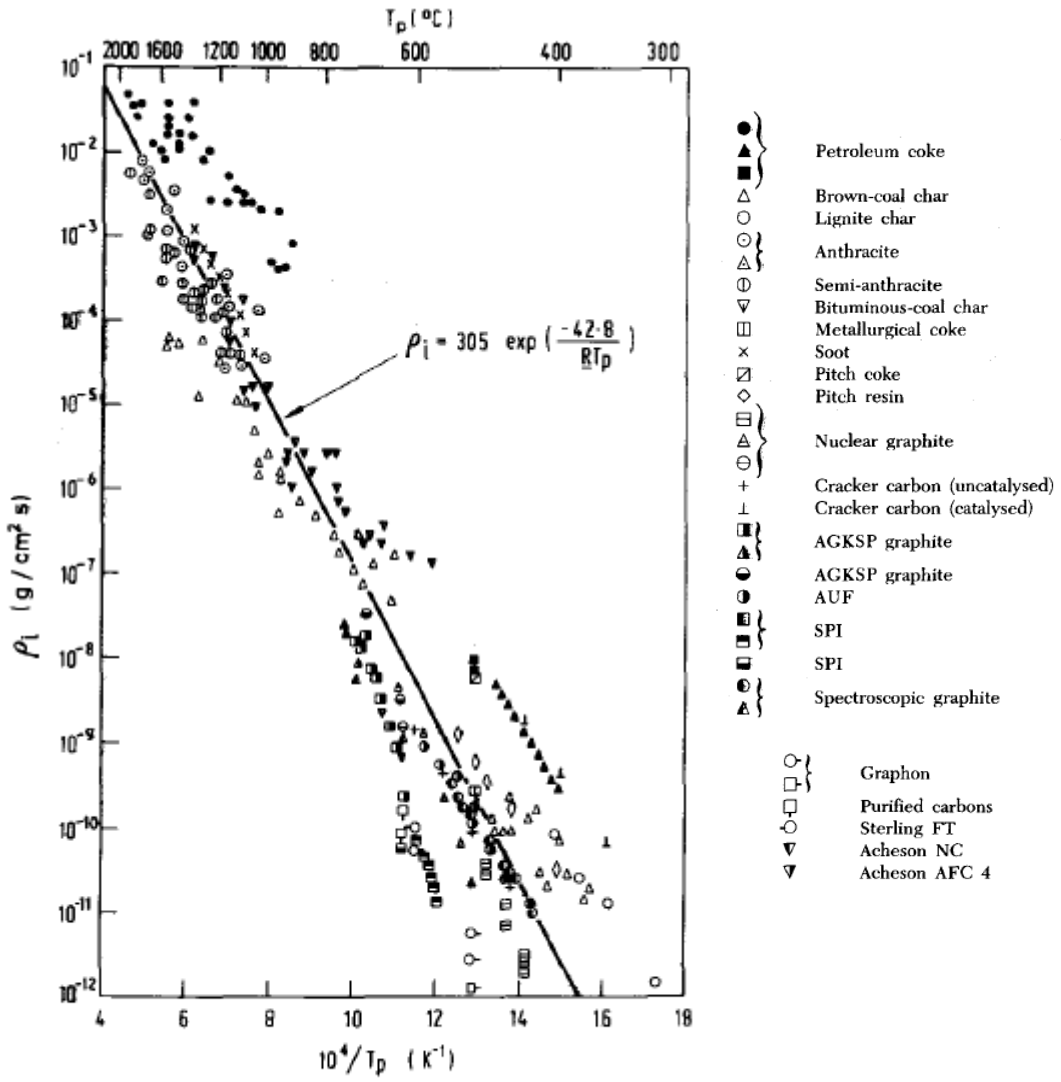

Figure 2.1: Intrinsic reactivity of various carbons when P_{O2} = 1 atm (Smith, 1982).

The organic matter present in the coal itself is heterogeneous in nature and consists of different macerals (microscopic components) as a result of which the coal of the same ultimate analysis may not necessarily have the same properties and coals of different composition may show similar behavior. The macerals differ from coal to coal w. r. t. both quality and quantity and hence during combustion of coal particles, different maceral constituents behave differently including the swelling, the yield of volatiles, char structures, the reactivity and ash chemistry. Hence the coals can be better classified according to the nature of the microscopic petrographic analysis. This classification is important for pulverized coal combustion and gasification. The organic material is

divided into three groups: Vitrinite (woody materials), Exitnite (spores, resins and cuticles) and Inertinite (oxidized plant material). For most of the coals the vitrinite group is the most abundant constituent. The microscopic studies show that coal may be made up of a single maceral or more usually association of macerals. Due to the optical properties of vitrinite, the vitrinite reflectance is used for the indicator of rank. Table 2.1 explains the classification of the coal based on the vitrinite reflectance which shows that the lignite (brown coal) has the lowest vitrinite reflectance (R_{max} = 0.41%) and the Anthracite has highest vitrinite reflectance (R_{max} = 7%) showing the highest rank. The coal micro lithotypes and ash/mineral content affects the devolatilization and char combustion rate. It is difficult to predict the devolatilization and char oxidation rates from their proximate and ultimate analysis as coals having similar properties can show different combustion behaviors. Hence knowledge about devolatilization rate and char reactivity is important to understand coal combustion. The intrinsic reactivity of char for various types of coal is shown in Figure 2.1, adopted from Smith (1982), which shows large variation in reactivity even though the effect of pore size and surface area are neglected. The wide range of reactivities presumably reflects the effects of the atomic structure of the carbons, as well as the effects of impurities in the solid reactants. There are several well-defined experimental methods to study devolatilization and char oxidation. The brief summary of such methods is shown in Table 2.2. The excellent literature review on experimental methods to study the coal pyrolysis/ devolatilization can be obtained from Solomon et al. (1992). Such experimental methods have helped in deriving useful information about the rates of devolatilization and reactivity of char oxidation which are majorly inputs to the combustion sub model while simulating combustion systems. The data obtained from such experiments are generally fitted to Arrhenius kinetic form to estimate the kinetic parameters: pre exponential factor (A) and Activation energy (E).

In this work, first TGA experiments were performed to understand the devolatilization and char oxidation reactivity of the high ash, low volatile sub bituminous type Indian coal. The model was developed to simulate TGA experimental data and kinetic parameters for devolatilization and char reactivity were estimated.

Table 2.2: Brief summary of experimental techniques for coal characterization

Experimental Technique: Thermo Gravimetric Analysis (TGA)		
References	Operating condtions	Key features
Cloke et al. (2002)	Non isothermal TGA	Intrinsic reactivity of 14 coal samples.
Alonso et al. (2001)	Non isothermal, HR = 25 $Kmin^{-1}$ Sample mass 13 mg; Air 50 ml /min (for oxidation, 1273 K); N_2 50 ml /min (for oxidation, 1173 K)	Effect of vitrinite and inertinite content on coal combustion
Morgan et al. (1986)	Standardization of sample mass (~5 mg), heating rate (20 $Kmin^{-1}$) and particle size (< 75 μm).	Predicted effect of rank on char reactivity
Cumming (1984)	Non isothermal, HR = 15 $Kmin^{-1}$ Sample mass 20 mg Air 75 $mlmin^{-1}$	Proposed reactivity assessment via a weighted mean activation energy. Tested 22 coal samples of all rank.

Experimental Technique: Drop Tube Furnace (DTF) / Entrain flow reactor (EFR) / Laminar flow reactor (LFR)/Wire mesh reactor (WMR)		
References	Operating condtions	Key features
Nandi and Vleeskens (1986)	Φ= 25 mm, L =1260 mm T = 1573-1773 K τp = 1.2 s	Studied effect of ash, vitrinite and inertinite on char burnout in DTF
Hurt et al. (1998)	T = 1423 K τp = 500 ms	Char conversion studies were performed. Model prediction of CBK and global rate were compared.
Cloke et al. (2003)	T = 1573 K Tp = 600 ms 5% O_2	Effect of inclusion of char morphological data in CBK model
Card and Jones (1995)	Φ= 25 mm, L =2500 mm T = 1573 K τp = 2.5 s	Developed light scattering technique to study coal combustion and fly ash formation in DTF
Zhang et al. (2005)	Φ= 200 mm, L =2500 mm T = 1523 K	Introduced AUSM turbulence chemistry model of char combustion to predict influence of particle temperature fluctuation on char combustion rate. In house CFD code was used to simulate DTF.
Yoshizava et al. (2006)	Φ= 42 mm, L =800 mm T = 400-1523 K HR = 10^2-10^3 Ks^{-1}	Swelling characteristic of 11 types of coal was analyzed.
Sujanti et al. (1999); Hindmarsh et al. (1995)		Wire mesh reactor (WMR)
Φ and L are internal diameter and length of DTF tube respectively		

Secondly, literature data on pulverized combustion of Anthracite coal in the drop tube furnace data was adopted and CFD model was developed to simulate pulverized coal combustion in DTF. Results of widely used 1D model were compared with 2D axisymmetric CFD model. Key aspects in estimation of kinetics from DTF experiments were highlighted. The next section deals with TGA analysis of coal.

2.2 Thermo gravimetric analysis of coal

Thermo gravimetric analysis (TGA) has been commonly employed for estimation of devolatilization rates and char reactivity measurements. These are all based on continuous weight loss measurements for a coal sample in inert medium (e. g. N_2) for devolatilization and in presence of air/dilute oxygen (~6 mol%) held in a temperature-controlled furnace. Typically, only small amount, 2–20 mg of sample is required and comparatively it is simple to operate. In general, TGA studies fall into two categories: a) isothermal, where the sample is maintained at a constant temperature, and b) non-isothermal, where the sample is heated at a constant rate (temperature ramp e.g. 20 $Kmin^{-1}$). For isothermal methods, measurements characterizing only the first 50% of weight loss are generally considered for char reactivity measurements and that may not be representative of the whole sample, particularly not of the less reactive components which are likely to be of most interest for predicting char burnout behavior. Continuing measurements beyond 50% conversion would allow these limitations to be overcome, but the reduction in rate of reaction means that run times are then significantly increased. At 773 K, a temperature often used for isothermal reactivity tests, and in air, a typical residual unburnt char from a utility boiler takes 3 hours to reach 50% conversion and more than 10 hours to reach 99% conversion. Hence the isothermal method is time consuming and also requires multiple runs. In contrary, non isothermal methods has the advantage of being able to achieve complete conversion in shorter experimental time. The reactivity can be assessed from the weight loss obtained as the char is heated at a constant rate usually with heating rate of 15 $Kmin^{-1}$ from 673 to 1173 K. Virtually all chars of interest for pulverized fuel combustion are converted by 1173 K i.e., within approximately 1 hour. Hence temperature-ramped non-isothermal method was adopted to

characterize the coal. Thermogravimetric (TG) and differential TG (DTG) curves are generally analyzed to estimate the characteristics temperatures like peak temperature at maximum weight loss rate, temperature at which 50% burn off occurs; burnout temperature where DTG profile reaches a 1% combustion rate at tail end of the profile, maximum dw/dt (% min^{-1}) and kinetics of combustion. The methodology and results are discussed in following section.

2.2.1 Experimental work

The coal of interest in the thesis work is the sub bituminous coal which is commonly used in thermal power plants in India that has medium volatiles (20-25%) and high ash content (> 35%). The inertinite content is > 50% (by volume) and vitrinite content is around 10-15% (by volume). Such pulverized coal sample (as on fired basis) was collected from power plant. The proximate and ultimate analysis is shown in Table 2.3.

Table 2.3: Composition of coal for TGA analysis

Proximate Analysis	Wt. %	Ultimate analysis	Wt. %
Moisture	12	C	37.03
Ash	41	H	2.26
Volatiles	23	N	0.85
Fixed carbon	24	S	0.33
		O	6.53
HHV (MJ kg^{-1})		14.63	

The thermo gravimetric analysis were carried out with Q 5000 IR (of TA Instrument, USA) TGA analyzer. The schematic of the same is shown in Figure 2.2.

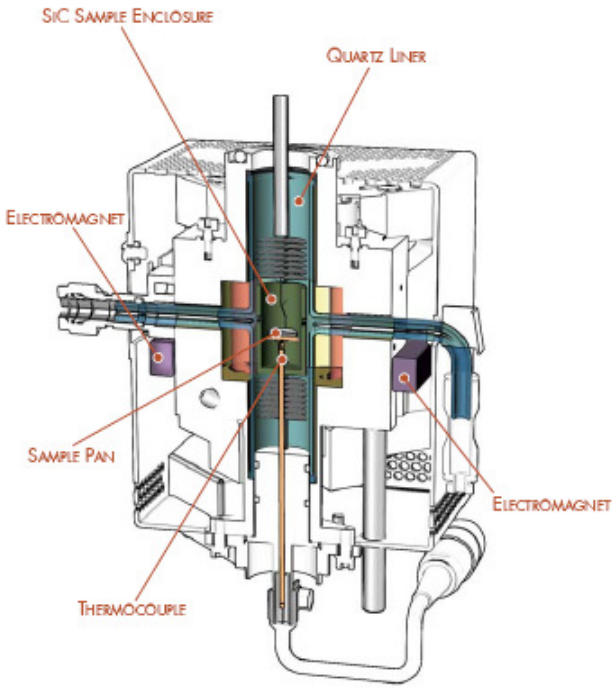

Figure 2.2: Sectional view of the TA 5000R TGA instrument (TA instruments)

The coal sample (~4.8-5 mg) was placed in platinum crucibles of 100 µL capacity suspended from the balance unit on hang-down hook. The air cooled furnace with maximum temperature of 1473 K, is heated with 4 Infrared (IR) bulbs. The sensitivity of the sample is less than 0.1 µg and having weighing accuracy of +/-0.1%. The linear heating rate can be achieved in the range of 0.1-500 $Kmin^{-1}$. The mass loss, time and temperature were recorded simultaneously to produce combustion profile. Raw data without any averaging or smoothing is saved to disk as a text file. Data analysis was achieved using thermal analyzer software (Thermal Analyst 5000, TA Instruments). Previous studies suggests that parameters like heating rate 10-50 $Kmin^{-1}$, mass of sample (<20 mg), flow rate of inert/air to the sample, etc. does not affect the overall trends of the results (Russell et al., 1998). Morgan et al. (1986) has suggested that to avoid ignition of the sample, the sample mass of 5 mg with 20 $Kmin^{-1}$ heating should be adopted and same was adopted in this study. Temperature-ramped non-isothermal method as discussed in Russell et al. (1998) was adopted to characterize the coal. The method for devolatilization and char oxidation are described below,

A ~4.5-5 mg coal sample was taken. N_2 gas was passed through the furnace section over the sample. The N_2 flow rate was kept 20 $mlmin^{-1}$ for the sample and 40 $mlmin^{-1}$ for the balance. Sample was heated with ramp of 20 $Kmin^{-1}$ from temperature 303 K to 383 K. Then it was kept at 383 K for 10 minutes so that the moisture present in the coal gets evaporated. Then the sample was heated to 1173 K with ramp of 20 $Kmin^{-1}$ so that the volatile material gets released from the coal and the chars and ash were left at the end. The weight loss was recorded with each 1 K rise in temperature. For char oxidation the furnace was quickly cooled to 673 K in presence of N_2 and then the air flow was purged over the sample with flow rate of 100 $mlmin^{-1}$ and 20 $mlmin^{-1}$ N_2 for the balance. Then the sample was heated to 1173 K with ramp of 20 $Kmin^{-1}$ so that the char gets oxidized. The weight loss was recorded with each 1 K rise in temperature.

2.2.2 Model equations and boundary conditions

- *Assumptions*
  a) The devolatilization is considered to be a first-order reaction based on the residual volatile content of the particle
  b) Char oxidation reaction is based on the external surface area of the coal particle and the oxygen partial pressure at the surface which was taken to be same as that of the bulk air
  c) The shrinking core assumption was taken where the size of the particle remains constant and density of the particle changes.
  d) Mono sized particles of mean particle size 70 µm was assumed
  e) Gas phase reactions were not modeled
  f) The change in particle temperature was proportional to heating rate

- *Devolatilization*

The single step kinetic rate model for devolatilization can be written as;

$$\frac{dM_t}{dt} = A_v e^{\left(-E_v / RT_p\right)} \left(M_t - M_f\right) \qquad 2.1$$

M_t is the mass of volatile at any time; M_f is the final mass of sample after the devolatilization is over, A_v is the pre exponential factor, E_v is the activation energy for devolatilization and T_p is the particle temperature.

It was assumed that the particle temperature is same as the gas temperature and is proportional to heating rate (HR). Hence the change in particle temperature can be written as,

$$\frac{dT_p}{dt} = HR, \qquad \therefore dt = \frac{dT_p}{HR} \tag{2.2}$$

Where, HR is the ramp heating rate (Ks^{-1}), T_p is particle temperature in K

Hence, we can write equation 2.1. for rate of devolatilization with change in particle temperature as,

$$\frac{dM_t}{dT_p} = \left(\frac{A_v}{HR}\right) e^{\left(-E_v/RT_p\right)} \left(M_t - M_f\right) \tag{2.3}$$

- *Char oxidation*

Similarly for the char oxidation, the rate of char oxidation with change in particle temperature can be written as,

$$\frac{dM_t}{dT_p} = \left(\frac{A_c}{HR}\right) e^{\left(-E_c/RT_p\right)} P_{O_2}^n A_p \tag{2.4}$$

$P_{O_2}^n$ is the O_2 partial pressure and n is order of the reaction (n=1). A_p is the particle surface area, A_c & E_c are pre exponential factor and activation energy for char oxidation respectively.

2.2.3 Results and discussion

- *Devolatilization*

Figure 2.3 shows two curves, (i) TG curve plotted as change in the normalized weight of volatile (%) w. r. t. temperature and superimposed with (ii) DTG curve (% sec^{-1}). The weight loss shows that the devolatilization starts around 600 K which was commonly observed for other type of coals. The rate of weight loss curve is also called as DTG (Differential thermo gravimetric) curve that also confirms the same. The DTG peak temperature (PT) which represents temperature at the maximum rate of weight loss of 0.1812 % sec^{-1} was reported as 719.4 K. The temperature at which the 50% weight loss occurs was recorded as 767.25 K. TGA model was simulated and fitted to experimental data so as to obtain kinetic parameters for devolatilization. The model could not capture the weight loss profile for devolatilization with single set of A_v and E_v and after several attempts; hence it was fitted into three temperature ranges. First the model was fitted in the temperature range of 600-830 K where the devolatilization starts and shows nearly > 60% weight loss. Then the model was fitted in second range of 830-940 K that accounts for ~20% weight loss and the third range was 940-1100 K where remaining 20% weight loss takes place. These zones are marked in Figure 2.4 and the comparison between the simulated and experimental results are also shown. The activation energy based on first range was not able to capture weight loss in second and third range and hence new set of the parameters were estimated for second and third range. For the Second and third range, activation energy was kept same and the pre exponential factor was changed so as to fit the experimental data. The kinetic parameter estimated for these three ranges are shown in Table 2.4.

Table 2.4: Devolatilization kinetic parameters

Temperature range (K)	Pre exponential factor, A_v (s^{-1})	Activation energy, E_v ($kJmol^{-1}$)
600-830	3282	82.42
830-940	32.44	62.48
940-1100	4.48	62.48

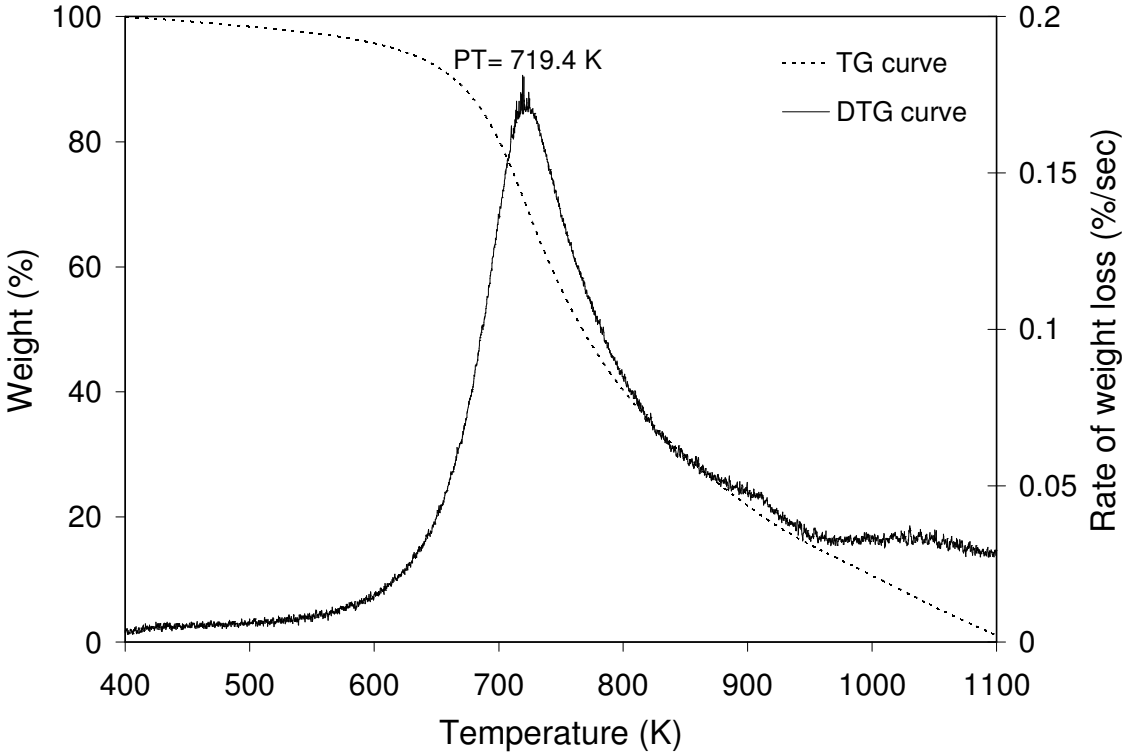

Figure 2.3: Plot of DTG curve (%sec^{-1}) super imposed over TG (%) for devolatilization

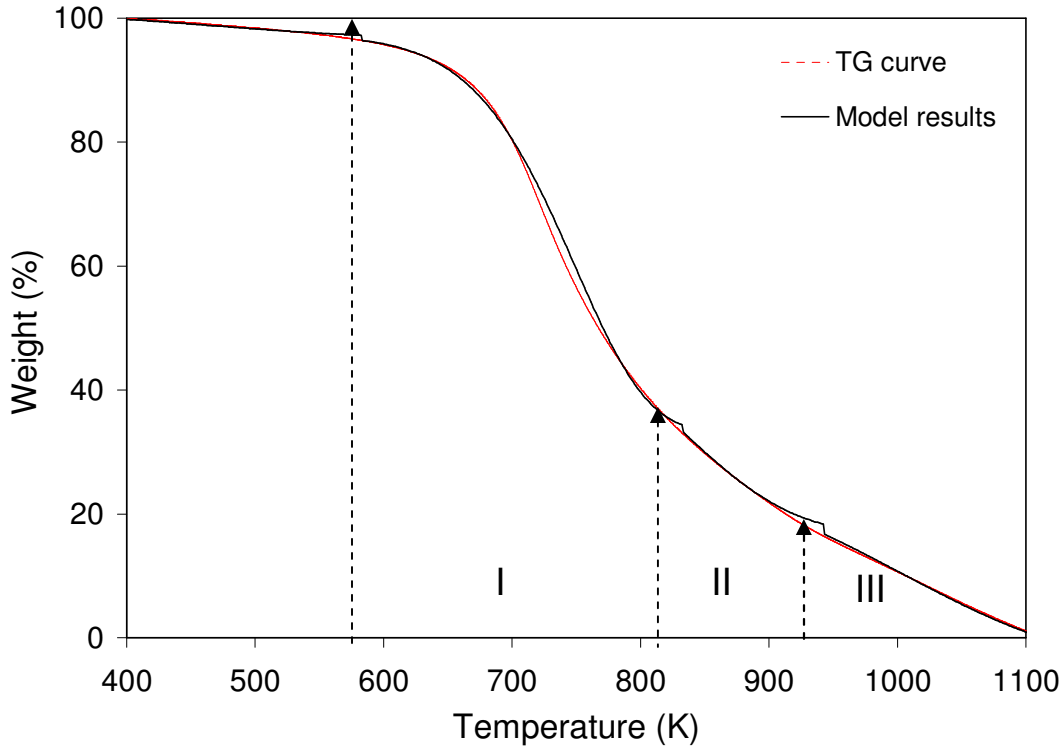

Figure 2.4: TGA model prediction for coal devolatilization

- *Char oxidation*

Figure 2.5 shows two curves, (i) TG curve plotted as change in the normalized weight of char (%) w. r. t. temperature and superimposed (ii) DTG curve (% sec^{-1}). The char was heated from 700 K to 1173 K and it was found that after 980 K there was negligible change in the weight loss and hence Figure 2.5 shows the data till 980 K which can be considered to be burnout temperature (BT) of char. The analysis of DTG curve for char oxidation shows two peaks temperatures PT1 and PT2 as shown in Figure 2.5. This two peak structure is common where the heterogeneity in the microlithotype of coal exist which is already discussed above. The PT1 shows burnout of the more reactive char which is primarily representing vitrinite content followed by less reactive Inertinite (PT2) peak. The curve also shows that the coal may have major component as Inertinite due to which a long tail of the curve is observed in DTG curve. The PT1 was observed at 769.1 K at maximum rate weight loss of 0.4394 % sec^{-1} and PT2 at 872.6 K at 0.1064 % sec^{-1}. TGA model was simulated and fitted to experimental data so as to obtain kinetic parameters for char oxidation (Figure 2.6). The model could not capture the weight loss profile for char oxidation with single set of A_c and E_c and minimum four ranges were required in which the whole weight loss curve was fitted (Figure 2.6). The first temperature range was from 700-773 K which is very fast step in which almost 40% of char gets reacted. The second temperature range was 773-805 K where around 20% change in weight takes place and was found to be slower than range I. Range III has temperature range of 800-913 K in which more than 30% of the char gets oxidized and remaining 10% char is oxidized in step IV of temperature range 913-1000 K. The model parameters in each range are listed in Table 2.5.

Table 2.5: Char oxidation kinetic parameters

Temperature Range (K)	Pre exponential factor, A_c ($kgm^{-2}Pa^{-1}s^{-1}$)	Activation energy, E_c ($kJmol^{-1}$)
700-773	8.96E+08	198.16
773-805	1.52E-04	14.09
805-913	4.41E-05	14.09
913-1000	5.33E-03	65.34

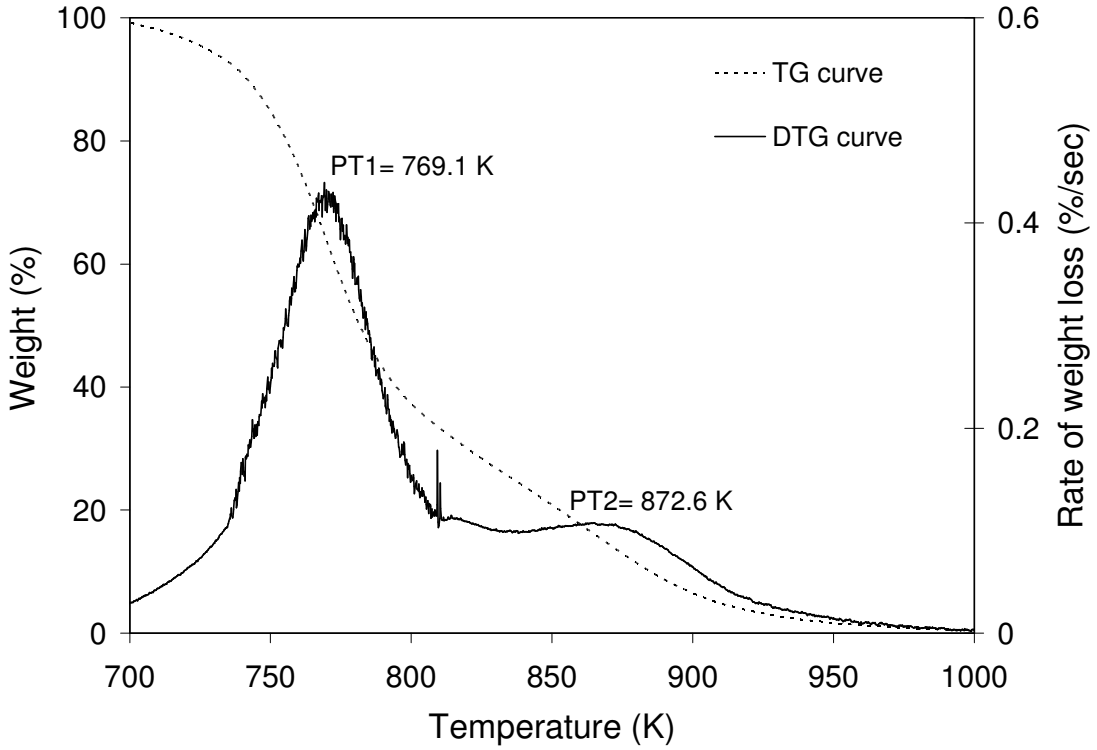

Figure 2.5: Plot of DTG curve (%sec^{-1}) super imposed over TG (%) of char oxidation

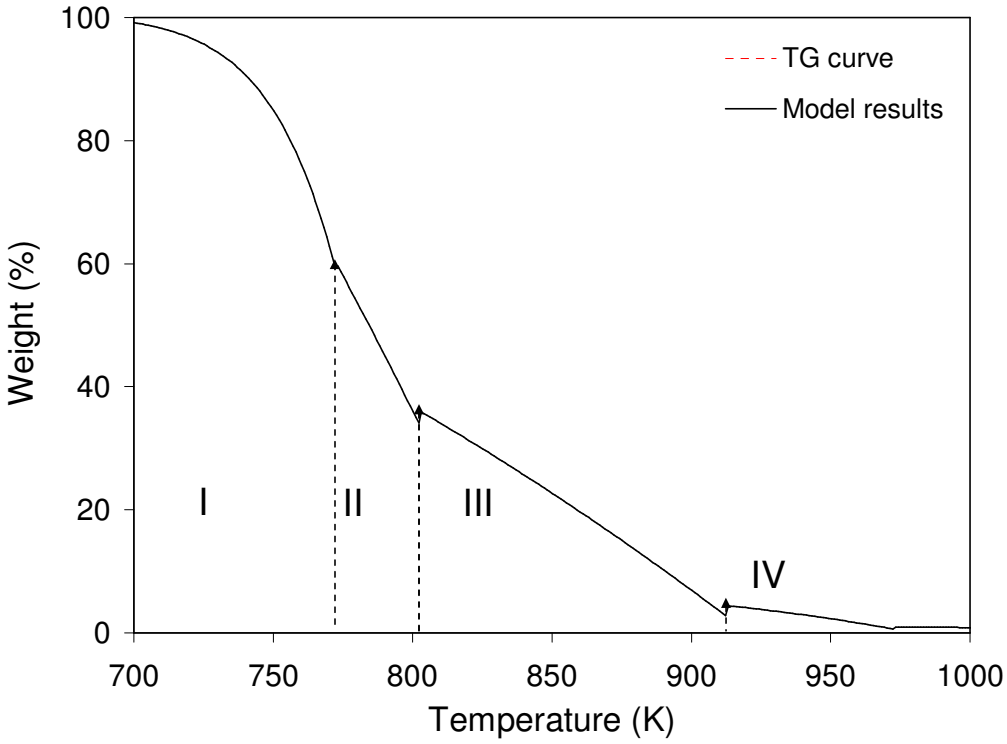

Figure 2.6: TGA model prediction for char combustion

The kinetic parameters for first range are quite different than other three ranges of temperature which shows very fast reactivity of coal. Once the reactive char gets oxidized, the rate of reaction slows down and same can be observed for II to IV step.

2.2.4 Conclusions

The use of non isothermal TGA experiments and mathematical model for derivation of kinetic parameters for devolatilization and char oxidation rates of sub bituminous type Indian coal have been described. Weight loss data was obtained from non-isothermal, ramp heating of coal sample and the mathematical model was developed to obtained kinetic parameters for the devolatilization and char oxidation. The key conclusions are listed below,

- DTG peak temperature for devolatilization was found to be as 719.6 K

- Three temperature ranges were required to fit the TGA model to experimental data in order estimate the devolatilization kinetic parameters

- The shape of Arrhenius plot for char oxidation shows two peaks which suggests heterogeneity of maceral present in the coal and long tail shows dominance of presence of Inertinite content in coal. The peak temperature were obtain as PT1= 769.1 K and PT2 = 872.6 K

- Four temperature ranges were required to fit the TGA model to experimental data in order estimate the char oxidation kinetic parameters

2.3 CFD modeling of pulverized coal combustion in DTF

The quality of coal can be estimated based on the proximate and ultimate analysis. But the chemical analysis does not necessarily represent the combustion behavior of coal, as it also requires the knowledge of devolatilization and char oxidation rates which are particularly important during coal switching in full scale boiler (Ballester et al., 2005). The devolatilization and char oxidation rates of different types of coal are generally obtained from laboratory experiments and TGA methods has been already discussed in section 2.2. TGA are useful to conveniently and quickly assess the devolatilization rates and intrinsic char reactivity at relatively low temperature (< 1300 K). TGA avoid the spurious effects due to diffusion limitations and also gives enough time for accurate measurements to take place (Russell et al., 1998). The heterogeneity of maceral content of char which shows two peaks in DTG plot can be easily assessed in TGA. Comparatively, DTF has short residence time (< 5 s), high heating rates (10^4-10^5 Ks^{-1}) and varying O_2 concentration which represent similar conditions to those as in practical systems like utility boilers. The char reactivity obtained from the TGA experiments is generally intrinsic reactivity of the char and the kinetic parameters obtained from DTF experiments, lumps the effect of internal ash layer diffusion with intrinsic reactivity and hence representing global/apparent kinetic rate parameter. These are particularly useful where the coal related information like porosity, pore diameter, effectiveness factor, surface area of char, are not readily available for particular type of coal. And hence DTF poses a better choice as it is more realistic to practical situation, has simpler geometric configuration and operational flexibility (residence time, operating temperature and O_2 concentration) to assess the combustion characteristic of coal.

The devolatilization and oxidation rates are usually represented by Arrhenius-type rate expression. The associated kinetic parameters (pre exponential factor and activation energy) are obtained by different methods like Arrhenius plot method or development of plug flow model which is fitted to coal burnout data obtained along the length of the DTF (Ballester et al., 2005; Smith, 1973 and Field, 1969). These estimated kinetic parameters are used as input parameters for combustion sub model in simulating large scale boiler

that can be based on lumped model approach (Boyd and Kent, 1986) or more recent computational fluid dynamic (CFD) models (Díez et al., 2004; Fan et al., 2001 and Yin et al., 2002). The Arrhenius plot method has several intrinsic drawbacks like the oxidation rate constant (K_c) is based on single representative particle size and the values of kinetic parameters obtained are specific to the set of experimental measurement obtained (Ballester et al., 2005). The plug flow models are generally simple, can account for particle size distribution and the complete combustion history of the coal particles along the length of DTF. But plug flow model doesn't account for the radial variations in velocity, temperature, O_2 concentration, particle trajectory and effects of inlet configuration. These may have influence on the predictions of the burnout behavior, as the particles at the same axial distance can experience different oxygen and temperature history at various radial locations. Also, the particle residence time depends upon the particle trajectory that it follows after injection. In order to account these effects it was required to develop multidimensional CFD model for DTF which can handle multiple complex and simultaneous processes like fluid flow, heat transfer, particle trajectories and chemical reactions.

Hence, this work attempts to numerically investigate the various key parameters that affect the coal burnout characteristics in DTF. The CFD model is developed based on the experimental data available in Ballester et al. (2005). The proximate and ultimate analysis of Anthracite coal is listed in Table 2.6.

Table 2.6: Coal composition (Ballester et al., 2005)

Proximate analysis	Wt. %	Ultimate analysis	Wt. %
Moisture	1.46	C	70.3
Ash	19.17	H	3.03
Volatiles	10.28	N	1.63
Fixed carbon	69.09	S	2.28
		O (by difference)	2.13
HHV ($MJkg^{-1}$)		27.59	

The sensitivity study on various model parameters was performed and their role in prediction of the burnout characteristic is discussed. The comparison between 1D and multidimensional model (2D axisymmetric) for the estimation of char kinetic parameters from drop tube furnace data has been discussed. The details of model equations are discussed below.

2.3.1 Model equations

The drop tube furnace has internal tube diameter 78 mm, total tube length of 1600 mm. There are two inlets; the first one is Fuel Air (FA) for the injection of transportation/pneumatic air with the coal particles at the center of the drop tube and second is for the coaxial entry for preheated gas stream (Figure 2.7-a). The detailed description of drop tube furnace and experimental procedure can be found in Ballester et al. (2005).

The underlying assumptions made in the development of the model are

- Instantaneous drying of coal particle was assumed and hence dry coal particles were injected from FA. The moisture present in the coal was added into the fuel air
- The oxygen first reacts with carbon to form CO, which diffuses into gas phase and subsequently gets oxidized to CO_2
- During the combustion of coal particles, the diameter of particle remains constant and the density of the particle changes

2D axisymmetric computational domain was used for drop tube furnace as the flow does not show any significant variation in azimuthal direction (Sheng et al., 2004). The schematic of 2D axisymmetric model is shown in Figure 2.7-a. As the discrete phase (coal) was present in low volume fraction (< 1%) the Eulerian/Lagrangian approach was employed to model two phase gas-solid flow. The gas flow in DTF was laminar (N_{Re} < 500). For steady state, 2D axisymmetric, continuity equations for continuous phase can be written as

$$\frac{1}{r}\frac{\partial}{\partial r}(\rho r U)+\frac{\partial}{\partial z}(\rho W) \quad = S_m \qquad 2.5$$

ρ is density of fluid, U and W are the fluid velocity in radial r and axial direction z. The S_m is the source term for the total mass added from the discrete phase.

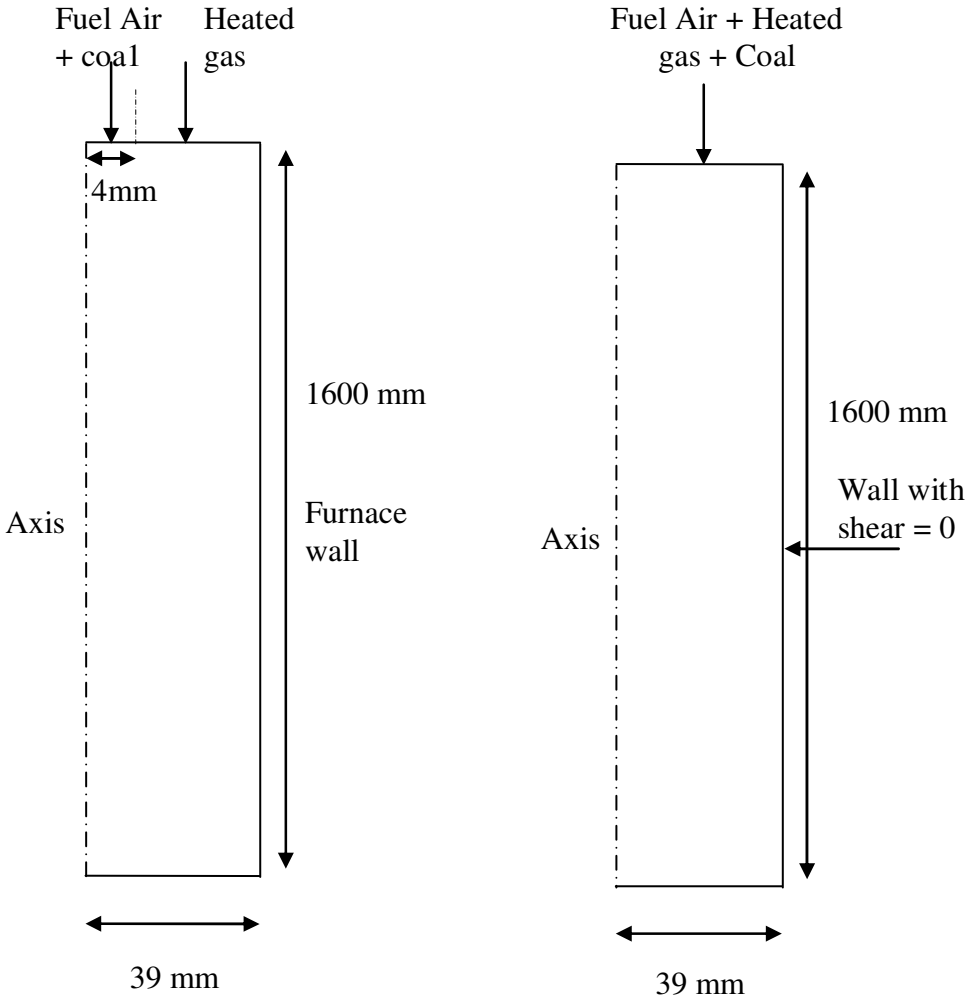

(a) 2D axisymmetric (b) 1D axisymmetric

Figure 2.7: Schematic of drop tube furnace

The species conservation equation can be written as

$$\frac{1}{r}\frac{\partial}{\partial r}(\rho r U m_k) + \frac{\partial}{\partial z}(\rho W m_k) = \frac{1}{r}\frac{\partial}{\partial r}\left(\rho D_{km} r \frac{\partial m_k}{\partial r}\right) + \frac{\partial}{\partial z}\left(\rho D_{km} \frac{\partial m_k}{\partial z}\right) + R_k + S_k \quad 2.6$$

m_k is mass fraction of species k, D_{km} is the diffusion coefficient for species k in the mixture, R_k is the net rate of production of species k by gas phase chemical reactions, S_k is the source of species k from dispersed phase. The net source of chemical species k due to reaction is computed as the sum of the Arrhenius reaction sources over the N_r reactions that the species participate in,

$$R_k = M_{w,k} \sum_{r=1}^{Nr} R_{k,r} \quad 2.7$$

$$R_{k,r} = \left(v'_{k,r} - v_{k,r}\right) K_r \prod_l \left[C_{l,r}\right]^{n_l,r} \quad 2.8$$

$C_{l,r}$ is the molar concentration of each reactant l^{th} species in reaction r, $\eta'_{l,r}$ exponent for each l^{th} reactant in reaction r, $v'_{k,r}$ and $v_{k,r}$ are stoichiometric coefficient for k^{th} species as product and reactant respectively, K is the kinetic rate constant

The source term S_k from the dispersed phase is written as

$$S_k = \frac{\Delta\left(\dot{m}_{pk}\right)}{V} \quad 2.9$$

$$S_m = \sum_k S_k \quad 2.10$$

Where $\dot{m}_{pk}$ is the particle mass flow rate of component k corresponding to the number of particles that crosses the cell, Δ is the change in the property across that cell and V is the cell volume.

The momentum equation for continuous phase in radial r and axial z direction can be written as

Radial momentum, r

$$\frac{1}{r}\frac{\partial}{\partial r}(\rho r U U)+\frac{\partial}{\partial z}(\rho W U) = \frac{1}{r}\frac{\partial}{\partial r}\left(\mu r\frac{\partial U}{\partial r}\right)+\frac{\partial}{\partial z}\left(\mu\frac{\partial U}{\partial z}\right)+F_z+S_U \qquad 2.11$$

Axial momentum, z

$$\frac{1}{r}\frac{\partial}{\partial r}(\rho r U W)+\frac{\partial}{\partial z}(\rho W W) = \frac{1}{r}\frac{\partial}{\partial r}\left(\mu r\frac{\partial W}{\partial r}\right)+\frac{\partial}{\partial z}\left(\mu\frac{\partial W}{\partial z}\right)+F_r+S_W \qquad 2.12$$

Source term for r momentum $S_U=-\frac{\partial p}{\partial r}+\frac{1}{r}\frac{\partial}{\partial r}\left(\mu r\frac{\partial U}{\partial r}\right)+\frac{\partial}{\partial z}\left(\mu\frac{\partial W}{\partial r}\right)-\frac{2\mu U}{r^2}$

Source term for z momentum $S_W=-\frac{\partial p}{\partial z}+\frac{1}{r}\frac{\partial}{\partial r}\left(\mu r\frac{\partial U}{\partial z}\right)+\frac{\partial}{\partial z}\left(\mu\frac{\partial W}{\partial z}\right)$

The momentum source term F, for a particular cell is calculated from every particle trajectory j crossing that cell

$$F_i=\frac{\Delta\left(\dot{m}_{pk}\,u_{p,i}\right)}{V} \qquad 2.13$$

Where $u_{p,i}$ is the velocity components of the particle in i^{th} direction (r or z)

Energy balalnce for gas phase can be written as

$$\frac{1}{r}\frac{\partial}{\partial r}(\rho r U h)+\frac{\partial}{\partial z}(\rho W h) = \frac{1}{r}\frac{\partial}{\partial r}\left(k r\frac{\partial T}{\partial r}\right)+\frac{\partial}{\partial z}\left(k\frac{\partial T}{\partial z}\right)+S_h \qquad 2.14$$

Where, k is the thermal conductivity of gas, h is an enthalpy. The volumetric source term, S_h is sum of heat of gas phase chemical reactions ($S_{h,rxn}$), heat added from discrete phase (S_Q) and radiation (S_R).

$$S_h = S_{h,rxn} + S_Q + S_R \tag{2.15}$$

$$h = \sum_k m_k h_k \quad \because h_k = \int_{Tref}^{T} C_{pk}\, dT \tag{2.16}$$

The heat released due to chemical reactions is

$$S_{h,rxn} = -\sum_k \frac{\left(h_k^0 + \int_{Tref}^{T} \Delta C_{pk}\, dT \right) R_k}{M_k} \tag{2.17}$$

Where, R_k the volumetric rate of creation of species k, h_k^0 is the formation enthalpy of species k at the reference temperature T_{ref}

The heat added from the discrete phase is due to char oxidation,

$$S_Q = \sum_j \frac{\left[(1 - f_{heat}) \Delta (\dot{m}_c) H_c \right]_j}{V} \tag{2.18}$$

The f_{heat} is the fraction of heat absorbed by the particle, H_c is heat released during char oxidation.

The radiative heat transfer in DTF was model by using discrete ordinate (DO) model. DO is considered to be more suitable for systems having optical thickness (= characteristic dimension of DTF * absorption coefficient) less than 1 (Fluent, 2007; Sheng, 2004). As the optical thickness was found to be less than 0.06 (0.078 [m] * 0.77 [m^{-1}]) for the DTF considered here, DO model was used to model the radiative heat transfer. DO model

solves the transport equation of radiation intensity, I in the direction $\vec{s}$ and can be written as

$$\nabla \cdot (I\,\vec{s}) + \left(a + a_p + \sigma_p\right) I(\vec{r},\vec{s}) = an^2 \frac{\sigma T^4}{\pi} + E_p + \frac{\sigma_p}{4\pi} \int_{\Omega=0}^{4\pi} I(\vec{r},\vec{s}^{\,'})\,\phi\left(\vec{s},\vec{s}^{\,'}\right) d\Omega^{'} \qquad 2.19$$

Where, I is radiant intensity, $\vec{r}$ is position vector, $\phi\left(\vec{s},\vec{s}^{\,'}\right)$ is scattering phase function, σ is Stefan Boltzmann constant, a is absorption coefficient of gas phase. Here, isotropic scattering (i.e., scattering that is equally likely in all directions) was assumed and for isotropic scattering $\phi\left(\vec{s},\vec{s}^{\,'}\right)$ =1. a_p is the equivalent absorption coefficient due to the presence of particulates, and is defined as

$$a_p = \lim_{V\to 0} \sum_{n=1}^{N} \varepsilon_{pn} \frac{A_{pn}}{V} \qquad 2.20$$

The equivalent emission E_p is defined as,

$$E_p = \lim_{V\to 0} \sum_{n=1}^{N} \varepsilon_{pn} A_{pn} \frac{\sigma T_{pn}^{\,4}}{\pi V} \qquad 2.21$$

The equivalent particle scattering factor σ_p, is given as

$$\sigma_p = \lim_{V\to 0} \sum_{n=1}^{N} \left(1 - f_{pn}\right)\left(1 - \varepsilon_{pn}\right) \frac{A_{pn}}{V} \qquad 2.22$$

and it is computed during particle tracking. The f_{pn} is the particle scattering factor associated with the n^{th} particle.

The discrete phase was modeled by using Lagrangian approach. The discrete phase momentum balance on single particle of size j, an be written as

$$\frac{\mathrm{d}u_{\mathrm{p,i,j}}}{dt} = \sum \mathrm{F_{i,j}} \qquad 2.23$$

Right hand side of equation (2.23) is the sum of the forces acting on the particle in i^{th} direction. If we consider only gravity and drag force acting on particle of size j, then we have

$$\sum F_{i,j} = \frac{(\rho_p - \rho_g)}{\rho_p} g + \frac{18\mu}{d_{p,j}^{\ 2}\rho_p}\frac{C_D \mathrm{Re}_p}{24}(u_{p,j,i} - v_i) \qquad 2.24$$

Where, ρ_P, d_p and $u_{p,i,j}$ are the density, diameter and velocity components of the particle of size j in i^{th} direction (r or z), μ is the viscosity of gas phase, g is gravitational constant and C_D is drag coefficient, v_i is the velocity component of gas phase (U or W). The particle Reynolds number was < 0.6. As Morsi and Alexander (1972) correlation cover this range, it was used to calculate C_D.

The trajectory of particles of size j in radial and axial direction can be calculated as

$$\frac{dx_{i,j}}{dt} = u_{p,i,j} \qquad 2.25$$

Species conservation equations for single particle can be written as:

$$\frac{d\left(M_{p0} m_k\right)}{dt} = S_{pk} \qquad 2.26$$

The M_{p0} is the initial mass of coal particle, m_k is the mass fraction of species k.

S_{pk} can be formulated by considering various particle level phenomena of interest such as devolatilization and surface reaction-char combustion. Hence the S_{pk} can be written as

$$S_{pk} = M_{p0}\left[\frac{dm_v}{dt} + \frac{dm_c}{dt}\right] \qquad 2.27$$

Where, the m_v and m_c is mass fraction of volatile and char respectively

It has been recognized that the single step models can successfully predict the devolatilization of coal provided that the coal specific kinetic parameters are known (Jones et al., 1999; Brewster et al., 1995). Hence the devolatilization was modeled using simple single step Arrhenius type kinetic rate model. The coal devolatilization rate for any particle can be written as (Badzioch and Hawksley, 1970)

$$Mp_0 \frac{dm_v}{dt} = -A_v\, e^{(-Ev/RT_P)} \left(Mp_v - Mp_f \right) \qquad 2.28$$

Where Mp_f indicates mass of coal particle after devolatilization and Mp_v is the mass of coal particle at any time, A_v is the pre exponential factor, E_v is the activation energy for devolatilization, T_p is the temperature of the particle.

Char combustion rate was calculated by using kinetic/diffusion model available in Fluent (Baum and Street, 1971; Field, 1969). It was assumed that the char gets oxidized to CO by following reaction.

$$C_{(s)} \quad + \quad 0.5\, O_{2\,(g)} \quad \rightarrow \quad CO_{\,(g)}$$

This model is simple in implementation and needs apparent kinetic rate constant which accounts for both chemical and internal pore diffusion resistance.

The rate of char oxidation for any particle can be written as, (Baum and Street, 1971; Field, 1969)

$$M_{p0} \frac{dm_c}{dt} = -A_p \frac{K_c K_d}{K_c + K_d} Y_{O_2} \frac{\rho_g R T_g}{MW_{O_2}} \qquad 2.29$$

The kinetic rate constant K_c for char oxidation reaction can be written as

$$K_c = A_C\, e^{(-E_C / RT_P)} \qquad 2.30$$

A_c is pre exponential factors and, E_c is the activation energy for char combustion.

The bulk gas phase diffusion coefficient K_d for oxidant (Field, 1969) can be given as,

$$K_d = \frac{5\times10^{-12}}{d_p}\left(\frac{T_g + T_p}{2}\right)^{0.75} \qquad 2.31$$

U is unburnt fraction of coal,

$$U = \frac{\sum_j N_{p,j} w_j \left(m_v + m_c + m_w + m_A\right)}{\sum_j N_{p,j} w_j \left(m_{v0} + m_{c0} + m_{w0} + m_{A0}\right)} \qquad 2.32$$

Where, w_j is the initial mass of particle of size j, m is the mass fraction at any time, $N_{p,j}$ is number of particles of size j, m is the mass fraction, subscript 0 indicates initial value at time t= 0.

$$N_{p,j} = \frac{w_j}{\left(\frac{\rho_p^0 \pi \left(d_{p,j}^0\right)^3}{6}\right)} \qquad 2.33$$

The sources of inter-phase transport are

$$\Delta\left(\dot{m}_{pk}\right) = \sum_j N_{p,j}\, w_j \frac{d\left(m_k\right)}{dt} \qquad 2.34$$

and

$$\Delta\left(\dot{m}_p\right) = \sum_k \Delta\left(\dot{m}_{pk}\right) \qquad 2.35$$

The volatile material was represented by single species as $C_{0.1}H_3O_{0.132}$ which is estimated from proximate and ultimate analysis of coal. Following two gas phase reactions were assumed.

$$CO_{(g)} + 0.5\ O_{2(g)} \rightarrow CO_{2(g)}$$

$$C_{0.1}H_3O_{0.132} + 0.784\ O_{2\,(g)} \rightarrow 0.1\ CO_{2(g)} + 1.5\ H_20_{(g)}$$

The rate of gas phase reactions of $C_{0.1}H_3O_{0.132}$ and CO resulting from the char combustion was determined by Arrhenius type rate expression.

$$K_r = A_r\ e^{(-E_r / RT)} \qquad 2.36$$

Energy balance for the single particle

$$M_p Cp_P \frac{dT_P}{dt} = \left(f_{heat} M_{p,0} \frac{dm_c}{dt} H_c \right) + Q_{rad} + Q_{conv} \qquad 2.37$$

Here, M_p is mass of particle at any time, C_{pp}, Qrad and Q_{conv} are the particle specific heat, radiative and convective heat transfer respectively.

The particle radiative heat transfer can be written as

$$Q_{rad} = \varepsilon_P \sigma A_p (T_R^{\ 4} - T_P^{\ 4}) \qquad 2.38$$

And the convective heat transfer can be written as

$$Q_{conv} = hA_P (T_g - T_P) \qquad 2.39$$

Where, ε_P is the emissivity of particle, σ Stefan-Boltzmann constant ($=5.67\times10^{-8}\,W/m^2K^4$), T_R is the radiation temperature $=\left(\frac{I}{4\sigma}\right)^{1/4}$ and h is heat transfer coefficient.

2.3.2 Boundary conditions

Char oxidation kinetic parameters for shrinking core assumption are listed in Table 2.7. The devolatilization kinetic parameter of Kobayashi et al. (1977) of BH11 coal type was used in the model is listed in Table 2.7.

Table 2.7: Kinetic parameters for 1D model

Devolatilization		Char oxidation			
Kobayashi et al. (1977)		Ballester et al. (2005)		Ballester et al. (2005)	
BH-11 type		Poly dispersed		Mono dispersed	
A_v	E_v	A_c	E_c	A_c	E_c
(s^{-1})	($Jkmol^{-1}$)	($kg/m^2s.Pa$)	($Jkmol^{-1}$)	($kgm^{-2}s^{-1}a^{-1}$)	($Jkmol^{-1}$)
1.58×10^{8}	1.29×10^{8}	0.88×10^{-3}	9.43×10^{7}	0.4×10^{-3}	$8.3\times10^{+7}$

Table 2.8: Devolatilization kinetic parameters for sensitivity study

(Kobayashi et al., 1977); VK-4 type		(Ballester et al., 2005)	
A_v	E_v	A_v	E_v
(s^{-1})	(J/kmol)	(s^{-1})	(J/kmol)
1.26×10^{7}	1.48×10^{8}	6×10^{5}	1.44×10^{8}

Table 2.9: Model parameters

Parameter	Value	References
Particle emissivity (ε_p)	0.9	Backreedy et al. (2006)
Particle scattering factor (f_p)	0.6	Backreedy et al. (2006)
Swelling factor (S_w)	1	
Heat fraction (f_{heat})	1	Boyd et al. (1986)
Particle density (ρ_p), kg/m^3	1700	Ballester et al. (2005)
Particle heat capacity (Cp_p), J/kg K	1700	
Emissivity of wall (silicon carbide wall)	0.96	Modest (2003)

- *1D model*

Single inlet was defined for Fuel Air, Heated Gas and was specified as mass flow rate (Figure 2.7-b) and the outlet was specified as outlet vent. Ballester et al. (2005) had assumed particle inlet temperature = 298 K and the gas inlet temperature to be same as reactor operating temperature. Same boundary conditions were used in 1D model. The gas and particle inlet conditions are specified in Table 2.10. The wall material was specified as silicon carbide and free slip condition was assigned to wall. The reflect condition was specified for the particles at the wall and escape condition was specified at the outlet. The operating temperature was specified to the wall with emissivity = 0.96 (Modest, 2003). The gas velocity was calculated based on the operating conditions and the same was patched in the computational domain.

Table 2.10: Operating conditions for 1D model

Wall operating temperature (K)	1313	1723
Mass flow rate (kgs^{-1})	3.585×10^{-4}	3.615×10^{-4}
Coal flow rate (kgs^{-1}, db)	8.211×10^{-6}	8.211×10^{-6}
Inlet Coal particle temperature (K) Inlet stream temperature (K)	1313	1723
Mass fraction of inlet stream		
O_2	0.085	0.092
CO_2	0.098	0.097
H_2O	0.08	0.08
O_2 at the outlet of DTF (mole %, db)	4	4

- *2D axisymmetric model*

Two separate inlets were specified for Fuel Air and Heated Gas. The pneumatic air and particles were injected from Fuel Air inlet and the coaxial entry of hot gas was introduced from Heated Gas inlet (Figure 2.7-a). The gas flow inlet was defined by mass flow rate, the outlet was specified as outlet vent. The gas and particle boundary conditions are specified in Table 2.11. The operating temperature was specified to the wall with emissivity = 0.96 (Modest, 2003). No slip condition was specified to the wall. For

discrete phase, the coal particles were injected from the Fuel air inlet by specifying it as group injection. The reflect condition was specified for the particles at the wall and escape condition was specified at the outlet. All other model parameters are listed Table 2.9. The simulations were performed at various operating temperatures (1313 K, 1448 K, 1573 K and 1723 K) and O_2 concentration (at the inlet of DTF = 4 mole %, db and = 8 mole %, db). The inlet temperature of Fuel Air and particles was modified than that was assumed in plug flow model. The higher temperature of pneumatic air at the smaller FA injection leads to high jet velocity (e.g. ~5.3 ms^{-1} for 1723 K). Instead of the same, particles were injected at reactor temperature and pneumatic air was injected at room temperature. The hot gas temperature was assumed to be same as reactor temperature.

Table 2.11: Operating conditions for 2D axisymmetric model

Burner inlet	Fuel Air	Heated Gas				
Wall temperature (K)		1313	1448	1573	1723	1573
Mass flow rate (kgs^{-1})	5.412×10^{-5}	3.044×10^{-4}	3.044×10^{-4}	3.059×10^{-4}	3.074×10^{-4}	3.141×10^{-4}
Coal flow rate (kgs^{-1}, db)		8.211×10^{-6}				
Inlet stream temperature (K)	298	1313	1448	1573	1723	1573
Coal Inlet stream temperature (K)		1313	1448	1573	1723	1573
Mass fraction of inlet stream						
O_2	0.232	0.0586	0.0586	0.063	0.068	0.112
CO_2	--	0.1149	0.1149	0.114	0.114	0.111
H_2O	0.002	0.094	0.094	0.094	0.093	0.091
O_2 at the outlet of DTF (mole %, db)		4	4	4	4	8

2.3.3 Numerical simulation

Commercial CFD solver, FLUENT (of Ansys Inc., USA) was used to solve the mass, energy and momentum governing equations. The Particle size distribution (PSD) data

was obtained from Ballester et al. (2005) which is shown in Figure 2.8. The Rosin-Rammler equation was fitted to the PSD of the coal particles and the model parameters mean particle diameter = 68 μm, spread parameter = 2.557 were obtained.

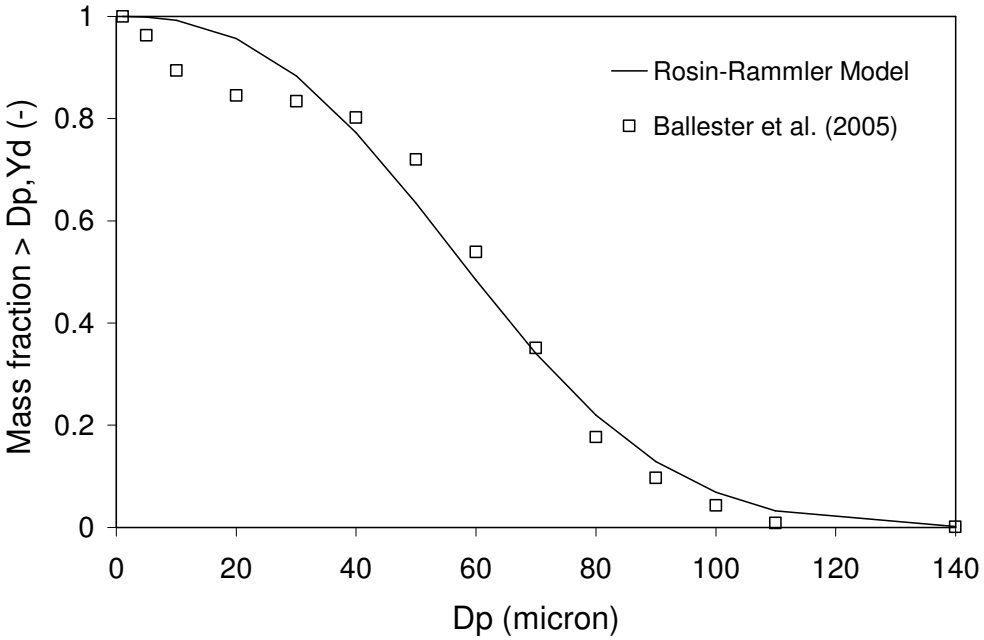

Figure 2.8: Rosin-Rammler fit to PSD data (Ballester et al. 2005)

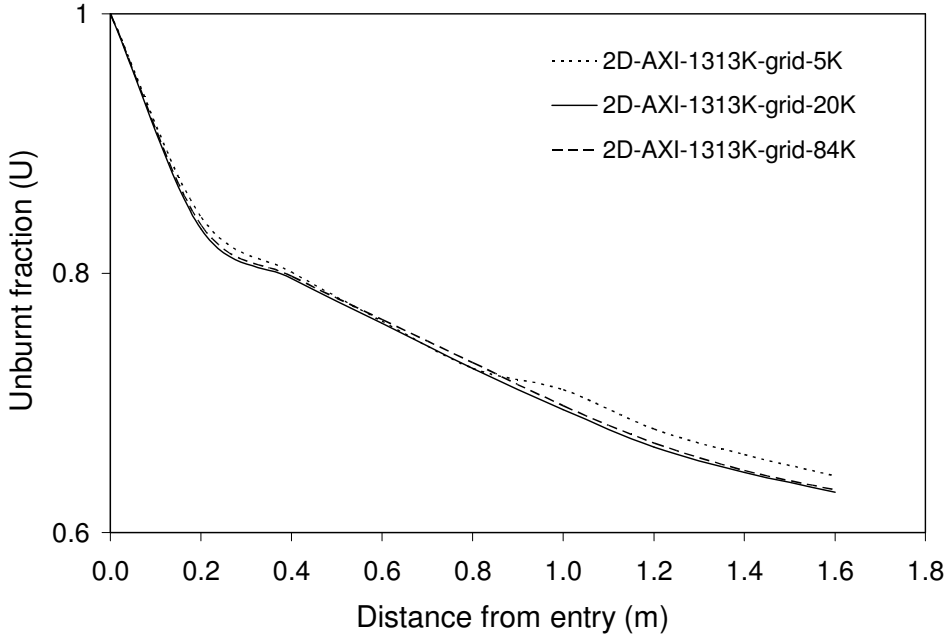

Figure 2.9: Effect of grid size on burnout profile of coal

The influence of number of computational cells was studied by performing simulations on uniform grid of size 5340 (20 x 267) to 83148 (78 x 1066). Figure 2.9 shows the effect of computational cells on prediction of coal burnout. Based on these results, the use of 20787 (39 x 533) cells seems to be adequate to capture the burnout profile. Hence 20787 cells were used in all the subsequent simulations.

Preliminary numerical experiments were carried out to evaluate different discretization schemes and based on this, second order accurate discretization scheme was used for all the subsequent simulations. Velocity and pressure coupling was handled by SIMPLE algorithm. For the 1D model, the velocity estimated based on the operating conditions was patch and simulations were performed without solving flow and where as for the 2D axisymmetric model, the flow was solved. The residuals of velocity components, species, energy, radiation were monitored. Various criteria like, insignificant change (<1%) in velocity, species, temperature profiles and combustion profile at various location of the DTF were used to decide appropriate level of convergence.

2.3.4 Results and discussion

Numerical investigation of combustion characteristic of pulverized coal in a drop tube furnace (DTF) has been performed. Two types of CFD models (1D and 2D axisymmetric) were developed and coal combustion data for DTF experiments available in literature was simulated. Simulations results obtained are discussed below.

- *1D model*

1D model of DTF was simulated to predict the coal burnout. The optimized kinetic parameters reported by Ballester et al. (2005) were used in this simulation (Table 2.7). First, the model was simulated using the poly dispersed particles and corresponding char oxidation kinetic parameters were $A_c = 0.88 \times 10^{-3}$ $kgm^{-2}s^{-1}Pa^{-1}$ and $E_c = 9.43 \times 10^{+7}$ $Jkmol^{-1}$. Simulation results of poly dispersed particle size for two operating temperatures 1313 K and 1723 K are shown in Figure 2.10. It was observed that the 1D CFD model qualitatively captures the burnout behavior of coal with kinetic parameters suggested by

Ballester et al. (2005). Also, the model predictions were checked at same operating conditions for mono dispersed particles of mean diameter (D_{43}) = 52.2 µm. The char oxidation parameters were A_c = 0.4 $\times 10^{-3}$ $kgm^{-2}s^{-1}Pa^{-1}$ and E_c = 8.3 $\times 10^{+7}$ $Jkmol^{-1}$. Simulation results for mono dispersed particles (Figure 2.10) shows that the burnout behavior is over predicted. Hence, this leads to similar conclusion of Ballester et al. (2005) that the char oxidation kinetic parameters should be estimated by considering the poly dispersed particle size. Based on this, 2D axisymmetric model was simulated only for polydispersed particle size.

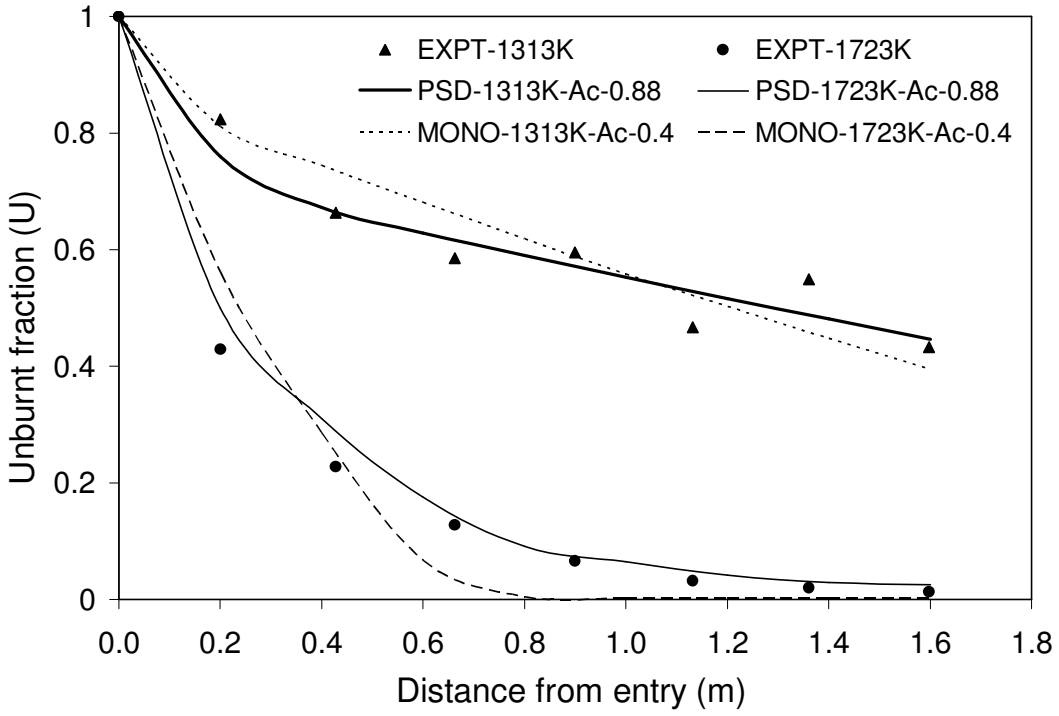

Figure 2.10: 1D model prediction for operating temperature 1313 K and 1723 K

- *2D axisymmetric model*

The coal combustion takes place by moisture evaporation, devolatilization, gas phase combustion of volatile species and char oxidation. Devolatilization plays important role in coal burnout and hence to understand its influence on burnout prediction, devolatilization rate was predicted by using kinetic parameters of two similar type of coals (Table 2.8) available in literature. Simulation results (Figure 2.11) shows that even though the amount of volatile present in coal was small enough (10.3 wt %), the model

predictions were sensitive to devolatilization kinetic parameters. The kinetic parameters reported by Ballester et al. (2005) shows convex nature till 0.6 m distance and does not show the trend observed in experiments. Model prediction for the kinetic parameters reported by Kobayashi et al. (1977) predicts the trends observed in experimental results. Hence for further simulation, the kinetic parameters for devolatilization i.e. BH11 of Kobayashi et al. (1977) were used.

Based on all above discussions, the 2D axisymmetric model was simulated. The kinetic parameters were similar to those used in 1D studies. Result shows (Figure 2.12) that the 2D axisymmetric model under predict the combustion profile with the char oxidation parameters that were based on 1D studies. Simulation results in Figure 2.12 are shown for two temperatures 1313 K and 1573 K and similar observation was found for all other operating conditions. Hence, the sensitivity studies were performed where initially the pre exponential factor (A_c) of the char oxidation was tuned and the activation energy (E_c) was kept constant so as to fit the experimental data. Figure 2.13 shows the effect of variation of pre exponential factor from $A_c = 0.88 \times 10^{-3}$ $kgm^{-2}s^{-1}Pa^{-1}$, 2.2×10^{-3} $kgm^{-2}s^{-1}Pa^{-1}$ and 2.7×10^{-3} $kgm^{-2}s^{-1}Pa^{-1}$ and $E_c = 9.43 \times 10^{+7}$ $Jkmol^{-1}$. It was observed that the model shows good fit to burnout profile with $A_c = 2.7 \times 10^{-3}$ $kgm^{-2}s^{-1}Pa^{-1}$. Subsequently, similar observation were obtained by performing the sensitivity over activation energy (E_c) from $E_c = 9.43 \times 10^{+7}$ $Jkmol^{-1}$ to $E_c = 8.1 \times 10^{+7}$ $Jkmol^{-1}$ by keeping pre exponential factor $A_c = 0.88 \times 10^{-3}$ $kgm^{-2}s^{-1}Pa^{-1}$ constant. The results show that good fit to the experimental data was obtained at $E_c = 9.43 \times 10^{+7}$ $Jkmol^{-1}$. This clearly shows that the char oxidation kinetic parameter plays significant role in the prediction of burnout profile.

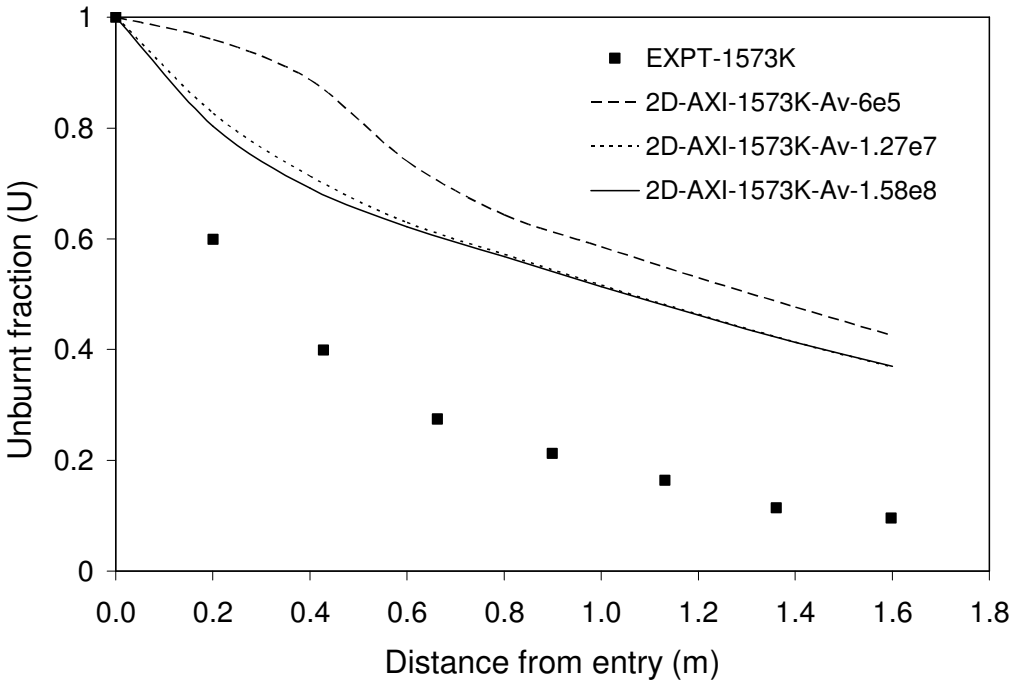

Figure 2.11: Sensitivity of devolatilization kinetic parameters on coal burnout

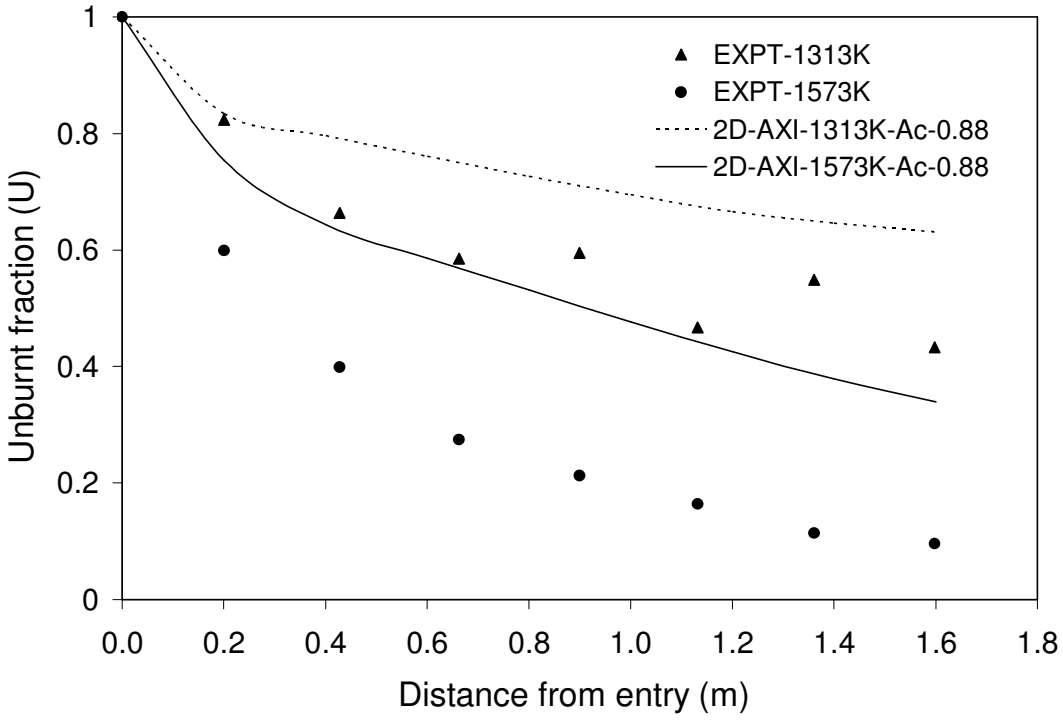

Figure 2.12: Model prediction of coal burnout for A_c =0.88 $kgm^{-2}s^{-1}Pa^{-1}$

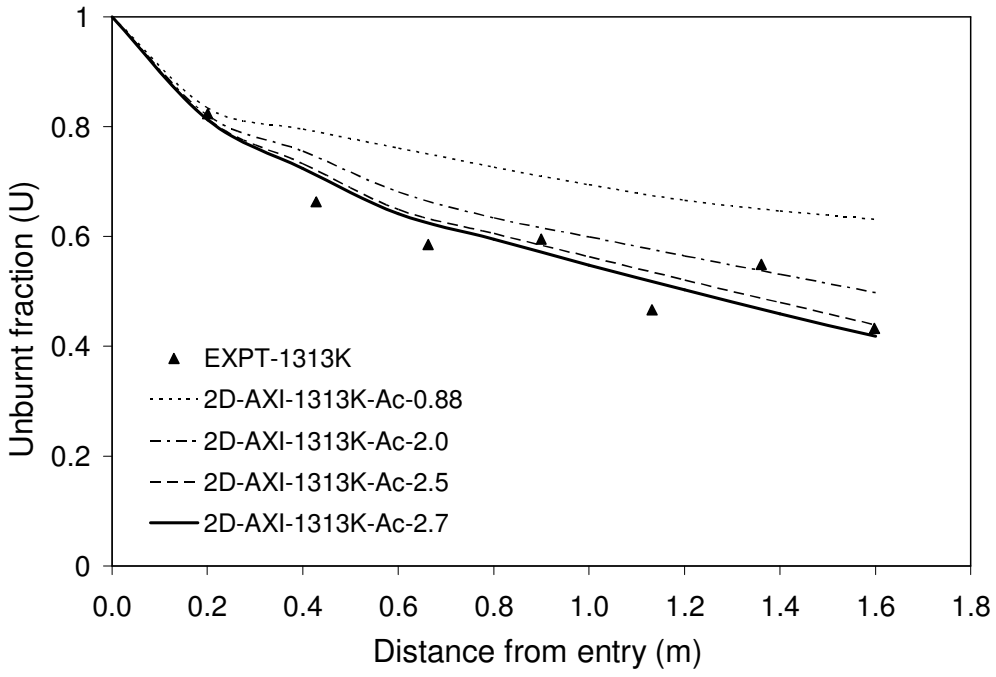

(a) 1313 K

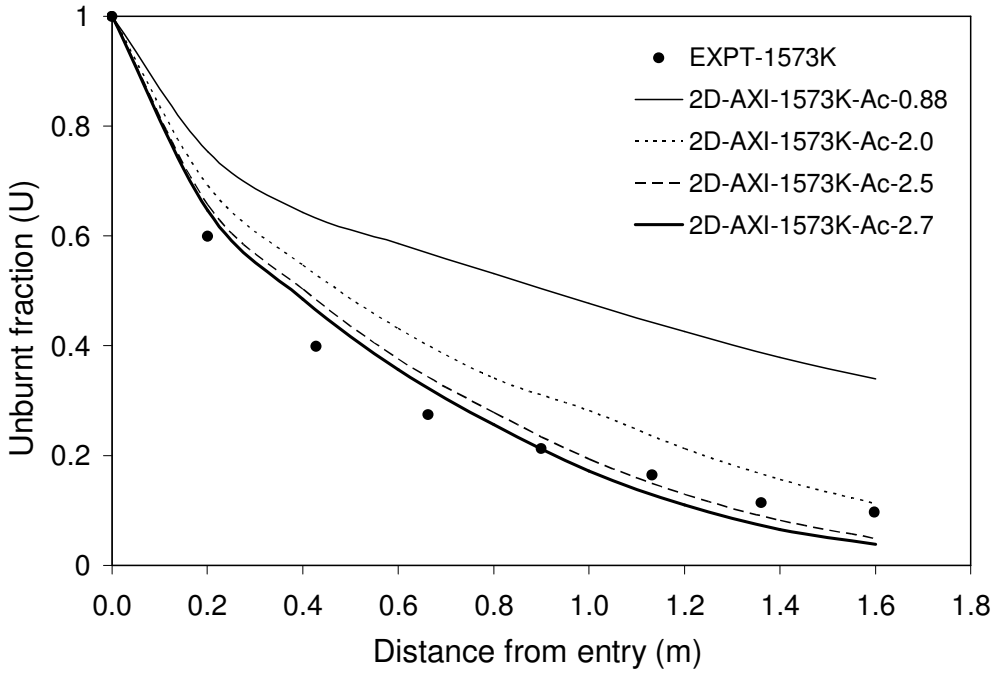

(b) 1573 K

Figure 2.13: Sensitivity of A_c on burnout profile

The above sensitivity studies had given the range in which the A_c and E_c can be varied so as to fit the experimental burnout data. Simulation was performed with $A_c = 1.8 \times 10^{-3}$ $kgm^{-2}s^{-1}Pa^{-1}$ and then the value of E_c was tuned to fit the experimental data. It was observed that $E_c = 9.0 \times 10^{+7}$ $Jkmol^{-1}$ shows good fit to the experimental data. Comparison of the model predictions for these three parameters at 1573 K is shown in Figure 2.14 that shows no significant difference in burnout prediction.

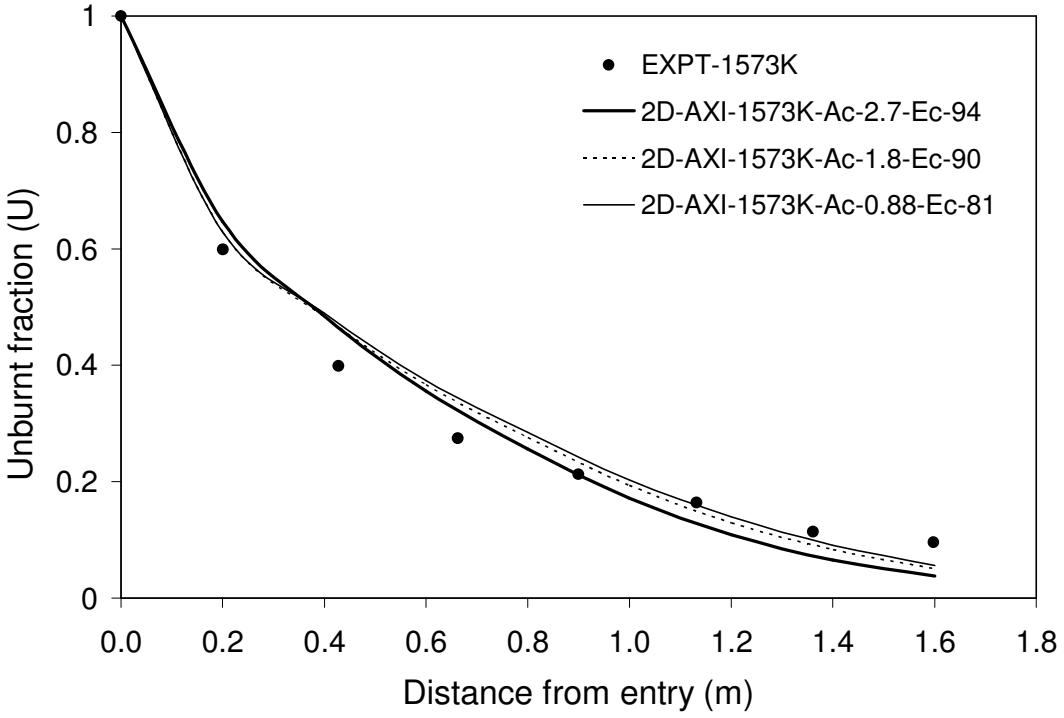

Figure 2.14: Simulation results for three sets of char oxidation parameters to predict coal burnout

Figure 2.15 shows burnout profile for char oxidation kinetic parameters for all operating temperature 1313 K, 1448 K, 1573 K, 1723 K. The char oxidation kinetic parameter was, $A_c = 2.7 \times 10^{-3}$ $kgm^{-2}s^{-1}Pa^{-1}$, $E_c = 9.43 \times 10^{+7}$ $Jkmol^{-1}$ and devolatilization kinetic parameter was $A_v = 1.58 \times 10^{8}$ s^{-1}, $E_v = 1.29 \times 10^{8}$ $Jkmol^{-1}$.

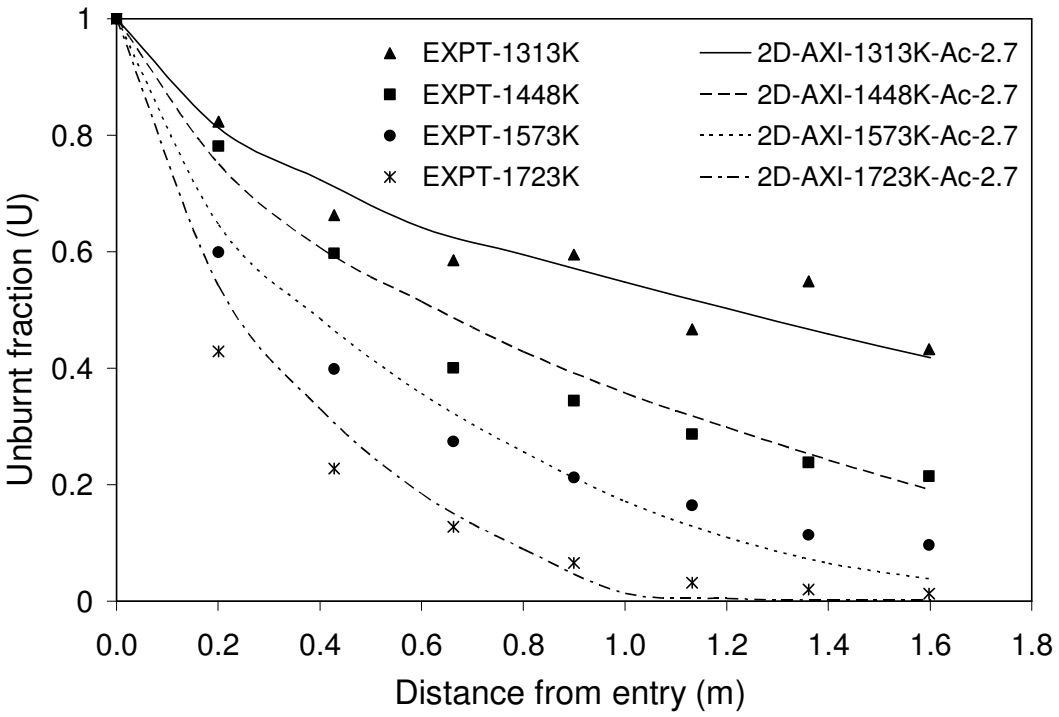

Figure 2.15: Model prediction for coal burnout for $A_c = 2.7 \times 10^{-3}$ $kgm^{-2}s^{-1}Pa^{-1}$

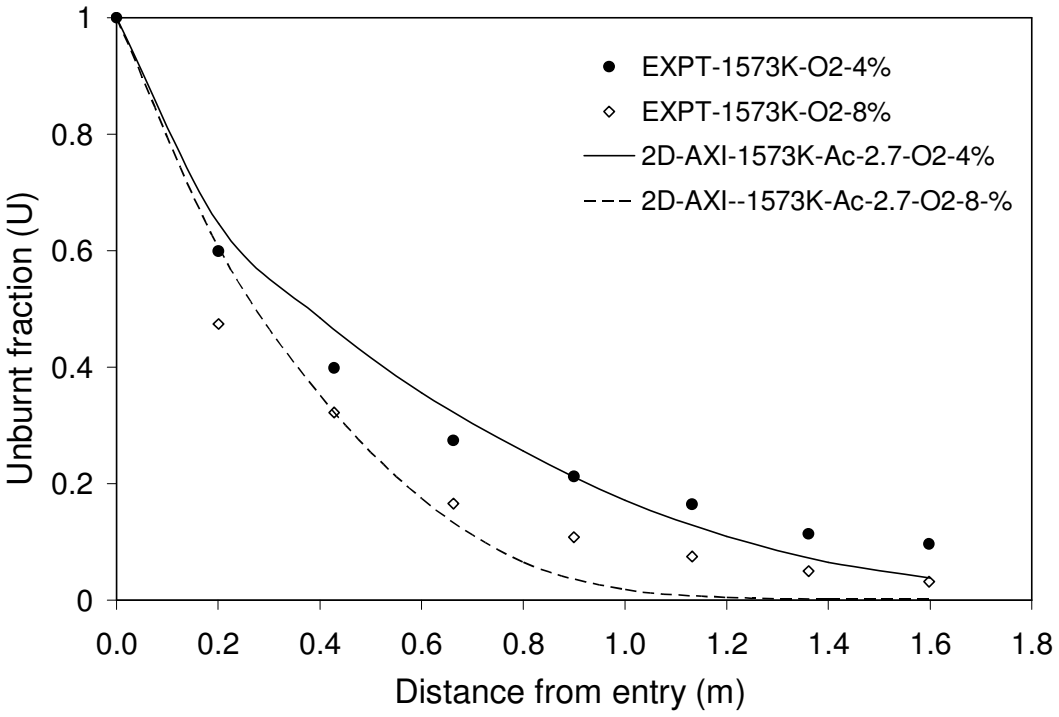

Figure 2.16: Effect of oxygen concentration on coal burnout (1573 K)

Simulations were also performed at the different oxygen concentration to understand the applicability of these evaluated parameters at various operating conditions. The operating conditions were adjusted such that the oxygen concentration at the outlet was increased to 8 (mole %, db). Figure 2.16 shows that the model was able to capture the qualitative trend of combustion profile at this operating condition.

- *Importance of 2D axisymmetric CFD model for DTF*

In order to simulate 1D behavior, the velocity was patched in the computational domain and the flow equation was not solved. The coal particles were injected from the all over the cross sectional area of inlet faces of DTF but in experiments, the particles were introduced from the central inlet with Fuel/pneumatic air. From the contour plot of rate of coal burnout of 2D axisymmetric model (Figure 2.17-a), it is evident that almost all the particles travel along the axis after injection into the DTF and no lateral dispersion of the particles were observed. Figure 2.17-a shows that the gas velocity along the axis is around 0.8 m/s to 0.9 m/s and around 0.1 m/s near to the wall region (for operating temperature 1723 K) where as for 1D model, the average velocity profile was ~ 0.38 m/s (Figure 2.17-b). The residence time distributions (RTD) of particles obtained from 2D axisymmetric and 1D simulations are shown in Figure 2.18. The mean residence time for 1D model was 3.869 s with standard deviation = 0.3919 s. For 2D axisymmetric model the mean residence time was observed to be 1.818 s with standard deviation =0.1176 s. The ratio of mean residence time of 2D axisymmetric model to 1D model was ~ 2.13 s. As the mean residence time of the particles for 2D axisymmetric model was smaller than the 1D model, the 2D axisymmetric model under predicted the combustion profile when the kinetic parameters based on the 1D model were implemented.

Hence the kinetic parameters cannot be obtained with the 1D assumption. The flow profile inside the DTF needs to be computed and the kinetic parameters should be evaluated based on this realistic information. The influence of inlet configuration on the flow profile is significant in DTF and hence any modeling effort should account the non uniformity at the inlet region and its effect on the flow profile.

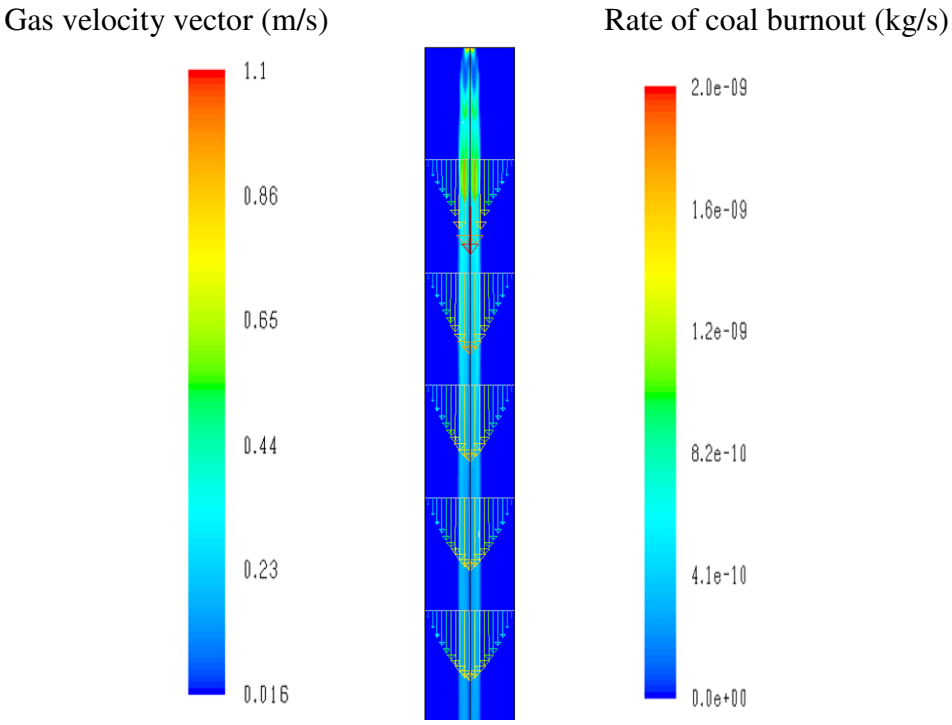

(a) 2D axisymmetric model (1723 K)

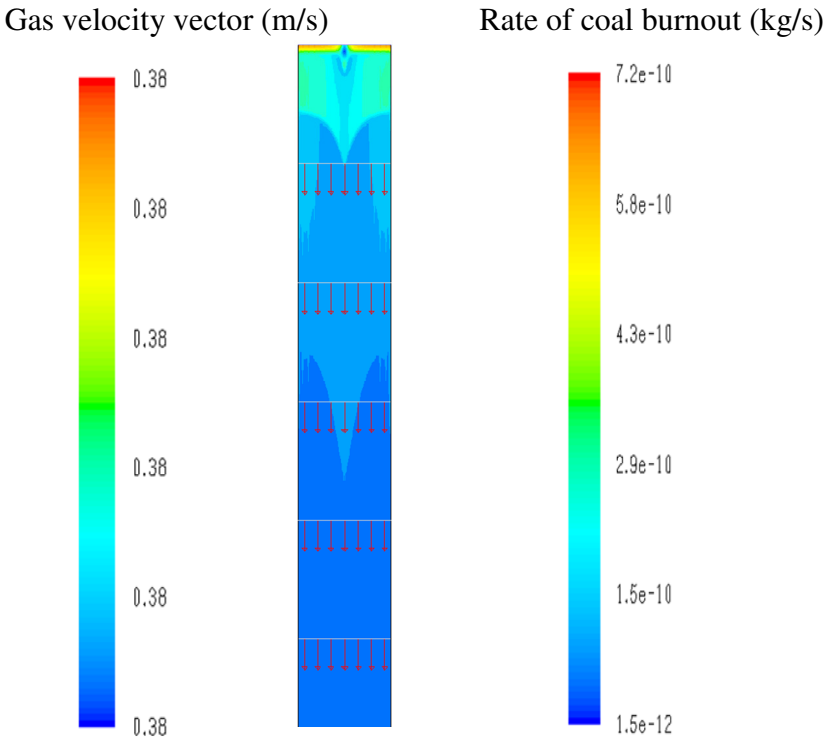

(b) 1D model (1723 K)

Figure 2.17: Contour plot of coal burnout superimposed with velocity magnitude vectors

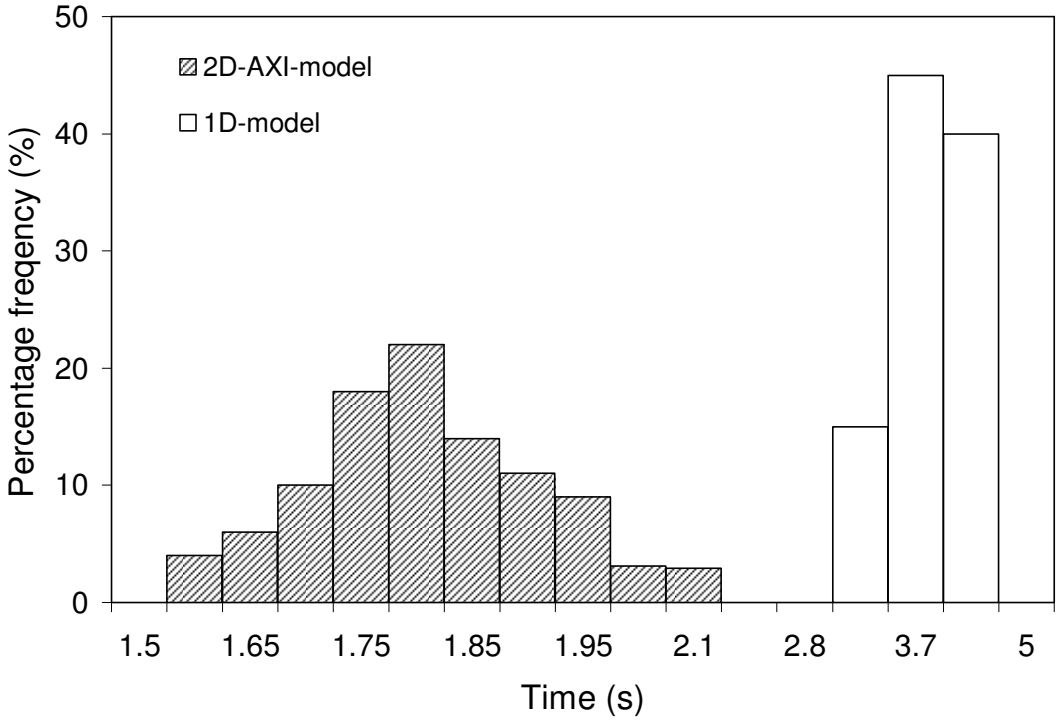

Figure 2.18: Residence time distribution (RTD) of coal particles for 2D axisymmetric and 1D model (1723 K)

2.3.5 Conclusions

CFD model of a laminar flow drop tube furnace was used to assess the influence of the model parameters and operating conditions on the burning characteristic of coal. It was observed that the estimation of kinetic parameters were sensitive to various assumption made while simplifying the model. The major observations and conclusions are listed below,

- 1D model with kinetic parameter for poly dispersed particle size of Ballester et al. (2005) captures the qualitative trends and quantitative burnout profile whereas mono dispersed particles leads to linear decay of coal burnout profile. Hence, the kinetic parameters should be estimated based on the consideration of particle size distribution which are the consistent with the observation of Ballester et al. (2005)

- Even though the amount of volatile was comparatively less in the anthracite coal (~ 10.3 wt%), the appropriate knowledge of the devolatilization kinetic parameters was essential to quantitatively predict the combustion profile

- 2D axisymmetric simulations show that as particles were injected from central injection, most of the particles travel along the axis of the DTF with maximum velocity (laminar flow), which leads to shorter residence time of the particle as compared to 1D model. This leads to under prediction of the burnout profile with char oxidation kinetic parameters proposed by Ballester et al. (2005). Hence it is important to simulate the gas flow, particle flow and inlet configuration of DTF. Therefore, the coal combustion kinetic parameters can be more realistic if they are estimated from the detailed multidimensional CFD model. Such parameters can be directly applicable in the combustion sub models simulating coal fired boilers

Chapter 3

CFD Modeling of Pulverized Coal Fired Boiler

3.1 Introduction

Coal fired boiler is one of the key equipment governing the overall energy efficiency of coal fired power stations. Performance of a coal fired boiler depends on several design and operating parameters. Generally, the boiler is designed for firing a specific type of coal and to avoid any undesirable situations, it is required to assess the possibility of firing any other type of coal and study the burnablity of that coal at lab scales. TGA as discussed in Chapter 2.2 is useful method to study and characterize various types of the coal and also it can predict the effect of maceral content on burnout profile of coal. However, the generally adopted Baum and Street (1970) model rely upon the global kinetic parameters for char oxidation that are estimated from DTF experiments. Chapter 2.3 discussed the advantages of detailed CFD model for DTF over traditional 1D model that can be effectively used for estimation of kinetic parameters as it takes care of geometric details and solves for various processes occurring simultaneously.

DTF has simple laminar flow structure and comparatively tangentially fired boiler has complex geometry and turbulent flow. Modeling of coal fired boilers involves various key issues namely, turbulent flow and transport process, motion of coal particles and turbulent dispersion, devolatilization, burning of char, combustion of volatile components, radiative heat transfer and so on. In order to predict the performance of the boiler it is required to adequately model various processes occurring in the boiler. It is essential to develop a comprehensive understanding of influence of furnace configuration, burner design and different operating parameters on overall performance of a coal fired boiler. Knowledge of temperature field within the boiler and local heat transfer coefficients at boiler tubes is of interest. Knowledge of particle trajectories (bottom ash as well as fly ash) is also one of the key interests in understanding long term performance of coal fired boiler. The particles may interact with pre-heater and super-heater tubes. Understanding of such interaction is important for estimating erosion rates. Over the years, CFD has evolved as a powerful design and predictive tool to simulate large utility boilers as it can handle multiple complex and simultaneous processes like fluid flow, heat transfer, particle trajectories and chemical reactions (Belosevic et al.,

2006; Pallares et al., 2005; Yin et al., 2002; Fan et al., 2001; Smoot et al., 1999 and Boyd & Kent, 1986).

The previous research was instrumental in understanding the applicability of various available turbulence, combustion and radiation models to predict the various processes occurring in the furnace and therefore, usually terminated at furnace exit. The standard k–ε gas turbulence model have been widely used (Asotani et al., 2008; Belosevic et al., 2006; Pallares et al., 2005 and Yin et al., 2002), also some derivatives of k–ε model like RNG k–ε model (Fan et al., 2001). Gas phase conservation equations are mostly time-averaged, but there are few suggestions on using the Favre-averaged equations (Smoot et al., 1999). A two-phase flow is usually described by Eulerian–Lagrangian approach with particle source in Cell method for coupling of the two phases. There are some exceptions where Eulerian–Eulerian approach (Li et al., 2003; Zhou et al., 2002 and Guo & Chan, 2000) are also implemented.

The combustion process includes moisture vaporization, devolatilization, char oxidation and homogenous gas phase reactions. Various models available to calculate volatile yield are constant rate (Baum & Street, 1970 and Pillai, 1981), single step (Badzioch and Hawksley, 1970) or two step Arrhenius kinetic rate (Kobayashi et al., 1977), Chemical Percolation Devolatilization (CPD) model (Fletcher et al., 1992), etc. It has been recognized that the single step models can successfully predict the devolatilization of coal provided that the appropriate coal specific kinetic parameters are known (Jones et al., 1999; Brewster et al., 1995). The char oxidation has been computed mainly by using global/apparent kinetic rate equation (Baum and Street, 1970) that couples the effect of internal ash layer diffusion with intrinsic reactivity. More recently advanced combustion model like Char Burnout Kinetic model (CBK) that can predict the effect of heterogeneity in maceral content, thermal deactivation and ash inhibition in late stages of combustion have been used for prediction unburnt char in Ash (Pallares et al., 2007 and Hurt et al. 1998). But global/apparent kinetic model are particularly useful where the coal related information like porosity, pore diameter, effectiveness factor, surface area of char, etc. are not readily available. Many efforts were made to improve the prediction

capabilities of the present CFD combustion models to obtain quantitative predictions of the char burnout (Pallares et al., 2007 & 2005; Backreedy et al., 2005 and Hurt et al. 1998) which suggests that the char burnout is not single dominated phenomena and depends upon many properties of coal and operating conditions. The homogenous gas phase reactions are treated either by species transport approach (with kinetic or mixing controlled reaction rate) (Li et al., 2003; Zhou et al., 2002 and Fan et al., 2001) or by using single or two mixture fraction approach (He et al., 2007; Pallares et al., 2005 and Yin et al., 2002).

Thermal radiation in the furnace is mostly modeled by P-1 model (Asotani et al.,2008; Vuthaluru et al.,2006 and Backreedy et al.,2006) or discrete ordinates (DO) model (He et al., 2007; Yin et al., 2002 and Zhou et al., 2002) and also with various approaches like six-flux model (Belosevic et al., 2006), Monte Carlo model (Fan et al., 2001 and Howell et al., 1968) and discrete transfer model (Xu et al., 2001 and Lockwood & Shah, 1981). The heat absorbing walls was modeled as constant temperature wall (Yin et al., 2002 and Zhou et al., 2002). The heat exchangers were modeled as either by porous volume approach (He et al., 2007 and Yin et al., 2002) or by constant temperature double sided walls (Yin et al., 2002).

CFD simulations of different types of pulverized coal fired boiler (wall or corner fired) were performed to obtain information about the various aspects of the boiler that experimental data alone cannot practically provide. Most of the previous CFD studies were mainly aimed at predicting the gas flow field, temperature and species distribution and particle trajectory within the boiler (Yin et al., 2002; Fan et al., 2001 & 1999). Much of the emphasis was given on the NO_x production in the boiler and methodology to reduce the same (Backreedy et al., 2005; Stanmore et al., 2000 and Xu et al., 2000). There were attempts to predict the temperature deviation that occurs in the upper furnace zone near the super heaters (Yin et al., 2002 and Xu et al., 1998) which suggests that the residual swirl is primary cause of the temperature deviation occurring in the boiler. The ash deposition on the heat exchangers are the common phenomena in the boiler and models have been developed for predicting the ash deposition on the heat exchangers

walls (Zhou et al., 2002 and Fan et al., 2001). The Fuel/Air ratio plays important role in overall oxygen concentration, temperature profile and residence time of the particles in the furnace and it affects the fuel NO_x formation and loss of unburnt char. The operational parameter like reduction in boiler heat load from standard operating conditions has influence on the boiler performance. Xu et al. (2001) had performed simulation studies to understand the effect of heat load on boiler performance for 300 MW_e wall fired boiler. Recently, Belosevic et al. (2008) has performed numerical studies to understand the effect of operating conditions on performance of 350 MW_e, wall fired boiler (for lignite coal) by developing their own customize code.

It was found in literature that, few numerical studies were performed to simulate 200 MW_e tangentially fired boiler. Hence present work discusses the development of 3D CFD model of 200 MW_e tangentially fired boiler, fired with medium volatile, high ash content sub bituminous type coal. Such studies are useful to enhance understanding of effect different operating conditions on boiler performance.

There are several steps involved in the development of 3D CFD model for boiler and some of the key steps are listed in the following:

- Geometry modeling of furnace: Geometry modeling based on engineering drawings was carried out. Various strategies to decompose furnace geometry to make it amenable to grid generation were developed.

- Grid generation: As quality of grid determines the quality of final simulations, every care was taken to generate good quality grid without increasing computational cells inordinately. Since the flow in furnace is characterized by a wide range of scales, grid generation is one of the most important steps. Both the accuracy of a solution and its cost in terms of necessary computer hardware and calculation time are dependent on the grid quality. Attempt was made to generate grids with not more than 1.5 million cells without compromising the accuracy.

- Selection of appropriate model and solution strategies: The computational models with appropriate grid and user defined programs/ libraries were solved using commercial CFD solver, FLUENT (of Ansys Inc., USA).

3.2 Boiler Geometry

It is essential to model the geometry of the pulverized coal fired boiler and to generate a suitable computational grid. The representation of the boiler geometry created in Gambit 2.1.6 for further use in the CFD model is shown in Figure 3.1-a. The typical dimension of the boiler is 25 m × 14 m × 52 m. The boiler consists of Furnace (consists of furnace and nose), Crossover pass (consists of platen superheater, reheater and final super heater) and Rear pass (consists of LTSH, lower and upper economizer). Each corner of the furnace has 4 operating Fuel Air (FA) burners (injects Primary Air and coal) and 5 Auxiliary Air (AA) burners (injects Secondary Air) that are arranged alternatively.

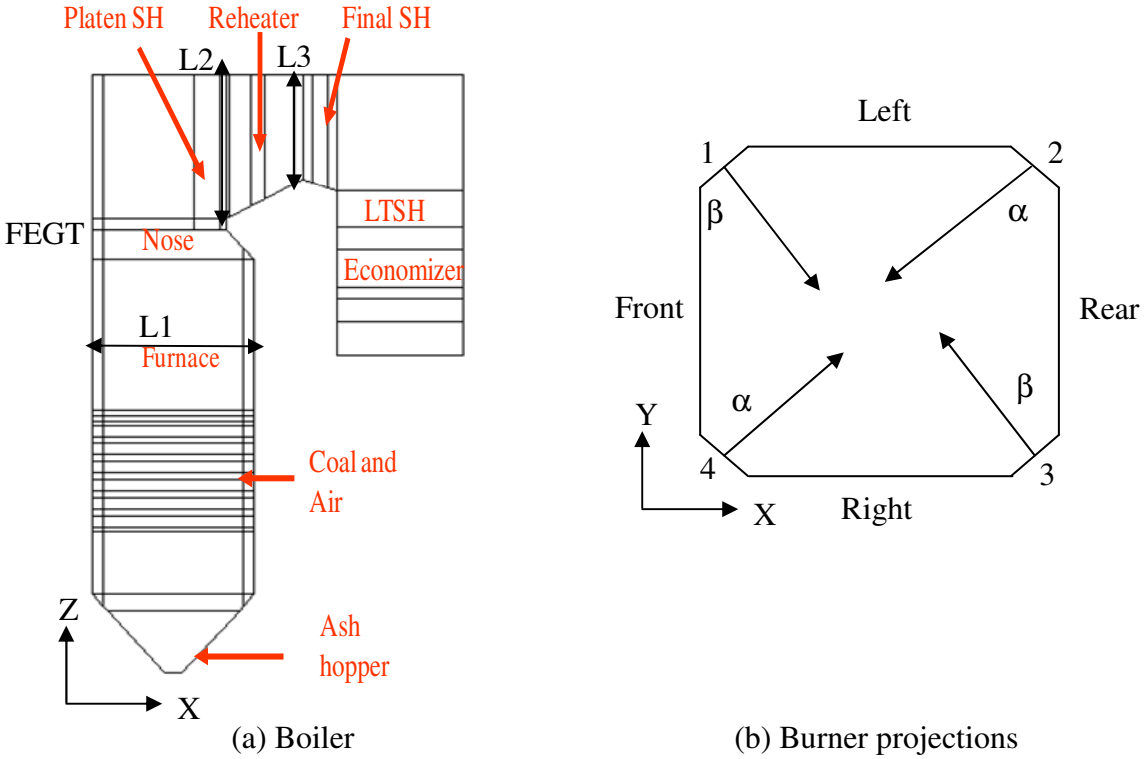

(a) Boiler (b) Burner projections

Figure 3.1: Schematic of 200 MW_e tangentially fired coal boiler
L1, L2, L3 are the Isolines. L1: X = 5 m, Z = 30 m; L2: X = 5 m, Z = 30 m; L3: X = 5 , Z = 30 m; FEGT : Furnace gas exit temperture

The air and coal is projected from the nozzles at an angle of α or β degree with respect to Y axis at a particular Z plane (Figure 3.1-b). The details of burners were not modeled and were represented as flat surface.

3.3 Grid generation

The grid has a significant impact on rate of convergence (or even lack of convergence), solution accuracy and CPU time required. Mesh quality for good solutions depends upon grid density; adjacent cell length/volume ratios and skewness. The mesh density should be high enough to capture all relevant flow features. The geometry was meshed with hexahedral cells and tetrahedral mesh at some parts. Figure 3.2 shows the generated grid at the cross section of the furnace. Initially geometry was meshed with 0.87 million cells. The grid was further refined to generate 1.4 million and 2.0 million cells to evaluate influence of grid size on predicted results. Influence of the computational cells on the solution accuracy is discussed in section 3.7.1.

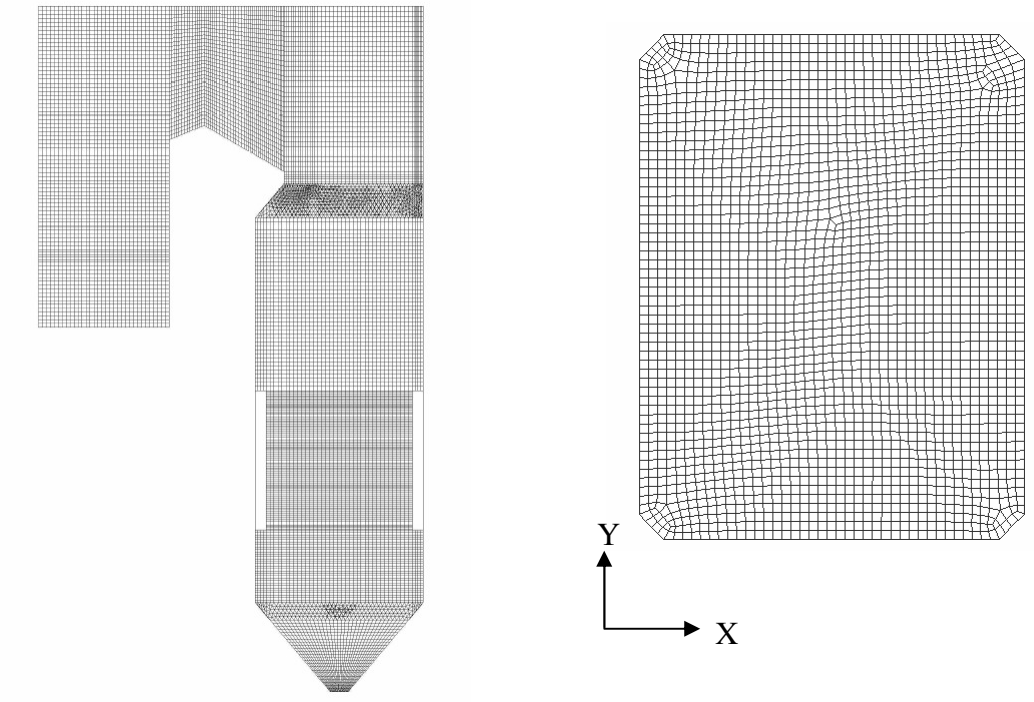

(a) Boiler (b) Furnace cross section

Figure 3.2: Boiler grid of 1465013 cells

3.4 Modeling of porous media

In order to represent the tube bundles (of 7 heat exchangers: platen SH, front and rear reheater, final SH, LTSH, Upper and lower economizers), a porous media approach was adopted. The flow characteristics of different tube bundles were quantified by simulating flow through these tube bundles using a 'unit cell' approach. A periodically repeating configuration of the tube bundles was identified and flow through such a periodic 'unit cell' was simulated over a range of velocities. The simulated results were implemented in appropriate user defined functions (UDFs). A library built using these UDFs was linked to standard FLUENT to implement the developed models into FLUENT. The heat exchangers were modeled as porous volumes. The porosity for each heat exchanger was calculated from the details of tubes (size, number, pitch etc).

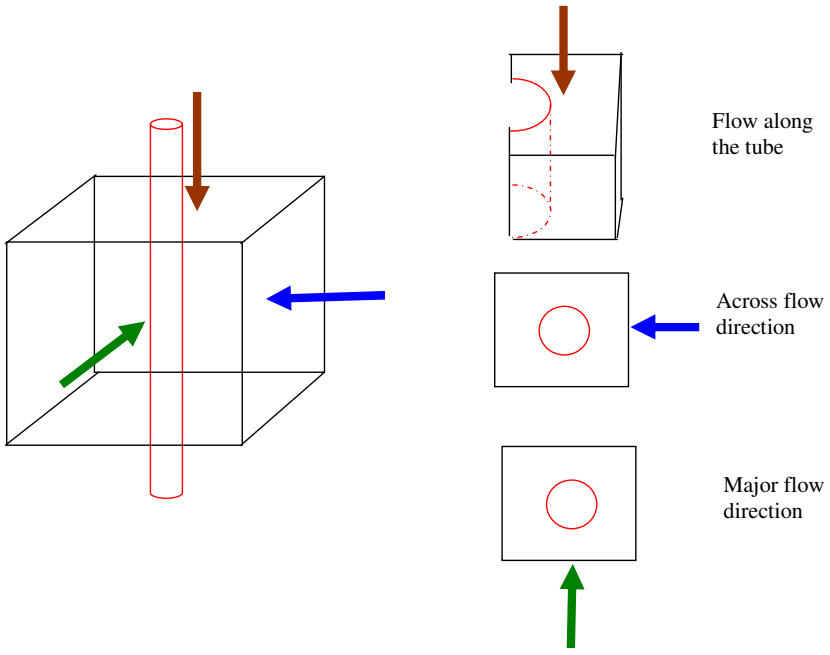

Figure 3.3: Schematic showing the flow directions for unit cell

In a tube bundle, several tubes of identical dimensions are placed with a specific pitch and specific arrangement. The flow through such a tube bundle quickly becomes periodic. This means flow around any tube in the bundle becomes identical to any other tube in the bundle. This is a valid approximation except for the tubes located at the end of

the bundle. Considering that the end effects are relatively minor, periodic flow or unit cell approach allows us to simulate and characterize the flow through bundle by modeling flow around a single tube. Following this approach, flow around a single unit cell was simulated over a range of gas velocities. Coefficients of viscous and inertial resistance were obtained from these numerically predicted results. The predicted pressure drop values were fitted as a function of velocity to obtain required resistance coefficients. A schematic of unit cell and three flow directions are shown in Figure 3.3. Simulations were performed for various gas velocities to calculate pressure drop per unit length (Pam^{-1}). The pressure gradient data was fitted with the velocity as

$$\frac{dP}{dz} = C_0 \mu v + C_2 \frac{1}{2} \rho v^2 \qquad 3.1$$

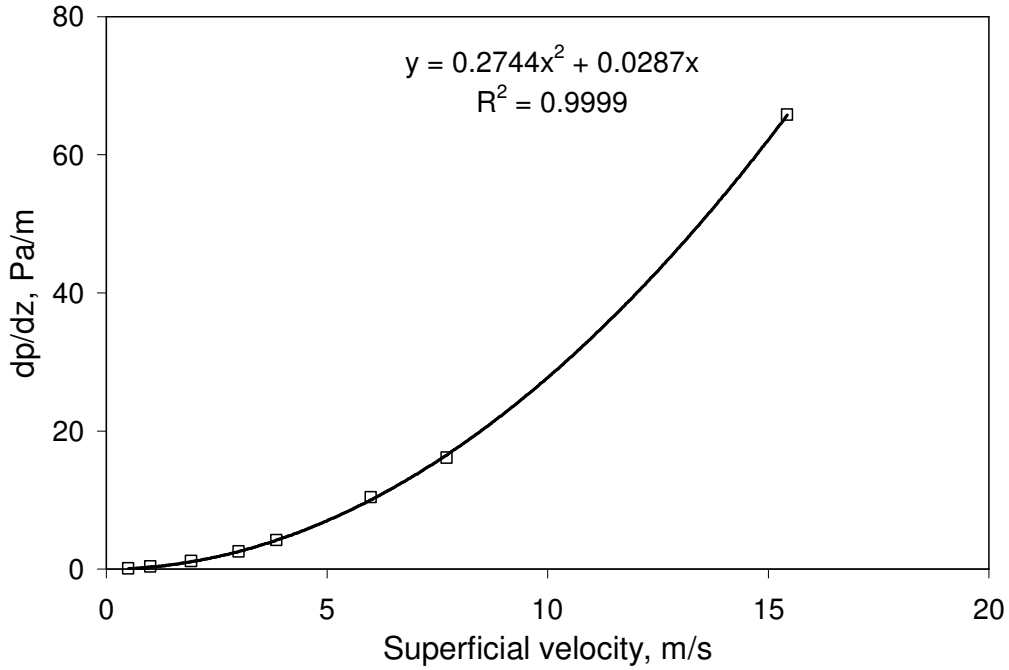

Figure 3.4: Pressure drop per unit length for platen superheater

The viscous and inertial resistance coefficients for all the internal heat exchangers for the three flow directions are listed in Table 3.1.

Table 3.1: Resistance coefficients for heat exchangers

(a) Major flow direction			
Sr. No.	Heat Exchanger	Viscous resistance coefficients ($C_{0,}$ m^{-2})	Inertial resistance coefficients ($C_{2,}$ m^{-1})
1	Platen SH	1607.84	0.448
2	Front RH	0.0	1.293
3	Rear RH	0.0	1.293
4	Final SH	1669.46	7.904
5	LTSH	1669.46	7.904
6	Upper Economizer	54913.17	8.212
7	Lower Economizer	54913.17	8.212

(b) Across flow direction			
1	Platen SH	130599.43	31.90
2	Front RH	30375.35	6.46
3	Rear RH	30375.35	6.46
4	Final SH	11047.62	9.47
5	LTSH	11047.62	9.47
6	Upper Economizer	0.0	4.65
7	Lower Economizer	0.0	4.65

(c) Flow along the tube			
1	Platen SH	40756.86	0.023
2	Front RH	12644.26	0.087
3	Rear RH	12644.26	0.087
4	Final SH	19266.89	0.041
5	LTSH	19266.89	0.041
6	Upper Economizer	24487.39	0.148
7	Lower Economizer	24487.39	0.148

3.5 Heat transfer at boiler internals

The tube bundle of heat exchangers in the boiler are periodically repeating geometries and hence heat transfer in such cases can be predicted by developing single periodic heat transfer module. This methodology was used to obtain Nusselt number correlations for heat exchanger like superheater, reheater and economizer. Numerical experiments were designed for a set of gas velocity values such that the Reynolds number (Re) will lie in a range of 3000 to 50000 that covers the entire range of flue gas velocities that might occur at boiler internals. First, the periodic flow was established by solving continuity, momentum and turbulence equations. The thermal boundary condition for tube walls of heat exchanger was specified as constant temperature, which was calculated from the average temperature of inlet and outlet of steam/water. Appropriate bulk temperature was specified for each heat exchanger and energy equation was solved to obtained periodic temperature profile. Then the heat transfer coefficient (h. t. c.) values were obtained with reference to bulk temperature of fluid. The typical temperature profiles developed for platen superheater is shown in Figure 3.5.

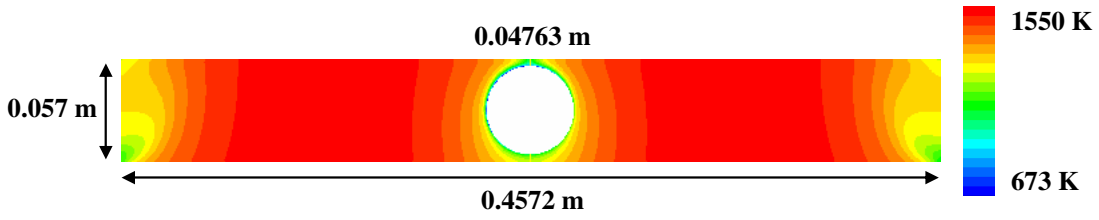

Figure 3.5: Temperature profile for platen superheater

The results of numerical experiments performed for heat exchangers like platen, reheater, final SH, LTSH, and economizer are shown in Figure 3.6-a to 3.6-e. The governing equation for Nusselt number is

$$Nu = c\,\mathrm{Re}^{m}\,\mathrm{Pr}^{1/3} \qquad 3.2$$

The data points are linearly fitted to obtain the values of constant c and m. The values of c and m for a wide range of Reynolds number (Re) are listed in Table 3.2.

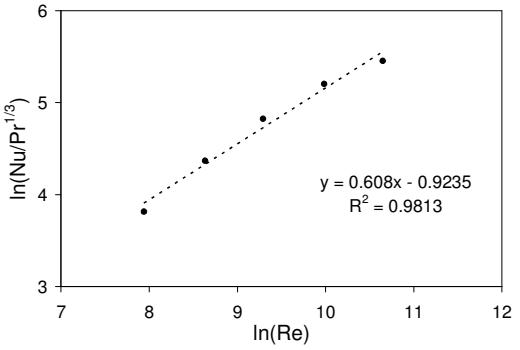

(a) Platen superheater

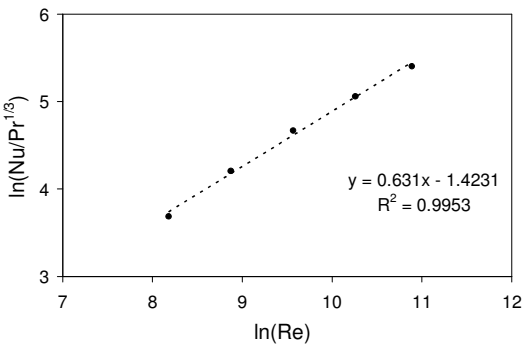

(b) Reheater (Front and Rear)

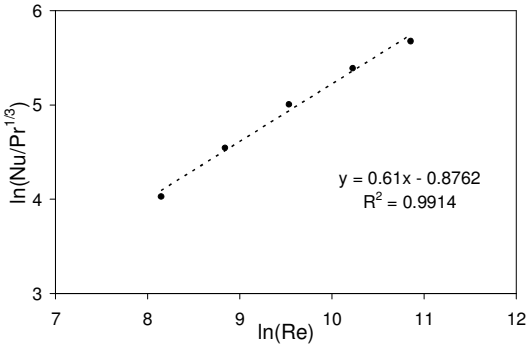

(c) Final superheater

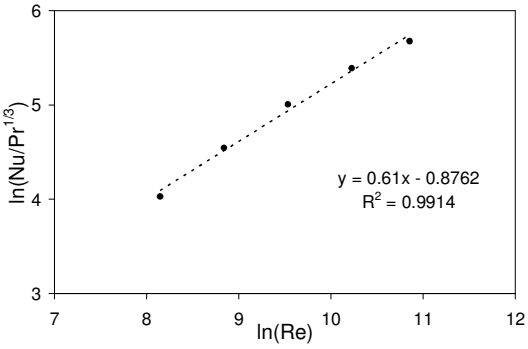

(d) LTSH

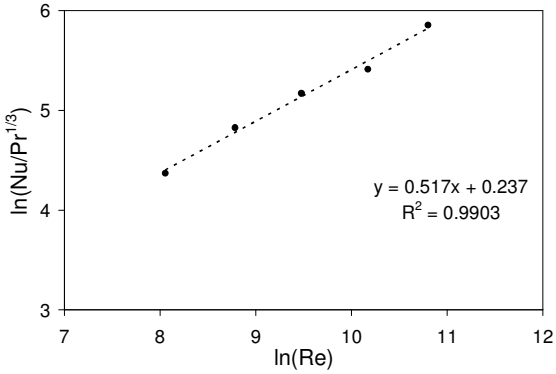

(e) Economizer (Lower and Upper)

Figure 3.6: log-log plot of ($Nu/Pr^{1/3}$) and Re for heat exchangers

Table 3.2: Predicted values of constants c and m for a range of Reynolds number

Heat Exchangers	c	m	Re
Platen SH	0.397	0.608	3000 to 45000
Reheater (Front and Rear)	0.241	0.631	3500 to 53500
LTSH	0.416	0.610	3500 to 51700
Final SH	0.416	0.610	3500 to 51700
Economizer (Lower and Upper)	1.267	0.517	3200 to 49000

Local heat transfer coefficient can be calculated as

$$Nu = \frac{hD}{k} \qquad 3.3$$

Where, h is local heat transfer coefficient, D is characteristic dimension, k is conductivity of flue gas. Based on this correlations, User define functions (UDF) were developed for accounting heat transfer to each heat exchanger.

3.6 Model equations and boundary conditions

The mathematical model is based on Eulerian description of the continuum phase and a stochastic Lagrangian description for the coal particles. The steady state mass conservation equation for gas phase, after Reynolds averaging, can be written as,

$$\nabla \cdot \left(\rho \vec{U}\right) = \sum_k \vec{S}_k \qquad 3.4$$

Where, the source term S_k is the mass of species k added to the continuous phase from the dispersed phase. The flow was assumed to behave similarly to incompressible flow, making density to be dependent only upon the temperature through reference pressure $\rho = \rho\,(T, P_{ref})$ which is reasonable assumption for the problems with Mach number under 0.3 (Pallares et al., 2005).

The species conservation equation can be written as

$$\nabla \cdot \left(\rho \vec{U}\, m_k \right) = \nabla \cdot \left(\left(\rho D_{km} + \frac{\mu_t}{Sc_t} \right) \nabla m_k \right) + R_k + S_k \qquad 3.5$$

m_k is mass fraction of species k, D_{km} is the diffusion coefficient for species k in the mixture, Sc_t is the turbulent Schmidt number ($\frac{\mu_t}{\rho D_t}$ where μ_t is the turbulent viscosity, D_t is the turbulent diffusivity and $Sc_t = 0.7$), R is the net rate of production of species k by chemical reaction, S_k is the source of species k from dispersed phase. The net source of chemical species k due to reaction is computed as the sum of the Arrhenius reaction sources over the N_r reactions that the species participate in

$$R_k = M_{w,k} \sum_{r=1}^{Nr} R_{k,r} \qquad 3.6$$

The discrete phase source term for species k is defined as,

$$S_k = \sum_j \frac{\left[\Delta \left(\dot{m}_{pk} \right) \right]_j}{V} \qquad 3.7$$

Where $\dot{m}_{pk}$ is the particle mass flow rate of component k corresponding to the j^{th} particle trajectory that crosses the cell.

The momentum conservation equation for gas phase (after Reynolds averaging) can be written as

$$\nabla \cdot \left(\rho \vec{U} \vec{U} \right) = -\nabla p - \nabla . \bar{\bar{\tau}} + \rho \vec{g} + \vec{F} \qquad 3.8$$

Where p is the static pressure, $\bar{\bar{\tau}}$ is the stress tensor (as described below). The left hand side term represents change in momentum per unit volume, caused by convection. On the right hand side, first term pressure force per unit volume, second term is viscous force per

unit volume, third term is the gravitational force per unit volume and fourth term is external force that arises from interaction with the dispersed phase.

The stress tensor, $\bar{\bar{\tau}}$ is given as

$$\bar{\bar{\tau}} = \mu_{eff}\left(\frac{\partial U_i}{\partial x_j} + \frac{\partial U_j}{\partial x_i}\right) - \frac{2}{3}\delta_{ij}\left(\mu_{eff}\frac{\partial U_k}{\partial x_k} + \rho k\right) \quad 3.9$$

δij is Kronecker delta function ($\delta ij = 1$ if i = j and $\delta j = 0$ if $i \neq j$), k is turbulent kinetic energy (normal turbulent stresses) and can be expressed as:

$$k = \frac{1}{2}\overline{u_i u_i} \quad 3.10$$

Here, μ_{eff} is referred as effective viscosity where $\mu_{eff} = \mu + \mu_T$ where, μ is the viscosity of gas phase, μ_T is turbulent or eddy viscosity.

For RNG k-ε model, effective viscosity is obtained from the knowledge of turbulent kinetic energy (k) and the turbulent energy dissipation rate (ε) and

$$\mu_{eff} = \mu\left(1 + \sqrt{\frac{C_\mu}{\mu}}\frac{k}{\sqrt{\varepsilon}}\right)^2 \quad 3.11$$

To close the set of equations, the local values of k and ε were obtained from the transport equations of k and ε (Launder and Spalding, 1972):

$$\frac{\partial(\rho U_i k)}{\partial x_i} = \frac{\partial}{\partial x_i}\left(\frac{\mu_T}{\sigma_k}\frac{\partial k}{\partial x_i}\right) + G - \rho\varepsilon \quad 3.12$$

$$\frac{\partial(\rho U_i \varepsilon)}{\partial x_i} = \frac{\partial}{\partial x_i}\left(\frac{\mu_T}{\sigma_\varepsilon}\frac{\partial \varepsilon}{\partial x_i}\right) + \frac{\varepsilon}{k}(C_1 G - C_2 \rho\varepsilon) \quad 3.13$$

G is the turbulence generation term and can be written as

$$G = \frac{1}{2}\mu_T \left[\nabla\overline{U} + \left(\nabla\overline{U}\right)^T\right]^2 \qquad 3.14$$

The transport equation contains four empirical parameters, which are listed in Table 3.3.

Table 3.3: Model constants for RNG k-ε Model (Ranade, 2002)

Sr. No.	Parameter	RNG k- ε
1	C_μ	0.0845
2	C_1	1.42
3	C_2	1.68
4	σ_k (Effective Prandtl number for k)	$\left\lvert\frac{\frac{1}{\sigma_k}-1.3929}{0.3929}\right\rvert^{0.6321}\left\lvert\frac{\frac{1}{\sigma_k}+2.3929}{3.3929}\right\rvert = \frac{\mu}{\mu_T}$
5	σ_ε (Effective Prandtl number for ε)	$\left\lvert\frac{\frac{1}{\sigma_\varepsilon}-1.3929}{0.3929}\right\rvert^{0.6321}\left\lvert\frac{\frac{1}{\sigma_\varepsilon}+2.3929}{3.3929}\right\rvert = \frac{\mu}{\mu_T}$

The momentum source from the discrete phase is added to the gaseous phase. The momentum source term F for a particular cell is calculated from every j^{th} particle trajectory crossing that cell

$$F = \sum_j \frac{\left[\Delta\left(\dot{m}_{pk}\, u_{p,i}\right)\right]_j}{V} \qquad 3.15$$

Where $u_{p,i}$ is the velocity components of the particle in x, y and z direction

Energy balalnce for gas phase

$$\nabla\cdot\left(\rho\vec{U}\,H\right) = \nabla\cdot\left(\frac{k_t}{C_p}\nabla H\right) + S_h \qquad 3.16$$

Under the assumption that the Lewis number (Le) = 1, the conduction and species diffusion terms combine to give the first term on the right-hand side of the above equation. Where, k_t is the turbulent thermal conductivity of gas, H is an total enthalpy.

The volumetric source term, S_h is sum of heat of chemical reactions ($S_{h,rxn}$), source term for discrete phase (S_Q), radiation (S_R) and heat sink to waterwalls and heat exchangers (S_E).

$$S_h = S_{h,rxn} + S_Q + S_R - S_E \tag{3.17}$$

The enthalpy can be estimated as

$$H = \sum_k m_k H_k \qquad \because H_k = \int_{Tref,k}^{T} C_{pk}\, dT + h_k^0\left(T_{ref,k}\right) \tag{3.18}$$

$h_k^0\left(T_{ref,j}\right)$ is the formation enthalpy of species k at the reference temperature $T_{ref,k}$

The heat added from the discrete phase is due to char oxidation.

$$S_Q = \sum_j \frac{\left[\left(1 - f_{heat}\right)\Delta\left(\dot{m}_c\right) H_c + Q_{rad} + Q_{conv}\right]_j}{V} \tag{3.19}$$

The f_{heat} is the fraction of heat absorbed by the particle, H_c is heat released during char oxidation, Q_{rad} and Q_{conv} are the radiative and convective heat transfer between gas and particle respectively.

The thermal radiation in the furnace of the boiler was the dominant mode of heat transfer. As the P-1 is considered to be more suitable for combustion systems having thick optical thickness, a*L >1 (Fluent, 2007), where a is the absorption coefficient and L is width or depth of the furnace. (0.1*14 = 1.4 > 1), the radiative heat transfer in boiler was model by using P-1 radiation model.

The radiation transport equation for P1 model can be written as

$$\nabla \cdot (\Gamma \nabla G) = (a + a_p) G - 4\pi \left(a \frac{\sigma T^4}{\pi} + E_p \right) \quad 3.20$$

The quantity Γ is $\Gamma = \frac{1}{3(a + a_p + \sigma_p)}$

Where, G is incident radiation $=4\sigma T^4$, σ is Stefan Boltzmann constant, a is absorption coefficient of gas phase, a_p is the equivalent absorption coefficient due to the presence of particulates, and is defined as

$$a_p = \lim_{V \to 0} \sum_{n=1}^{N} \varepsilon_{pn} \frac{A_{pn}}{V} \quad 3.21$$

The equivalent emission E_p is defined as,

$$E_p = \lim_{V \to 0} \sum_{n=1}^{N} \varepsilon_{pn} A_{pn} \frac{\sigma T_{pn}^4}{\pi V} \quad 3.22$$

The equivalent particle scattering factor σ_p, is given as

$$\sigma_p = \lim_{V \to 0} \sum_{n=1}^{N} (1 - f_{pn})(1 - \varepsilon_{pn}) \frac{A_{pn}}{V} \quad 3.23$$

and is computed during particle tracking. The f_{pn} is the scattering factor associated with the n^{th} particle.

The expression for $\nabla \cdot (\Gamma \nabla G)$ can be directly substituted into the energy equation to account for heat sources (or sinks) due to radiation.

The discrete phase was modeled by using Lagrangian approach considering the effect of dilute particle phase on fluid flow (two way coupling). Due to large particle-to-gas density ratio $\left(\rho_p / \rho_g > 1000\right)$, effects of static pressure gradients, virtual mass, Basset, Saffman, and Magnus forces were neglected (Guo et al., 2003). Due to dilute flow assumption the particle-particle collision was also neglected. Hence, momentum balance over a single particle of size class i, can be written by only considering gravity and drag force acting on particle.

The discrete phase momentum balance on single particle can be written as

$$\frac{\mathrm{d}u_{\mathrm{p,i}}}{dt} = \frac{(\rho_p - \rho_g)}{\rho_p} g + \frac{18\mu}{d_p{}^2 \rho_p} \frac{C_D \mathrm{Re}}{24} (u_{p,i} - v_i) \qquad 3.24$$

First term on the right hand side of equation 3.24 is the net gravitational force acting on the particle and second term is the drag force acting on particle.

Where, ρ_P, d_p and $u_{p,i}$ are the density, diameter and velocity components of the particle in i^{th} direction (i = x, y or z), μ is the viscosity of gas phase, g is gravitational constant and C_D is drag coefficient, v_i is the velocity component of gas phase (x, y or z direction). Morsi and Alexander (1972) correlation was used to calculate C_D.

Once the velocity flow field is calculated from the above force balance equation, the trajectory of particles can be calculated as

$$\frac{\mathrm{dx_i}}{dt} = u_{\mathrm{p,i}} \qquad 3.25$$

Species conservation equations for discrete phase can be written as:

$$\frac{d\left(M_P m_k\right)}{dt} = S_{pk} \qquad 3.26$$

The M_p is the mass of particle, m_k is the mass fraction of species k.

The particle source term in equation 3.26 can be written as

$$\Delta\left(\dot{m}_{pk}\right)=\frac{d\left(M_p m_k\right)}{dt} \qquad 3.27$$

and

$$\Delta\left(\dot{m}_p\right)=\sum_k \Delta\left(\dot{m}_{pk}\right) \qquad 3.28$$

S_{pk} can be formulated by considering various particle level phenomena of interest such as devolatilization and surface reaction-char combustion.

Hence the S_{pk} can be written as

$$S_{pk}=M_p\left[\frac{dm_v}{dt}+\frac{dm_c}{dt}\right] \qquad 3.29$$

Where, m_v and m_c is mass fraction of volatile and char respectively.

The coal devolatilization rate for any particle can be written as (Badzioch and Hawksley, 1970)

$$\frac{dm_v}{dt}=-A_v\, e^{(-E_v/RT_P)}\left(M_{p_v}-M_{p_f}\right) \qquad 3.30$$

Where Mp_f indicates mass of coal particle after devolatilization and Mp_v is the mass of coal particle at any time, A_v is the pre exponential factor, E_v is the activation energy for devolatilization, T_p is the temperature of the particle

Char combustion rate was calculated by using kinetic/diffusion controlled model available in Fluent (Baum and Street, 1970; Field, 1969). It was assumed that the char gets oxidized to CO by following reaction.

$$C_{(s)} \quad + \quad 0.5\, O_{2\,(g)} \quad \rightarrow \quad CO_{\,(g)}$$

This model is simple in implementation and needs apparent kinetic rate constant which accounts for both chemical and internal pore diffusion resistance. The rate of char oxidation for any particle can be written as, (Baum & Street, 1970 and Field, 1969)

$$M_{p0}\frac{dm_c}{dt} = -A_p \frac{K_c K_d}{K_c + K_d} Y_{O_2} \frac{\rho_g R T_g}{MW_{O_2}} \qquad 3.31$$

A_p is the external surface area of particle, Y_{O_2} is oxygen mass fraction, R universal gas constant, T_g is gas temperature, MW_{O_2} is molecular weight of O_2, ρ_g is density of gas

The kinetic rate constant (K_c) for char oxidation reaction is

$$K_c = A_c\, e^{(-E_c/RT_P)} \qquad 3.32$$

Where, A_c is pre exponential factor and, E_c is the activation energy for char combustion.

The bulk gas phase diffusion coefficient for oxidant (Field, 1969) can be given as,

$$K_d = \frac{5\times10^{-12}}{d_p}\left(\frac{T_g + T_p}{2}\right)^{0.75} \qquad 3.33$$

Energy balance for the discrete phase

$$M_p Cp_P \frac{dT_P}{dt} = \left(f_{heat} M_p \frac{dm_c}{dt} H_{rxn}\right) + Q_{rad} + Q_{conv} - \sum \frac{dM_P}{dt} h_{fg} \qquad 3.34$$

Here, C_{pp}, f_{heat}, H_{rxn} , Q_{rad} and Q_{conv} are the particle specific heat, fraction of heat absorb by particle, heat of char oxidation reaction, radiative and convective heat transfer respectively. The f_{heat} is the fraction of heat absorbed by the coal particle during the char oxidation. H_{fg} is the latent heat of evaporation of volatile/moisture.

The particle radiative heat transfer can be written as

$$Q_{rad} = \varepsilon_P \sigma A_p (T_R^{\,4} - T_P^{\,4}) \qquad 3.35$$

And the convective heat transfer can be written as

$$Q_{conv} = hA_P (T_g - T_P) \qquad 3.36$$

Where, ε_P is the emissivity of particle, σ Stefan-Boltzmann constant ($=5.67\times10^{-8}\, W/m^2K^4$), T_R is the radiation temperature $=\left(\frac{I}{4\sigma}\right)^{1/4}$ and h is heat transfer coefficient.

The heat transfer coefficient, h_c was evaluated using the correlation of Ranz and Marshall (1952) as

$$\frac{h_c d_p}{k_g} = 2 + 0.6(\mathrm{Re}_p)^{1/2}(\mathrm{Pr})^{1/3} \qquad 3.37$$

The volatile material was represented by single species as $CH_{2.08}O_{0.38}$. Following gas phase reactions were assumed.

$$CH_{2.08}O_{0.38\ (g)} + 1.33O_{2\ (g)} \rightarrow CO_{2\ (g)} + 1.04H_20_{\ (g)}$$

$$CO_{(g)} + 0.5\,O_{2(g)} \rightarrow CO_{2(g)}$$

The rate of gas phase combustion at low temperature is kinetic rate controlled and once the flame is ignited, the reaction rate becomes mixing limited. Hence the rate of gas phase combustion was determined by Arrhenius type kinetic rate / eddy dissipation model. The gas phase reaction rate is evaluated based on the minimum of the reaction rate estimated by Arrhenius type kinetic rate model and eddy dissipation model. The eddy

dissipation model is based on the work of Magnussen and Hjertager (1976) which describes the turbulence-chemistry interaction. The net rate of production of species k due to reaction r, $R_{k,r}$, is given by the smaller (i.e., limiting value) of the two expressions below:

$$R_{k,r} = v'_{k,r} M_{w,k} A \rho \frac{\varepsilon}{k} \min_R \left(\frac{Y_R}{v'_{R,r} M_{w,R}} \right) \quad 3.38$$

$$R_{k,r} = v'_{ki,r} M_{w,k} AB \rho \frac{\varepsilon}{k} \left(\frac{\sum_P Yp}{\sum_j^N v''_{j,r} M_{w,j}} \right) \quad 3.39$$

$Y_{p,}$ mass fraction of any product species, p, Y_R, mass fraction of a particular reactant, R, A, empirical constant = 4.0, B, empirical constant = 0.5. In Equations 3.38 and 3.39, the chemical reaction rate is governed by the large-eddy mixing time scale, k/ε as in the eddy-breakup model of Spalding (1969).

The molar rate of creation/ destruction of species k in reaction r in Arrhenius form can be written as

$$R_{k,r} = \left(v'_{k,r} - v_{k,r} \right) K_r \prod_l \left[C_{l,r} \right]^{n_l, r} \quad 3.40$$

$C_{l,\,r}$ is the molar concentration of each reactant l^{th} species in reaction r, $\eta'_{l,r}$ exponent for each l^{th} reactant in reaction r, $v'_{k,r}$ and $v_{k,r}$ are stoichiometric coefficient for k^{th} species as product and reactant respectively, K_r is the kinetic rate constant for any reaction r and can be expressed as

$$K_r = A_r \, e^{(-E_r / RT)} \quad 3.41$$

A_r and E_r are the pre exponential factor and activation energy for the gas phase reaction r, T is the gas temperature, R is gas constant. The gas phase reaction rate is evaluated based on the minimum rate obtained from equations 3.38, 3.39 and 3.40.

- *Boundary conditions*

The gas flow inlets for FA and AA were defined as velocity inlet and the outlet was specified as pressure outlet. The waterwalls were defined as constant temperature walls. The emissivity = 0.8 was specified to the all water wall for accounting the radiative heat transfer. No slip condition was specified to the wall. For discrete phase, the coal particles were injected as surface injection. The reflect condition was specified for the particles at the wall and escape condition was specified at the outlet. Particles were modeled as discrete phase with particle size distribution (PSD) that was furnished. The PSD was fitted to appropriate Rosin-Rammler (RR) equation and the RR model inputs required for specifying PSD in CFD model like mean diameter and spread were estimated for the same (Table 3.4).

Table 3.4: Particle size distribution (wt. %) of coal

Sample	Mass fraction				Rosin Rammler parameters	
	-75 μ	-150 μ to +75 μ	-300 μ to +149 μ	+300 μ	Mean particle diameter (μm)	Spread parameter
Sub bituminous	0.75	0.166	0.078	0.006	60	1.156

The water walls were assumed as constant temperature walls. Appropriate heat sink terms were added to all the internal heat exchangers which were modeled based on porous media approach discussed in section 3.4 and 3.5. The emissivity of heat exchanger tube bundles was specified as 0.6 and the tube wall temperature was estimated from the average value of the input and output temperature of steam. Model constants for RNG k-ε model are listed in Table 3.3. The appropriate kinetic parameters for devolatilization and char oxidation were obtained from the open literature for similar type of coal. Coal composition is shown in Table 2.3. Devolatilization and char oxidation kinetic

parameters are given in Table 3.5. Gas phase oxidation kinetic parameters are listed in Table 3.6. Operating conditions are shown in Table 3.7. The overall model parameters are listed in Table 3.8.

Table 3.5: Devolatilization and char oxidation kinetic parameters

Devolatilization (Sheng et al.,2004)		Char oxidation (Sheng et al.,2004)	
A_v (s^{-1})	E_v (J $kmol^{-1}$)	A_c ($kgm^{-2}s^{-1}Pa^{-1}$)	E_c (J $kmol^{-1}$)
2×10^5	6.7×10^7	0.0053	8.37×10^7

Table 3.6: Gas phase oxidation reaction kinetic parameters

Volatile combustion (Guo et al., 2003)		CO oxidation (Kim et al, 2000)	
A_{vol} (m^3 $kmol^{-1}s^{-1}$)	E_{vol} (J $kmol^{-1}$)	A_{CO} (m^3 $kmol^{-1}s^{-1}$)	E_{CO} (J $kmol^{-1}$)
2.56×10^{11}	1.081×10^8	8.83×10^{14}	9.98×10^7

Table 3.7: Operating conditions

Excess Air (%)	20
Fuel Air mass flow rate (kgs^{-1}) (Temperature 350 K)	75
Auxiliary Air mass flow rate (kgs^{-1}) (Temperature 553 K)	149
Coal flow rate (kgs^{-1}) (Temperature 350 K)	39

Table 3.8: Model parameters for base case simulation study

Parameter	Value	References
Particle emissivity	0.9	Backreedy et al. (2006)
Particle scattering factor (f_p)	0.6	
Swelling factor (S_w)	1	
Heat fraction (f_{heat})	1	Boyd and Kent (1986)
Particle density (ρ_p, kgm^{-3})	1400	
Particle heat capacity (Cp_p, $Jkg^{-1}\ K^{-1}$)	1680	
Number of particle streams tracked	10240	
Gas absorption coefficient	WSGGM	
Burner tilt (degree)	0	
Operating heat load (MW_e)	200	

3.7 Numerical simulation

Commercial CFD solver, FLUENT (of Ansys Inc., USA) was used to solve the mass, energy and momentum governing equations for gas and particles. Velocity and pressure coupling was handled by the SIMPLE algorithm. The differential equations were discretized by using second order upwind scheme for momentum, turbulent kinetic energy, turbulent dissipation rate, species and energy. The pressure was discretized by using standard scheme. The simulations were performed on 1465013, 3-D non uniform hybrid type (hexahedral + tetrahedral) grid cells. The effect of grid size on the solution accuracy was performed and the selected grid provides the optimal combination of grid independence and computational economy. First the single phase cold flow simulations were performed by injecting air with mass flow rate of 225 kg/s distributed among the FA and AA burners. These cold flow studies were performed for selection of appropriate grid size and to understand the applicability of various turbulence models. Once the flow field was established, then solid coal particles were injected flow in cold condition and gas-solid flow was established, then temperature (1500 K) was patched in the burner zone and coal combustion was solved without radiative heat transfer at very low under relaxation factor (URF) for particle and temperature equations. The heat generated due to

coal combustion increases the temperature of furnace above 2300 K and the radiative heat transfer was solved initially at low URFs and further increasing to maximum 1, once solution gets stabilized. It systematically cools down the burner section temperature to more realistic value of around 1800 K. Once the solution was established, the URFs of temperature, radiation and discrete phase were increased to their maximum possible values (eg. Energy = 0.95, DPM = 0.5). Various convergence criteria like, insignificant change (<1%) in velocity, species, temperature profiles and heat transferred to exchangers were observed at various locations in the boiler.

3.8 Results and discussion

The simulation result of 200 MW_e CFD model are discussed below. The predicted results were compared with the few global boiler design parameters obtained from power plant like CO_2, H_2O and O_2 concentration at the economizer outlet, unburnt char in ash, heat transferred to heat exchangers and waterwall, FEGT, temperature at the inlet of each heat exchanger and at economizer outlet. Due to restrictions, the comparison between the simulation results and design parameters was not possible to disclose over here thesis and hence are not included in this section and only key CFD model results are discussed below;

3.8.1 Influence of grid size

Single phase air flow simulations were performed with different computational cells to quantify influence of computational cells on the predicted results. The predicted velocity magnitude profiles is shown in Figure 3.7 for three difference cases (with 0.87, 1.4 and 2.0 million cells). It can be seen that the predicted result at the Line 1, Line 2 show small influence of the number of computational cells (Figure 3.7). It can be seen that no significant change in velocity magnitude can be observed between results predicted with 1.4 to 2.0 million cells. Therefore, all the subsequent simulations were carried out with 1.4 million computational cells (1465013 grid cells).

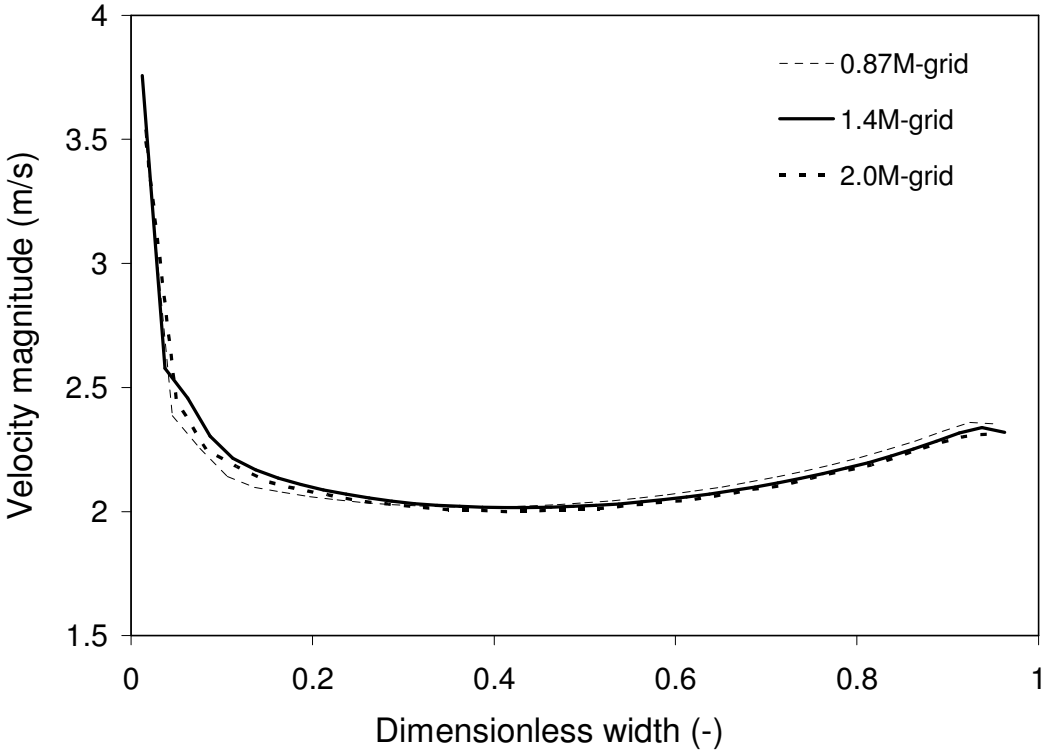

(a) Line L2

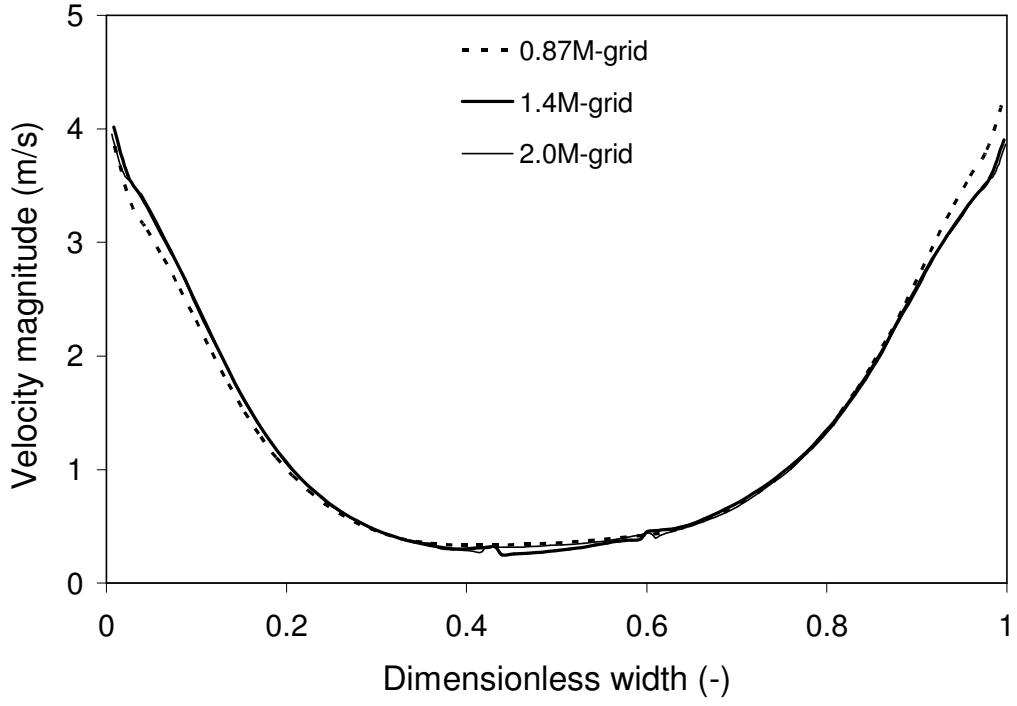

(b) Line L1

Figure 3.7: Influence of number of computational cells on velocity magnitude

3.8.2 Influence of turbulence models

Since the flow in coal fired boiler is turbulent, it is important to select an appropriate turbulence model. As mentioned there, two equations turbulence models were found to be most appropriate and widely used in literature for simulating pulverized coal fired boiler.

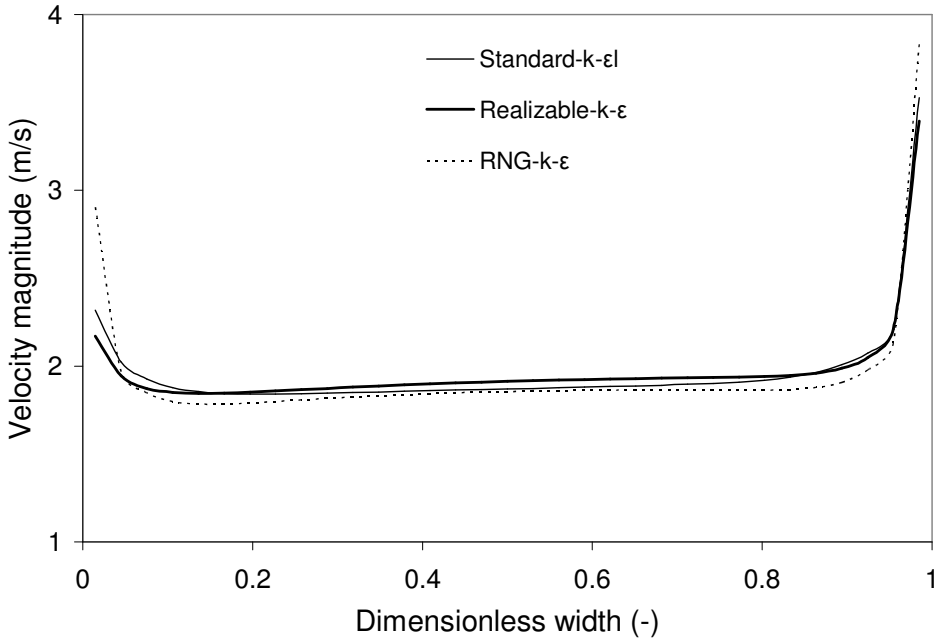

(a) Line L3

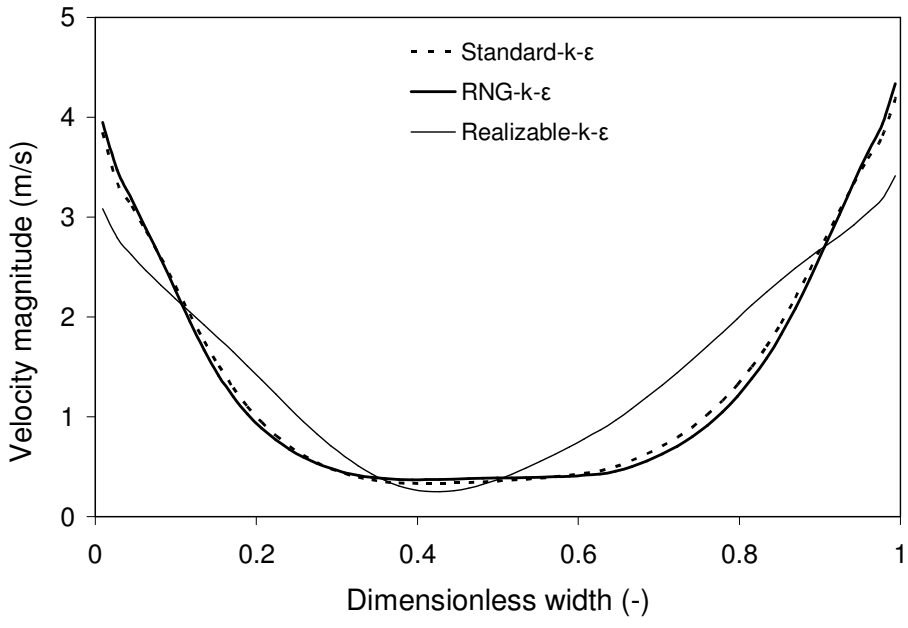

(b) Line L1

.Figure 3.8: Influence of turbulence models on velocity magnitude (ms^{-1})

Three different two-equation turbulence models, namely (1) standard k- ε model, (2) renormalization group (RNG) version of the standard k- ε model and (3) realizable k- ε model were considered. The simulation results of single phase air flow study are shown in Figure 3.8. The predicted results at L3 in the crossover pass (Figure 3.8-a) indicate no significant influence of the turbulence models like standard, renormalization group or realizable on the predicted velocity profile. The predicted results of different turbulence models were also compared in the furnace zone where flow is circulating in nature. As a sample of such comparison, predicted velocity profiles with three turbulence models at L1 are shown in Figure 3.8-b. It can be seen that predicted results of the standard k-ε model and the RNG k- ε model of turbulence agree with each other quite well. The results predicted with the realizable k-ε model show some deviation from these results. There is no adequate data available to discriminate between these models. Results predicted with renormalization group (RNG) version of k- ε model and the standard k-ε model agree with each other and hence further work was carried out with the RNG k-ε model, since the RNG k–ε model is superior to the standard k–ε model for flow prediction with swirl or sharp change in the calculation domain.

3.8.3 Temperature profile

Predicted temperature distribution on a typical vertical plane (plane Y, y=6.5 m & plane Z, z=25 m) is shown in Figure 3.9. The burner section is distinguished hot zone in Y plane with higher local temperature (1500-1800 K) observed in the zone where major combustion reactions are taking place and heat is liberated. The plane Z at the cross section of the furnace passing through the fuel air burner port at 25 m is shown in the Figure 3.9-b. The cold air jets (350-400 K) can be observed near the inlet at the corner which is starting point of the jests and then gets heated due to the heat generation along the path that increases the local temperature to around 1750 K. The FEGT (furnace gas exit temperature, z = 41 m) was around 1327 K. As the flue gas flows from the furnace exit to the boiler exit, the temperature gradually decreases due to the heat transfer from the flue gas to the furnace walls, re-heaters, super-heaters and economizer. The estimated heat flux to the water walls in the burner section was ~121 kWm^{-2} and 90 kWm^{-2} in the

sections above and below the burner zone. The estimated gas side heat transfer coefficient to the water walls at the burner zone was ~130 $Wm^{-2}K^{-1}$ and around 150 kWm^{-2} for the sections above and below the burner zone. The flue gas average temperature at the boiler exit (after lower economizer) was 665 K.

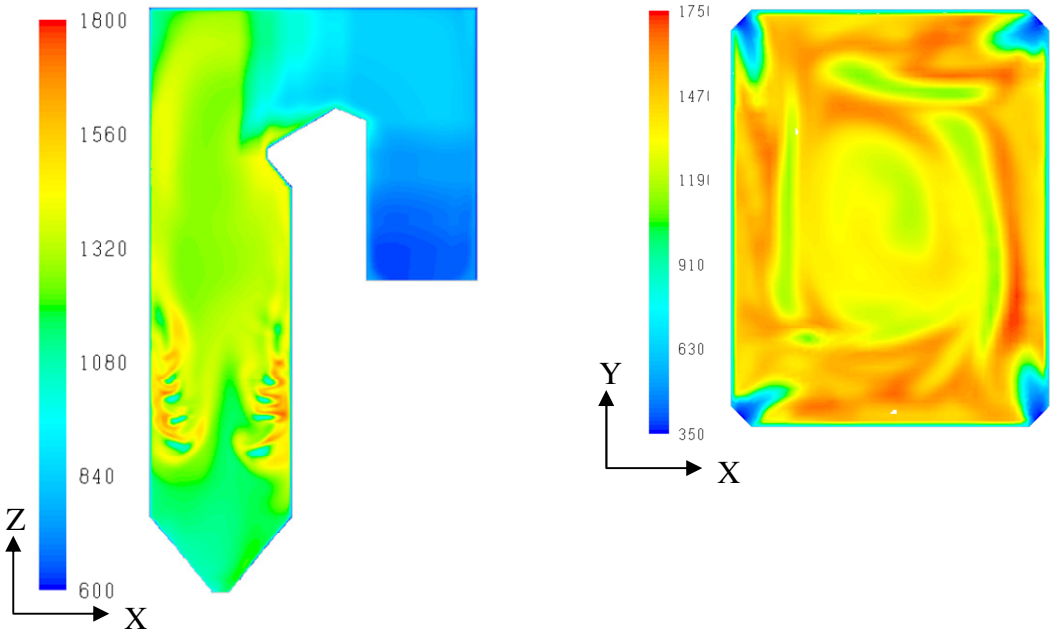

(a) Y = 6.5 m (b) Z = 25 m (FA)

Figure 3.9: Temperature profile within boiler (K)

3.8.4 Gas flow

A typical flow field in Y plane, y = 6.5 m is shown in Figure 3.10-a in the form of vector plots. Four distinguished high gas velocity jets (20-25 ms^{-1}) are observed in the burner section of the furnace, representing the combusting mixture of fuel air and coal. The gas enters from the burners above the ash hopper. It can be seen that most of the gas has upward movement and small fraction of gas flows downward towards the ash hopper and then flows upward. The flow moves upward towards platen super heater and bends around the nose of the furnace to enter into the cross over pass. From the crossover pass the flow bends toward the outlet of the boiler. Flow field on the horizontal plane cutting one row of the burners is shown in Figure 3.10-a. It can be seen that the four jets coming

from the burners form a strong counter clockwise circulatory flow. The gas flow jet when enters the furnace is pushed towards the wall by another jet that is coming from the left hand side corner and the jet coming from the left side is directed towards the inner core of the furnace. This structure is repeated at four corners that forms the rotational imaginary circle (Fireball) at the center. Tangential burners generate rotational flow in the furnace and hence flow in the upper pass of the furnace is rotational in nature. This can be observed in the Figure 3.10-a where in the upper part of furnace, the gas has higher velocity near walls than that of the center of the furnace. The swirling nature of flow continues till the Nose section of the furnace and then starts breaking due to the presence of the suspended Platen super heater.

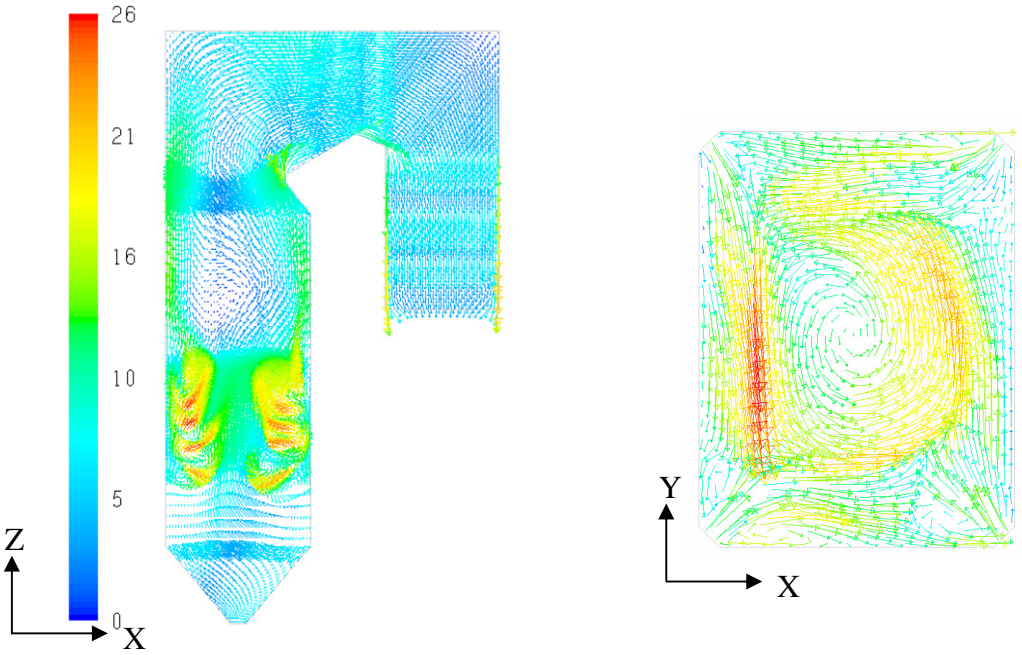

(a) Y = 6.5 m (b) Z = 25 m (FA)

Figure 3.10: Velocity magnitude vector plot (ms^{-1})

Part of the flow moves towards the front side wall of the boiler which still is rotational in nature and then leads to horizontal entry into the platen SH. While passing through the heat exchangers that are porous volumes, the velocity of the flue gas increases due to restrictions offered by heat exchangers. The flow in crossover pass and rear pass does not show the swirling nature and shows moreover flat structure. The percentage frequency

plot for pathlength and residence time is shown in Figure 3.11-a and b respectively. The mean residence time and traveling length of the flue gas within the boiler was estimated as 11.2 s (standard deviation = 4.5 s) and 73.8 m (standard deviation = 18.6 m), respectively.

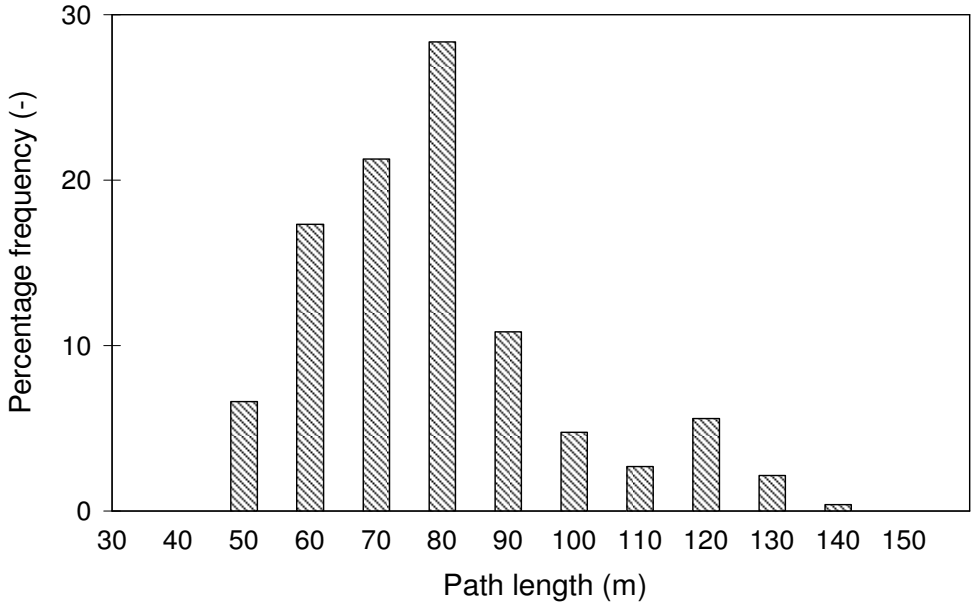

(a) Path length

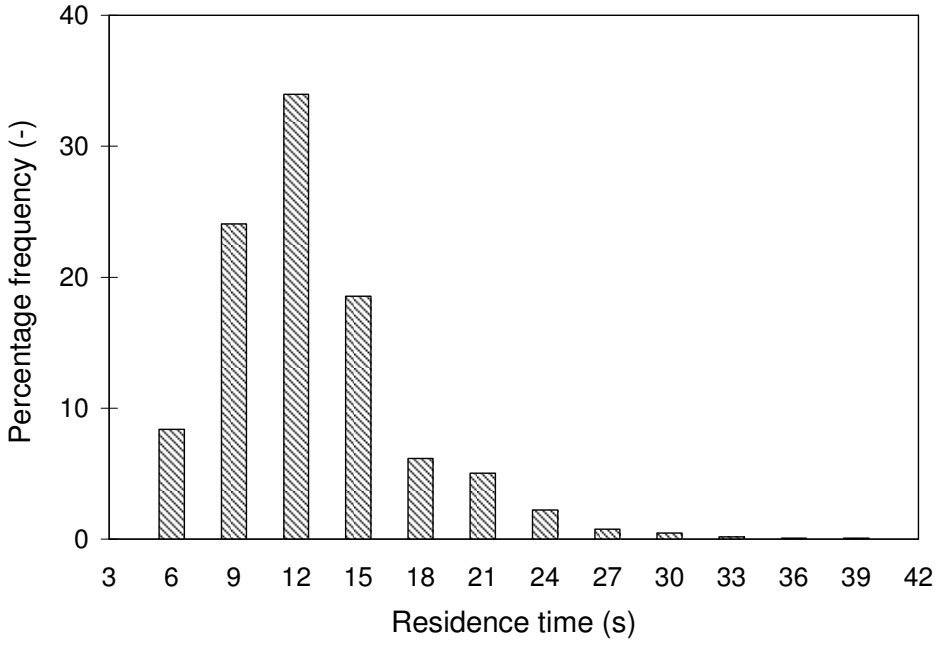

(b) Residence time

Figure 3.11: Frequency distribution plot of the gas flow path lines at the boiler exit

3.8.5 Particle trajectories

The simulated particle trajectories (colored by z velocity of particles) are shown in Figure 3.12. Since injected coal particles are rather small and the flow is very dilute, most of the particles follow the gas phase motion and leave the solution domain (boiler) with flue gases. The trajectories show complicated three-dimensional flow characteristics which promote the mixing of the air and coal particles and enhancing heat transfer via bulk motion. The total ash present in the coal was about 15.83 kg for the considered case. The simulated results show that the only ~2% of initial ash was recovered as bottom ash (i.e. from the bottom outlet of the furnace) and rest ~98% of initial ash was carried away by the flue gas.

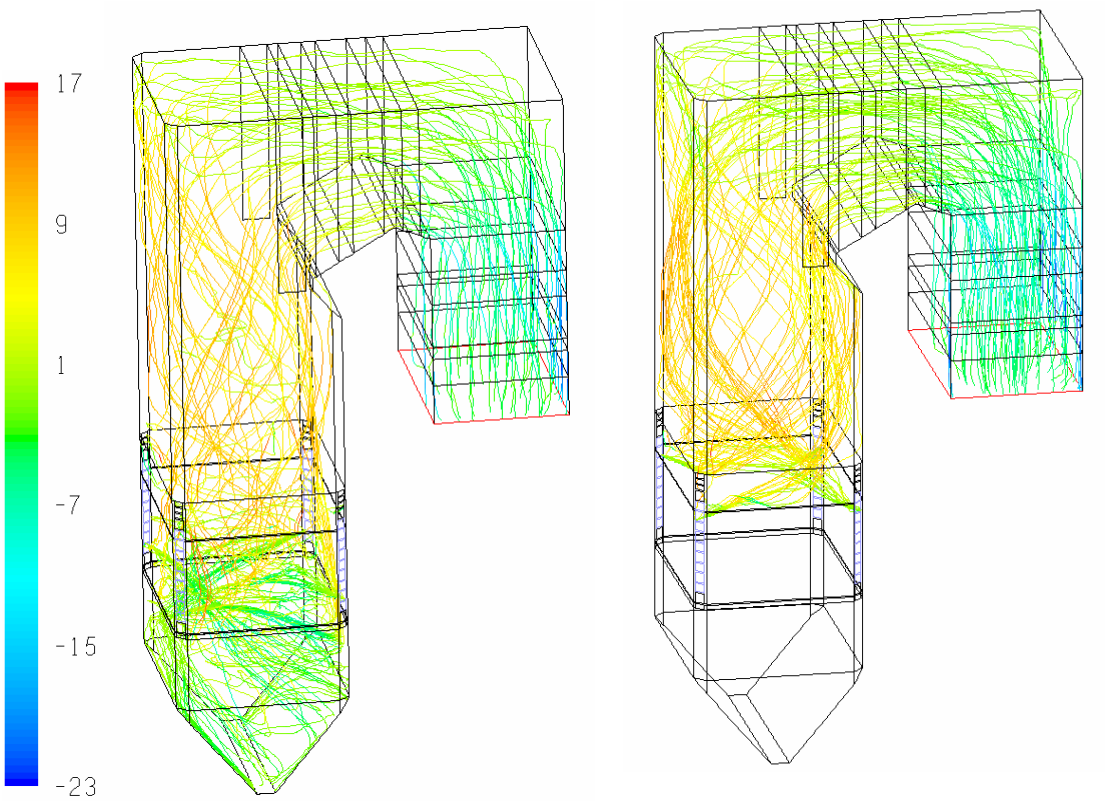

(a) Injected from last FA burner (b) Injected from first FA burner

Figure 3.12: Coal particle trajectories colored by z velocity (ms^{-1})of the particle

The flue gas and coal particles injected from the lower burners, initially circulate in the bottom of the furnace and the ash hopper, and eventually travel up through the high-temperature and swirling-flow region (so-called fire-ball) formed in the central region of

the furnace (Figure 3.12-a), while the flue gas and coal particles from the higher burners pass directly upwards from the fire-ball region (Figure 3.12-b). Model predicts that nearly 86% of the char and 100% volatile material were released in the burner section itself. The remaining 10% of char material was oxidized in section above the burner and the last 4% in the bottom section of the burner. As a result, the residence times of the flue gas and coal particles injected from the higher burners are shorter in comparison to the flue gas and coal particles injected from the lower burners. The mean residence time of the particles coming out with fly gas is around 11 s with standard deviation of 5 s and that falls down as bottom ash has mean residence time around 8 s with standard deviation of 13 s.

3.8.6 Species profile

The predicted concentration distribution of oxygen and carbon dioxide over a typical vertical plane is shown in Figure 3.13 and 3.14 respectively.

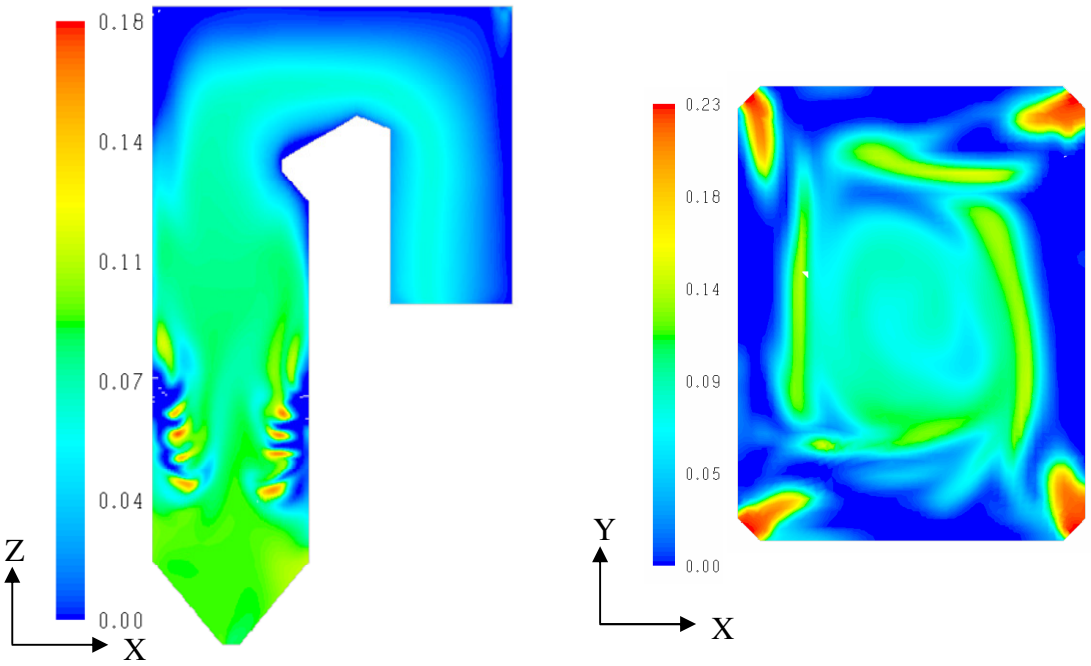

(a) Y = 6.5 m (b) Z = 25 m

Figure 3.13: O_2 concentration plot (mass fraction)

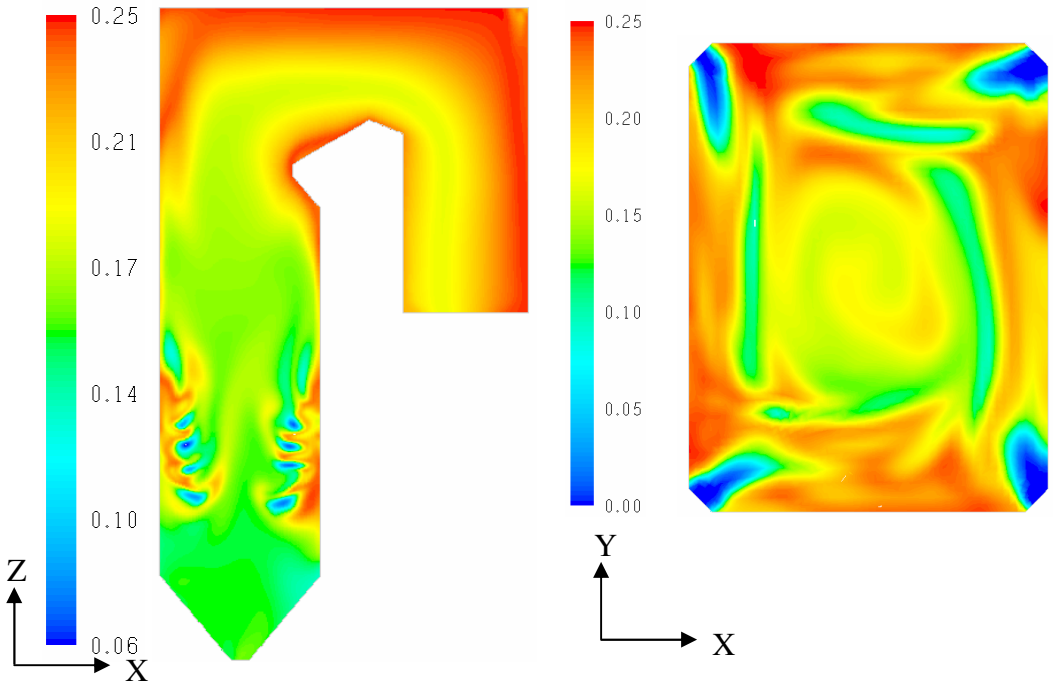

(a) Y = 6.5 m (b) Z = 25 m

Figure 3.14: CO_2 concentration plot (mass fraction)

It can be seen that the O_2 concentration is high near to the burner tip and it rapidly decreases as volatile material and char reacts with O_2 (Figure 3.13-b). An opposite trend to this was observed for the CO_2 concentration distribution (see Figure 3.14-b). The value of carbon dioxide increases from zero at the burner tip to nearly 24-25% along the length of the burner jet (Figure 3.14-b). The oxygen mass at the FEGT was ~4 (mole %) and 3.4 (mole %) at the boiler exit respectively.

3.8.7 Heat transfer to heat exchangers

Heat generated due to coal combustion reaction gets transferred to water wall and suspended super heater and Reheaters. The predicted heat transferred to internal heat exchangers are listed in Table 3.9 which shows that nearly 40% of total heat transferred is absorbed by water wall and rest is transferred to the heat exchangers tube bundles. The furnace section of the boiler is majorly radiation dominated and convective heat transferred plays small role in the overall heat transfer. Quantification of the same is given in Table 3.9 which shows that nearly 89% of the total energy absorbed by

waterwall is due to radiative heat transfer where as the LTSH absorbs nearly 63% of total energy due to radiation.

Table 3.9: Heat transferred to heat exchangers

Heat exchangers	Heat transferred (MW)	Convective heat transferred (%)	Radiative heat transferred (%)
Water wall	211	11	89
Platen SH	120	34	66
Front RH	70	40	59
Rear RH	30	45	57
Final SH	19	59	41
LTSH	41	37	63
Upper ECO	35	50	49
Lower ECO	14	45	56

3.8.8 Char burnout in boiler

The combustion performance in the boiler is justified by char burnout which is considered to be slower step among all the combustion processes. To combustion efficiency is expressed based on total conversion of char which is listed in Table 3.10.

Table 3.10: Char unburnt in ash

Total coal flow rate towards top (kgs^{-1})	37.86
Total coal flow rate towards bottom (kgs^{-1})	0.736
Total char flow rate towards top (kgs^{-1})	9.09
Total char flow rate towards bottom (kgs^{-1})	0.177
Char burnout at top (%)	95.00
Char burnout at bottom (%)	100.00

The simulation results shows that nearly 5% unburnt char is present ash.

3.8.9 Characteristics of crossover pass of 200 MW_e boiler

Most of the large capacity utility boilers use the four angle-tangential firing systems. The main advantage of this kind of the firing system is that it works efficiently for a wide variety of coals. The inherent strengths of the tilting tangential firing system are its high combustion efficiency, consistent thermal performance and low emissions. In this type of firing system, the fireball formed within the furnace delivers thermal energy uniformly to each of the furnace wall, independent of unit load or fuel input combinations. A feature unique to tangentially fired boiler is the ability to regulate furnace heat absorption for steam temperature control, which is done by tilting the fuel and air nozzle assemblies up or down automatically. Superheat and reheater temperatures can thus be controlled with minimal plant heat rate impact. Global furnace aerodynamics provides effective furnace volume utilization for higher heat absorption and lower bulk gas temperatures compared to wall-fired boilers. Complete combustion is assured by the combination of maximum residence time and vortex turbulence. But vortex turbulence of the tilted tangential firing system intensely affects the thermal load distribution in the convection horizontal gas passage (crossover pass), which increases the thermal load deviation. Development of high-capacity utility boilers, operating at high temperatures and pressures, results in increased thermal load deviation of the boiler in the lateral direction with horizontal gas passage. In spite of its many advantages, the thermal load deviation is inherent for the tangentially firing system and cannot be eliminated completely. The extreme steam temperature deviation experienced in the SH and RH of a utility boiler can seriously affect its economic and safe operation. This temperature deviation is one of the root causes of the boiler tube failures (BTF), which causes about 40% of the force power station outages (Xu et al, 2000). The steams temperature deviation is mainly die to the thermal load deviation in the lateral direction of the SH and RH. This variation is difficult to measure in situ using direct experimental techniques. Significant efforts have been expended to predict the BTF and to determine mechanisms responsible for the BTF by utility boiler companies, boiler manufacturers, and by academic researchers (Yin et al. , 2002; Dooley, 1997; Chen, 1997; Xu, 1994; Collins,1993; Liu, 1993; Wang, 1984, 1992 and 1993; Abbott et al., 1992; Yang, 1989 & 1991 and Bian, 1987;)

The CFD model was developed to simulate the various complex phenomena of tangentially fired boiler, including gas-solid turbulent flow, coal combustion and the radiative and convective heat transfer. The simulation results can be useful to understand overall flow field, temperature and species profile within the boiler and to predict one of the common problems which was discussed above of the gas temperature deviation in the crossover pass zone of the boiler. Hence the analysis of boiler CFD simulation results was performed to quantify of the extent of temperature deviation in the crossover pass section. The results are discussed below;

In tangentially fired boiler flow enters from the corner burners and forms rotating fireball type of structure in the horizontal plane of the combustion zone. This swirling flow leaves the combustion zone and while entering into the crossover pass the flow goes towards the right side wall. This leads to the uneven distribution of the flow in the entrance region of the crossover pass where Platen SH and Reheaters are located. Vector plot of the velocity magnitude over an isoplane at height z = 47 m is shown in Figure 3.15-a. The flow from the furnace section enters the platen super heater from front wall and the vector plot in Figure 3.15-a shows the tendency of the flow going toward the right side wall. For the boiler as the firing is done in counterclockwise and hence the flow shifts towards the right side wall.

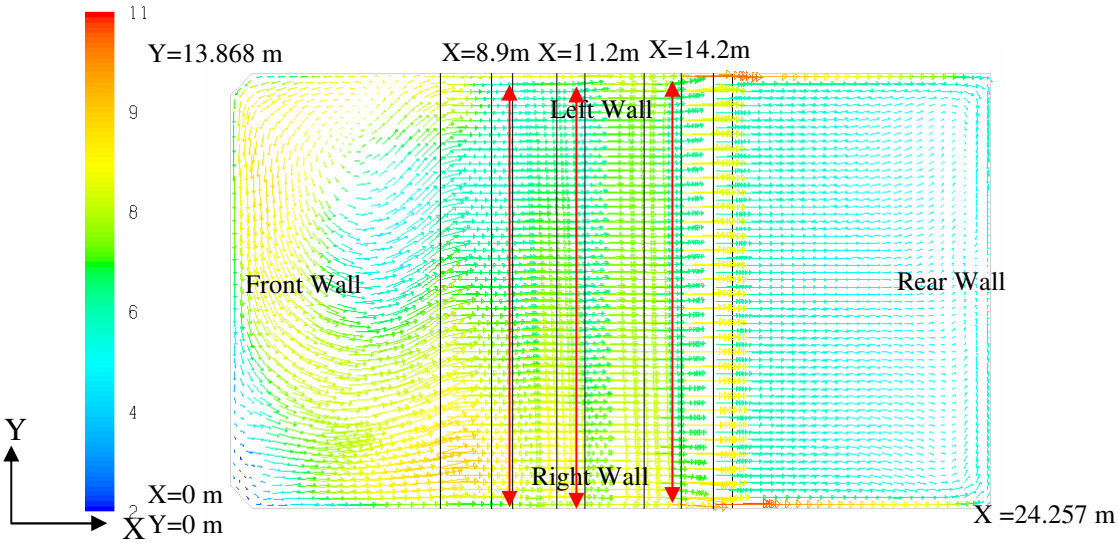

(a) Velocity magnitude vector plot (ms^{-1})

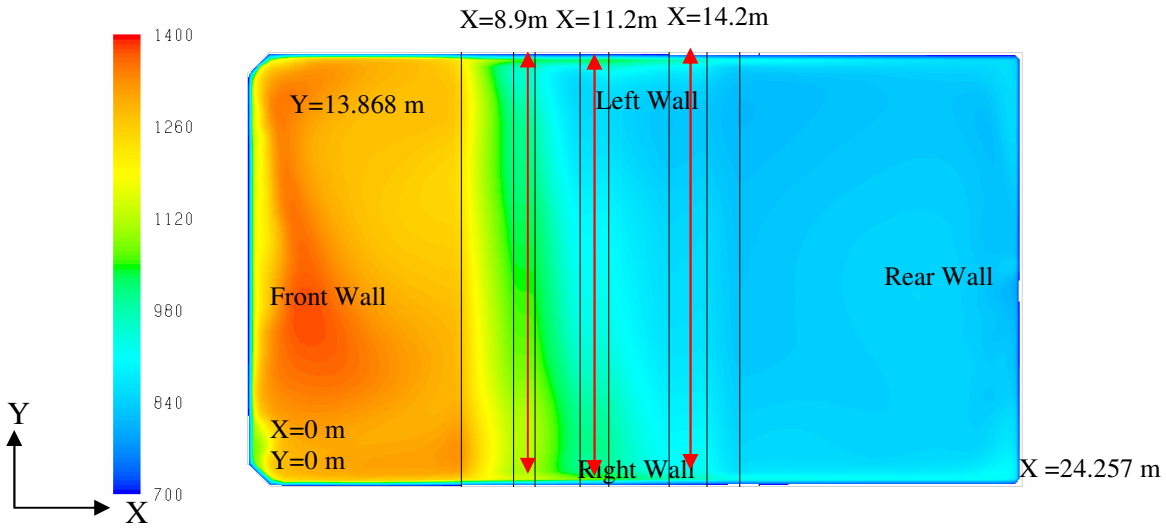

(b) Temperature contour plot (K)

Figure 3.15: Simulation result at crossover pass at plane Z = 47 m

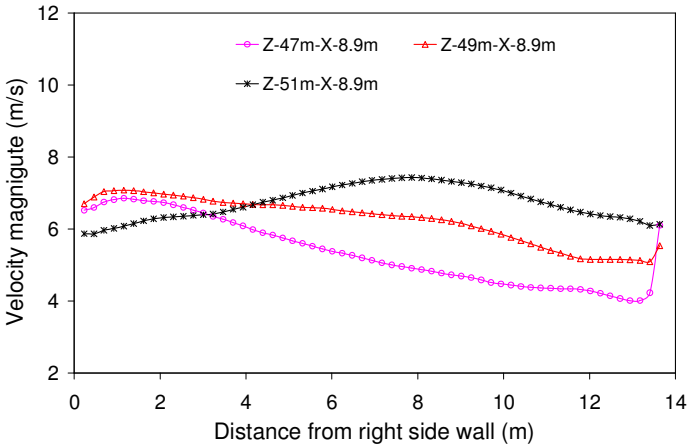

(a) X = 8.9 m

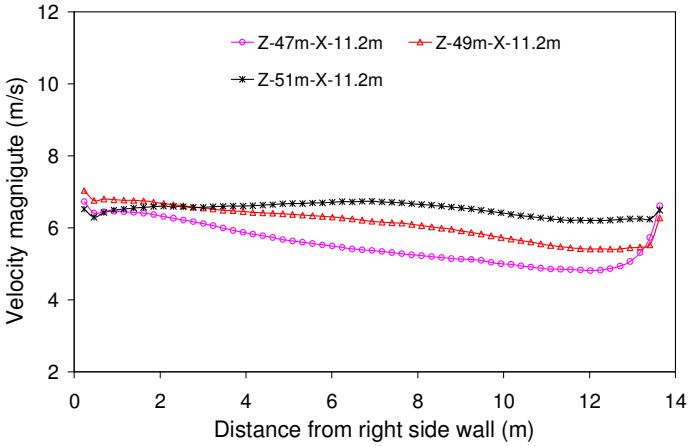

(b) X = 11.2 m

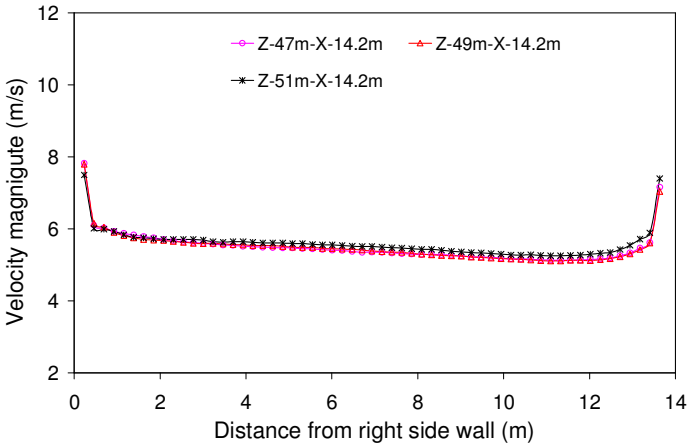

(c) X = 14.2 m

Figure 3.16: Velocity magnitude line plot at crossover pass

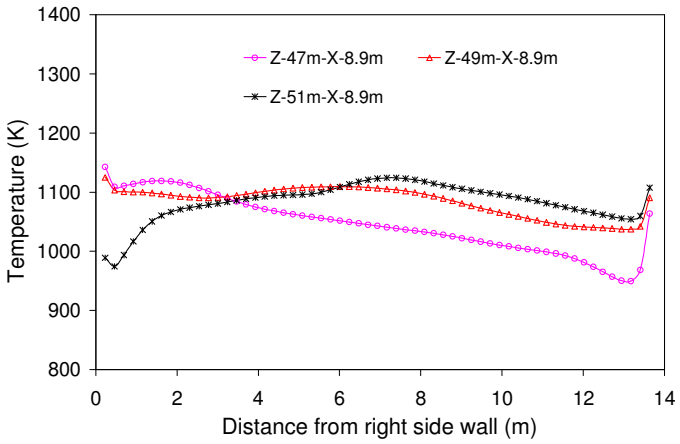

(a) X = 8.9 m

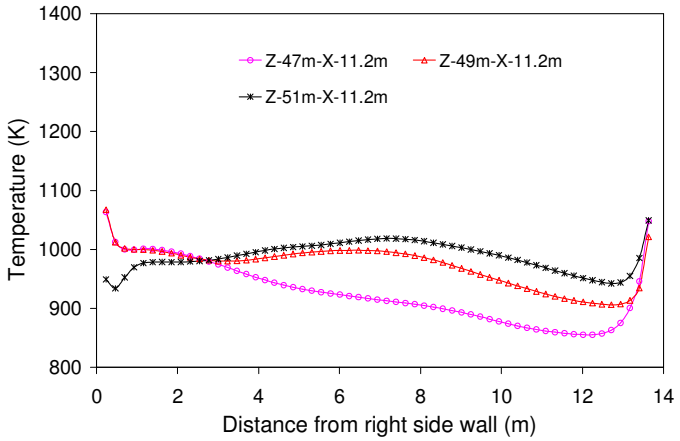

(b) X = 11.2 m

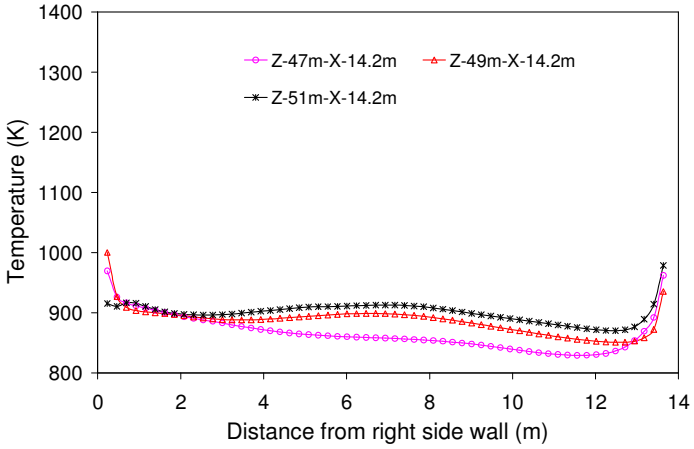

(c) X = 14.2 m

Figure 3.17: Temperature profile along a line plot at crossover pass

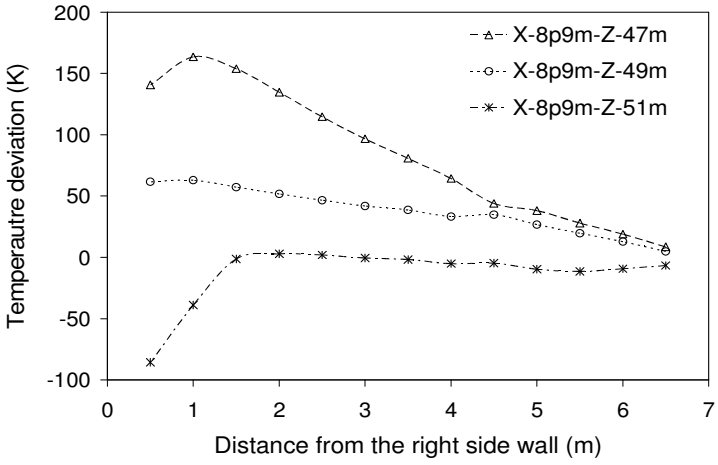

(a) X = 8.9 m

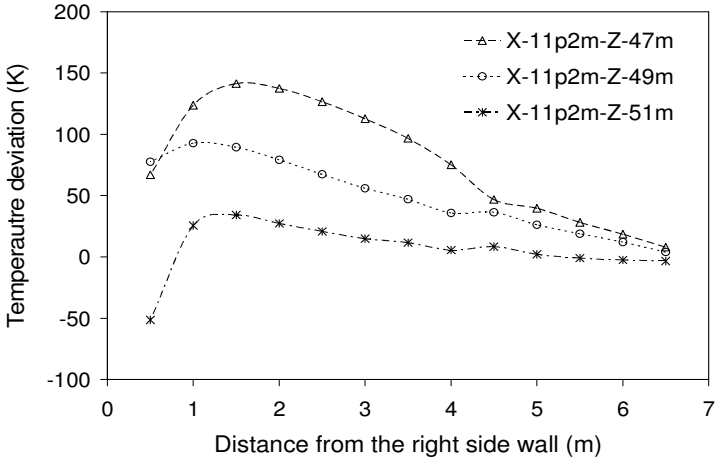

(b) X = 11.2 m

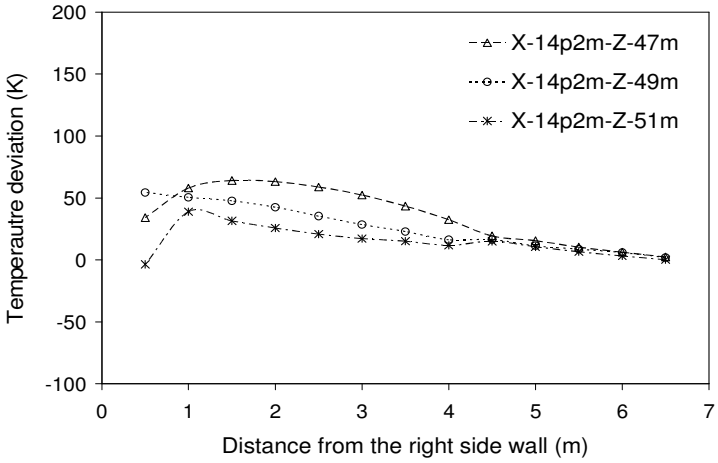

(c) X = 14.2 m

Figure 3.18: Plot of temperature deviation from right side wall of the boiler at various X

Figure 3.16 shows the velocity plots on the isolines drawn at various (heights) Z locations (z = 47 m, 49 m, 51 m) at particular X distance, (a) x = 8.9 m (before FRH), (b) 11.2 m (before RRH) and (c) 14.2 m (before Final SH) from the front wall. When the flow passes through the Platen SH, the flow gets guided due to presence of the tube bundle and starts aligning between right and left wall. But the effect of imbalance flow gets carried forward to the Reheater and the high velocity zone can be observed in Figure 3.16-b at right side wall. When flow comes out of the Reheater and goes to the Final SH, Figure 3.16-c shows that the left-right imbalance has almost diminished.

The effect of this mass imbalance leads to high temperature in the right side wall and comparatively a cooler left side wall. The temperature profile over an isoplane at height Z = 47 m is shown in Figure 3.15-b. The profile clearly shows a hot spot towards the right hand side wall to the entrance of the Platen SH. This leads to comparatively hotter gas contact with right wall side tubes than left side. Similar to velocity, the temperatures was plotted at various isolines and are shown in Figure 3.17. This clearly indicate that the difference in the temperatures any similar locations from left and right side wall.

The quantification of imbalance of flow was done by plotting the temperature deviation along any X isolines. The two temperature values at nearly same locations from the right and left walls were compared and the difference between right side wall and left side wall temperatures was termed as temperature deviation. Plot of the same for various X isolines is shown in the Figure 3.17. The effect was prominently observed at the entry of the Front RH and rear RH that shows the temperature deviation as high as >150 K (maximum ~166 K) at height Z = 47 m (Figure 3.18-a & b). As we move up towards the roof of the boiler the deviation decreases. When the flow reaches at the entry of the Final SH, it was observed that he deviation decreased to around <50 K from right side wall. Hence this study concludes that the maximum deviation of ~166 K was observed at the entry of Front RH at distance Z = 47 m and X = 8.9 m. These results show good comparison with the literature value of 150 K for 210 MW_e (Yin et al., 2002).

3.9 Conclusions

CFD model was developed to simulate the 200 MW_e tangential coal fired boiler. The boiler performance at the normal operating conditions was simulated. The different characteristics like temperature profile, species concentration, flow field, uneven temperature distribution in crossover pass were predicted. Sensitivity study at operating parameters like excess air and heat load was performed. The important observations of the study are highlighted below;

I. Comprehensive CFD model was developed for simulating coal combustion in boiler and it was based on following approaches,
    a. RNG k-ε model for turbulence
    b. E-L approach with two-way coupling
    c. P-1 radiation model
    d. Single step kinetic devolatilization
    e. Kinetic/diffusion controlled char oxidation
    f. Finite rate/ Eddy dissipation rate model for gas phase combustion

II. Model was able to predict the temperature & species distribution, fireball formation, coal particle trajectory , crossover pass characteristics and heat transferred to internal heat exchangers

III. At normal operating conditions, 200 MW_e shows maximum 166 K temperature deviation in the crossover pass which are generally present in similar capacity boilers.

Chapter 4

Effect of Operating Conditions on Boiler Performance

4.1 Introduction

CFD simulations of 200 MW_e pulverized coal fired boiler in Chapter 3 have led to various insights to the behavior of complex processes occurring within the boiler. The various steps and issues involved in the development of comprehensive CFD model for boiler are discussed in previous chapter. The model was able capture various key features like temperature and species profile, unburnt char in ash, heat transfer and crossover pass characteristics of the boiler and emerged as robust tool for the analyzing performance of pc fired boiler. The overall performance of boiler is dependent upon many factors including operating conditions such as local oxygen concentration, coal quality & its properties, burner positions, thermal load, etc. The quantity of coal and air can be monitored and controlled before introduction into the boiler. When the coal and air are mixed, combustion takes place in the furnace, and the next monitoring point is the furnace exit gas temperature (FEGT, at height z = 41 m in the furnace), which has a major impact on boiler performance and reliability. The management of FEGT is linked to the optimum controls to be exercised in operating parameters. The undesired conditions like increased slagging/fouling/corrosion rate of the water wall and heat exchanger tubes occurs if there is a deviation in the desired FEGT value and that also leads to creep damage and loss of efficiency due to higher boiler exit temperature.

CFD models can be useful to perform numerical investigation of effect of operating conditions on boiler performance. Such studies are useful to optimize the operating conditions, reduce pollutant emissions, investigate malfunctions in the equipment, evaluate different corrective measures and also improve the design of new boilers. This study presents the extension of the CFD modeled discussed in Chapter 3 to simulate the effect of key operating parameters on boiler performance. The details are discussed in next section.

4.2 Sensitivity study for effect of operating conditions

CFD model discussed in the Chapter 3 was considered as the base case with 20 % excess air and zero operating tilt. The sensitivity studies were performed by identifying

operating parameters such as Excess air, burner tilt, boiler heat load and coal blends that plays key role in the performance of pulverized coal fired boiler. The simulation results are discussed below;

4.2.1 Excess air (i.e. Fuel/Air ratio)

The optimum excess air or Fuel/Air ratio that is to be fed to the boiler is important factor as it affects the loss of combustion in the form of unreacted char and pollutant formation. The excess air also absorbs the part of combustion energy to attain the combustion temperature. Hence, it was necessary to characterize the sensitivity of the excess air on the boiler performance. The base case was simulated with 20% excess air in chapter 3 and over here sensitivity studies were performed for excess air of 10% and 5%. The operating conditions are listed in Table 4.1.

Table 4.1: Operating conditions for excess air

	Excess Air		
	20% *	10%	5%
Fuel Air mass flow rate (kgs^{-1}) (Temperature 350 K)	75	69	66
Auxiliary Air mass flow rate (kgs^{-1}) (Temperature 550 K)	149	135	129
Coal flow rate ($kg\ s^{-1}$) (Temperature 350 K)	39	39	39
* standard operating condition			

The effect of excess air on the temperature distribution along the height of the furnace is shown Figure 4.1-a. The results show that the crossectional average temperature across the furnace height increases by 50-100 K when excess air was changed from 20% to 5% and such effect can be strongly observed in the bottom section of the furnace (below burner zone). The FEGT temperature was changed from 1327 K to 1338 K when excess air was changed from 20% to 5%. The effect on the oxygen concentration was more profoundly observed in Figure 4.1-b where the cross-section average mass fraction of O_2 was plotted along the height of the furnace.

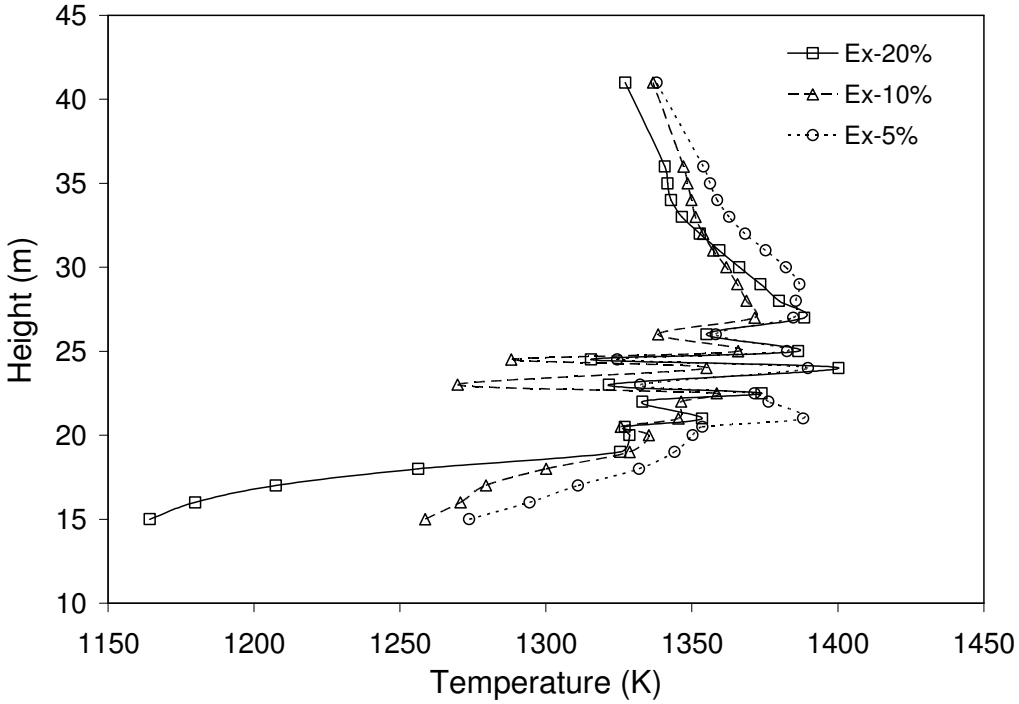

(a) Crossectional average temperature

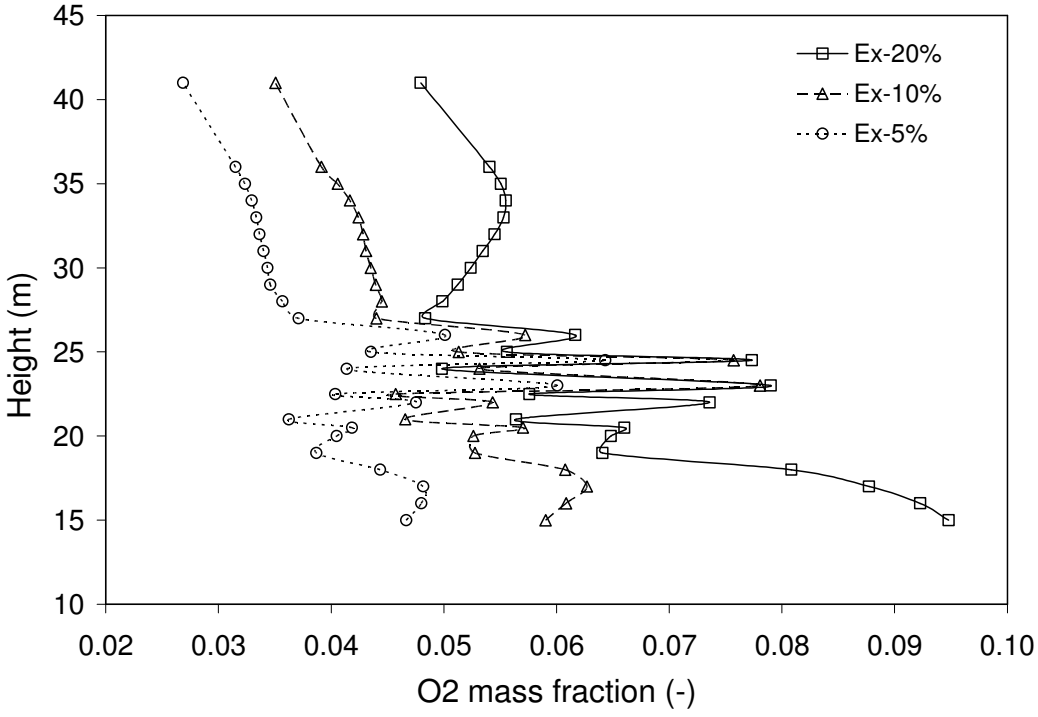

(b) Crossectional average O_2 mass fraction profile

Figure 4.1: Effect of excess air on boiler performance

The FEGT O_2 mass fraction was changed from 0.04791 to 0.0267 when the excess air was changed from 20% to 5%. The O_2 mass fraction at the plane Z = 15 m at top of the hopper was changed from 0.095 to 0.047 when the excess air was changed from 20% to 5%.

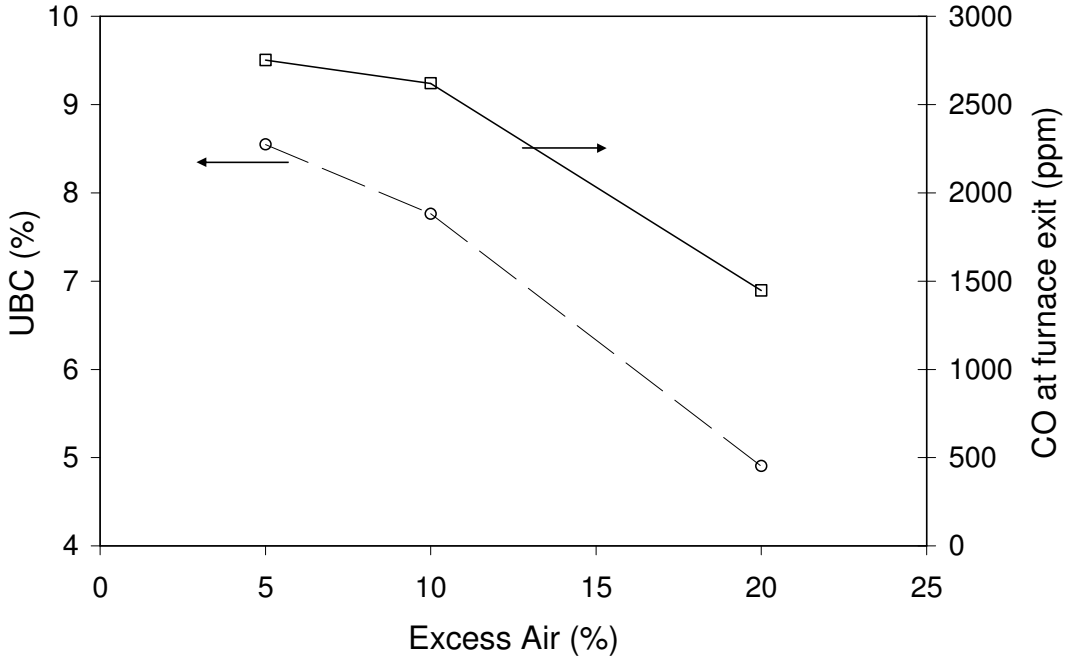

Figure 4.2: Effect of excess air on CO concentration (ppm) at the furnace exit (FEGT) and total char burnout

The reduction in the oxygen concentration affects the CO level in the furnace and it was observed that the CO level at the FEGT was increased from 1448 ppm to 2753 ppm (Figure 4.2). The excess air affects the combustion efficiency of the boiler and it was observed that the total unburnt char (UBC) in the ash was increased from 5 % to 8.5 % was reduced from 20 % to 5 % (Figure 4.2).

4.2.2 Burner tilt

Aerodynamics is crucial for the performance of the pulverized coal (pc) fired boilers and it can be drastically influenced by position and tilt of the jets. The burner tilting is synchronizing the movement of air nozzles in vertical direction (upward/downward) in

angle θ less than ± 20^{o} (Figure 4.3). The position of flame center in the furnace can be changed to adjust the superheat and reheat temperature. It is useful in changing the combustion conditions and heat release rate in the burner area, and in decreasing slagging and overheat temperature. If wrongly designed, serious ash slag will occur in the ash hopper when the nozzles are tilted downwards. Hence it is important to characterize effect of burner tilt on the performance of 200 MW_e boiler. In previous chapter, CFD simulation of 200 MW_e boiler was performed with zero burner tilt and was considered as base case. The effect of burner tilt on boiler performance was systematically quantified in terms of the overall heat transferred to different sections of the water wall in furnace and coal burnout.

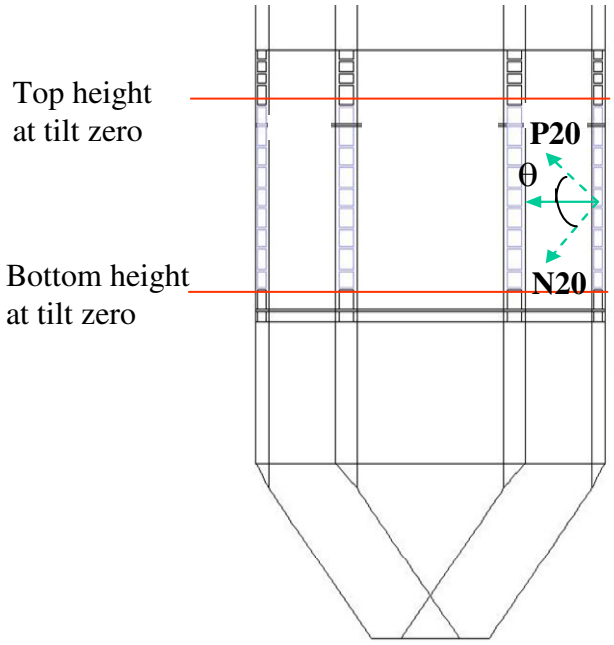

Figure 4.3: Schematic showing burner tilt

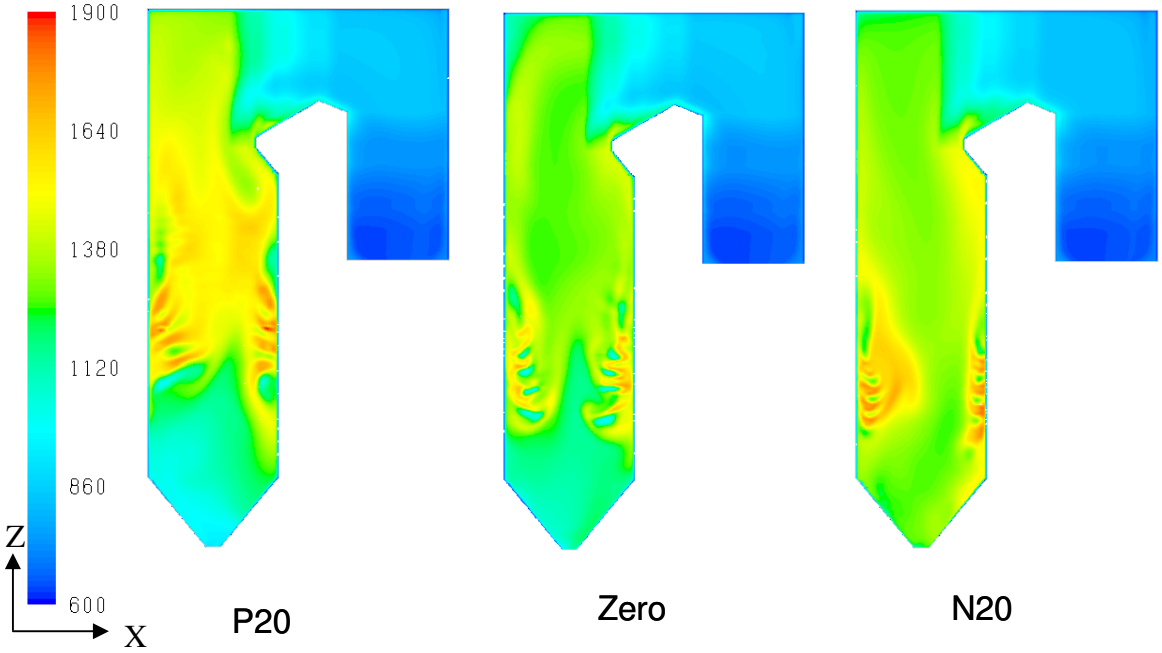

(a) Temperature (K) profile at plane Y= 6.5 m

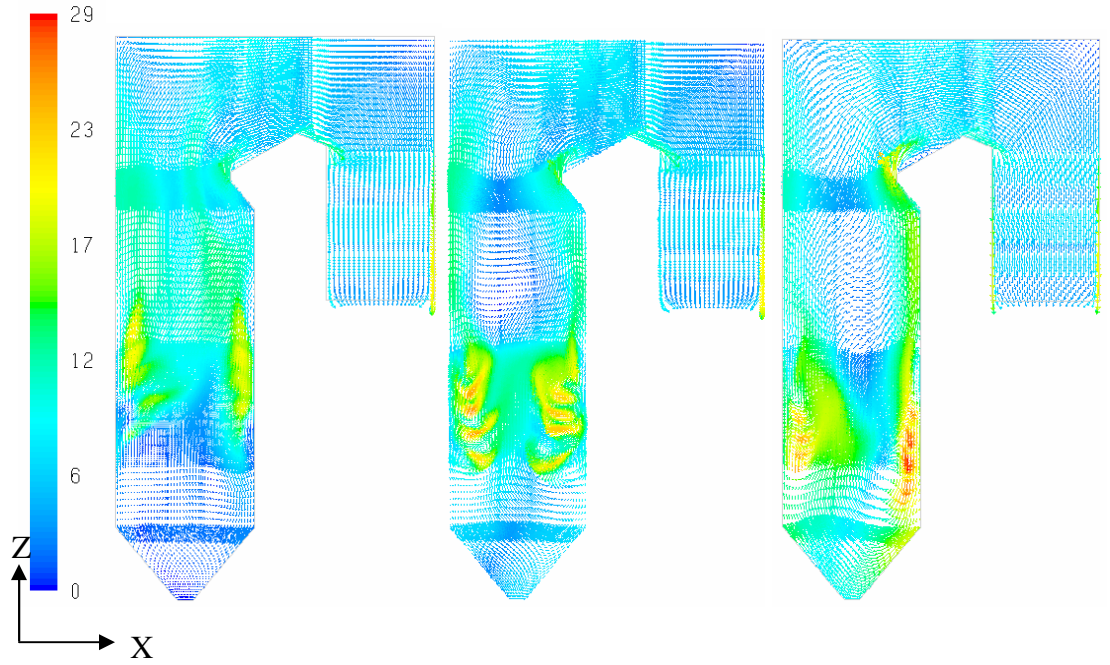

(b) Velocity profile (velocity magnitude, ms^{-1}) at plane Y = 6.5 m

Figure 4.4: Effect of burner tilt on boiler performance

The boundary conditions are listed in Table 4.2 and 4.3.

Table 4.2: Velocity boundary conditions (for all burner tilts)

	Fuel Air & Coal				Auxiliary Air			
Corner number	1	2	3	4	1	2	3	4
V_x	6.221	-8.00	-6.221	8.00	18.43	-23.69	-18.43	23.69
V_y	-10.353	-8.58	10.353	8.58	-30.67	-25.40	30.67	25.40

Table 4.3: Z velocity (V_z in ms^{-1}) boundary conditions (Burner tilts)

	Fuel Air & Coal		Auxiliary Air	
Tilt degree	1 & 3 corner	2 & 4 corner	1 & 3 corner	2 & 4 corner
+20	4.131	4.011	12.237	11.881
+10	2.097	2.036	6.213	6.032
-10	-2.097	-2.036	-6.213	-6.032
-20	-4.131	-4.011	-12.237	-11.881

Effect of burner tilt was simulated by changing the inlet flow velocity conditions such that the fuel air, coal particles and auxiliary air were injected at an angle of $+20^o$, $+10^o$ in upward direction and -10^o, -20^o in downward direction with reference to horizontal position. The change in burner tilt shifts the combustion zone in upward or downward direction affecting the overall flow characteristics of the boiler.

Figure 4.4-a shows the effect of burner tilt on the overall temperature profile in the boiler at plane Y, y = 6.5 m. Results clearly shows that the combustion reaction zone shifts away from the burner zone and that cause the movement of the hot zone in the furnace. This affects the heat transfer to water wall characteristics of the furnace. Figure 4.4-b shows the velocity magnitude vector plot at Y plane, y = 6.5 m for burner tilts $+20^o$, 0^o

and -20^{o}. According to the positive or negative tilt the flow will be directed towards the upper section or hopper section of the furnace.

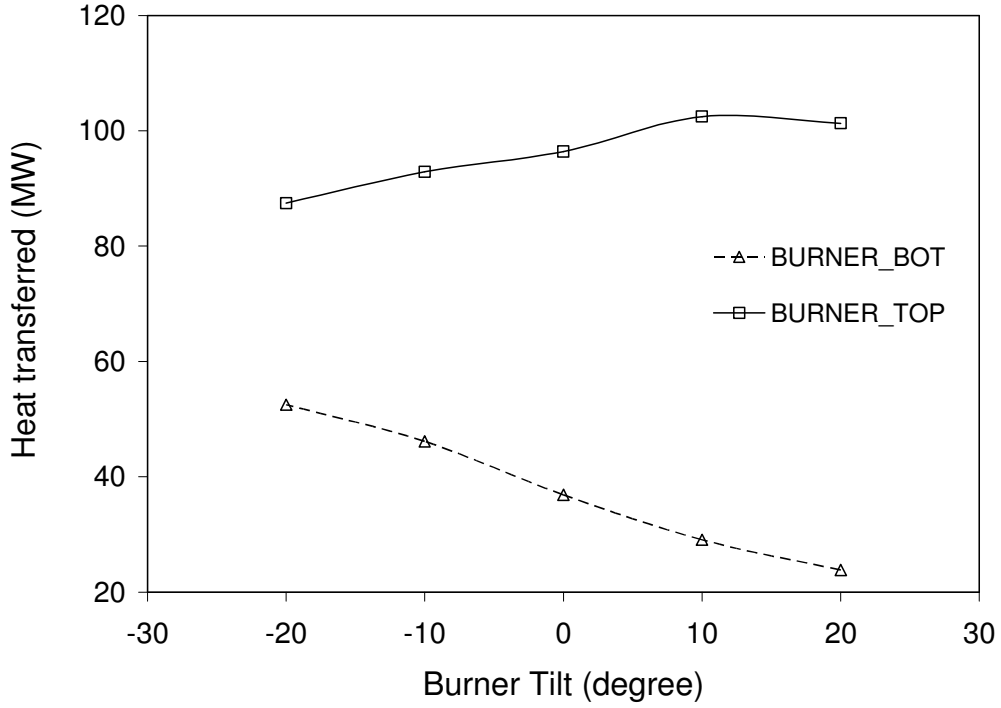

Figure 4.5: Effect of burner tilt on heat transferred to water wall in furnace zone

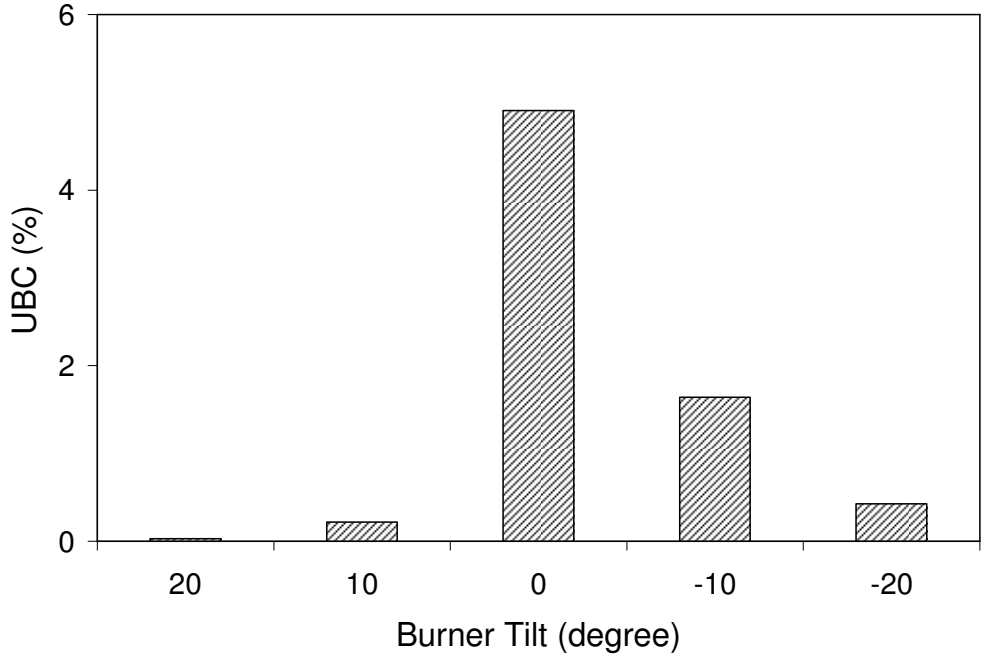

Figure 4.6: Effect of burner tilt on total unburnt char (UBC) in the boiler

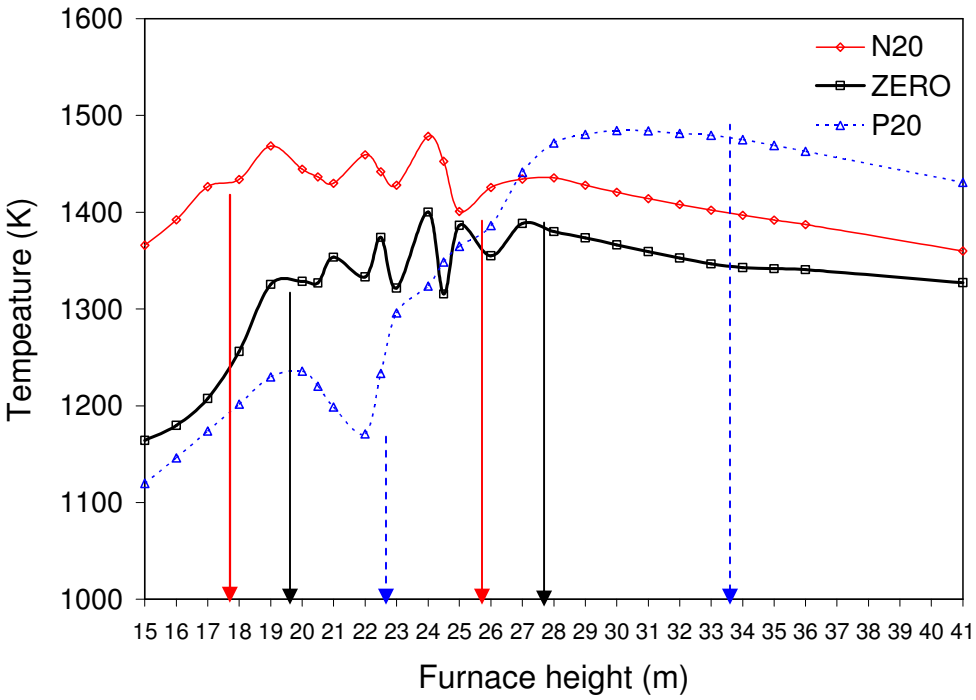

Figure 4.7 : Effect of burner tilt on crossectional average temperature (K)

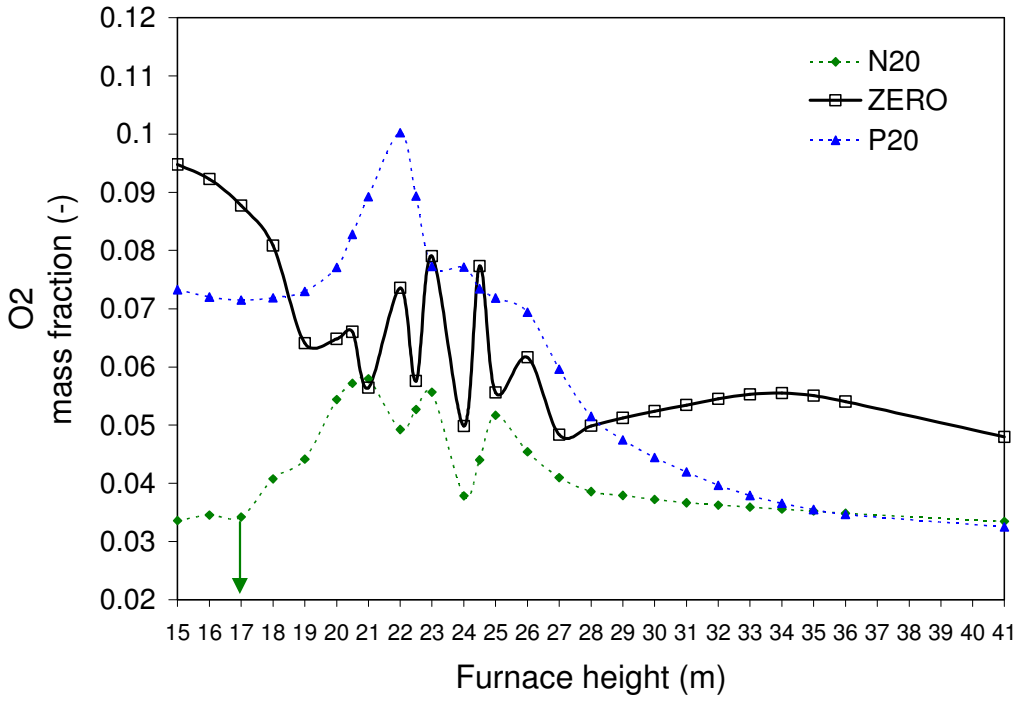

Figure 4.8 : Effect of burner tilt on crossectional average O_2 mass fraction

Figure 4.5 shows the effect of combustion zone shifting affects the heat flux distribution to the waterwalls above and below the burner section. Results show that the heat transfer to waterwall section above the burner (height from z = 27 m to 52 m) increases from 87 MW to 101 MW and for section below the burner (height from z = 9 m to 20 m) to decreases from 53 MW to 23 MW when the burner tilt in changed from the -20 to +20 respectively. Figure 4.6 shows the effect of burner tilt on the unburnt char (UBC). It was observed that, for the base case of zero tilt the UBC was ~ 5%. As discussed above, the burner tilt changes the overall dynamics gas and solid flow, temperature and species profile in the boiler. It has significant impact on the residence time of particle in combustion zone and the local history of temperature and oxygen that particle passes while moving through the furnace. It was observed that the total UBC decreases when the burner tilt is shifted either up or down (Figure 4.6). The results for the +20 tilt shows lowest UBC was observed than that of any other tilt. Figure 4.7 and 4.8 shows the crossectional average temperature (T_{plot}) and O_2 concentration profile (O_{2plot}) respectively along the height of the furnace when burner tilt were shifted from ZERO to $\pm 20^{o}$.

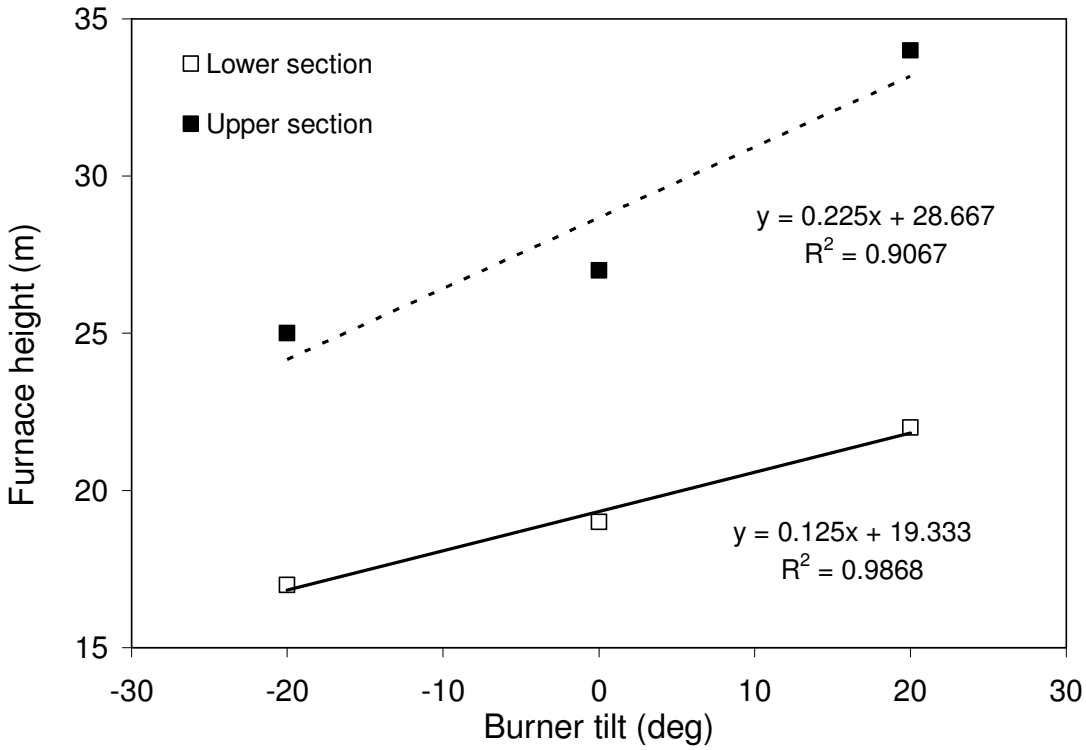

Figure 4.9: Effect of burner tilt on shifting of hot zone

To quantify the effect of burner tilt on the shifting of reaction/hot zone in the furnace, methodology was proposed to obtain a correlation from analyzing simultaneously the T_{plot} and O_{2plot}. First, the ZERO tilt T_{plot} was observed such that the upper and lower bounds of the combustion/burner section can be marked. To mark the lower section for ZERO tilt on the T_{plot}, the point after which the average plane temperature starts decreasing suddenly was considered as lower bound for ZERO tilt. This observation was also confirmed with O_2 plot where the O_2 concentration rises suddenly in the lower section. The lower bound for ZERO tilt case was found to be 19 m. Similar approach was useful at the upper section where the average furnace temperature starts decreasing was marked as upper bound of the reaction/hot zone and observed to be 27 m. For the zero tilt, reaction/hot zone was found in the burner section where array of physical burners (FA & AA) were injecting coal and air into the furnace. Hence to understand movement of these upper and lower boundaries with burner tilts, the simulation results of average plane temperature and O_2 concentration for +20 and -20 were plotted on the T_{plot} and O_{2plot}. Similar approach that was used for the ZERO tilt was applied on T_{plot} and O_{2plot} to estimate the lower and upper bound. The results obtained from these analysis was then fitted to a linear equation to obtain a generalized equation to predict the movement of the reaction/hot zone when the burner tilts are applied (Figure 4.9).

The equations obtained for the movement of the upper and lower boundaries are given below,

The shift of top plane of the hot zone;

$$Z = 0.225\,\theta + 28.667$$

The shift of bottom plane of the hot zone;

$$Z = 0.125\,\theta + 19.333$$

Where Z is the vertical height, θ is the burner tilt angle in degrees (generally -20 to +20). Hence burner tilt plays important role in the boiler performance. The effect of the burner tilt was quantified in the form of correlation to predict the shift in the hot combustion zone according to the movement of the burner. This equation is specific to the

tangentially fired 200 MW_e boiler of similar configuration as the aerodynamics of other scale (350 MW_e, 500 MW_e) boilers may be different. But similar methodology can be adapted to other scales of the boiler in order to predict the shift in the combustion zone due to change in burner tilt. This correlation has great importance in the development of phenomenological model as such correlations can be directed implemented in phenomenological model.

4.2.3 Effect of boiler heat load

The influence of boiler load reduction from normal operating condition of 200 MW_e has been numerically examined. The load was decreased by reducing the air and coal flow rate by first 20% and then by 40% distributing evenly to each burners in the operation. The operating conditions are listed in Table 4.4.

Table 4.4: Operating conditions for boiler heat load

	Turndown by	
	20%	40%
Fuel Air mass flow rate (kgs^{-1}) (Temperature 350 K)	60	45
Auxiliary Air mass flow rate (kgs^{-1}) (Temperature 553 K)	119.2	89.4
Coal flow rate (kgs^{-1}) (Temperature 350 K)	31.2	23.4

The average furnace exit temperature (FEGT) changed from 1327 K of standard operating condition to 1252 K for 40% turndown condition (Figure 4.10-a). Compare to the full scale, the crossectional average temperature for 40% turndown decrease by nearly 100 K. The turndown has decreased the gas and particle velocity in the boiler which increases the residence time of the particle. The mean residence time of the particle for full scale, 20% and 40% turndown was found 11 s, 13 s and 19 s respectively and correspondingly char combustion was found to be 95%, 97% and 97.7%. Figure 4.10-b shows the comparison for the heat transferred to the water wall and platen superheater.

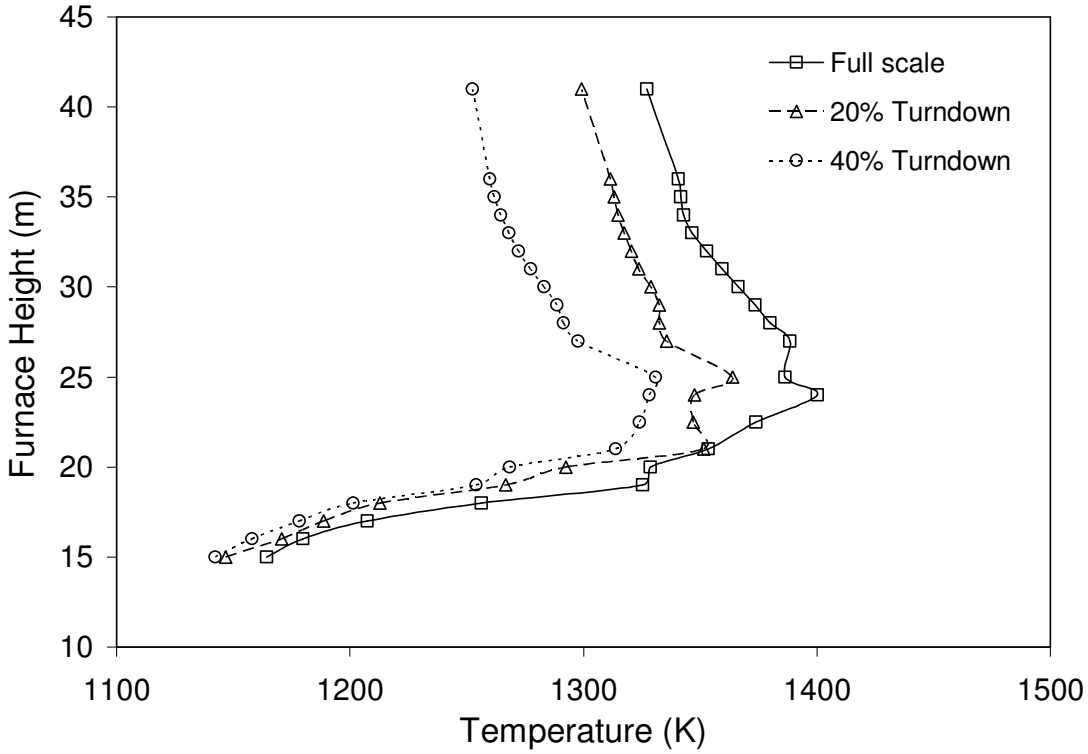

(a) Crossectional average furnace temperature (K)

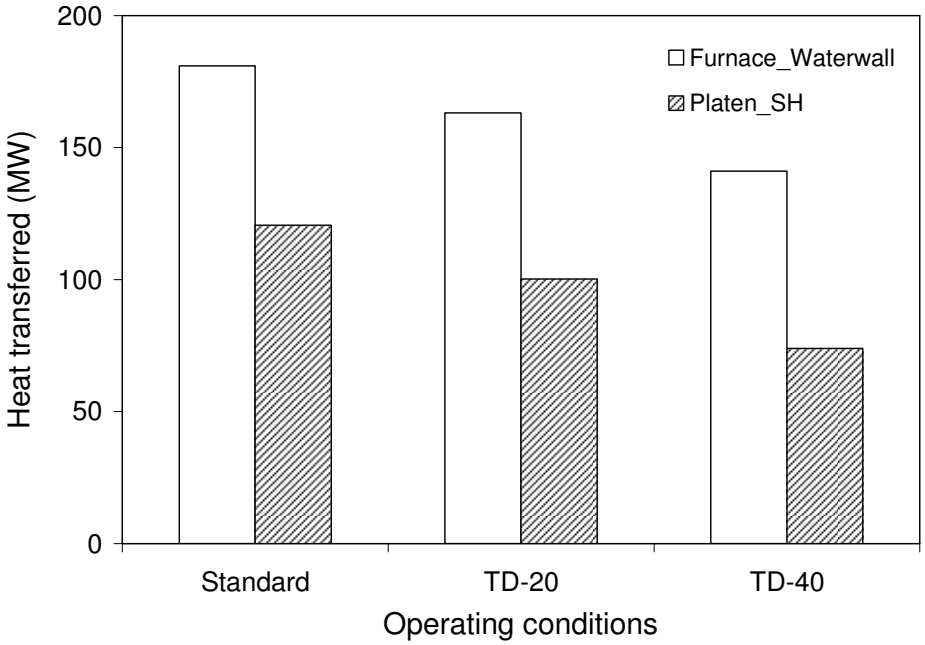

(b) Heat transferred to waterwall of furnace and platen SH

Figure 4.10: Effect of boiler heat load on boiler performance

The total heat transfer to the waterwall in furnace section decreases from 181 MW to 141 MW and for platen super heater the heat transfer decreased from 120 MW to 74 MW.

4.2.4 Coal Blends

Blending of various types of coal at utility boilers has been widely adopted as a viable option due to its economical and environmental impact (Wall et al., 2001). It gives better control over the pollutant emissions, coal quality and ash deposition. It is useful in improving combustion behavior, enhancing fuel flexibility, mitigating operation problems (e.g. ash deposition), and reducing the fuel cost. Power plants may also passively use blended coals provided by coal suppliers who use coal blending to make a cheaper coal or to modify the properties of a coal with a known problem, such as slagging, sulphur content, volatile content and burnout problems. In the last decades, extensive studies have been performed to characterize the combustion of coal blends (Su, *et al.*, 2003 & 2001; Wall et al., 2001 and Carpenter, 1995). It has been recognized that the properties related to fuel composition (e.g. proximate and ultimate analysis data, heating value, etc.) remain additive after blending, whilst many characteristics related to the combustion exhibit non-additive, i.e. synergistic, behaviour. For example, ignition, flame stability, slagging and fouling cannot be predicted by the additivity . Previous studies show that the combustion behavior of a coal blend is complex than combustion of single coal and its effect on boiler performance are imperfectly understood and which has been motivating developing reliable techniques to predict and evaluate the combustion behaviors of coal blends for process optimization, coal selection and blending .

The experimental approaches have been employed to assess the combustion performance of pulverized coal blends fired in boilers based on bench-scale (Milenkova et al., 2003; Rubiera et al., 2002; Peralta et al., 2002 & 2001; Arenillas et al., 2002; Su, et al., 2001; Artos, 1993; Beeley et al., 2000 and Haas et al., 2001), pilot scale (Ikeda et al., 2003; , Su, et al., 2001; Beeley et al., 2000 and Maier et al., 1994) or on full scale (Helle et al., 2003 and Beeley et al., 2000) data. From the experimental data, some empirical indices, using such as volatile matter content, fuel ratio and maceral composition, were also derived to empirically predict the ignitability, flame stability, and combustion of coal

blends. However, bench-scale experiments were found difficult to reproduce the combustion of coal blends prevailing in practical pulverized fuel furnace. For instance, normal drop tube furnace cannot operate with high particle concentration comparable to that in real furnaces, therefore is not adequate to represent the interactions between coal particles (Artos, 1993 and Haas et al., 2001). Investigation of combustion characteristics of blends via experimental methods is typically expensive & can be labour-intensive, also it can be dangerous to extrapolate the pilot scale data directly to full scale boiler. The conclusions are often difficult to extrapolate to unknown coals and blends. The empirical indices, validated by a limited number of experimental data, hence, may not be very reliable (Sheng et al., 2004).

Hence, it is requisite to predict the combustion behavior of blends of different rank coal and of high and low ash content coals before firing them in boiler such that any unforeseen problems can be avoided. Another technique, which potentially can be an accurate and cost effective tool in analysis of coal blends, is computation fluid dynamics (CFD) modeling. Over the years, the CFD has gained its reputation of being an effective tool in identifying and solving problems related to pulverized coal combustion and the details of the same was discussed in the earlier chapters of the thesis. CFD modeling of coal blends, unfortunately, attracted less attention and only a couple of works (Shen et al., 2009; Backreedy et al., 2005; Sheng et al., 2004; Arenillas et al., 2002 and Beeley et al., 2000) have been reported in the open literature. Beeley et al. (2000) modeled the combustion of coal blends in a pilot-scale test furnace based on two separate distinct coal streams with inputs of individual component properties. Arenillas et al. (2002) evaluated the application of CFD to model the combustion of binary coal blends in a bench-scale drop tube furnace (of internal diameter 20 mm and length 1420 mm) to predict the NO_x emissions and char burnout. In their simulation, one mixture fraction/pdf (probability distribution function) approach was used to model the combustion process and the blend was represented only as a single coal with properties obtained by weighted averaging relevant properties of the component coals, without adequate description of the chemical and physical interactions between components. Consequently, the non-additivity particularly from widely different rank coals was not reproduced. Sheng et al. (2004)

have simulated pc combustion in a pilot-scale furnace (150 kW down fired furnace) and the predictions were compared and also validated against the measurements on the ignition, burnout and NO_x emission from the combustion of coal blends in the furnace. Backreedy et al. (2005) demonstrated with experimental validation that the coal model for coal blends could be applied successfully to both an entrained flow reactor (of internal diameter 40 mm and length 2000 mm) and an industrial furnace (350 MW_e). Recently, Shen et al. (2009) has simulated pulverized coal combustion in blast furnace and successfully validated the coal burnout with experimental data. These are the encouraging developments over last decades that have taken place to apply CFD tool to simulation pulverized coal combustion in furnaces.

More such studies are required to make CFD as a robust tool for predicting the burnout behaviour of various types of coal especially where presently fired high ash coal can be blended with low ash coal and high volatile coal that will help to reduce the pollutant emissions. Hence in this work, 3D CFD model was developed to simulate 200 MW_e tangentially fired boiler when fired with coal blends of sub bituminous coal (High ash, medium volatile) and Imported lignite (low ash, high volatile).

Table 4.5: Coal composition for blends

Sub bituminous (Indian)				Lignite (Imported)			
Proximate		Ultimate		Proximate		Ultimate	
Components	Wt. %	Components	Wt. %	Components	Wt. %	Components	Wt. %
Fixed carbon	26.9	C	37.2	Fixed carbon	44.1	C	62.3
Volatiles	21.7	H	2.4	Volatiles	41.3	H	3.8
Ash	47.5	N	0.67	Ash	4.5	N	1.18
Moisture	3.9	S	0.15	Moisture	10.1	S	1.15
		O (by diff.)	8.18			O (by diff.)	17.0
		HHV ($kcalkg^{-1}$)	3260			HHV ($kcalkg^{-1}$)	5840

The properties of the coal are listed in Table 4.5. The kinetic parameters required for coal combustion was adopted from literature are listed in Table 4.6 and the operating conditions are shown in Table 4.7. The PSD of coal is given in Table 3.4.

Table 4.6: Kinetic parameters for imported coal (Lignite)

Devolatilization (Zhang et al., 1991)		Char oxidation (Visona et al.,1999)	
A_v (s^{-1})	E_v (J $kmol^{-1}$)	A_c ($kgm^{-2}s^{-1}Pa^{-1}$)	E_c (J $kmol^{-1}$)
1.34×10^{5}	7.41×10^{7}	0.0042	7.55×10^{7}

* Refer Table 3.5 for kinetics of sub bituminous coal and Table 3.6 for gas phase combustion

Table 4.7: Operating conditions for blends

Case	A	B	C	D
Blends of sub bituminous and lignite coal (%)	100-0	90-10	80-20	70-30
Fuel Air (kgs^{-1}) (Temperature 350 K)	74.304	74.10	73.945	73.81
Auxiliary Air (kgs^{-1}) (Temperature 550 K)	146.839	146.44	146.129	145.87
Coal flow rate (kgs^{-1}) (Temperature 350 K)				
Sub bituminous	38.05	32.12	26.9	22.25
Lignite (Imported)	0	3.56	6.9	9.5

CFD simulations were performed to predict the burnout behavior of these blends when fired in full scale 200 MW_e boiler. Figure 4.11 shows the CFD model simulation results to predict the effect of the blends on the unburnt char (UBC). CFD simulation predictions shows that the UBC for 100% sub bituminous coal was around 4.2% and shows variation

of maximum ± 2% of this value when the with the increase in imported coal share till 30% of total blend.

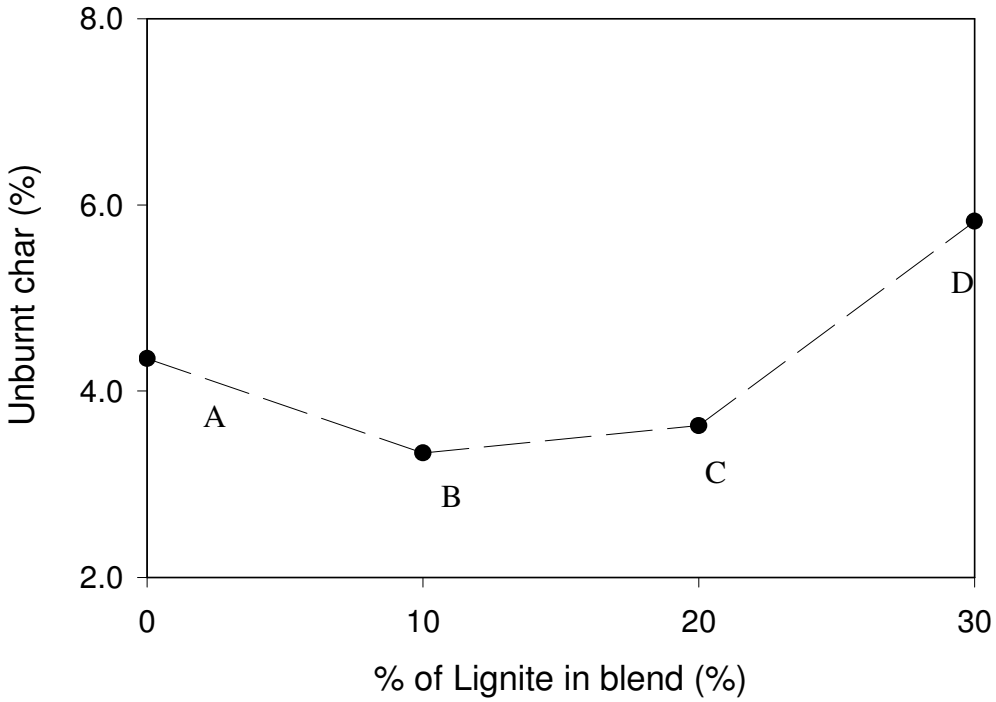

Figure 4.11: Effect of blend on unburnt fraction of char in ash

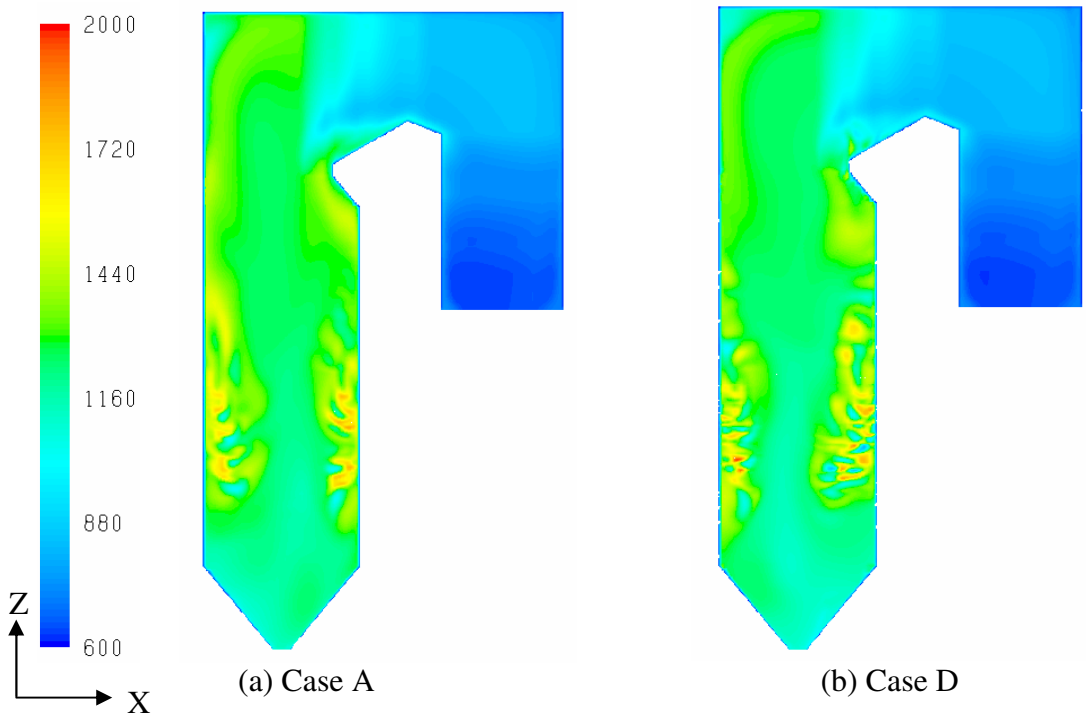

(a) Case A (b) Case D

Figure 4.12: CFD prediction of temperature profile (K) for blend of 30% imported coal and 70% Indian coal at Y plane y = 6.5 m

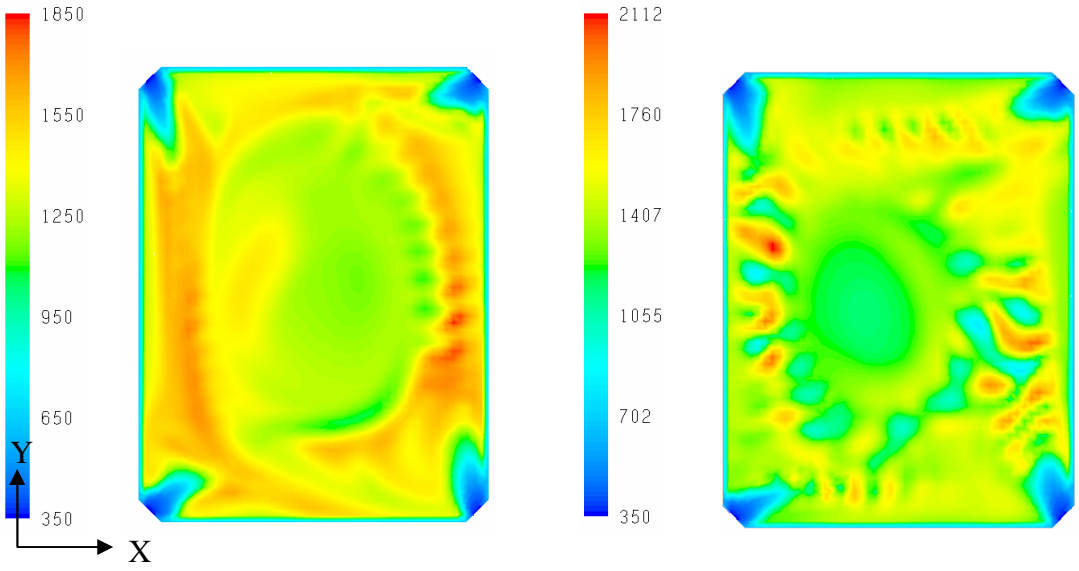

(a) Case A (b) Case D

Figure 4.13: CFD prediction of temperature profile (K) for case A and D at Z plane z = 21 m

Figure 4.12 and 4.13 shows CFD model prediction for temperature profile at corresponding Y (y = 6.5 m) and Z plane (z = 21 m, FA burner) of the boiler for case A and D (refer Table 4.7). The comparison shows that the temperature profile of blends is quite different that single coal due to the different devolatilization and char combustion rates for each type of coal. Hence, it confirms the non additive nature of blend and shows that each coal burns separately. Figure 4.13 shows that the maximum flame temperature (hot spots) in the furnace cross section has increase from ~1850 K to 2112 K. This can be expected as the imported coal has large amount of volatile content (41.3%) that burns faster as compared to char leading to more localize heat generation.

4.3 Conclusions

- Excess air: total unburnt char (UBC) in the ash was increased from ~5% to ~8.5%, when excess air was reduced from 20% to 5% and the CO level at the furnace exit was increased from 1448 ppm to 2753 ppm

- Burner tilt: The effect of the burner tilt is quantified in the form of correlation to predict the shift in the hot combustion zone according to the movement of the burner. This equation is specific to the tangentially fired 200 MW_e boiler of similar configuration as the aerodynamics of other scale (350 MW, 500 MW) boilers may be different. But similar methodology can be adapted to other scales of the boiler

- Thermal load: The average furnace exit temperature changed from 1327 K of standard operating condition to 1252 K for 40% turndown condition. The heat transfer to the water wall in furnace section decreases from 181 MW to 141 MW and for platen super heater the heat transfer decreased from 120 MW to 74 MW

- Coal Blends: The char burnout was changed by ± 2% when the lignite in coal blend was increased from 0% to 30%. The high volatile content of the lignite increases the local flame temperature as that was observed in with case A. The difference in reactivity also shows hot spots developed in the upper section of the furnace

Chapter 5

Phenomenological Modeling of Coal Fired Boiler

5.1 Introduction

Pulverized coal fired boiler is a workhorse of the power plant and efforts are being made continuously to improve its reliability, consistency and performance. In Chapter 3, the CFD model for simulating 200 MW_e pc fired boiler was discussed. The simulated model was able to predict the temperature and species profile, heat transfer, char burnout and crossover pass characteristics. The developed CFD model of boiler was used to understand effects of operating parameters such as excess air, burner tilt, heat load and coal blends on boiler performance. These results are discussed in Chapter 4 which shows that the model was successful in capturing key aspects of boiler performance. However, simulations using the CFD model require large computational resources and turnaround time. These models are therefore not appropriate for quick analysis and on-line optimization. In this work therefore we have developed a phenomenological model of pulverized coal boiler based on mixing cell/reactor network model (RNM) approach. In such an approach, a boiler is generally represented by less than hundred cells (zones). The model is therefore computationally quite efficient compared to the CFD models. In order to use such models in practice, it is however necessary to ensure that approximations underlying the development of such models are realistic and they capture key processes occurring in boilers.

Various lower order computational models have been developed for the boilers in past to predict the heat transfer, temperature and concentration profile (see for example, zone model by Hottel and Sarofim, 1967; Monte Carlo model by Gosman, 1973 and Howell, 1968). The zone and Monte Carlo models solve for the heat transfer if the combustion and gas flow patterns are given. These models were used as engineering tool to predict boiler performance. However, these models depend upon the information about the gas flow pattern that was obtained from upon engineering intuition (Lowe, 1975). Such approximations can be overcome by developing various methodologies to extract useful information from the CFD simulation of boiler. The key aspects like flow path and its distribution to each cell, particle trajectories and dimensions of the zone can be obtained

based on the detailed analysis of CFD simulation results. Such approach can provide useful insight while developing reactor network model for boiler.

In this chapter, CFD simulations results of a 200 MW_e boiler (discussed in Chapters 3 & 4) were analyzed to develop phenomenological model for simulating the boiler. The overall methodology of using CFD simulation results, details of the phenomenological model and simulated results are discussed in this chapter. In order to be able to account for parameters like burner tilt, appropriate empirical correlations developed in Chapter 4 was implemented in the model developed here. Based on this approach a simple tool called BOST (Boiler Optimization and Simulation Tool) was developed. The details of the same are discussed in the next section.

5.2 Methodology for Reactor Network Model (RNM)

Reactor network modeling approach is usually practiced by dividing the computational domain into compartments/ zones with shapes and volumes based on the prior information about the flow field, species composition, temperature distribution and geometric configuration. Each zone is modeled as either mixed flow reactor (MFR) or plug flow reactor (PFR). Multiple reactors can be used forming a network that are connected to each other exchanging mass and energy amongst these reactors. The flow connections between adjacent zones are required for this purpose. This information was obtained from the CFD models of the boiler described in previous two chapters. Reactor network models have been widely used for modeling the effects of mixing non-idealities in process equipment, presenting a realistic trade-off of computational efficiency and predictive accuracy between simple models based on idealized descriptions of mixing and full computational fluid dynamics (CFD) simulations.

Recent advances in CFD models can provide detailed modeling of imperfect mixing and reaction. As CFD models are computationally intensive, RNM-CFD approach is an attractive option to apply detailed flow, mixing and heat transfer information obtained from CFD into comparative less computationally intensive RNM model. Such models are applied to model LDPE reactors by Ray and Wells (2005). Osawe et al. (2002) applied an

approach to combine simulations generated using the Fluent CFD package with Aspen plus flow sheet modeling package. Their approach either integrates CFD models in their full complexity into Aspen or uses a multidimensional interpolation technique to obtain needed values from the database of precomputed steady-state CFD results. Bezzo et al. (2000) developed a framework that integrates CFD model in their full form inside of the gPROMS process simulation environment. This approach allowed the Fluent CFD package to compute momentum balance and quantities such as heat-transfer coefficients, where as process simulator computed the larger flow-sheet simulations. Further work along these lines by Bezzo et al. (2000) presents a general approach for determining flow quantities from nonreactive CFD simulations and applying them in zonal reaction model. Such approaches are useful where complex chemistry (like diesel engine combustion having more than 100 reactions) can be solved into RNM and where as flow information is extracted from non reactive CFD model. Hence it was proposed to develop reactor network model for tangentially pc fired boiler with coupling of offline steady state CFD simulations. The details of the model development are given below.

The overall approach to develop RNM of a boiler was to initially identify the distinctive zones in the boiler using the results of the CFD model and then formulate a strategy to connect these zones to establish a network. The boiler has 3 major parts: Furnace, Crossover pass (CP) and Second pass (SP). Furnace region has a complex flow structure especially in the burner zone and where as CP and SP comparatively have more uniform flow structure. The CFD results and the basic geometry of the 200 MW_e boiler were critically analyzed to identify different zones. It was observed that furnace has 5 important parts as (i) Hopper, (ii) Burner zone, (iii) zone above burner section, (iv) zone below burner section and (v) Nose. As most of the reactions take place in the burner zone it was also termed as combustion zone. Its location was marked for zero burner tilt position with the known physical locations of operating burners. Based on this, the zones at the top and bottom of the combustion zone were fixed to their respective physical location which will complete furnace part till nose section.

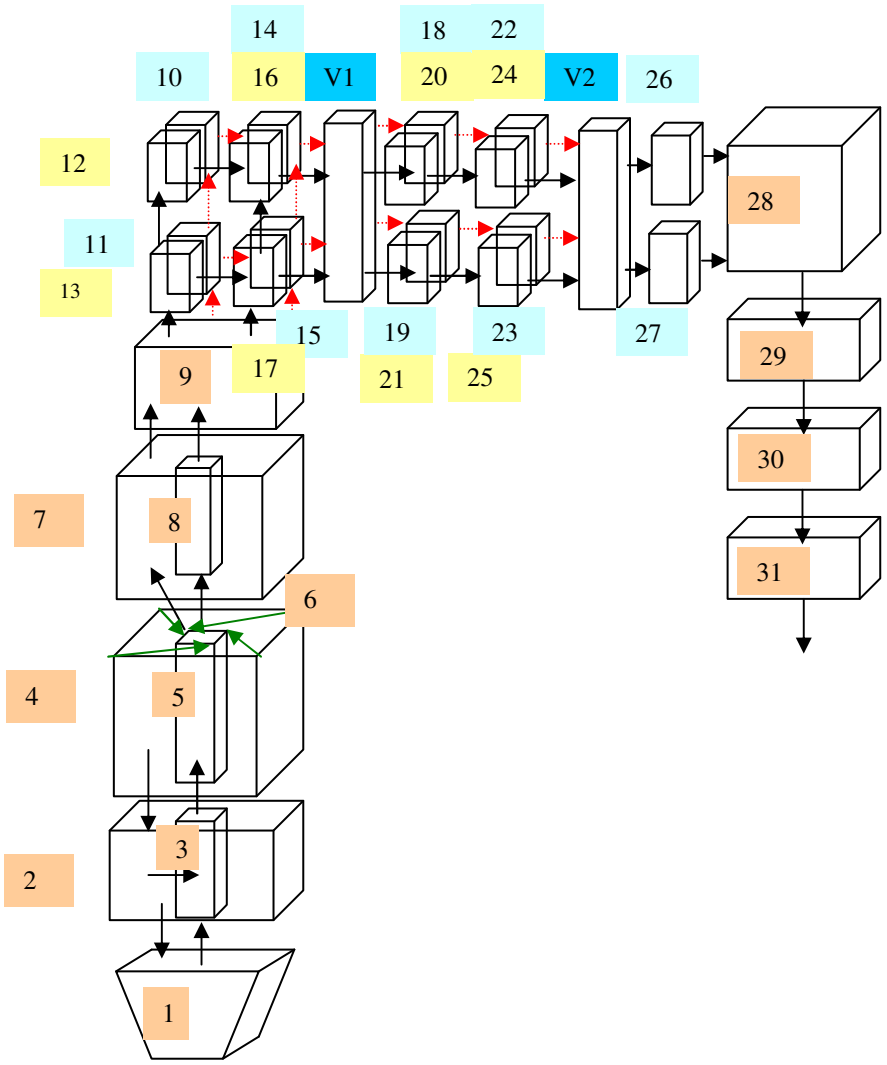

Zone number in yellow color boxes indicates right side wall and similarly blue color indicates left side wall of the boiler

Figure 5.1: Reactor network model for boiler

1: HOPPER;

2: COMBUSTION BOTTOM (CB) GAP; 3: COMBUSTION BOTTOM (CB) CORE;

4: FIREBALL GAP; 5:FIREBALL; 6: BURERJET;

7: COMBUSTION TOP (CT) GAP; 3: COMBUSTION TOP (CT) CORE;

9: NOSE; 10 TO 13: PRE PLATEN; 14 TO 17: PLATEN;

V1: VIRTUAL VOLUME; 18 TO 21: FRONT RH; 22 TO 25: REAR RH;

V2: VIRTUAL VOLUME; 26 TO 27: FINAL SH;

28: PASS2TOP; 29: LTSH;30:U-ECO;31:L-ECO

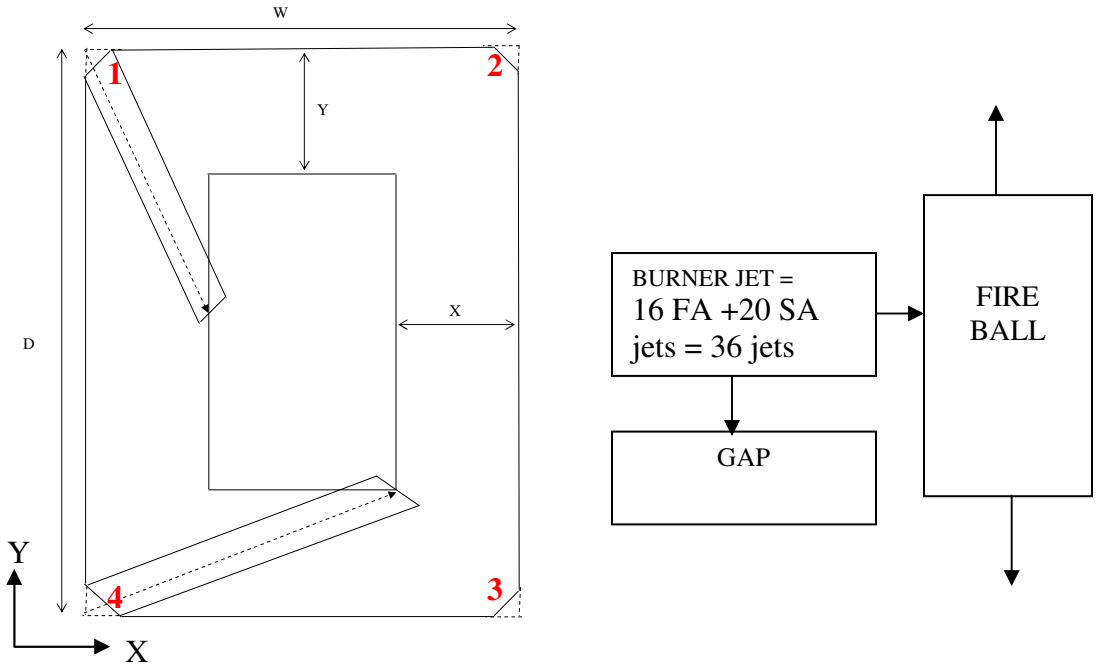

(a) Schematic of cross section of the furnace

(b) Schematic of single jet and Fireball

Figure 5.2: Combustion zone

The crossover and second pass had zones, each enclosing a heat exchangers tube bundle. Each zone was modeled as single continuous stirred tank reactor (CSTR). For accounting the crossover pass effect, each heat exchanger zone in crossover pass was split into multiple CSTR. Based on this, the boiler domain was finally discretized into 31 distinct zones that are shown in Figure 5.1. Further, each zone can be again split (except Fireball, Hopper and Platen) into more number of internal CSTRs in series along the direction of flow to obtain spatial distribution of temperature and species profile. The details about each zone are discussed in next paragraph.

The COMBUSTION zone shown in Figure 5.2 is important section of boiler where the coal and air is injected. Based on the analysis of the velocity, species and temperature profiles on a crossectional plane passing through one of the operating fuel air burner, the combustion zone was split into three parts BURNER JET, FIREBALL and FIREBALL GAP (Figure 5.2-b). There were total 36 jets (16 FA +20 SA jets = 36 jets) injected from the corner of the boiler entering in to the central FIREBALL. All the jets were combined

together into a single zone, BURNER JET that starts from the corner of the furnace and exhausts burning coal and combustion products into the FIREBALL which is located in the center of the furnace.

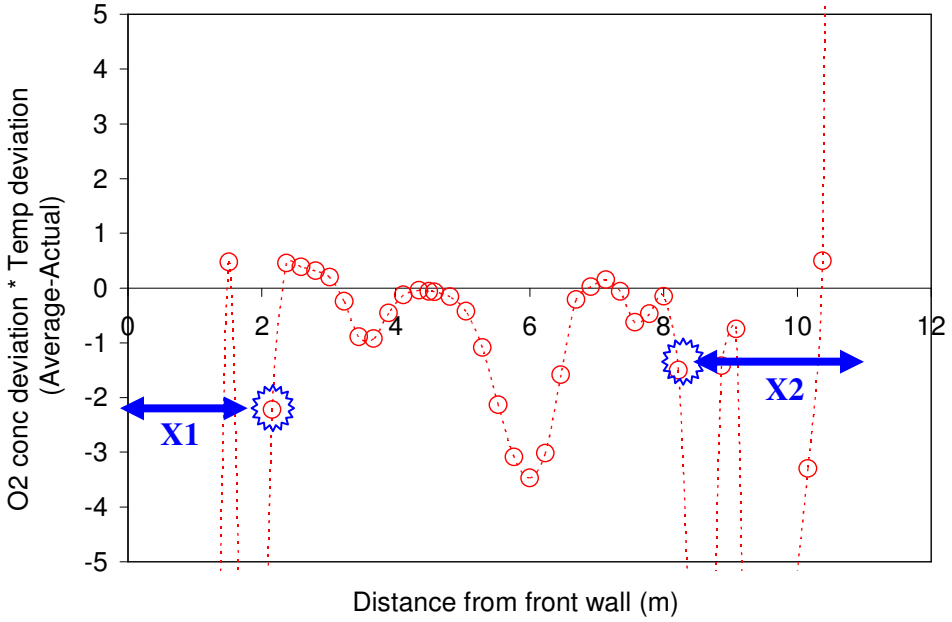

(a) Deviation of O_2 conc*T on line X = 5.25 m

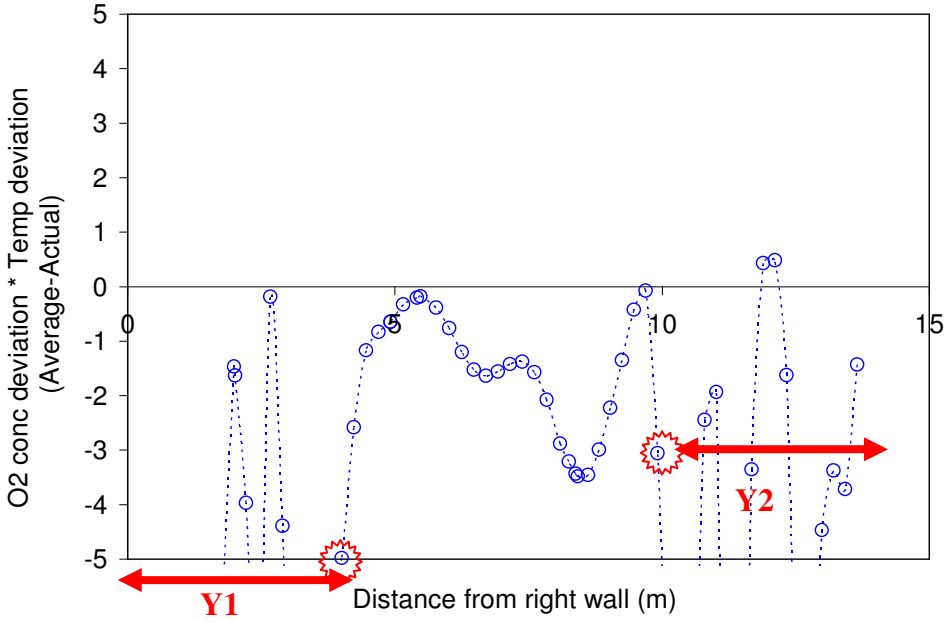

(b) Deviation of O_2 mass fraction*T on line Y = 6.934 m

Figure 5.3 : Plots for estimation of dimensions X and Y

The cross-sectional area of the BURNETJET was the sum of the cross-sectional area of the all burner 36 burner ports. The length of the BURNETJET depends upon the dimensions of the FIREBALL. As the shape of the furnace was rectangular, the FIREBALL was also assumed to be rectangular in shape and its dimensions are dependent upon the values of the X & Y as shown in Figure 5.2-a. The values of X and Y were estimated based on analysis of CFD results. Once the values of X and Y are obtained, the dimensions of BURNER JET and FIREBALL GAP can be estimated from simple geometric calculations. Following methodology was developed to extract the values of X and Y from CFD simulation results of 200 MW_e boiler and stepwise procedure is described below;

I. Examine temperature and O_2 mass fraction on isolines passing through the center of the furnace in X and Y direction on a Z plane that passes through the center of any Fuel Air burner port
II. Calculate number average of temperature and O_2 mass fraction of the Isolines
III. Calculate standard deviation of actual value from the average value at each point on the Isoline for temperature and O_2 mass fraction
IV. Multiply the deviation in O_2 mass fraction with that temperature and plot it along the Furnace Width or Depth (for X or Y respectively) as shown in Figure 5.3. This coupling is important as in COMBUSTION zone heat liberated due to O_2 consumption leads to change in gas temperature.
V. Estimate boundaries of FIREBALL
    - Start from center of the furnace and more toward the wall and stop when the deviation values goes out of the range bound [+5 to -5]. This is width or depth of FIREBALL (distance between two red marks as shown in Figure 5.3).
    - The remaining part is the distance of FIREBALL (X or Y) from wall of the furnace. As the distance of FIREBALL from opposite wall can come out to be different, hence the X or Y was estimated by numbered average value of X1 & X2 or Y1 & Y2 respectively.

- The range bound is decided based on the analysis of CFD results, e.g. for the Figure 5.3, the range bound for estimation of Y dimension was [5,-5] and for estimation of X dimension was [5,-5].
- Based on this analysis the X and Y dimensions were estimated as; X = 2.26 m and Y = 3.98 m

The volume remained in the COMBUSITON zone after subtracting the volumes of BURNERJET and FIREBALL was termed as FIREBALL GAP (Figure 5.2-a). The walls surrounding the GAP zones are the water walls. The zones above and below the COMBUSITON zone has inner volume and a volume surrounding the inner volume as shown in Figure 5.2. The width and depth of central volume was assumed to have same as the FIREBALL. The area and volume for zones like NOSE and above of that was estimated from geometric details of the boiler. It should be noted that the dimensions of the zones like BURNER TOP and BURNER BOTTOM were dependent upon the dimensions of the COMBUSTION zone. The height of COMBUSTION zone was estimated from the burner tilt correlations obtained from CFD simulations (Figure 4.9). According to the change in burner tilt the height of COMBUSTION zone changes and hence the dimension of zones above and below COMBUSTION zone changes. Hence the heights of zones in the furnace are dynamic in nature and depend upon parameters like burner tilt.

The PLATEN, REHEATER, FINAL SH, LTSH and ECONOMIZER zones have heat exchanger bundles and to these tube bundles radiative and convective heat is transferred from flue gas to produce high pressure and temperature steam. The common characteristic found in tangentially fired boilers are the uneven flow distribution in crossover pass which leads to high temperature towards the one side wall of boiler (temperature deviation). The detailed CFD analysis of the same is discussed in Chapter 3. In order to capture the temperature deviation effect in the crossover pass of the boiler, the zones in crossover pass were discretized into four sections left, right, top and bottom zones (Figure 5.1). This configuration was kept identical for the crossover pass till the reheater section. The flow distribution in each of these zones was estimated from CFD

simulations. For the FINAL SH, only top and bottom sections were considered as it was observed that the effect gets diminished when flue gas reaches the FINAL SH. Rest of the sections of second pass like LTSH and ECONOMIZER were considered as CSTRs in series

Once the location of each zone was fixed, the volume of each zone was estimated from the geometric details of the boiler. The next step was to establish convective heat and mass flow connections between all the zones. Flow field obtained from the CFD simulations (Figure 4.4) was used to establish reactor network model flow connections. The burner jets feeds combusting material in the FIREBALL and the vector plot as shown in Figure 4.4 indicates that small part of fluid that moves down towards the HOPPER section and the remaining part moves directly towards the top of section of the furnace. The fluegas that comes down from the FIREBALL goes to zone combustion bottom (CB) GAP zone where part of the gas again splits into HOPPER and CB CORE. The flue gas that comes to HOPPER then moves upwards through the CB CORE and then through the FIREBALL GAP. The flue gas that comes to CB CORE from the CB GAP also moves upwards through FIREBALL GAP.

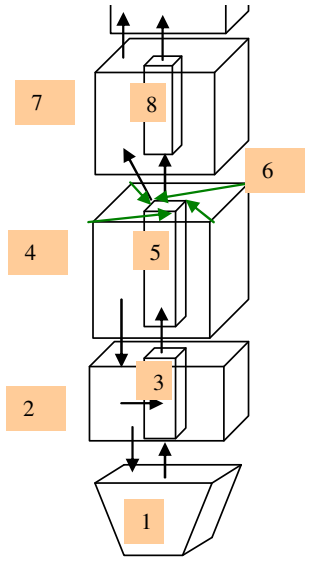

Figure 5.4: Schematic shows flow connections for bottom section

This observation was supported by contour plots of positive/negative z velocity at plane z =20 m (below the lower most operating AA burner) & z = 15 m (top of the Hopper) which are shown in Figure 5.4. The mass flow rate of flue gas flowing downward was determined on clip planes of negative z velocity. Based on this, the information about the distribution of flow at both heights z= 15 & 19 m was obtained. The fluegas from the combustion zone moves upwards towards the NOSE of the boiler through Combustion top (CT) zone.

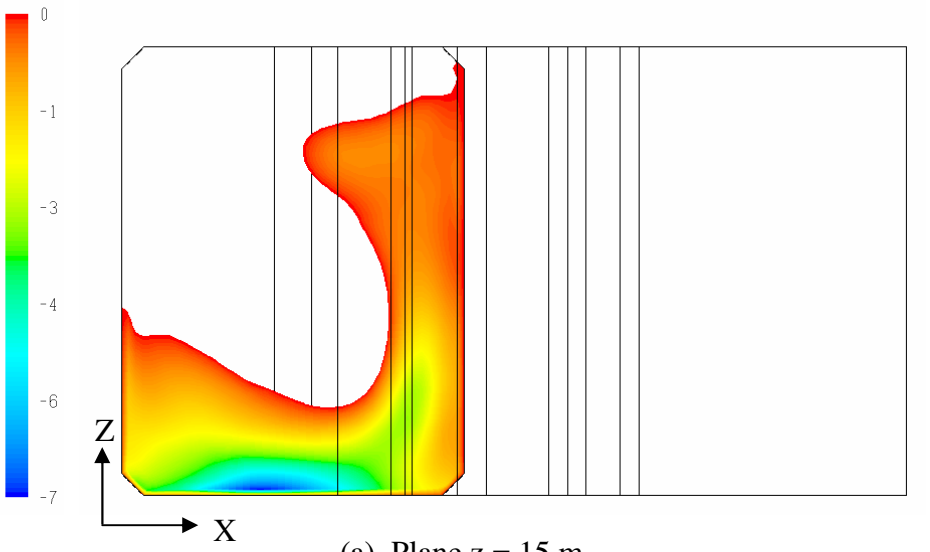

(a) Plane z = 15 m

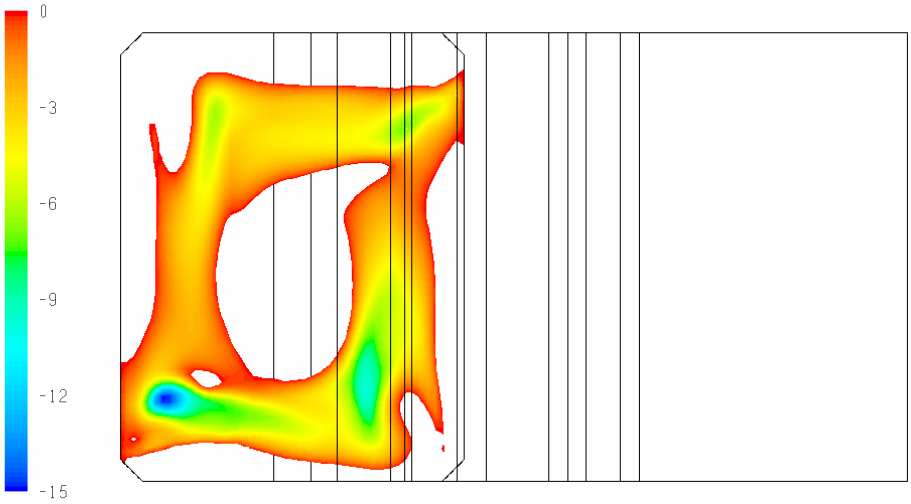

(b) Plane z = 20 m

Figure 5.5: Contour plot showing the negative z velocity (ms^{-1}) at two cross-sections of the furnace

The structure of the CT is same as CB which was split into two parts as CT CORE surrounded by CT GAP. The dimensions of the CT CORE were assumed to be the same as the FIREBALL. The fluegas gas that moves upwards splits into these two co axial zones and for each zone, mass flow rate was estimated from the flow field obtained from the CFD model. It was observed that around 30% of the total flue gas flow rate goes to the CT CORE.

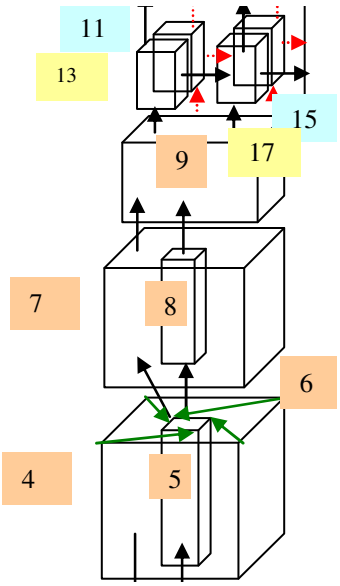

Figure 5.6: Flow connection for fireball-CT-NOSE

The section above the CT is NOSE was modeled as single CSTR. It collects the mass from CT GAP and CORE. The flue gas from the NOSE moves towards the crossover pass of the boiler. The zone above the NOSE was split into two equal volumes PRE PLATEN and PLATEN zone (Figure 5.6). The PLATEN zone has platen SH tube bundle where as PRE PLATEN was void space where the part of the fluegas that comes from the NOSE was directed. For counter current fireball, it was observed that in the upper furnace zone, the fluid has tendency of moving towards the right side wall of the boiler which leads to temperature deviation in the upper furnace zone and crossover pass zone in left and right side wall. It was also noted that the temperature deviation varies with the vertical height in the upper furnace zone (refer Chapter 3, Section 3.8.9). Hence the each zone like PRE PLATEN, PLATEN, FRONT and REAR REHEATER were further split

into four sub zones as LEFT, RIGHT, TOP and BOTTOM (Figure 5.6). It was observed from the CFD simulations that the temperature deviation diminishes after Reheater. Therefore the Final super heater was modeled as two sub zones as TOP and BOTTOM. The mass flow distribution for each zone was estimated from the simulated CFD model.

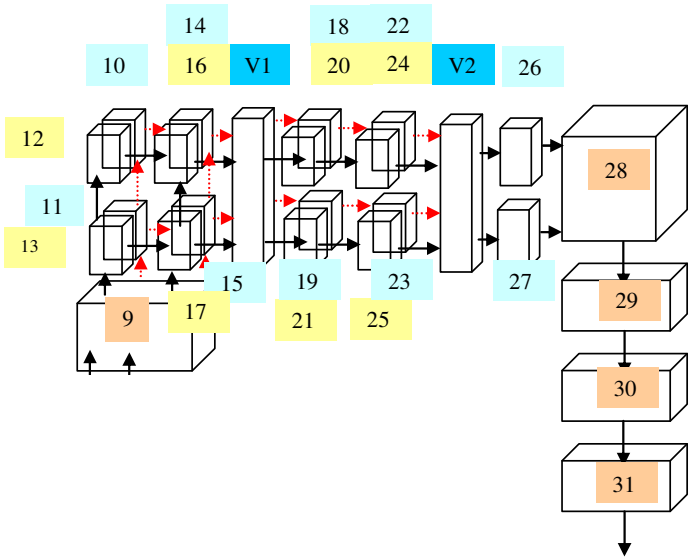

Figure 5.7: Flow connection for platen SH to Economizer

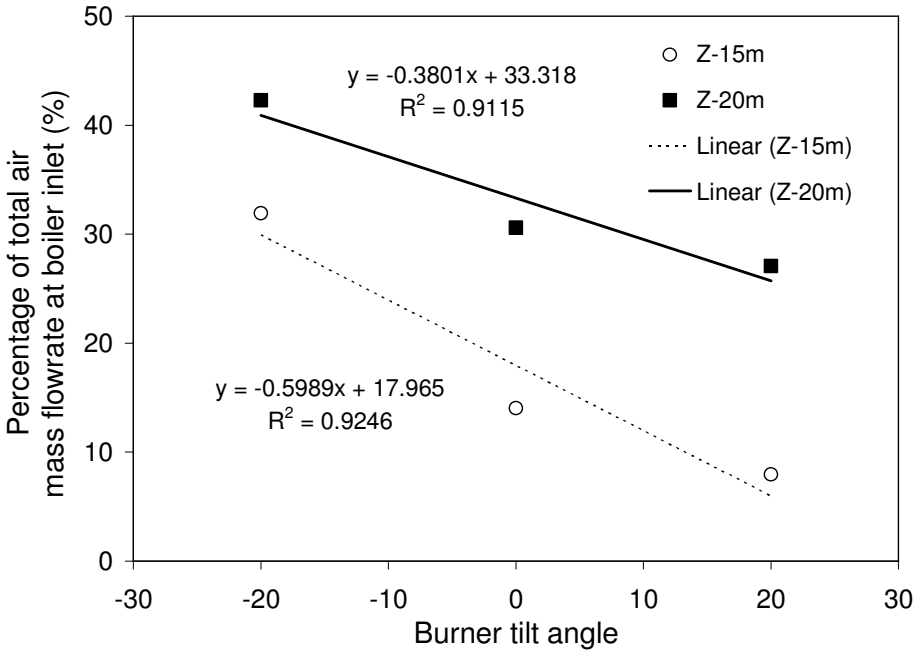

Figure 5.8: Effect of burner tilt on mass flow distribution in the lower part of furnace

The fluid from final super heater passes further towards the Pass2TOP, LTSH, UECO and LECO (Figure 5.7). Each zone can have 'n' internal CSTRs. From Platen to LECO zones the gas exchanges heat with water wall/steam wall and heat exchangers. The flue gas with fly ash leaves the boiler from the LECO zone. The burner tilt also affects the flow distribution in the furnace and hence effect of the same was analyzed from the CFD simulations and was expressed in terms of correlations (Figure 5.8). This figure shows that there is a significant effect of burner tilt on the flow distribution in the lower part of the furnace. The correlations for the predicting effect of burner tilt on the percentage of total flue gas mass flow rate that is moving down towards the bottom of the furnace is as follows;

$$F_{20\,m}\ (\%) = -0.3801\ \theta + 33.318$$

$$F_{15\,m}\ (\%) = -0.5989\ \theta + 17.965$$

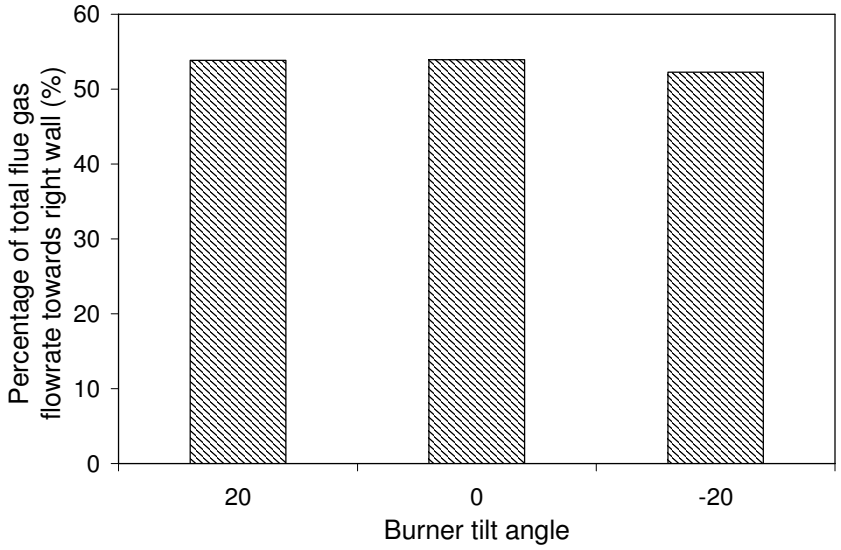

Figure 5.9: Effect of burner tilt on the mass flow distribution in crossover pass (Front RH)

The effect of burner tilt on the flow distribution at the crossover pass was also analyzed as shown Figure 5.9. It shows that there is a negligible effect of burner tilt on the flue gas

mass flow rate distribution towards the right side zone (including top and bottom) of Front Reheater.

Particle motion in the boiler needs to be represented adequately in such a RNM. For this purpose, four streams of particles were considered. Simulated particle trajectories from the CFD model were critically examined to approximate the motion of particles in RNM. Based on this analysis, an approximate model for the particle motion was constructed. It was assumed that the particles follow the path of fluid. The particle level processes like heating, devolatilization and reactions were modeled and simulated in the Lagrangian framework. The trajectories of four particle streams through various zones are listed in Table 5.1.

Table 5.1: Particle trajectory through the various zones

Particle stream 1	Particle stream2	Particle stream 3	Particle stream 4
6	6	6	6
5	5	4	5
7	8	2	4
9	9	3	2
10	13	5	1
13	17	8	
17	19	9	
19	21	12	
26	26	14	
28	28	18	
29	29	20	
30	30	24	
31	31	28	
		29	
		30	
		31	

The mass flow distribution of the coal particles that are moving down towards the bottom of the furnace were estimated from the CFD simulation results. Figure 5.10 shows the plot of % of particles moving down towards the bottom of the furnace at two heights z = 20 m. The simulation result was linearly fitted to obtain correlation to predict effect of burner tilt on the particle mass flow rate distribution in bottom section of the furnace. The

mean residence time of the coal particles at various cross sections in the furnace were obtained from the CFD simulations and are given in the in Table 5.2. This information was useful to estimate the residence time for all other zones.

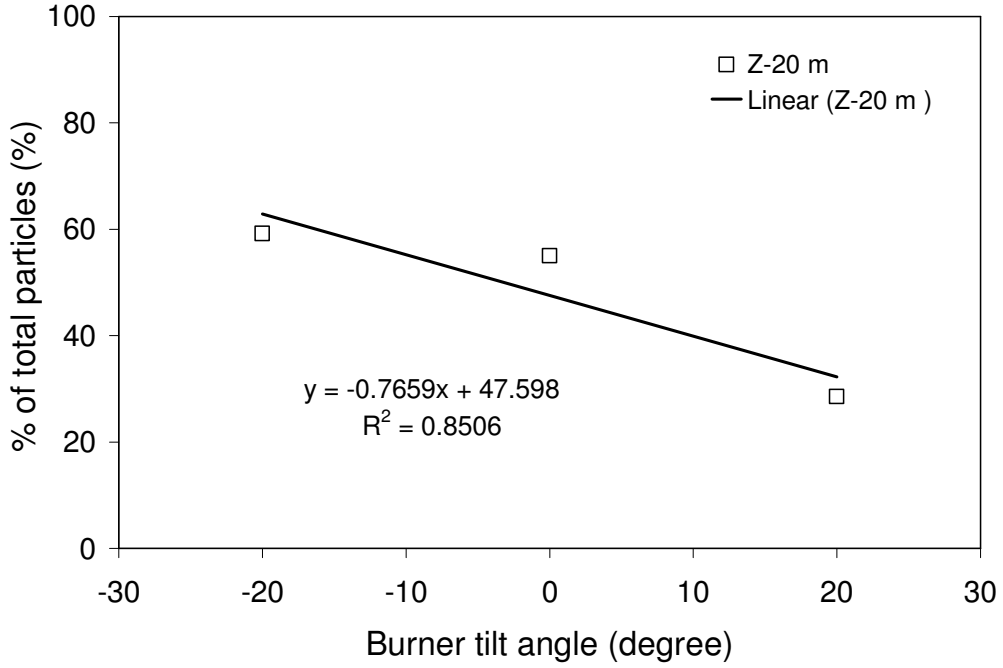

Figure 5.10: Effect of burner tilt on the percentage of total particles going down to bottom section of the furnace

Table 5.2: Particle residence time in various zones

Particle location	Particle mean residence time (s)
Exit as bottom ash	7.50
Entering Hopper	6.59
Entering CB GAP	2.48
FEGT (exit of NOSE)	4.18
Entering Final SH	7.46
Boiler exit	11.07

This completes the basic formulation methodology for the RNM and the model equations for each zone are described in next section.

5.3 Model equations and boundary conditions

Methodology was developed to formulate appropriate reactor network model to simulate boiler. Each MFR comprised of two phases: continuous gas and discrete solid phase (coal particles). Mass and energy conservation equations were written for both the phases over each MFR. Solid flow was modeled using the Lagrangian framework. The coal devolatilization was modeled as single step kinetic controlled, char oxidation as diffusion / kinetically controlled. Homogenous gas phase reactions are kinetic/ mixing controlled based on Eddy Dissipation Concept which is same as discussed in Chapter 3. Radiative heat transfer was modeled based on Hottel Zone method (1957). The details of the model are given below.

5.3.1 Continuous phase

The continuous gas phase was modeled based on the Eulerian approach. Conservation equations for each CSTR can be written as;

- *Overall mass balance for k^{th} zone*

$$\frac{d\left(\rho^{k,n}V^{k,n}\right)}{dt} = \sum_{i\neq k}\Phi_{k,k}F_{out}^{i,n} - F_{out}^{k,n} + \sum_{j}S_{j}^{k,n} \qquad 5.1$$

Where, n is any internal CSTR, i is any zone other than k and j is the any gas component.

- *Component balance for the k^{th} zone*

The species conservation equation for the n^{th} internal CSTR of k^{th} zone can be written as,

$$\frac{d\left(\rho^{k,n}V^{k,n}m_{j}^{k,n}\right)}{dt} = \sum_{i\neq k}m_{j}^{i,n}\Phi_{k,k}F_{out}^{i,n} - m_{j}^{k,n}F_{out}^{k,n} + R_{j}^{k,n} + S_{j}^{k,n} \qquad 5.2$$

Where,

ρ Gas density of the k^{th} zone and n^{th} internal CSTR kg m^{-3}

F	Mass flow rate coming into/ going out of CSTR	kgs^{-1}
V	Volume of n^{th} internal CSTR of k^{th} zone	m^3
A	Cross sectional area	m^2
m_j	Mass fraction of species j	–
R_j	Net rate of production or consumption of species j by chemical reaction	kgs^{-1}
S_j	Source of species j from dispersed phase	kgs^{-1}
$\Phi_{k,k}$	Parameter that connects the outlet of all CSTR to current k^{th} CSTR	

- *Energy balalnce*

The enthalpy conservation equation for the n^{th} internal CSTR of k^{th} zone can be written as,

$$\frac{d\left(\rho^{k,n}V^{k,n}h^{k,n}\right)}{dt} = \sum_{i\neq k} h_{out}^{i,n}\Phi_{k,k}F_{out}^{i,n} - h_{out}^{k,n}F_{out}^{k,n} + S_{gas-rxn}^{k,n} + S_{char}^{k,n} + S_{rad}^{k,n} \quad 5.3$$

Where, h is the total enthalpy

$$h^{k,n} = \sum_j m_j^{k,n}h_j^{k,n} \quad 5.4$$

Where h_j is enthalpy of j^{th} species defined as

$$h_j^{k,n} = h_j^0 + \int_{T_{ref}}^{T_{k,n}} C_{p,j}\,dT \quad 5.5$$

Where,

h_j^0	Standard heat of formation of species j	J kg^{-1}
$S_{gas-rxn}$	Source term of heat of chemical reactions	W
S_{rad}	Heat transfer by radiation from all other zones	W
S_{char}	Source term for discrete phase char oxidation	W

The heat released due to chemical reactions is

$$S_{rxn}^{k,n} = -\sum_{r} \Delta H_r R_r^{k,n} \qquad 5.6$$

The heat of reaction, ΔH_r is defined as,

$$\Delta H_r = \Delta H_r^0 + \int_{Tref}^{T_{k,n}} \Delta C_p \, dT \qquad 5.7$$

The heat transfer to the water wall and heat exchangers of the each CSTR due to convection is given as,

$$S_{Conv-ww}^{k,n} = h_{ww}^{k,n} A_{ww}^{k,n} \left(T_g - T_{ww}\right)^{k,n} + h_{HTX}^{k,n} A_{HTX}^{k,n} \left(T_g - T_{HTX}\right)^{k,n} \qquad 5.8$$

The heat transfer coefficient for convective heat transfer to heat exchangers was estimated based on the Nusselt number correlation (eq. 3.3) discussed in Chapter 3. The constants of the equation were adopted from the Table 3.3. The heat transfer coefficient for the water walls was estimated from the CFD simulations based on the total convective heat transferred to water walls.

5.3.2 Discrete phase

The particle size distribution was fitted to Rosin-Rammler equation (Figure 5.11). The Rosin-Rammler distribution function is based on the assumption that an exponential relationship exists between the particle diameter, d_p, and the mass fraction of particle with diameter greater than d_p is

$$Y_d = e^{(-d_p/\overline{d_p})^n} \qquad 5.9$$

Where $\overline{d_p}$ the mean diameter and n is the spread parameter.

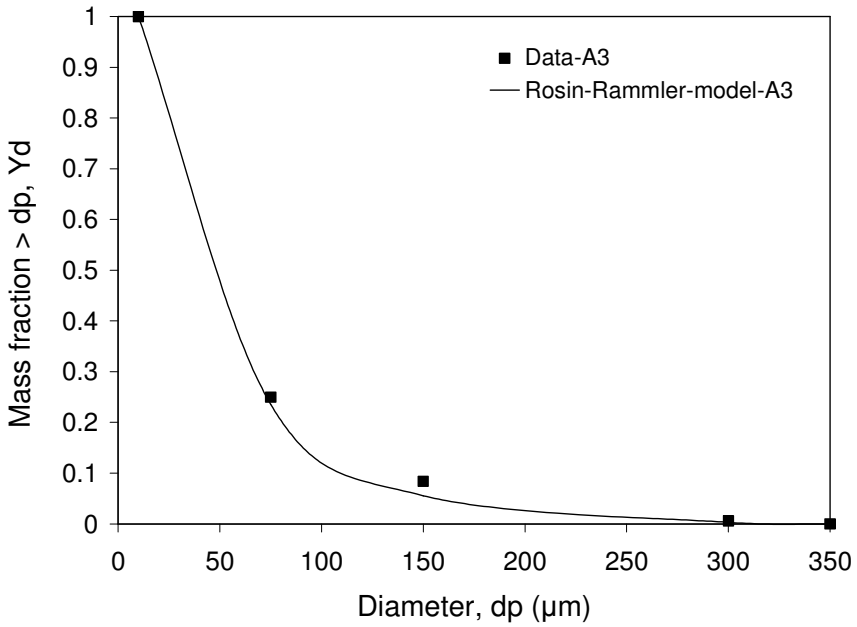

Figure 5.11: Rosin-Rammler model equation fit to particle side distribution

The Rosin-Rammler parameters are, mean particle diameter = 68 µm, spread parameter = 1.18

- *Particle momentum balance*

The discrete phase was modeled by using the Lagrangian approach. The discrete phase momentum balance over a single particle of size class i, can be written (by only considering gravity and drag force acting on particle) as,

$$\frac{\mathrm{d}u_{\mathrm{p,i}}}{d\theta} = \frac{(\rho_{p,i}-\rho_g)}{\rho_{p,i}} g + \frac{18\mu}{d_{p,i}{}^2 \rho_{p,i}} \frac{C_{D,i}\,\mathrm{Re}_{p,i}}{24}(u_{p,i}-u_g) \qquad 5.10$$

ρ_P	Particle density	kg m^{-3}
d_p	Particle diameter	m
u_p	Particle velocity	ms^{-1}
g	Gravitational constant	ms^{-2}
C_D	Drag coefficient	
µ	Viscosity of gas phase	$kgms^{-1}$
u_g	Velocity component of gas phase	ms^{-1}
i	particle size class	

The drag coefficient, C_D was estimated based on Morsi and Alexander (1972) correlation.

The change in mass of particle is mass loss due to devolatilization and char oxidation,

$$\frac{d\left(M_{p,i}\right)}{d\theta} = -\left(\frac{d\left(M_{p0,i}m_{v,i}\right)}{d\theta} + \frac{d\left(M_{p0,i}m_{c,i}\right)}{d\theta}\right) \qquad 5.11$$

The combustion models employed are described below,

- *Devolatilization*

The coal devolatilization rate can be written as (Badzioch and Hawksley, 1970):

$$\frac{d\left(M_{p0,i}m_{v,i}\right)}{d\theta} = -A_v\, e^{(-E_v/RT_{P,i})}\left(U - 1 + m_{v0,i} + m_{w0,i}\right)M_{p0,i} \qquad 5.12$$

M_{p0}	Initial mass of the particle	Kg
$m_{v,0;}\, M_{w,0}$	Mass fraction of volatiles and moisture initially present in the particle	-
U	Unburnt fraction as defined in equation 5.18	-
E_v	Activation energy for devolatilization	J $kmol^{-1}$
A_v	Pre exponential factor for devolatilization	s^{-1}
T_p	Temperature of the particle	K

In the devolatilization phase, particle diameter was assumed to remain constant and the particle density was allowed to decrease to account for the reduction in particle mass due to the devolatilization.

- *Surface reaction-char oxidation*

Char combustion rate was calculated based on the assumption that the char gets oxidized to CO by the following reaction:

$$C_{(s)} + 0.5O_{2\,(g)} \rightarrow CO_{(g)}$$

The rate of char oxidation can be written as, (Baum and Street, 1971; Field, 1970)

$$\frac{d\left(M_{p0,i}m_{c,i}\right)}{d\theta} = -A_{p,i}\frac{K_c K_{d,i}}{K_c + K_{d,i}} Y_{O2}\frac{\rho_g RT_g}{MW_{O_2}} \quad 5.13$$

The kinetic rate constant (K_c) for char oxidation reaction is

$$K_c = A_c\ e^{(-E_c/RT_P)} \quad 5.14$$

Where,

A_c	Pre-exponential factor	$kgm^{-2}s^{-1}Pa^{-1}$
E_c	Activation energy for char combustion	J $kmol^{-1}$

The bulk gas phase diffusion coefficient (K_d) for oxidant (Field, 1970) can be given as,

$$K_{d,i} = \frac{5\times10^{-10}}{d_{p,i}}\left(\frac{T_g + T_{p,i}}{2}\right)^{0.75} \quad 5.15$$

The change in density of coal particle can be written as (Smith, 1971)

$$\rho_{P,i} = \rho_{Po,i}\left(U_i\right)^{\beta} \quad 5.16$$

$$d_{P,i} = d_{Po,i}\left(U_i\right)^{\alpha} \quad 5.17$$

Where, $3\alpha + \beta = 1$

U is unburnt fraction of coal and which can be written as

$$U_i = \frac{M_{v,i} + M_{c,i} + M_{w,i} + M_{A,i}}{M_{v0,i} + M_{c0,i} + M_{w0,i} + M_{A0,i}} \quad 5.18$$

- *Particle heat balance*

$$\frac{d\left(M_{p,i}Cp_P T_{P,i}\right)}{d\theta} = \left(f_{heat}Q_{char,i}\right) + Q_{rad,i} + Q_{conv,i} \qquad 5.19$$

Where, C_{pp}, f_{heat}, H_{rxn} , Q_{rad} and Q_{conv} are the particle specific heat, fraction of heat absorb by particle, heat of char oxidation reaction, radiative and convective heat transfer respectively. The f_{heat} is the fraction of heat absorbed by the coal particle during the char oxidation.

$$Q_{char,i} = \frac{d\left(M_{p0,i}m_{c,i}\right)}{d\theta} H_{char-rxn} \qquad 5.20$$

The radiative heat transfer can be written as

$$Q_{rad,i} = \varepsilon_P \sigma A_{p,i}(T_g^{\,4} - T_{p,i}^{\,4}) \qquad 5.21$$

The convective heat transfer can be written as

$$Q_{conv,i} = h_{c,i}A_{P,i}(T_g - T_{p,i}) \qquad 5.22$$

The heat transfer coefficient, h_c was evaluated using the correlation of Ranz and Marshall (1952) as

$$\frac{h_{c,i}d_{p,i}}{k_g} = 2 + 0.6(\mathrm{Re})^{0.5}(\mathrm{Pr})^{0.33} \qquad 5.23$$

Where,

ε_P	emissivity of particle	(-)
σ	Stefan-Boltzmann constant $= 5.67\times10^{-8}$	$Wm^{-2}K^{-4}$

h	heat transfer coefficient	$Wm^{-2}K^{-1}$
k_g	Conductivity of gas	$Wm^{-1}K^{-1}$

- *Discrete phase source term*

The mass source term from discrete phase can be written as

$$S_{k,n} = \int_0^{\tau_{k,n}} \left(R_v + R_c\right) d\theta \qquad 5.24$$

Where R_v and R_c are the rate of devolatilization and char oxidation and $\tau_{k,n}$ is residence time of the particle in any n^{th} internal CSTR of k^{th} zone .

$$R_v = \sum_{i=1}^{N} N_{p,i} \frac{d\left(M_{p0,i} m_{v,i}\right)}{d\theta}, \qquad R_c = \sum_{i=1}^{N} N_{p,i} \frac{d\left(M_{p0,i} m_{c,i}\right)}{d\theta} \qquad 5.25$$

Where N is the total size class, Np,i is the total number of particle of size class i

5.3.3 Homogenous gas phase reactions

The net source of chemical species j due to reaction is computed as the sum of the Arrhenius reaction sources over the N_r reactions that the species participate in as:

$$R_j = V\, Mw,_j \sum_{r=1}^{Nr} R_{j,r} \qquad 5.26$$

The volatile material was represented by single species as $CH_{2.08}O_{0.33}$ based on proximate and ultimate analysis of coal. Following homogenous gas phase reactions were considered.

$CO_{(g)} + 0.5\ O_{2\,(g)} \rightarrow CO_{2(g)}$

$CH_{2.08}O_{0.33(g)} + 1.33\ O_{2\,(g)} \rightarrow CO_{2(g)} + 1.04H_20_{(g)}$

The molar rate of creation/ destruction of species j in reaction r can be written as

$$R_{rxn\,j,r} = \left(v'_{j,r} - v_{j,r}\right) K_r \prod_l \left[C_{l,r}\right]^{n_l,r} \qquad 5.27$$

$C_{l,\,r}$	Molar concentration of each reactant l^{th} species in reaction r	kmol m^{-3}
$\eta'_{l,r}$	Exponent for each l^{th} reactant in reaction r	
$v'_{j,r}, v_{j,r}$	Stoichiometric coefficient for j^{th} species as product and reactant respectively	
K_r	Kinetic rate constant for reaction r where , $K_r = A_r\, e^{(-E_r/RT)}$	$m^3kmol^{-1}s^{-1}$
A_r	Pre exponential factor for gas phase reaction r	$m^3kmol^{-1}s^{-1}$
E_r	Activation energy for gas phase reaction r	J $kmol^{-1}$

The effective rate of gas phase combustion under the conditions prevailing in coal fired boilers may not be equal to the intrinsic kinetic reaction rate because of possible limitations imposed by mixing. When intrinsic rate of gas phase reactions is much higher than the rate of mixing of oxygen and combusting species, the effective rate is controlled by the rate of mixing. Magnussen and Hjertager (1976) have proposed the eddy-dissipation model to represent interaction between turbulent mixing and intrinsic chemical reactions. As per this model, the rate of production of species j due to reaction r, $R_{EBUj,r}$, is given by the smaller (i.e., limiting value) of the expressions given below:

$$\mathrm{R}_{EBU\,j,r} = A\rho\frac{\varepsilon}{k}\min\left(\frac{Y_{ox}}{\nu_{j,r}}, Y_{fuel}\right) \qquad 5.28$$

Where, Y_{ox} is the mass fraction of the oxidant and Y_{fuel} of the fuel reactant. In Equations 5.28, the chemical reaction rate is governed by the large-eddy mixing time scale, k/ε as in the eddy-breakup model of Spalding (1969). The gas phase reaction rate is evaluated based on the minimum of the reaction rate estimated by Arrhenius type kinetic rate model and eddy dissipation model.

$$R_{j,r} = \min\left(R_{rxn\,j,r}, R_{EBU\,j,r}\right) \quad 5.29$$

5.3.4 Radiation model

The most usual numerical methods for analyzing the radiative spaces are the Monte Carlo, heat flux method and zone method. Indeed, by using these methods the radiative heat transfer in an absorbing, emitting, scattering medium can be analyzed. In this study, the zone method has been employed for predicting the temperature and heat flux on the water walls of the boiler. Hottel and Cohen (1935) have developed this method for analyzing the radiation heat transfer in an enclosure containing gray gas with certain properties. Later, Hottel and Sarofim (1967) used this method for more complex geometries. Ever since, this model has been widely used by researchers for modeling industrial radiative enclosures such as boiler furnaces (Diez et al, 2005; Batu and Selçuk, 2002). In this method, the whole space of the furnace is split into zones and the enclosure's walls are divided into finite surface parts (zones). The main assumption is using an existing uniform temperature and properties within the volume and surface zones. The heat transfer between a pair of zones depends on coefficients that are called the heat exchange area. The radiative source terms is balance between total heat exchanged by any zone with other surface and volume zones and total emission from the existing zone

The net radiative heat source for any zone k;

$$S_{rad,k} = \left(\sum_i \overline{G_k S_i} E_{s,i} + \sum_i \overline{G_k G_i} E_{g,i}\right) - 4K_k V_k E_k \quad 5.30$$

In order to evaluate the radiative exchange between the zones, it is required to calculate the total exchange areas $\overline{G_k S_i}$ and $\overline{G_k G_i}$. Hottel and Sarofim (1957) have discussed in detailed method to determine total exchange area. The E_g and E_s are the black emissive power of the gas and surface respectively. The total exchange areas are evaluated from the direct exchange areas. The directed exchange area can be calculated as;

$$g_k s_j = \int_{A_j} \int_{V_k} K \cos\theta_j \, e^{(-kr_{kj})} \, dV_k dA_j \qquad 5.31$$

$$g_k g_j = \int_{V_k} \int_{V_j} \frac{K^2 \, e^{(-kr_{kj})}}{\pi r_{kj}^2} dV_k dV_j \qquad 5.32$$

Also, the total exchange for one zones with all other zones is given by

$$\sum_{i \neq k} g_k g_i + \sum_j g_k s_j = 4KV_{g,k} \qquad 5.33$$

In this equations, r_{ij} is the center to center distance between two elements, are the angle between the normal vector of surface element and the above mentioned vector and K is the absorption coefficient of the gas.

5.3.5 Boundary conditions

The flowrate, temperature of air and coal at the inlet are listed in Table 3.7. The kinetic parameters for gas phase reactions are listed in Table 3.6. The geometric detials of boiler, heat exchagner surface area, tube emissivity, porosity of each heat exchanger zone, particle size distribution (PSD) of coal particles and their properties are same as specified in chapter 3 (Table 3.8). Radiation exchange coefficient for each zone is shown in Appendix- I.

5.3.6 Solution methodology

The solution procedure employed is shown in Figure 5.12. The required model inputs about geometry and operating conditions were supplied to the model. In the preprocessor, the dimensions of each zone based on the burner tilt were calculated. From these dimensions the crossectional area and volumes of each zone were estimated.

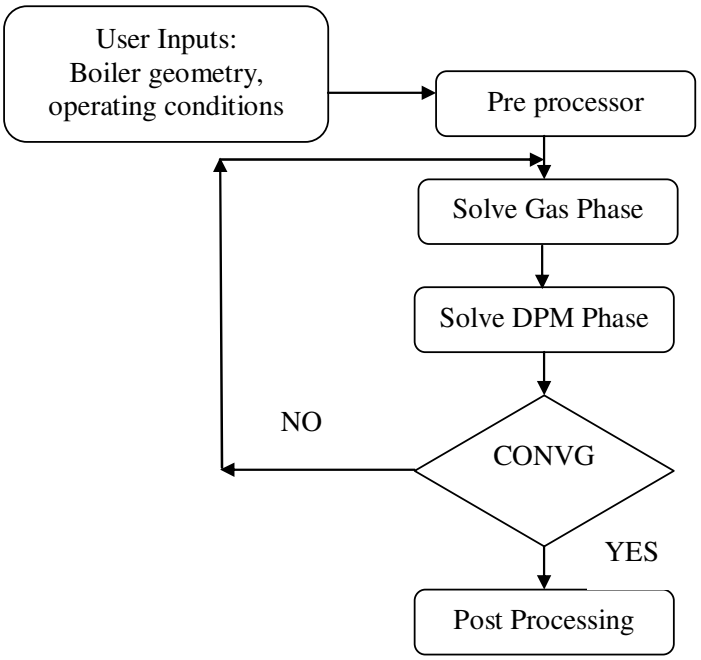

Figure 5.12: Solution methodology

Then, the gas phase mass and energy equations were solved for total residence time of gas phase. After solving gas phase, discrete phase source term for each zone were estimated by solving particle mass, momentum and energy equations. For the first iteration, the discrete phase source term for each zone was specified as zero. In the second iteration, the source term estimated in previous iteration was added to gas phase. Various convergence criterion like root mean square (RMS) error in gas temperature, heat transfer to heat exchangers and also mass and heat balance of each cell were checked (<0.1% of previous iteration), failing to which the model again solves the gas phase till the convergence was achieved which typically needs 15-20 iterations. The details about number of the ode equations solved are shown below;

Gas phase:

- No. ODE for each zone = 6 (5 Comp. + 1 Energy)
- Total zones = 31 (Fixed)
- Internal CSTRs in each zone = N_i (User input)
- Total no. ODE = $(6)\times \sum N_i$

Particle phase:

- No. of particle sizes = 10
- No. ODE for each size class = 5 (1 Vel.+ 3 Comp. + 1 Energy)
- Number of trajectories = 4
- Total no. ODE = 200 (=10 × 4 × 5)

The modified Gear's method implemented in ODEPACK was used to solve ordinary differential equation using LSODE (Livermore Solver for Ordinary Differential Equations) subroutine. The programming platform used over here was FORTRAN.

Figure 5.13 shows the convergence plot for RMS error in temperature. It shows that model takes about 10 iterations to converge to specified convergence criterion.

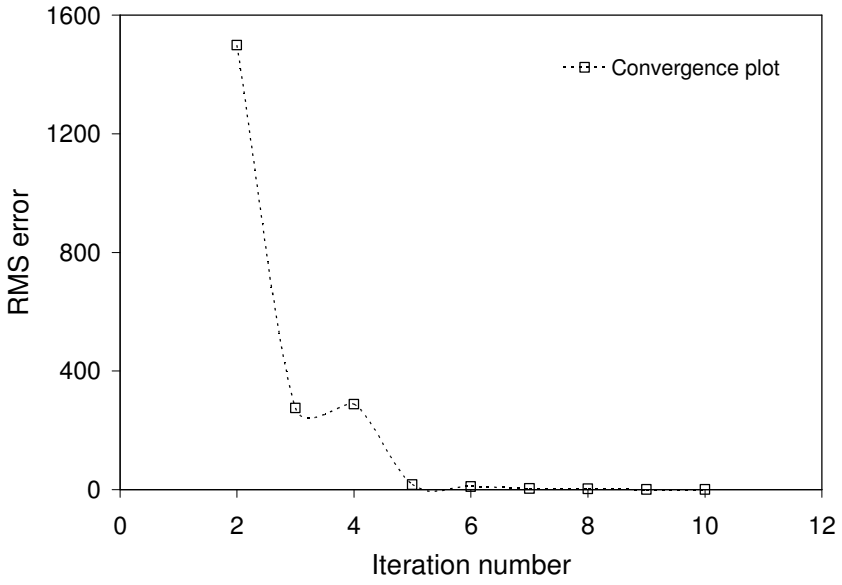

Figure 5.13 : Convergence plot for RMS error in the temperature of zones

5.4 Results and discussion

The integrated model (BOST) presented in the previous section was used to simulate performance of 200 MW_e pc fired boiler. The base case simulation was initially performed and the model predictions were compared with the CFD simulation results discussed in Chapter 3. The predicted results are summarized below.

Temperature profile:

The temperature profile obtained from the simulation is plotted in Figure 5.14. There are few zones where number of CSTRs in respective zone is more than 1. Hence for such zones, number average of temperature of CSTRs in that zone was estimated and plotted in Figure 5.14.

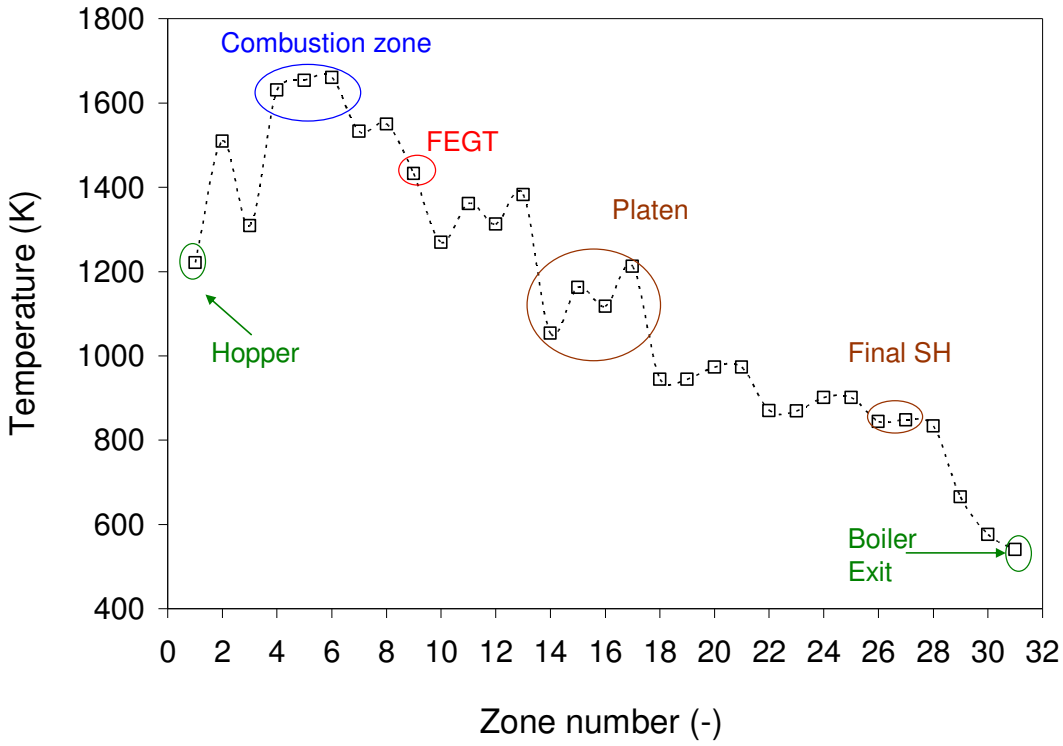

Figure 5.14: Gas temperature across the boiler

The first zone is HOPPER which shows the temperature of 1221 K. The second and third zones are GAP (2) and CORE (3) below the COMBUSTION zone. The part of flow from COMBUSTION zone travels downward from zone 4 to 2 and further gets redistributed

into zone 3 and 1. Hence it can be seen that the zone 2 is at temperature of 1509 K and where as zone 3 is at 1308 K. The zone 2 and 3 were divided into 5 CSTRs each. Figure 5.15 shows the gas temperature of each CSTR.

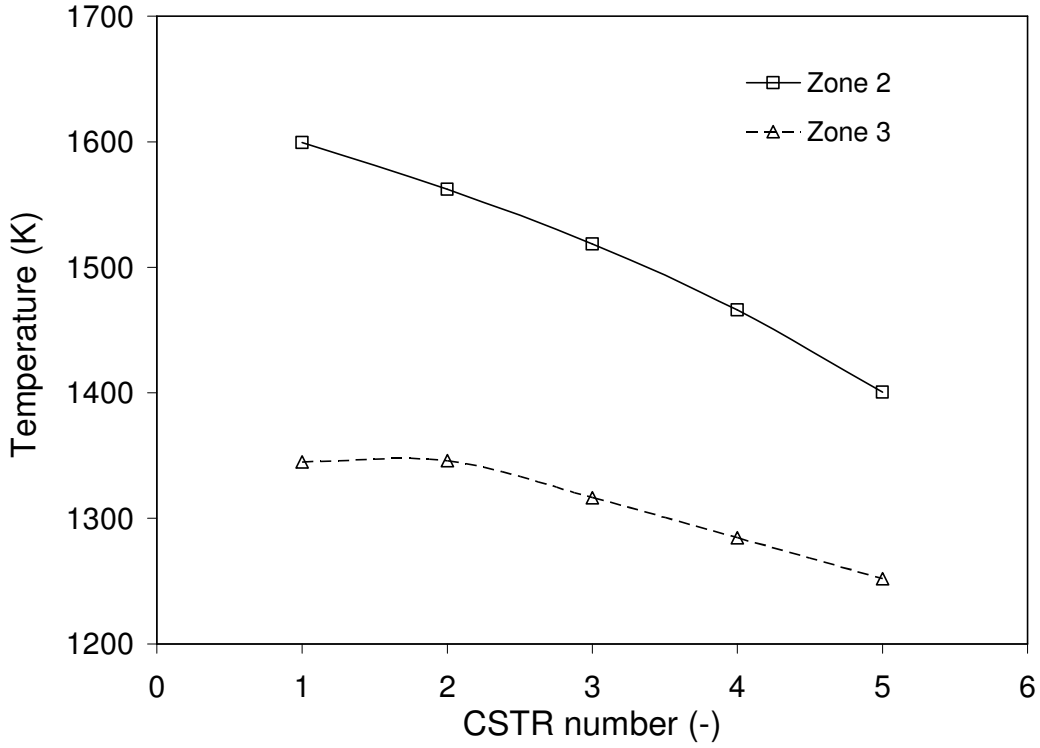

Figure 5.15: Gas temperature profile of zone below the Combustion zone

The zones 4 and 5 were modeled as single CSTR, and have temperature of 1630 K and 1654 K respectively. The burner jet (6) has 5 internal CSTRs and the temperature profile for each CSTR is shown in Figure 5.16. The temperature profile for zone 7 and 8 which are above the combustion zone are also shown in Figure 5.16. The temperature of the Burner jet has increased from inlet feed temperature to 1444 K in first CSTR indicating that major of the reactions taking place in the first CSTR of zone 6. The temperature has finally increased to 1756 K. The localized temperature around 1750 K was predicted across burner jet in CFD simulations. The furnace exit gas temperature (FEGT) was measured at the outlet of the Nose zone (9) as 1432 K and where as the CFD model has predicted area weighted plane average temperature as 1327 K.

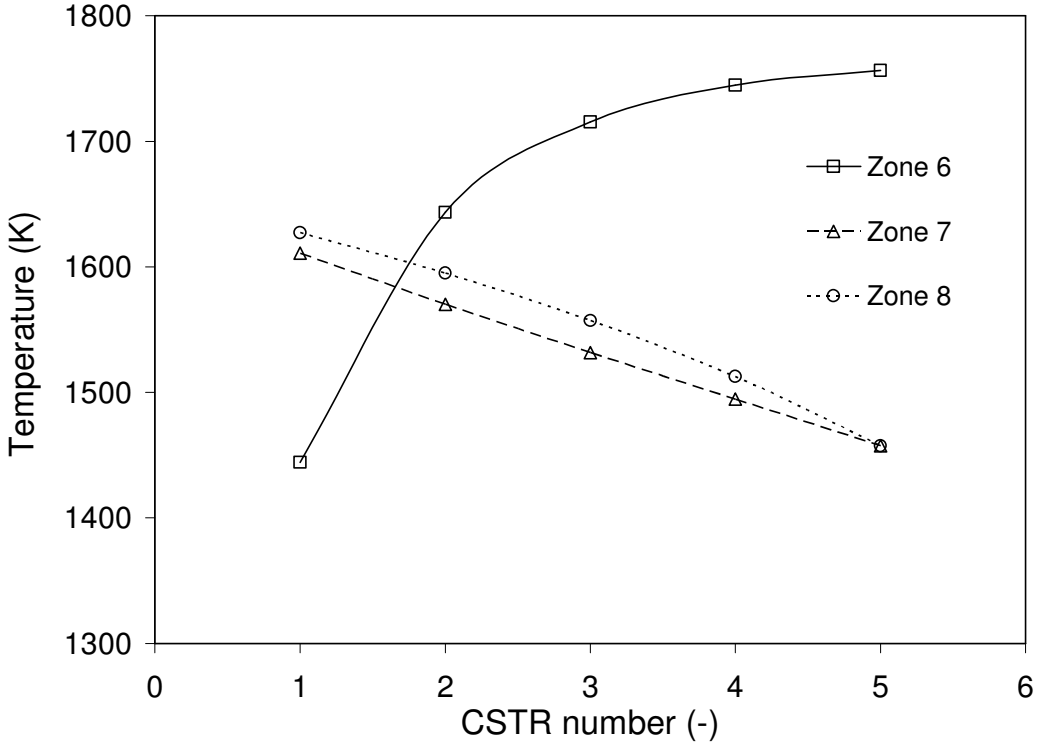

Figure 5.16: Gas temperature profile of zone above the Combustion zone

The model also has ability to predict the imbalance in mass flow distribution in the crossover pass of the boiler which is discussed in Chapter 3. Based on the CFD analysis the imbalance in mass flow rate was estimated and same distribution was incorporated in the present model. The predicted temperature deviation in the cross over pass is shown in the Figure 5.17 (a) and (b). Results show that the model is able to predict the temperature deviation characteristics of the crossover pass. The CFD model predicts the maximum temperature deviation of 166 K and the BOST has predicted the same as 64 K. The difference is due to fact that CFD predictions are based on resolving temperature distribution into finer grids where as in BOST it is based on difference between only two volume as left and right.

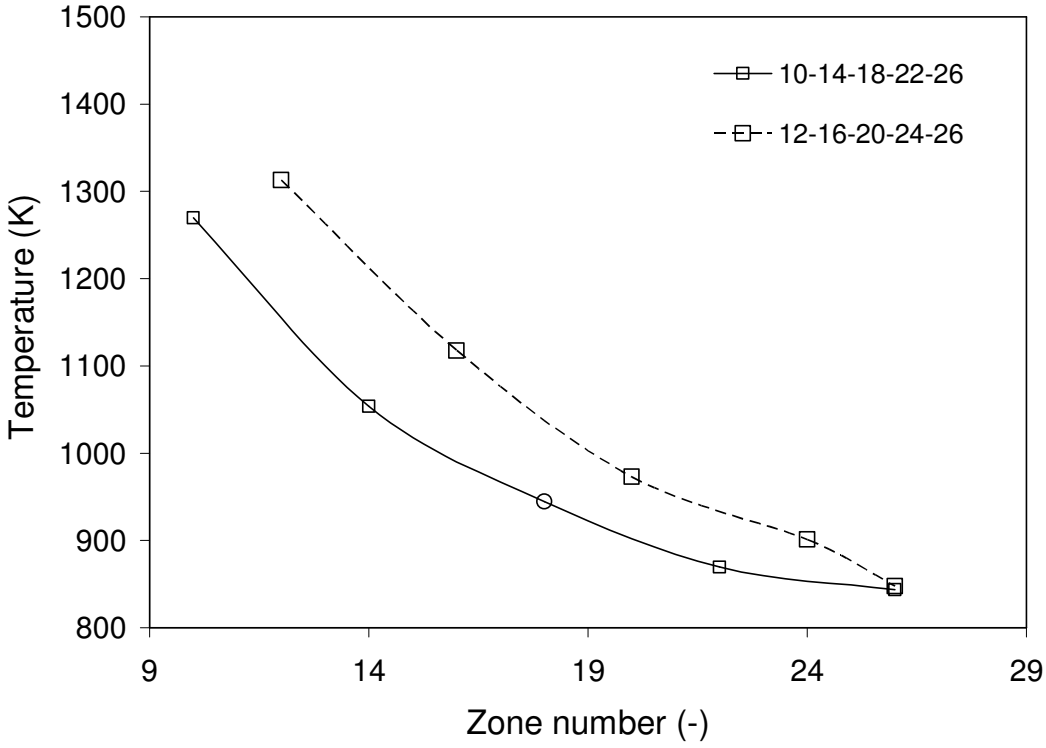

Figure 5.17: (a) Temperature profile at crossover pass of top zones

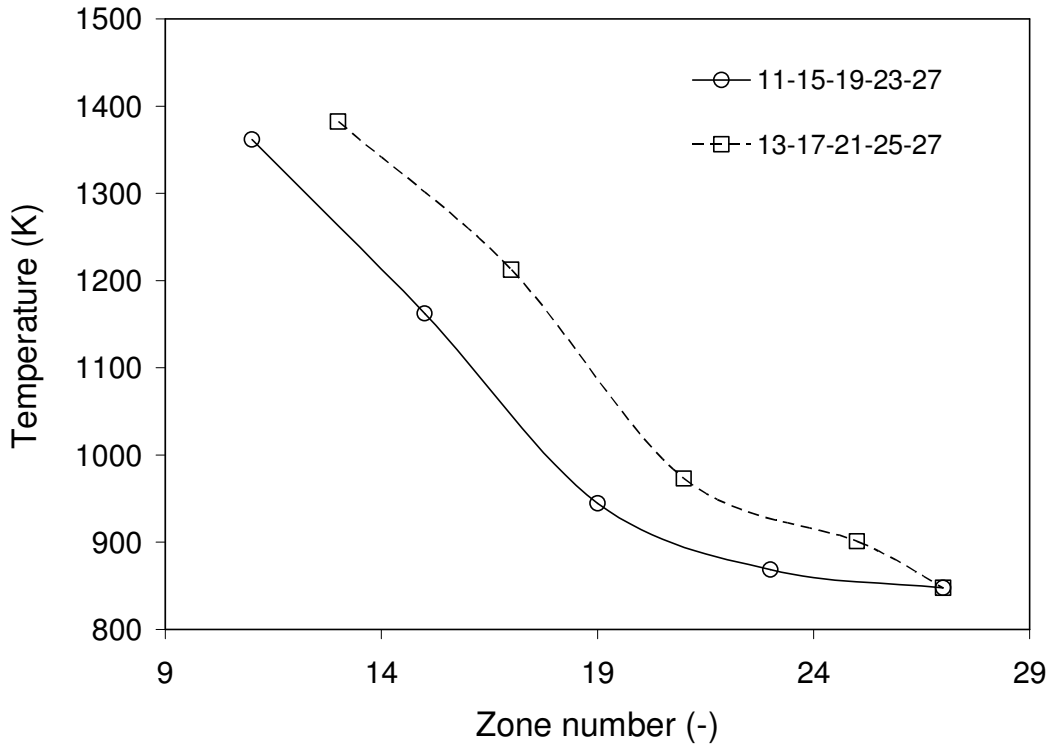

Figure 5.17: (b) Temperature profile at crossover pass of bottom zones

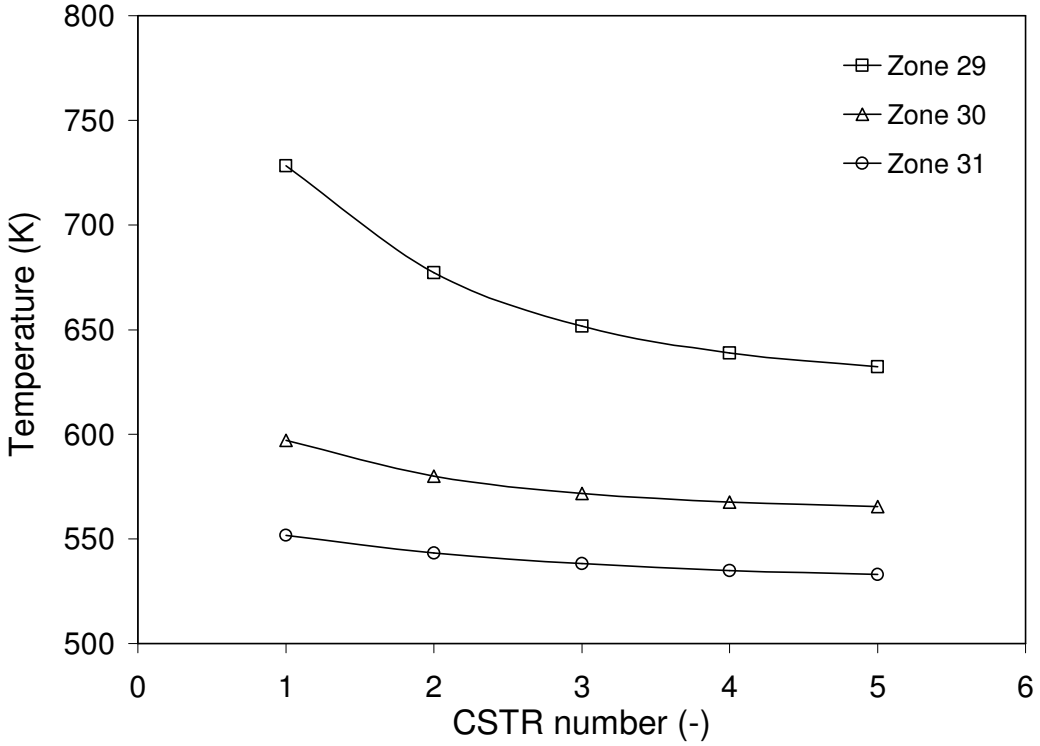

Figure 5.18: Temperature profile of second pass of boiler LTSH, Upper and Lower Economizer

The temperature profile of second pass zone from LTSH to Lower economizer is shown in Figure 5.18. Each of these zones has 5 CSTRs each and the gas temperature along the flow direction for each CSTR is shown in Figure 5.18. The boiler exit temperature was found to be 540 K. The heat transferred to the heat exchangers are listed in Table 5.3 below.

Table 5.3: Heat transfer to heat exchangers

Heat exchangers	Heat transferred (MW)	
	CFD	BOST
Water wall	211	264
Platen SH	120	109
Front RH	70	43
Rear RH	30	21
Final SH	19	12.9

LTSH	41	58.2
Upper ECO	35	19.5
Lower ECO	14	10.4
Total heat transferred	540	538

Comparison shows the few degree of deviation in the heat transfer to individual heat exchanger. But model has qualitatively able to predict the heat transfer in the boiler to each individual heat exchanger.

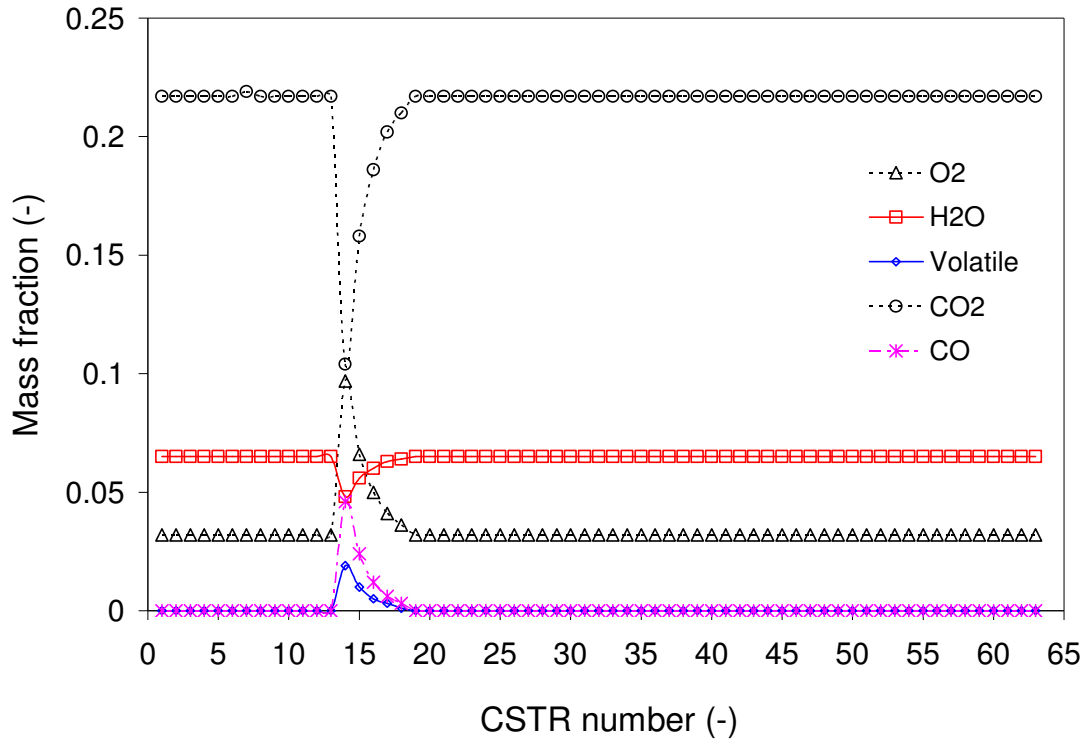

Figure 5.19: Spceies mass fraction profile across the boiler

Species mass fraction for each CSTR is shown in the Figure 5.19. Typically the change in the species concentration was observed in only combustion zone indicating that the reaction was completed in this zone. Model has predicted O_2 mass fraction 0.032 at the boiler exit and CFD simulation shows the same value as well. The BOST was further implemented to simulate the effect of burner tilt on the performance of the furnace. The predicted results are shown in Figure 5.20. The burner tilt correlation has been

implemented in the BOST along with its effect on geometric configuration and as well as the flow distribution into the bottom section of the furnace. Figure 5.20 shows the movement of the fireball zone (and same is applicable to total combustion zone) as an effect of burner tilt.

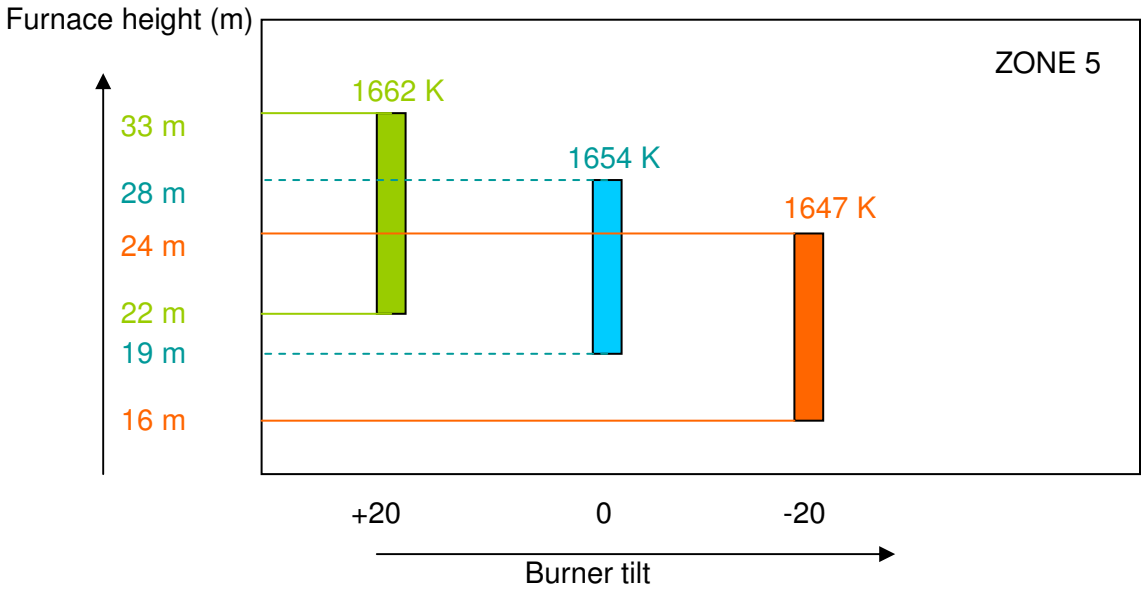

Figure 5.20: Effect of burner tilt on movement of Fireball zone

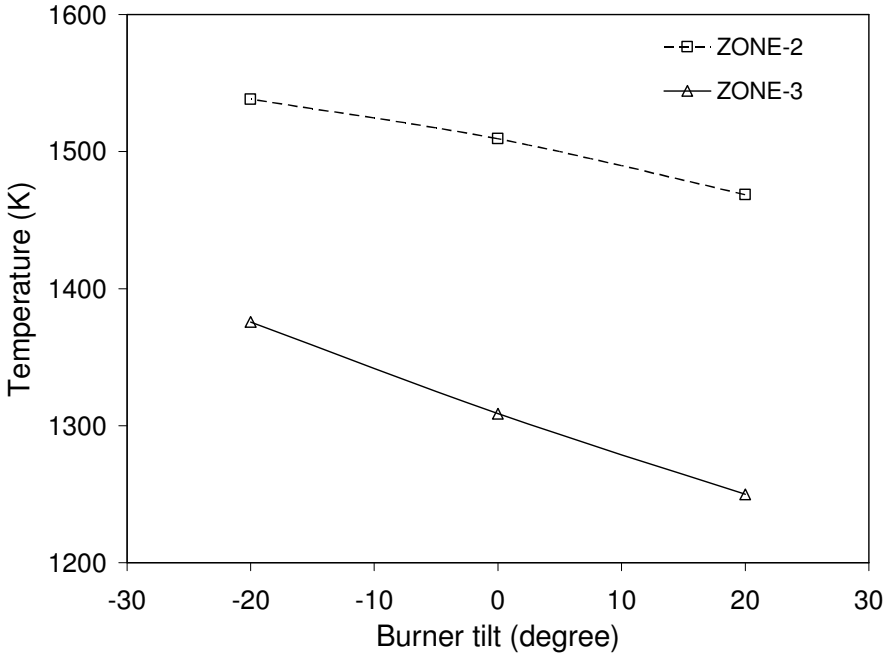

Figure 5.21: Effect of burner tilt on the bottom section of the furnace

The effect of tilt is tested at two extreme conditions of +20 and -20 burner tilt and model was able to predict the movement of hot zone as a function of tilt. For zero tilt, the burner top and boundary limits are 19 and 28 m and has temperature of 1654 K. But for +20 tilt the hot zone has shifted in upward direction to 22 and 33 m. This effect can be observed on the numbered average temperature of the bottom section in Figure 5.21 which shows that the zone 3 temperature will decrease by 126 K when burner tilt is changed from -20 to +20. This clearly shows that BOST can be successfully used to predict the effects of operating conditions like burner tilt on boiler performance.

As discussed in previous sections that the accuracy of the model depends upon the inputs from the CFD model about flow distribution, particle residence time, tilt correlation etc. which is specific to a particular type of geometric configuration and generation capacity of the boiler. However the proposed approach can be extended and used in a straightforward manner for other configurations (and generation capacity) of boiler. CFD models for particular set of systems can be developed and based on few CFD simulations the coefficients of various correlations that are proposed in the methodology are required be evaluated from these CFD simulation. Based on this inputs the BOST becomes a generalized tool to simulate performance of coal fired boiler.

5.5 Conclusions

Phenomenological model was developed to simulate 200 MW coal fired boiler. The model is based on the information extracted from offline CFD model developed for 200 MW_e boiler. Appropriate methodology was developed to obtain key information from the CFD models. Key conclusions are given below,

- Comparison with the CFD model shows the phenomenological model was able to simulate performance of the boiler and was able to predict key features of the boiler with reasonable accuracy

- Model shows ability to predict the effect of burner tilt on hot zones

- Model was able to predict the crossover pass characteristic of the tangentially fired boiler. Model was able predict the 68 K temperature deviation in left and right side volume of crossover pass section.

- The proposed methodology, CFD models and the BOST can be useful as generalized tool to simulate pc fired boiler of various configurations

Chapter 6

Summary and Scope for Future Work

In the present work, a multilayer methodology was developed to study various aspects of tangentially fired pulverized coal boiler of a utility power plant. TGA experiments were performed to study kinetics of coal combustion. Computational models based on detailed computational fluid dynamics (CFD) and conventional reaction engineering approach (REN) was developed to capture influence of key design (furnace dimensions) and operating parameters (burner tilt) on overall performance of boiler. Key aspects of the developed models and scope of future work is discussed below.

- **Kinetics of pulverized coal combustion**

TGA experiments were performed to understand devolatilization and char oxidation characteristics of the sub bituminous high ash content (40%) coal. The experimental data was simulated by TGA model to obtain kinetic parameters for the devolatilization and char oxidation. CFD model for the drop tube furnace was developed to estimate the kinetics of char oxidation from the available literature data on char burnout. This study emphasized the importance and use of 2D axisymmetric CFD model over conventional 1D (ideal plug flow) model in estimation of kinetic parameters.

- **CFD modeling of pulverized coal fired boiler**

A detailed CFD model was developed for 200 MW_e boilers and the effects of various operating parameters were studied. The Eulerian-Lagrangian approach was used to simulate the flow, mass and heat transfer in the boiler. The model was used to understand flow, temperature and species concentration field within a typical boiler. The crossover pass characteristic (uneven distribution of flow and temperature) of tangentially fired boiler was predicted. The model was also used to quantify sensitivity of these fields with key design and operating parameters. The base case was used to understand the sensitivity of excess air, burner tilt and thermal heat load on boiler performance. Simulations were performed to understand the performance of

boiler when the high ash content sub bituminous coal was blended with imported low ash content lignite coal in various ratios. The developed CFD model was able to predict the trends generally observed in literature.

- **Phenomenological model for coal fired boiler**

An appropriate methodology was adopted to develop phenomenological model for simulating pc fired boilers. This model framework BOST uses the information gained from detailed CFD model and uses reaction network models to create readily usable engineering scale model for actual plant implementation. The phenomenological model was based on the mixing cell approach, each zone representing key section of boiler. The positioning and sizes of different zones depend upon the underlying fluid dynamics. The effect of key operating protocols like burner tilt was accounted through appropriate correlations developed from CFD simulations. The developed framework provides a powerful platform to simulate coal fired boilers with reasonable computing resources and in real time.

The research work of this thesis presents systematic approach in developing state of art models for boilers. Studies were performed to understand various aspects like chemistry (kinetics of devolatilization and char oxidation), physics (two phase reactive turbulent flow, radiative heat transfer) and engineering (effect of operational parameters) to predict the performance of the boiler.

- **Scope for future work**

    - Developing a model to predict the ash deposition and erosion of heat exchanger surfaces for high ash content coal firing boiler

- Implementation of advanced combustion model that will take care of heterogeneity in maceral content of binary coal blends. Also model for NO_x and SO_x prediction can be implemented for coal blends

- Extension of BOST to other capacities of boiler and also incorporation of advanced coal combustion model (CBK approach) to increase generality of model

- For BOST, the automatic zoning of boiler computation domain based on coupling with the CFD model simulation results

References

- Abbott, R.C.; Tiley, R. and Gehl, S. (1992), New software directs the ®ght against boiler tube failure, Power Engineering, 96, 59-62
- Allen, M. G.;Butler, C. T.;Johnson, S. A.;Lo, E. Y. and Russo, F.(1993), An imaging neural network combustion control system for utility boiler applications, *Combustion and Flame,* **94,** 205-214
- Alonso, M. J. G.;Borrego, A. G.;Alvarez, D.;Kalkreuth, W. and Menéndez, R.(2001), Physicochemical transformations of coal particles during pyrolysis and combustion, *Fuel,* **80,** 1857-1870
- Arenillas, A.;Backreedy, R. I.;Jones, J. M.;Pis, J. J.;Pourkashanian, M.;Rubiera, F. and Williams, A.(2002), Modelling of no formation in the combustion of coal blends, *Fuel,* **81,** 627-636
- Artos, V. and Scaroni, A. W.(1993), T.G.A. And drop-tube reactor studies of the combustion of coal blends, *Fuel,* **72,** 927-933
- Asotani, T.;Yamashita, T.;Tominaga, H.;Uesugi, Y.;Itaya, Y. and Mori, S.(2008), Prediction of ignition behavior in a tangentially fired pulverized coal boiler using cfd, *Fuel,* **87,** 482-490
- Backreedy, R. I., Fletcher, L.M., Ma, L. Pourkashanian, M. and Williams, A. (2006), Modelling pulverized coal combustion using a detailed coal combustion model, Combust. Sci, and Tech., 178, 763–787
- Backreedy, R.I., Jones, J. M., Ma, L. Pourkashanian, M. and Williams, A., Arenillas, A., Arias, B. Pis, J. J. and Rubiera, F.(2005), Prediction of unburned carbon and Nox in a tangentially fired power station using single coals and blends, Fuel, 84,2196-2203
- Badzioch, S. and Hawksley, P.G.W. (1970), Kinetics of Thermal Decomposition of Pulverized coal particles, Ind. Eng. Chem. Process Design and Development, 9,521-530.
- Ballester, J., Jimenez, S. (2005), Kinetic parameters for the oxidation of pulverized coal as measured from drop tube tests, Combustion and Flame,142, 210–222

- Baranski, J. (2002), Physical and numerical modeling of flow pattern and combustion process in pulverized fuel Fired boiler, Ph.D thesis, Royal Institute of Technology, Sweden.
- Baum, M.M. and Street P.J. (1970), Predicting the combustion behavior of coal particles, Combust. Sci, and Tech., 3(5), 231–243
- Batu, A. and Selçuk, N. (2002), Modeling of Radiative Heat Transfer in the Freeboard of a Fluidized Bed Combustor Using the Zone Method of Analysis. Turkish Journal of Engineering and Environmental Sciences 26, 49
- Beeley T, Cahill P, Riley G, Stephenson P, Lewitt M, Whitehouse M. (2000) The effect of coal blending on combustion performance. DTI Report No. COAL R177, DTI/Pub URN 00/509, London
- Belosevic, S., Sijercic, M., Oka, S. and Tucakovic, D. (2006), Three-Dimensional modeling of utility boiler pulverized coal tangentially fired furnace, International Journal of Heat and Mass Transfer, 49, 3371-3378
- Belosevic, S., Sijercic, M., Oka, S. and Tucakovic, D. (2008), A numerical study of a utility boiler tangentially-fired furnace under different operating conditions, Fuel, 87, 3331-3338
- Bezzo, F.; Macchietto, S. and Pantelides, CC, (2003), General hybrid multizonal CFD approach for bioreactor modeling, AIChE J., 49, 2133
- Bian, Q.L. (1987), The experimental study of the boiler tube failure for the high temperature superheater of 1000 ton/h utility boiler at Wangting Power Station, Boiler Technology, 4, 1-9
- Boyd, R. K. and Kent, J.H. (1986), Three-dimensional furnace computer modeling, In 21st Symp. (Int'l) on combustion, The Combustion Institute, 265-274
- Brewster, B. S., Smoot, L.D. Barthelson, S.H. and Thornock, D. E. (1995), Model Comparisons with Drop Tube Combustion Data for Various Devolatilization Sub models, Energy & Fuels, 9, 870-879
- Card, J. B. A. and Jones, A. R.(1995), A drop tube furnace study of coal combustion and unburned carbon content using optical techniques, *Combustion and Flame,* **101,** 539-547

- Carpenter, A. M. (1995), Coal blending for power stations, IEA Coal Research, London
- Central Electricity Authority (CEA), Ministry of Power, INDIA (2009)
- Chen, J.-Y.;Mann, A. P. and Kent, J. H.(1992), Computational modelling of pulverised fuel burnout in tangentially fired furnaces, *Symposium (International) on Combustion,* **24,** 1381-1389
- Chen, Z.H. (1997), The calculation and analysis of the flow distribution and the thermal variation of the single-phase fluid flowing through the manifold systems in boilers, Journal of University of Shanghai for Science and Technology, 19, 160-178
- Choudhury D. (1993), Introduction to the renormalization group method and turbulence modeling, Fluent Inc. Technical Memorandum,TM-107, 1993.
- Chui, E. H. and Raithby, G. D.(1993), Computation of radiant heat transfer on a nonorthogonal mesh using the finite-volume method, *Numerical Heat Transfer, Part B: Fundamentals: An International Journal of Computation and Methodology,* **23,** 269-288
- Cloke, M.;Lester, E. and Thompson, A. W.(2002), Combustion characteristics of coals using a drop-tube furnace, *Fuel,* **81,** 727-735
- Cloke, M.;Wu, T.;Barranco, R. and Lester, E.(2003), Char characterisation and its application in a coal burnout model, *Fuel,* **82,** 1989-2000
- Coda, B. and Tognotti, L.(2000), The prediction of char combustion kinetics at high temperature, *Experimental Thermal and Fluid Science,* **21,** 79-86
- Collins, S. (1993), Computer calculation provides early warning of boiler tube leaks, Power, 137, 72
- Cumming, J. W.(1984), Reactivity assessment of coals via a weighted mean activation energy, *Fuel,* **63,** 1436-1440
- Diessel, C.F.K. (1992), Coal-bearing depositional systems, Springer-Verlag, Berlin
- Díez, L. I.; Cortés, C. and Campo A.(2004), Modelling of pulverized coal boilers: review and validation of on-line simulation techniques, Applied Thermal Engineering, 25-10, 1516-1533

- Dooley B. (1997), Don't let those boiler tubes fail again, Power Engineering, 56-61
- Eaton, A. M.;Smoot, L. D.;Hill, S. C. and Eatough, C. N.(1999), Components, formulations, solutions, evaluation, and application of comprehensive combustion models, *Progress in Energy and Combustion Science,* **25,** 387-436
- Essenhigh, R. H. and Mescher, A. M.(1996), Influence of pressure on the combustion rate of carbon, *Symposium (International) on Combustion,* **26,** 3085-3094
- Essenhigh, R. H.;Klimesh, H. E. and Fortsch, D.(1999), Combustion characteristics of carbon: Dependence of the zone i-zone ii transition temperature (tc) on particle radius, *Energy & Fuels,* **13,** 826-831
- Essenhigh, R.H. (1981), In: Lowry H.H. editor: Chemistry of coal utilization, 2nd volume. Wiley, New York, USA
- Falcitelli, M.;Tognotti, L. and Pasini, S.(2002), An algorithm for extracting chemical reactor network models from CFD simulation of industrial combustion systems, *Combustion Science and Technology,* **174,** 27-42
- Fan, J. R.;Zha, X. D. and Cen, K. F.(2001), Study on coal combustion characteristics in a w-shaped boiler furnace, *Fuel,* **80,** 373-381
- Fan, J., Sun, P., Zha, X. and Cen, K. (1999), Modeling of Combustion Process in 600 MW Utility Boiler Using Comprehensive Models and Its Experimental Validation, *Energy Fuels,* 13-5,1051 -1057
- Fan, J., Xha, X. D., Sun, P. and Cen, K. (2001), Simulation of ash deposit in a pulverized coal fired boiler, Fuel, 80, 645-654
- Fan, J.; Qian, L.; Ma,Y.; Sun, P. and Cen, K. (2001), Computational modeling of pulverized coal combustion processes in tangentially fired furnaces, Chemical Engineering Journal, 81-1, 261-269
- Field, M.A. (1969), Rate of combustion of size graded fractions of char from a low-rank coal between 1200K and 2000K, Combustion and Flame, 13 , 237–252
- Fiveland, W.A. and Jamaluddin, A.S. (1989), Three-Dimensional Spectral Radiative Heat Transfer Solutions by the Discrete Ordinates Method, Heat Transfer Phenomena in Radiation, Combustion and Fires, 43-48.

- Fletcher, T.H. and Kerstein, A.R.(1992) Chemical percolation model for devolatilization: 3 Direct use of 13C NMR data to predict effect of coal type, Energy and Fuels, 6: 414
- Fluent-6 User's Guide (2007), Ansys Inc. USA
- Gavalas, G. R., *Coal Pyrolysis,* Elsevier, Amsterdam,1982.
- Gosman, A. D. and Lockwood, F. C.(1973), Incorporation of a flux model for radiation into a finite-difference procedure for furnace calculations, *Symposium (International) on Combustion,* **14,** 661-671
- Gosman, A. D.; Pun, W. M.; Ramchal, A. K.; Spalding, D. B., and Wolfshtein, M. (1969), Heat and Mass Transfer in recirculating flows, Academic Press, London.
- Guo, Y. C. and Chan, C. K. (2000), A multi-fluid model for simulating turbulent gas–particle flow and pulverized coal combustion, Fuel, 79- 12, 1467-1476
- Guo, Y. C., Chan, C. K. and Lau, K.S. (2003), Numerical studies of pulverized coal combustion in a tubular coal combustor with slanted oxygen jet, Fuel,82-8, 893-907
- Haas, J.;Tamura, M. and Weber, R.(2001), Characterisation of coal blends for pulverised fuel combustion, *Fuel,* **80,** 1317-1323
- He, B., Zhu, L., Wang, J. Liu, S., Liu, B., Cui, Y., Wang, L. and Wei, G. (2007), Computational fluid dynamics based retrofits to Reheater panel Overheating of No.3 boiler of Dagang Power Plant, Computers & Fluids,36,435-444
- Helle, S.;Gordon, A.;Alfaro, G.;García, X. and Ulloa, C.(2003), Coal blend combustion: Link between unburnt carbon in fly ashes and maceral composition, *Fuel Processing Technology,* **80,** 209-223
- Hindmarsh, C. J.;Thomas, K. M.;Wang, W. X.;Cai, H. Y.;Güell, A. J.;Dugwell, D. R. and Kandiyoti, R.(1995), A comparison of the pyrolysis of coal in wire-mesh and entrained-flow reactors, *Fuel,* **74,** 1185-1190
- Hottel H. C. and Cohen E. S. (1935), Radiant heat exchange in a gas-filled enclosure: Allowance for nonuniformity of gas temperature. AIChE J.,4(1), 14
- Hottel, H. C. and Sarofim, A. F. (1967), Radiative Transfer, McGraw-Hill, N.Y.

- Howard, J. B., Fong,W. S., and Peters,W. A., in *Fundamentals of the Physical Chemistry of Pulverized Coal Combustion, NATO ASI Series, Series E: Applied Sciences, No. 137,* (J. Layaye and G. Prado, eds.), Martinus Nijhoff, Netherlands, 1987, p. 77.
- Howell, J. R. (1968), Application of Monte Carlo to Heat Transfer Problems, *Advances in Heat Transfer,* Academic Press, New York.
- Huang, Y.;Yan, Y. and Riley, G.(2000), Vision-based measurement of temperature distribution in a 500-kw model furnace using the two-colour method, *Measurement,* **28,** 175-183
- Hurt R., Sun, J. and Lunden M.(1998), A kinetic Model of Carbon Burnout in Pulverized Coal Combustion, Combustion and Flame, 113 , 181–197
- Hurt, R. H. and Gibbins, J. R.(1995), Residual carbon from pulverized coal fired boilers: 1. Size distribution and combustion reactivity, *Fuel,* **74,** 471-480
- Ikeda, M.;Makino, H.;Morinaga, H.;Higashiyama, K. and Kozai, Y.(Emission characteristics of nox and unburned carbon in fly ash during combustion of blends of bituminous/sub-bituminous coals[small star, filled], *Fuel,* **82,** 1851-1857
- Jones, J.M.; Patterson P.M.; Pourkashanian , M.; Williams , A.; Arenillas, A.; Rubiera, F. and Pis, J.J.(1999), Modeling Nox formation in coal particle combustion at high temperature: an investigation of the devolatilization kinetic factors, Fuel 78,1171–1179
- Jones, W. P. and Whitelaw, J. H.(1982), Calculation methods for reacting turbulent flows: A review, *Combustion and Flame,* **48,** 1-26
- Jüntgen, H. and Van Heek, K. H.(1979), An update of german non-isothermal coal pyrolysis work, *Fuel Processing Technology,* **2,** 261-293
- Kim, Y. J.; Lee, J. M. and Kim, S. D.(2000), Modeling of coal gasification in an internally circulating fluidized bed reactor with draught tube, *Fuel,* **79,** 69-77
- Kobayashi, H., Howard, J.B. and Sarofim, A.F. (1977), Coal devolatilization at high temperatures, Proc. Combust. Inst., 16**,** 411–425
- L. J. *Muzio*, *D. Eskinazi, and S. F. Green*, *Acoustic Pyrometry*: *New Boiler Diagnostic*. *Tool*, *Power Eng*., *vol. 11*, *pp. 49–52*, *1989*

- Launder, B.E. and Spalding, D. B. (1972), Lectures in Mathematical Models of Turbulence, Academic press, London, England
- Li, Z.Q., Wei, F and Jin, Y.(2003), Numerical simulation of pulverized coal combustion and NO formation, Chemical Engineering Science 58, 5161-5171
- Liu, W.J. (1993), The improved measure and cause analysis of partial overheat for 1025 ton/h utility boiler reheater, Boiler Technology, 7, 4-12
- Lockwood, F. C. and Shah, N. G.(1981), A new radiation solution method for incorporation in general combustion prediction procedures, *Symposium (International) on Combustion,* **18,** 1405-1414
- Lowe, A.;Wall, T. F. and Stewart, I. M.(1975), A zoned heat transfer model of a large tangentially fired pulverized coal boiler, *Symposium (International) on Combustion,* **15,** 1261-1270
- Magnussen, B. F. and Hjertager B. H. (1976), On mathematical models of turbulent combustion with special emphasis on soot formation and combustion, In 16th Symp. (Int'l.) on Combustion*,* The Combustion Institute.
- Maier, H.;Spliethoff, H.;Kicherer, A.;Fingerle, A. and Hein, K. R. G.(1994), Effect of coal blending and particle size on nox emission and burnout, *Fuel,* **73,** 1447-1452
- Mcilvaine, (2008), Report on world power generation projects,
- Milenkova, K. S.;Borrego, A. G.;Alvarez, D.;Xiberta, J. and Menendez, R.(2003), Tracing the origin of unburned carbon in fly ashes from coal blends, *Energy & Fuels,* **17,** 1222-1232
- Miller, B. G. (2005), Coal Energy Systems, Elsevier Academic Press,5
- Miura, K.(2002), A new and simple method to estimate f(e) and k0(e) in the distributed activation energy model from three sets of experimental data, *Energy & Fuels,* **9,** 302-307
- Modest, M. F. (2003) ,Radiative heat transfer, Academic press
- Morgan, P. A.;Robertson, S. D. and Unsworth, J. F.(1986), Combustion studies by thermogravimetric analysis: 1. Coal oxidation, *Fuel,* **65,** 1546-1551
- Morsi, S.A. and Alexander, A.J. (1972), An Investigation of Particle Trajectories in Two-Phase Flow Systems, J. Fluid Mech**,** 55(2), 193-208

- Mullinger, P. and Jenkins, B. (2008), Industrial and process furnace, First edition, Butterworth Heinemann publications
- Murthy, J. Y. and Mathur, S. R. (1998), Finite volume method for radiative heat transfer using unstructured meshes, *Journal of Thermophysics and Heat Transfer,* **12** 313-321
- Niksa, S., *Coal Combustion Modelling,* Perspectives IEAPER/31, IEA Coal Research, London, 1996.
- Ohtake, K. and Okazaki, K.(1988), Optical ct measurement and mathematical prediction of multi-temperature in pulverized coal combustion field, *International Journal of Heat and Mass Transfer,* **31,** 397-405
- Osawe, M., Felix, P., Syamlal, M., Lapshin,I., Clectus, KJ and Zitney, SE,(2002), An integrated process simulation and CFD environment using the CAPE-OPEN interface specifications, Proc of AIChE Annual Meeting, Indianapolis, IN
- Pallarés, J., Arauzo, I. and Williams, A. (2007) , Integration of CFD codes and advanced combustion models for quantitative burnout determination, Fuel, 86-15, 2283-2290
- Pallares, J., Arauzo, I., Diez, L. I. (2005), Numerical prediction of unburned carbon levels in large pulverized coal utility boilers, Fuel, 84, 2364-2371
- Peralta, D.; Paterson, N. P.;Dugwell, D. R. and Kandiyoti, R.(2001), Coal blend performance during pulverised-fuel combustion: Estimation of relative reactivities by a bomb-calorimeter test, *Fuel,* **80,** 1623-1634
- Peralta, D.; Paterson, N. P.;Dugwell, D. R. and Kandiyoti, R.(2002), Development of a reactivity test for coal-blend combustion: The laboratory-scale suspension-firing reactor, *Energy & Fuels,* **16,** 404-411
- Perry, J. H. (1982), Aerodynamics of burner jets designed for brown coal-fired boilers: literature survey, Report (State Electricity Commission of Victoria. Research and Development Dept.) ; no. GO/82/53.
- Pillai, K.K. (1981), The Influence of Coal Type on Devolatilization and Combustion in Fluidized Beds, *J. Inst. Energy*, 142.

- Raithby, G. D. and Chui, E. H.(1990), A finite-volume method for predicting a radiant heat transfer in enclosures with participating media, *Journal of Heat Transfer,* **112,** 415-423
- Ranade, V. V. (2002), Computational flow modeling for chemical reactor engineering, Academic Press, London
- Ranz, W. E. and Marshall, W. R.(1952), Evaporation from drops, part I., *Chemical Engineering Progress,* **48,** 141-146
- Ranz, W. E. and Marshall, W. R.(1952), Evaporation from drops, part II., *Chemical Engineering Progress,* **48,** 173-180
- Ray, H. W. and Wells, G. J. (2005), Methodology for Modeling Detailed Imperfect Mixing Effects in Complex Reactors, AIChE J., 51/5, 1508
- Rubiera, F.;Arenillas, A.;Arias, B. and Pis, J. J.(2002), Modification of combustion behaviour and no emissions by coal blending, *Fuel Processing Technology,* **77-78,** 111-117
- Russell, N. V.; Beeley, T. J.; Man, C. K.; Gibbins J. R. and Williamson, J. (1998), Development of TG measurements of intrinsic char combustion reactivity for industrial and research purpose Fuel Processing Technology, Volume 57-2, 113-130
- Sahu, R.; Northrop, P. S.;Flaganâ, R. C. and Gavalas, G. R.(1988), Char combustion: Measurement and analysis of particle temperature histories, *Combustion Science and Technology,* **60,** 215-230
- Serio, M. A.;Hamblen, D. G.;Markham, J. R. and Solomon, P. R.(2002), Kinetics of volatile product evolution in coal pyrolysis: Experiment and theory, *Energy & Fuels,* **1,** 138-152
- Sheng, C.; Moghtaderi, B.; Gupta, R. and Wall, T. F. (2004), A computational fluid dynamics based study of the combustion characteristics of coal blends in pulverized coal-fired furnace, Fuel 83, 1543–1552
- Sheng, C.;Moghtaderi, B.;Gupta, R. and Wall, T. F.(2004), A computational fluid dynamics based study of the combustion characteristics of coal blends in pulverised coal-fired furnace, *Fuel,* **83,** 1543-1552

- Siegel, R. and Howell, J. R. (1981), Thermal radiation heat transfer, 2nd edition, Hemisphere Pub. Corp., USA
- Sivathanu, Y. R. and Faeth, G. M.(1990), Generalized state relationships for scalar properties in nonpremixed hydrocarbon/air flames, *Combustion and Flame,* **82,** 211-230
- Smith, I. W. (1982), The combustion rates of coal chars: A review, *Symposium (International) on Combustion,* **19,** 1045-1065
- Smith, I. W.(1973), Combustion rate of bituminous coal char in the temperature range 800K-1700K, Fuel, 52-57
- Smith, I. W.(1979),The intrinsic reactivity of carbons to oxygen, Fuel, 57, 409
- Smith, K. L., Smoot, L. D., and Fletcher, T. H., (1993), *Fundamentals of Coal Combustion* (L. D. Smoot, ed.), Elsevier, Amsterdam, 18.
- Solomon, P. R. and Fletcher, T. H.(1994), Impact of coal pyrolysis on combustion, *Symposium (International) on Combustion,* **25,** 463-474
- Solomon, P. R.; Serio, M. A. and Suuberg, E. M.(1992), Coal pyrolysis: Experiments, kinetic rates and mechanisms, *Progress in Energy and Combustion Science,* **18,** 133-220
- Stanmore B.R. and Visiona, S.P. (2000); Prediction of Nox emissions from a number of coal-fired power station boilers, Fuel Processing Technology 64, 25–46
- Su, S.; Pohl, J. H. and Holcombe, D.(2003), Fouling propensities of blended coals in pulverized coal-fired power station boilers, *Fuel,* **82,** 1653-1667
- Su, S.;Pohl, J. H.;Holcombe, D. and Hart, J. A.(2001), Slagging propensities of blended coals, *Fuel,* **80,** 1351-1360
- Su, S.;Pohl, J. H.;Holcombe, D. and Hart, J. A.(2001), Techniques to determine ignition, flame stability and burnout of blended coals in p.f. power station boilers, *Progress in Energy and Combustion Science,* **27,** 75-98
- Sujanti, W.;Zhang, D.-K. and Chen, X. D.(1999), Low-temperature oxidation of coal studied using wire-mesh reactors with both steady-state and transient methods, *Combustion and Flame,* **117,** 646-651

- Sun, J., Hurt, R.H., Niksa, S., Muzio, L., Mehta, A. and Stallings, J. (2003). A simple numerical model to estimate the effect of coal selection on pulverized fuel burnout, Combust. Sci. and Tech., 175, 1085–1108.
- Viskanta, R. and Mengüç, M. P.(1987), Radiation heat transfer in combustion systems, *Progress in Energy and Combustion Science,* **13,** 97-160
- Viskanta, R., (1966), Radiation Transfer and Interaction of Convection with Radiation Heat Transfer, Advances in Heat Transfer, 3, 175-252
- Vleeskens, J. M. and Nandi, B. N. (1986), Burnout of coals- Comparative bench-Scale experiments on pulverized fuel and fluidized bed combustion, Fuel, 65,797
- Vuthaluru, R. and Vuthaluru H.B. (2006), Modelling of a wall fired furnace for different operating conditions using FLUENT, Fuel Processing Technology, 87,633–639
- Vuthaluru, R. and Vuthaluru, H. B.(2006), Modelling of a wall fired furnace for different operating conditions using fluent, *Fuel Processing Technology,* **87,** 633-639
- Wall, T. F.;Duong, H. T.;Stewart, I. M. and Truelove, J. S.(1982), Radiative heat transfer in furnaces: Flame and furnace models of the ifrf m1- and m2-trials, *Symposium (International) on Combustion,* **19,** 537-547
- Walsh, P. M. (1997) Analysis of carbon loss from a pulverized coal-fired boiler, Energy Fuels, 11, 965.
- Walsh, P. M.(1997), Analysis of carbon loss from a pulverized coal-fired boiler 11965-971
- Wang, M. H. (1984), Thermal deviation of the same row in the convective superheater and reheater of utility boiler, Power Engineering, 2, 11-17
- Wang, M. H. (1986), The calculation of thermal deviation for plate superheater, Power Engineering, 2, 7-14
- Watanabe, H. And Otaka, M.(2006), Numerical simulation of coal gasification in engrained flow gasifier, Fuel, 85, 1935-1943
- Williams, A.; Pourkashanian, M. and Jones, J. M. (2000), The combustion of coal and some other solid fuels, *Symposium (International) on Combustion,* **28,** 2141-2162

- Williams, A.; Pourkashanian, M. and Jones, J. M. (2001), Combustion of pulverised coal and biomass, *Progress in Energy and Combustion Science,* **27,** 587-610
- Xu, L. J. (1994), Research and analysis of boiler tubes failure diagnosis for superheater and reheater, Journal of Energy Research and Utilization, 33 (3), 34-38
- Xu, M., Azevedo, J. L. T. and Carvalho, M. G. (2000), Modelling of the combustion process and NO_x emission in a utility boiler, Fuel, 79-13, 1611-1619
- Xu, M., Yuan, J. Ding, S. and Cao, H. (1998), Simulation of the gas temperature deviation in large-scale tangential coal fired utility boilers, Comput. Methods Appl. Mech. Engrg., 155,369-380
- Xu, M.; Azevedo, J. L. T. and Carvalho, M. G.(2001), Modeling of a front wall fired utility boiler for different operating conditions, *Computer Methods in Applied Mechanics and Engineering,* **190,** 3581-3590
- Yang, R.G. (1989), BTF cause and diagnosis for the reheater of 1160 ton/h utility boiler at Baoshan Iron and Steel Group Corp, Boiler Technology, 8, 1-8
- Yang, R.G. (1991), The improved measure and diagnosis of boiler tube failure for the reheater of 1160 ton/h utility boiler, Boiler Technology 2, 5-8
- Yin, C.; Caillat, S.; Harion, J; Baudoin, B. and Perez, E. (2002), Investigation of the flow, combustion, heat-transfer and emissions from a 609 MW utility tangentially fired pulverized-coal ,Fuel,81-8,997-1006
- Yoshizawa, N.;Maruyama, K.;Yamashita, T. and Akimoto, A.(2006), Dependence of microscopic structure and swelling property of dtf chars upon heat-treatment temperature, *Fuel,* **85,** 2064-2070
- Zhang, D.; Wall, T. F.; Harris, D.J.; Smith, I. W.; Chen, J. and Stanmore, B. R.(1992), Experimental studies of ignition behavior and combustion reactivity of pulverized fuel particles, Fuel, 71-11,1239-1246
- Zhang, Y.;Wei, X.-L.;Zhou, L.-X. and Sheng, H.-Z.(2005), Simulation of coal combustion by ausm turbulence-chemistry char combustion model and a full two-fluid model, *Fuel,* **84,** 1798-1804

- Zhou, L. X., Li, L. Li, R. X. and Zhang, J. (2002), Simulation of 3-D gas-particle flows and coal combustion in a tangentially fired furnace using a two-fluid-trajectory model, Powder Technology, 125, 226-233
- Zolin, A.;Jensen, A. and Dam-Johansen, K.(2001), Coupling thermal deactivation with oxidation for predicting the combustion of a solid fuel, *Combustion and Flame,* **125,** 1341-1360

List of Publications

- Conferences

- D.F. Gupta and V.V. Ranade (2009). CFD simulations of firing coal blends in 210 MW_e boiler, Advances in Chemical Engineering and Process Technology (ACEPT09), National Chemical Laboratory (NCL), Pune

- D.F. Gupta and V.V. Ranade, (2008). CFD Simulations of Pulverized Coal Combustion in Drop Tube Furnace, poster presented on Science Day 2009, NCL, Pune

- D.F. Gupta and V.V. Ranade, (2008). Phenomenological Modeling of coal fired boiler based on CFD simulations, ISCRE20, Kyoto, Japan

- D.F. Gupta and V.V. Ranade, (2008). Modeling of coal fired boiler, poster presented on Science Day 2008, NCL, Pune

- D.F. Gupta, V.V. Ranade, K. BhanuPrakash and R.R. Sonde, (2006). Modeling of Pulverized Coal Fired Boiler: Validations using cold air velocity tests, BHEL Conference, Hyderabad

Appendix –I

Radiation exchange coefficients

Gas to gas exchange coefficients (g-g)

	1	2	3	4	5	6	7	8	9	10
1	0	2.55	4.52	0.77	0.83	0.17	0.38	0.33	0.04	0.01
2	2.55	0	4.08	1.7	1.59	0.64	0.59	0.18	0.02	0.005
3	4.52	4.08	0	1.53	2.62	0.58	0.56	0.52	0.06	0.028
4	0.77	1.7	1.53	0	4.02	6.22	1.8	1.36	0.15	0.033
5	0.83	1.59	2.62	4.02	0	1.49	1.66	1.84	0.14	0.028
6	0.17	0.64	0.58	6.22	1.49	0	0.65	0.61	0.06	0.003
7	0.38	0.59	0.56	1.8	1.66	0.65	0	24.69	2.03	0.283
8	0.33	0.6	0.52	1.36	1.84	0.61	24.69	0	2.43	0.263
9	0.04	0.06	0.06	0.15	0.14	0.06	2.03	2.43	0	0.093
10	0.01	0.005	0.028	0.033	0.028	0.003	0.283	0.263	0.093	0
11	0.01	0.005	0.028	0.033	0.028	0.003	0.283	0.263	0.093	0
12	0.01	0.005	0.028	0.033	0.028	0.003	0.283	0.263	0.093	0
13	0.01	0.005	0.028	0.033	0.028	0.003	0.283	0.263	0.093	0
14	0.005	0.005	0.013	0.033	0.028	0.003	0.283	0.278	0.098	1.352
15	0.005	0.005	0.013	0.033	0.028	0.003	0.283	0.278	0.098	1.352
16	0.005	0.005	0.013	0.033	0.028	0.003	0.283	0.278	0.098	1.352
17	0.005	0.005	0.013	0.033	0.028	0.003	0.283	0.278	0.098	1.352

	11	12	13	14	15	16	17
1	0.01	0.01	0.01	0.005	0.005	0.005	0.005
2	0.005	0.005	0.005	0.06	0.005	0.005	0.005
3	0.028	0.028	0.028	0.013	0.013	0.013	0.013
4	0.033	0.033	0.033	0.033	0.033	0.033	0.033
5	0.028	0.028	0.028	0.028	0.028	0.028	0.028
6	0.003	0.003	0.003	1.11	0.003	0.003	0.003
7	0.283	0.283	0.283	0.283	0.283	0.283	0.283
8	0.263	0.263	0.263	0.278	0.278	0.278	0.278
9	0.093	0.093	0.093	0.098	0.098	0.098	0.098
10	0	0	0	1.352	1.352	1.352	1.352
11	0	0	0	1.352	1.352	1.352	1.352
12	0	0	0	1.352	1.352	1.352	1.352
13	0	0	0	1.352	1.352	1.352	1.352
14	1.352	1.352	1.352	0	0	0	0
15	1.352	1.352	1.352	0	0	0	0
16	1.352	1.352	1.352	0	0	0	0
17	1.352	1.352	1.352	0	0	0	0

Gas to gas exchange coefficients (g-s)

	S1	S2	S3	S4	S5	S6
G1	67.84	18.2	4.19	1.26	0.06	0.04
G2	8.85	53.92	7.8	1.95	0.1	0
G3	9.48	11.17	1.42	0.27	0.02	0
G4	2.46	6.27	57	7.29	0.31	0
G5	2.32	1.18	15.46	1.39	0.06	0
G6	0.6	2.37	25.17	2.05	0.07	0
G7	0.48	1.66	5.02	152.92	4.45	0
G8	0.67	2.36	9.49	115.16	5	0
G9	0.06	0.18	0.92	11.88	14.34	25.41
G10	0.013	0.045	0.113	1.08	1.315	29.11
G11	0.013	0.045	0.113	1.08	1.315	29.11
G12	0.013	0.045	0.113	1.08	1.315	29.11
G13	0.013	0.045	0.113	1.08	1.315	29.11
G14	0	0	0	0	0	31.665
G15	0	0	0	0	0	31.665
G16	0	0	0	0	0	31.665
G17	0	0	0	0	0	31.665